J. Heyrovský Institute of Physical Chemistry of the ASCR, v. v. i.

PhD Thesis

MoO_3 supported on mesoporous molecular sieves – new catalysts for alkene metathesis and alkyne polymerization

Ing. Pavel Topka

Supervisor: Prof. Ing. Jiří Čejka, DrSc.

Consultant: RNDr. Hynek Balcar, CSc.

Declaration

I hereby declare that the submitted PhD Thesis was completed by myself and no other. I have not used any sources or materials other than those that I cited and indicated in the list of references.

Moreover, I declare that the following PhD Thesis has not been submitted further in this form or any other form, and has not been used to obtain any other equivalent qualifications at any other organization/institution.

Additionally, I have not applied for, nor will I attempt to apply for any other degree or qualification in relation to this work.

Prague, July 16, 2008

.....
Ing. Pavel Topka

Acknowledgements

This work was done at the Department of Synthesis and Catalysis of the J. Heyrovský Institute of Physical Chemistry of the ASCR, v. v. i. in Prague.

I would like to thank Prof. Ing. Jiří Čejka, DrSc., my supervisor, for his help. Many thanks belong to RNDr. Hynek Balcar, CSc., my consultant, for his understanding and support over the years. I thank all the people from the group of Prof. Čejka for all kind help and fruitful discussions. Thanks go to Ing. N. Žilková for GC analysis, Dr. A. Zukal and Dr. J. Rathouský for nitrogen adsorption measurements, Dr. L. Brabec for recording SEM images, Dr. J. Dědeček for taking NMR spectra, and Dr. Z. Bastl for XPS measurements.

Acknowledgements go to Prof. Francis Verpoort and his group from the Department of Inorganic and Physical Chemistry of the Ghent University, Belgium, for their kind help during my stay there. I also thank Dr. Eric Marceau and Dr. Xavier Carrier from Laboratoire de Réactivité de Surface, Université Pierre et Marie Curie - Paris 6, France, for their assistance and help with Raman spectroscopy.

Summary

The main emphasis of the PhD thesis focuses on the development of new type of heterogeneous catalysts for metathesis of alkenes based on molybdenum oxide supported on siliceous mesoporous molecular sieves MCM-41, MCM-48, and SBA-15. The key idea is to improve the activity of molybdenum oxide catalyst in this reaction utilizing high surface area and narrow pore size distribution of the support material. For the preparation of the catalysts, innovative and environmentally friendly thermal spreading method was employed.

The catalysts and the supports were characterized by X-ray powder diffraction and nitrogen adsorption measurement. It was shown that MoO_3 disperses over the surface of mesoporous silica. No collapse of support structures during the preparation of the catalysts was observed even at the highest loadings (16 wt. % Mo).

Metathesis of 1-octene was carried out in a liquid phase using a stirred glass batch reactor. The catalyst was activated under the stream of dry air at 500 °C, whereas the catalytic reaction was performed under argon atmosphere. The metathesis of 1-octene proceeded at ambient or slightly elevated temperature and without the presence of solvent. At 40 °C, the most active MoO_3/MCM-41 catalyst with 6 wt. % Mo allowed to achieve 75 % conversion of 1-octene after 360 min of the reaction with selectivity to 7-tetradecene being 84 %. The initial turn-over frequency of MoO_3/MCM-41 catalyst (6 wt. % Mo) at 40 °C was 0.014 s^{-1}, i.e. more than four times higher in comparison with conventional MoO_3/SiO_2 catalyst with the same loading operating under the same reaction conditions. Among the catalysts prepared from different Mo compounds and using different preparation procedures, that prepared by thermal spreading of MoO_3 exhibited the highest activity together with high selectivity. The conversion achieved after 360 min of the reaction at 40 °C with MoO_3 based catalysts loaded with 8 wt. % Mo decreased in the order MoO_3/MCM-41 > MoO_3/MCM-48 > MoO_3/SBA-15 > MoO_3/SiO_2 (70, 32, 18, and 8 %, respectively), while the selectivity was slightly increasing (from 82 to 95 %). Catalysts of lower loadings (from 4 to 8 wt. % Mo) exhibited higher specific activity than the catalysts with the highest loading (16 wt. % of Mo). The differences in catalytic activity were correlated with the structure of the catalysts before the reaction using XRD, XPS, DR UV-VIS and Raman spectroscopy. It was shown that dispersion of molybdenum depends on Mo loading and kind of support

used. Whereas for low loadings, isolated monomeric molybdenum species were prevailing, with higher Mo content the concentration of surface polymolybdates increased and finally for the highest loaded catalysts 2.5 - 5 nm crystallites of MoO_3 appeared on the external surface of the support. The differences in the dispersion of Mo are probably connected with different number of surface OH groups of individual supports, as determined by FTIR spectroscopy. No leaching of molybdenum species was observed during the reaction and the concentration of Mo in the products was lower than 0.005 ppm. When the spent catalyst was washed with hexane and reactivated at 500 °C for 0.5 h under the stream of dry air, the same activity and selectivity was achieved as with fresh catalyst.

In metathesis of unsaturated ethers and esters, the activity of the catalysts was much lower even with the aid of tetramethyltin as cocatalalyst (e.g. 33 % conversion of 4-allylanisole after 360 min of the reaction over MoO_3/MCM-41 catalyst with 8 wt. % Mo at 40 °C; toluene was used as a solvent, the initial substrate-to-catalyst molar ratio was 24 and the tin-to-molybdenum molar ratio was 0.9).

Good results were achieved in polymerization of aliphatic 1-alkynes. In the case of 1-hexyne, 64 % yield of the polymer (M_w = 30 000, M_w/M_n = 2.3) together with 22 % yield of higher oligomers (M_w = 2 700) and cyclotrimers was achieved after 180 min of the reaction over MoO_3/MCM-41 with 6 wt. % Mo at 40 °C. On the other hand, with *tert*-butylacetylene, 2-hexyne, and phenylacetylene, only low yields of corresponding polymers were obtained under the same conditions (11, 1, and 1 %, respectively). For catalysts with 6 wt. % Mo, poly(1-hexyne) yield after 180 min of the reaction increased in the order MoO_3/SiO_2 < MoO_3/MCM-48 < MoO_3/MCM-41 < MoO_3/SBA-15 (4, 22, 38, and 64 %, respectively) together with M_w of the polymers (6 800, 8 800, 23 000, and 30 000, respectively). It was shown that 1-octene acted as a chain transfer agent, which supported the assumption that the polymerization of 1-hexyne over MoO_3/MCM-41 catalyst proceeds via metal carbene mechanism. In comparison with corresponding MoO_3 based catalysts, Schrock carbene complex Mo(=CHCMe$_2$Ph)(=N-2,6-*i*-Pr$_2$C$_6$H$_3$)[OCMe(CF$_3$)$_2$]$_2$ anchored on MCM-41 and SBA-15 (loading 1 wt. % Mo) exhibited slightly lower polymer yields (34 and 59 %, respectively) and significantly lower molecular weights of poly(1-hexyne)s (M_w 7 500 and 4 900, respectively).

Keywords: alkene metathesis, alkyne polymerization, molybdenum heterogeneous catalysts, mesoporous molecular sieves, MCM-41, MCM-48, SBA-15, polyacetylenes.

Souhrn

Hlavní důraz je v disertační práci kladen na vývoj nového typu heterogenních katalyzátorů pro metathese alkenů, založených na oxidu molybdenovém naneseném na křemičitanových mesoporésních molekulových sítech MCM-41, MCM-48 a SBA-15. Cílem bylo zvýšit aktivitu katalyzátorů na bázi oxidu molybdenového v této reakci díky využití vysokého specifického povrchu a úzké distribuce velikosti pórů nosiče. Pro přípravu katalyzátorů byla použita metoda „thermal spreading“, která je šetrná k životnímu prostředí.

Připravené nosiče a katalyzátory byly charakterizovány pomocí difrakce rentgenových paprsků a adsorpce dusíku. Bylo ukázáno, že oxid molybdenový se disperguje na povrchu mesoporésních křemičitanů. Kolaps struktury nosiče nebyl během přípravy katalyzátorů pozorován ani při nejvyšším zatížení (16 hmotnostních % Mo).

Metathese 1-oktenu byla studována v kapalné fázi za použití míchaného vsádkového reaktoru. Katalyzátor byl aktivován v proudu suchého vzduchu při teplotě 500 °C, zatímco katalytická reakce probíhala pod argonovou atmosférou. Metathese 1-oktenu byla vedena za laboratorní nebo mírně zvýšené teploty bez přítomnosti rozpouštědla. Při teplotě 40 °C byla za pomoci nejaktivnějšího katalyzátoru MoO_3/MCM-41 se 6 hm. % Mo za 360 minut dosažena konverze 1-oktenu 75 % při selektivitě na 7-tetradecen 84 %. Počáteční aktivita katalyzátoru MoO_3/MCM-41 (6 hm. % Mo) při 40 °C byla 0.014 s^{-1}, tedy více než čtyřikrát vyšší ve srovnání s konvenčním katalyzátorem MoO_3/SiO_2 se stejným obsahem Mo pracujícím za stejných reakčních podmínek. Mezi katalyzátory připravenými z různých sloučenin molybdenu různými procedurami vykázal katalyzátor připravený z MoO_3 metodou „thermal spreading“ nejvyšší aktivitu spolu s vysokou selektivitou. Konverze dosažená po 360 minutách reakce při 40 °C s katalyzátory založenými na oxidu molybdenovém s obsahem 8 hm. % Mo klesala v pořadí MoO_3/MCM-41 > MoO_3/MCM-48 > MoO_3/SBA-15 > MoO_3/SiO_2 (70, 32, 18 a 8 %), zatímco selektivita mírně vzrůstala (od 82 do 95 %). Katalyzátory s nižším obsahem Mo (od 4 do 8 hm. % Mo) vykázaly vyšší aktivitu než katalyzátory s nejvyšším obsahem Mo (16 hm. % Mo). Rozdíly v katalytické aktivitě byly korelovány se strukturou katalyzátorů před reakcí pomocí technik XRD, XPS, DR UV-VIS a Ramanovy spektroskopie. Bylo ukázáno že disperse Mo závisí na obsahu

molybdenu a na druhu použitého nosiče. Zatímco pro nízký obsah molybdenu převládají isolovaná Mo species, při vyšším obsahu molybdenu vzrůstá koncentrace povrchových polymolybdátů a nakonec u katalyzátorů s nejvyšším obsahem Mo se na externím povrchu objevují krystalky MoO_3 o rozměru 2.5 až 5 nm. Pomocí FTIR spektroskopie bylo ukázáno, že rozdíly v dispersitě Mo jsou pravděpodobně způsobeny rozdílným počtem povrchových OH skupin různých nosičů. Nebylo pozorováno vymývání Mo během reakce a koncentrace molybdenu v produktech byla nižší než 0.005 ppm. Pokud byl katalyzátor po reakci promyt hexanem a reaktivován při teplotě 500 °C po dobu 30 min v proudu suchého vzduchu, bylo dosaženo stejné aktivity a selektivity jako v případě původního katalyzátoru.

V metathesi nenasycených etherů a esterů byla aktivita katalyzátorů mnohem nižší i při použití tetrametylcínu jako kokatalyzátoru (např. konverze allylanisolu po 360 minutách reakce za použití katalyzátoru MoO_3/MCM-41 s osmi hm. % Mo byla jen 33 %; jako rozpouštědlo byl použit toluen, počáteční molární poměr katalyzátor:substrát byl 24 a molární poměr Sn:Mo byl 0.9).

Dobrých výsledků bylo dosaženo v polymerizaci alifatických 1-alkinů. V případě 1-hexinu byl po 180 minutách reakce s katalyzátorem MoO_3/MCM-41 (6 hm. % Mo) při 40 °C získán výtěžek polymeru 64 % (M_w = 30 000, M_w/M_n = 2.3) a vyšších oligomerů (M_w = 2 700) a cyclotrimerů 22 %. Na druhou stranu, v případě *tert*-butylacetylenu, 2-hexinu a fenylacetylenu bylo dosaženo pouze nízkých výtěžků příslušných polymerů (11, 1 a 1 %). Pro katalyzátory se šesti hm. % Mo stoupal výtěžek polymeru po 180 minutách reakce v pořadí MoO_3/SiO_2 < MoO_3/MCM-48 < MoO_3/MCM-41 < MoO_3/SBA-15 (4, 22, 38, a 64 %) stejně jako jeho molekulová hmotnost M_w (6 800, 8 800, 23 000, a 30 000). Bylo ukázáno, že 1-okten působí jako přenašeč, což podporuje hypotézu že polymerizace 1-hexinu na katalyzátoru MoO_3/MCM-41 probíhá metalokarbenovým mechanismem. Ve srovnání s odpovídajícími katalyzátory založenými na oxidu molybdenovém, Schrockův karbenový komplex Mo(=CHCMe$_2$Ph)(=N-2,6-*i*-Pr$_2$C$_6$H$_3$)[OCMe(CF$_3$)$_2$]$_2$ zakotvený na MCM-41 a SBA-15 (1 hm. % Mo) vykázal v polymeraci 1-hexinu mírně nižší výtěžky (34 a 59 %) a podstatně nižší molekulové hmotnosti polymeru (M_w 7 500 a 4 900).

Klíčová slova: metathese alkenů, polymerizace alkinů, molybdenové heterogenní katalyzátory, mesoporésní molekulová síta, MCM-41, MCM-48, SBA-15, polyacetyleny.

CONTENT

1 INTRODUCTION

Alkene metathesis opens new industrial routes to important petrochemicals, polymers and specialty chemicals. The discovery of the functional-group tolerant ruthenium-based catalysts resistant to moisture and oxygen by Grubbs et al. denotes recently a booming research in the area. However, these catalysts based on homogeneous systems lack the typical advantages of heterogeneous catalysts as easy recovery and separation. Furthermore, the high price prevents their widespread utilizing. Therefore, heterogeneous catalysts based on tungsten, molybdenum and rhenium oxides supported on silica or alumina remain the most important systems for industrial large-scale applications. Tungsten and molybdenum oxide catalysts require higher reaction temperatures (100 – 400 °C), at which side reactions decreasing metathesis selectivity occur. Only expensive rhenium oxide catalysts exhibit a high activity and selectivity at temperatures below 100 °C.

In 1992, the synthesis of MCM-41, the first member of a new family of mesoporous molecular sieves, opened a new area in the preparation of heterogeneous catalysts. A silicate structure with tunable pore size, high surface area and narrow pore size distribution makes the mesoporous molecular sieves ideal for catalysts supporting.

Combining the excellent properties of mesoporous support with low-cost molybdenum oxide active phase, new type of catalysts for metathesis of alkenes may be designed. Taking the advantages of heterogeneous catalyst, easy separation of the reaction products together with simple recovery of the catalyst could be maintained. Moreover, by replacing the conventional silica as a support by mesoporous molecular sieves, their high surface area can be utilized to obtain highly dispersed molybdenum species, which would allow achieving high activity of the catalysts under mild reaction conditions. Finally, low acidity of siliceous support promises an increased selectivity of these new catalysts.

2 AIMS OF THE THESIS

The objectives of this PhD thesis can be summarized as follows:

1. To design new type of catalysts for metathesis of alkenes based on molybdenum oxide and siliceous mesoporous molecular sieves.

2. To determine the properties of new catalysts using physicochemical methods.

3. To propose optimum activation conditions, molybdenum oxide loading and reaction temperature in metathesis of linear alkenes.

4. To find differences in activity and selectivity related to the type of mesoporous silica and to compare new catalysts with conventional MoO_3/SiO_2 catalyst.

5. To compare the new catalysts prepared by thermal spreading of MoO_3 with catalysts prepared using different methods and different types of molybdenum compounds.

6. To examine the process of catalysts deactivation and to suggest the method for the reactivation of the catalyst.

7. To verify the activity of new catalysts in metathesis of unsaturated ethers and esters.

8. To validate the activity of new catalysts in metathesis of alkynes.

9. To characterize the catalysts by spectroscopic methods and to find differences among individual types of catalysts.

10. To estimate relationships between the structure and activity of the catalysts.

3 THEORETICAL PART

3.1 Alkene metathesis

Alkene metathesis is one of the very few fundamentally novel organic reaction discovered in the last 50 years. The word *metathesis* comes from Greek *meta* (change) and *tithemi* (place). In organic chemistry, it describes the exchange of alkylidene fragments around the carbon-carbon (C=C) double bond. In the presence of transition metal compounds (mainly that based on W, Mo, Re, Ru), two C=C double bonds react with an active site to form two new C=C double bonds, exchanging substituents attached to the carbon atoms during the reaction (Fig. 3.1a) [1].

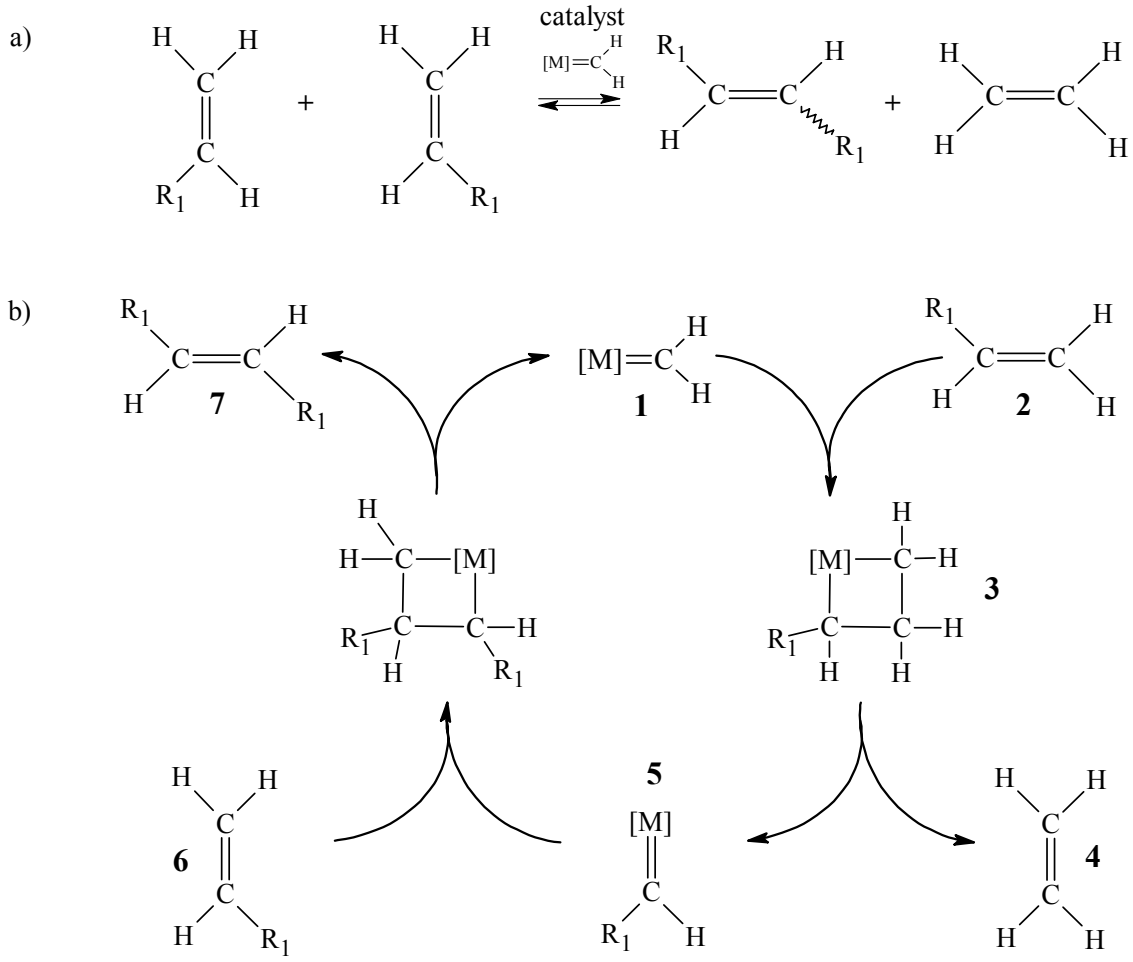

Figure 3.1

Alkene metathesis: a) overall reaction and b) reaction mechanism as exemplified by metathesis of terminal alkene (R = alkyl). The wavy bond shows that the R^1 groups can be located on the same side of the double bond or on different sides [2].

The generally accepted mechanism of alkene metathesis was originally proposed by Hérisson and Chauvin in 1971 [3] and involves a reaction between transition metal alkylidene complex **1** and alkene **2** to form metallacyclobutane intermediate **3** (Fig. 3.1 b). This metallacycle is unstable and cleaves in the opposite manner to form new alkylidene **5** and new alkene **4**. Finally, this new alkylidene is regenerated by the reaction with alkene **6** to provide second alkene **7** and original alkylidene complex **1**.

When two different alkenes react with each other, we speak about cross-metathesis. On the other hand, if two molecules of the same alkene undergo metathesis with each other, the reaction is called self-metathesis (or just metathesis). In this case, two types of metathesis reaction proceed:

(i) productive metathesis, and

(ii) non-productive (degenerate) metathesis [4].

In the first case, the metallacyclobutane intermediate is formed in such way that after its decomposition two new products are formed. On the other hand, in the latter case, the substrate molecules are arranged into the intermediate in such manner that the reaction products are the same as starting molecules. Non-productive metathesis is generally much faster than productive metathesis [1]. Productive and non-productive metathesis can be recognized by using isotope labeled alkenes (Fig. 3.2).

a) $CH_2{=}CH{-}CH_3 + CD_2{=}CD{-}CD_3 \rightarrow CH_2{=}CD_2 + CD_3{-}CD{=}CH{-}CH_3$

b) $CH_2{=}CH{-}CH_3 + CD_2{=}CD{-}CD_3 \rightarrow CD_2{=}CH{-}CH_3 + CH_2{=}CD{-}CD_3$

Figure 3.2
Alkene metathesis: a) productive and b) non-productive metathesis can be distinguished by metathesis of labeled and unlabeled propene.

In principle, alkene metathesis is a reversible thermoneutral reaction, with statistical distribution of reactant and product molecules. Thus, the equilibrium can be easily shifted either by the excess of the substrate or by removing of the product. The latter is the case of 1-alkene metathesis. One of the reaction products, ethene, is spontaneously releasing from the reaction mixture, which allows achieving conversions

higher than 50 %. On the other hand, internal alkenes can be converted to 1-alkenes using a high pressure of ethene.

Alkene metathesis is closely connected with two another types of reactions with similar mechanisms: ring opening metathesis polymerization and ring closing metathesis (Fig. 3.3).

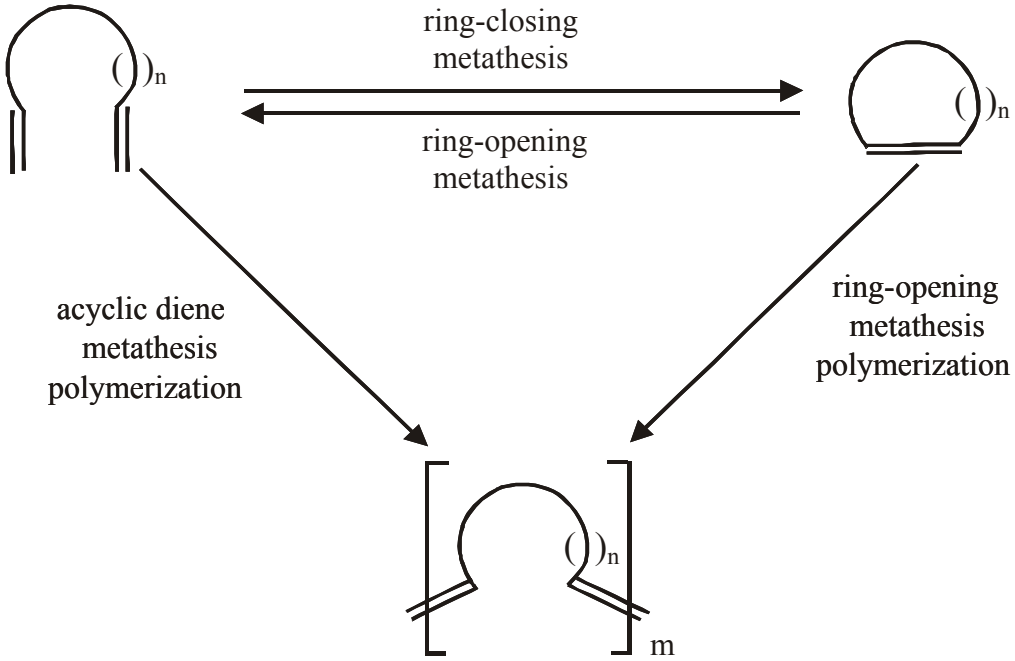

Figure 3.3

Ring-opening metathesis polymerization, ring-closing metathesis and related reactions [5].

Metathesis of alkenes is symmetrically forbidden reaction and therefore proceeds only in the presence of transition metal compounds that possess proper electronic structure, which enables the formation of metallacyclobutane intermediate. The most successful metal compounds are based on tungsten, molybdenum, rhenium and ruthenium. Both homogeneous and heterogeneous catalysts can be employed.

3.1.1 Homogeneous catalysts

Classical homogeneous catalysts are based on chlorides of molybdenum, tungsten or another transition metal. They need a cocatalyst (an alkylating agent with Lewis acid properties, e.g. $EtAlCl_2$), making possible the in-situ generation of carbene, which is the catalytically active species. These "ill-defined" systems were recently replaced by "well-defined" catalysts based on Ru (Grubbs catalysts) and Mo (Schrock catalysts)

alkylidene complexes (Fig. 3.5), which contain stable metallocarbene active site directly in their structure [6,7].

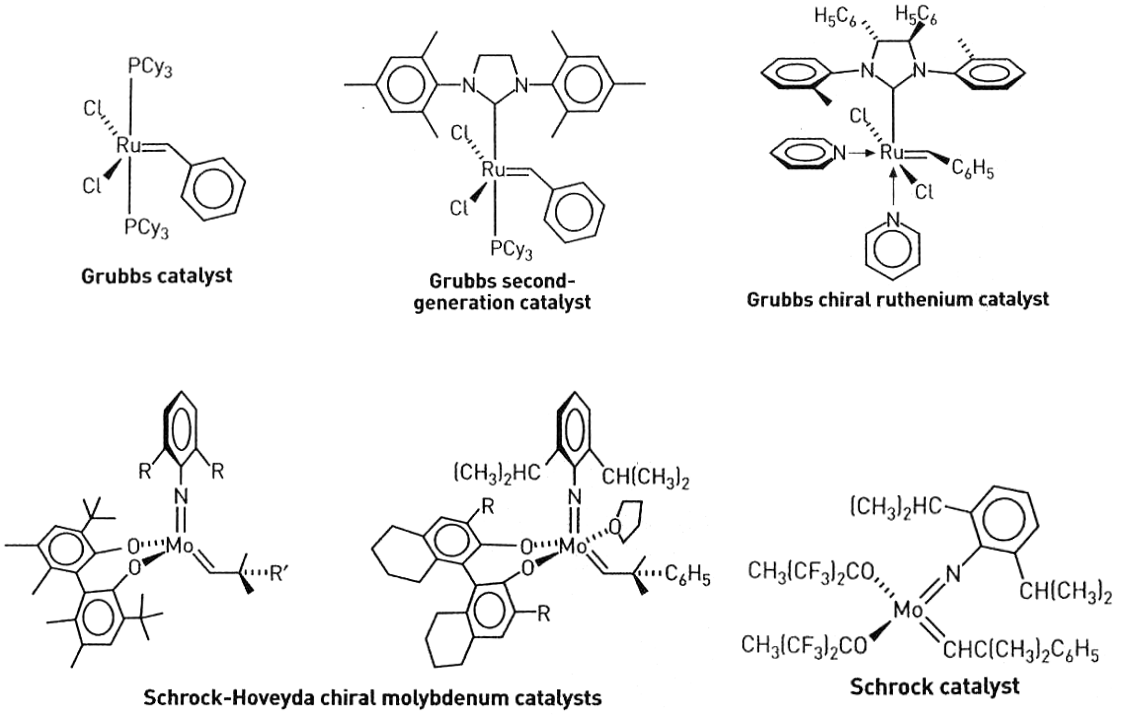

Figure 3.5
Modern homogeneous metathesis catalysts [8].

Both Grubbs and Schrock catalysts are very efficient systems for alkene metathesis and metathesis polymerization. They work at low reaction temperatures (25 – 80 °C), provide good selectivities, and are compatible with a variety of functional groups in comparison with ill-defined catalyst. The choice of the catalyst depends on the nature of the substrate; however, only Grubbs Ru catalysts are resistant to moisture and oxygen and show significant tolerance to functional groups (such as esters, amides, ketones, and even alcohols, water and acids). The main drawbacks of the well-defined catalysts are the bimolecular decomposition to their dimers via intermolecular halide exchange reaction [9] and the necessity to use complex process to separate the products from the catalyst. This can lead to metal contamination of the products and also hinders the recycling or the regeneration of the catalyst [10].

With the development of these novel catalysts, new applications of alkene metathesis in organic synthesis (preparation of raw materials, agrochemicals, fragrances, and pharmaceuticals via cross-metathesis) and in the preparation of highly

functionalized and regular polymers via ring opening metathesis polymerization have been made possible [11,12].

Generally, Grubbs catalysts have been successfully employed in ring-opening metathesis polymerization, ring-closing metathesis reactions to produce disubstituted alkenes, ethenolysis (cross-metathesis with ethene, i.e., cleavage of C=C double bond), cross-metathesis of terminal alkenes, and the preparation of 1,3-dienes via enyne metathesis [13]. For example, Boehringer Ingelheim recently reported the use of alkene metathesis over Grubbs catalyst for the commercial preparation of macrocyclic hepatitis C therapeutics [5]. Ethenolysis of feedstocks derived from bio-renewable seed oils (such as methyl oleate) is employed to produce useful commercial raw materials (1-decene and methyl 9-decenoate in the case of methyl oleate) with Grubbs first generation catalyst [14]. Dicyclopentadiene is polymerized with ruthenium-catalyzed ring-opening metathesis polymerization and the polymer is utilized in wide variety of products such as ballistic panels or large equipment body parts. The ruthenium system can be also employed in living polymerization of norbornene derivatives, controlling both molecular weight and the functionality of the polymer (by sequential adding of monomers with different functional groups) [11]. The ability of the second-generation Grubbs catalysts to couple alkenes with α,β-unsaturated carbonyls has been utilized to prepare A,B-alternating copolymers by ring-opening insertion metathesis polymerization. The product of the cross metathesis of 1-hexene with hexenylacetate over Grubbs catalyst can be readily converted into a pheromone of the peach twig borer moth, which can be used for environmentally friendly insect control instead of the use of broad-spectrum pesticides [11].

Moreover, Schrock catalysts were employed in alkyne metathesis and alkyne polymerization as well, making also possible stereoselective syntheses as that one of civetone, important perfume ingredient. Wide variety of asymmetric reactions was developed, e.g. ring-opening/ring-closing metathesis or ring-opening/cross metathesis to yield various products as drugs or enzymes [12].

Robert H. Grubbs and Richard R. Schrock together with Yves Chauvin were awarded the Nobel Prize for Chemistry in 2005 for “the development of the metathesis method in organic synthesis”.

Recently, some attempts have been made to immobilize Schrock and Grubbs catalysts on polymeric (based on polystyrene or polynorbornene) and inorganic supports (e.g. mesoporous silica MCM-41) [15]. Although the catalyst was leaching resistant and

exhibited metathesis activity close to that achieved with parent complex, the problems with reusability and short lifetime due to the decomposition of the catalyst still have to be solved.

For large-scale industrial applications, heterogeneous catalysts remain the preferable choice because of low cost, high stability, easy catalyst regeneration and the possibility of easier separation of a catalyst from the reaction mixture.

3.1.2 Heterogeneous catalysts

Typical heterogeneous catalysts are oxides (less often carbonyls or halides) of W, Mo and Re supported on silica, alumina or silica-alumina. They can operate as such but often require addition of cocatalyst (R_4Sn, R_4Pb, R_4Zn, R_nAlCl_{3-n}, where R = H, methyl, ethyl, butyl, phenyl; n = 1, 2, 3) and sometimes also promoter (CoO, ethanol, phenol). In the case of heterogeneous catalysts, the metallocarbene active site is formed upon the contact of the catalyst with the cocatalyst, if present, or by interaction of the substrate alkene with the transition metal centre [16]. There are two the most accepted routes to the first metal carbene (Fig. 3.6): in both of them, at first a π-complex (**3** or **5**) between the reacting alkene **1** and the transition metal **2** is formed. After that, the π-complex transforms either via a 1,2-hydrogen shift mechanism (Fig. 3.6a) or via a hydride transfer (Fig. 3.6b) to form the metal carbene **4** or **7**, respectively [17].

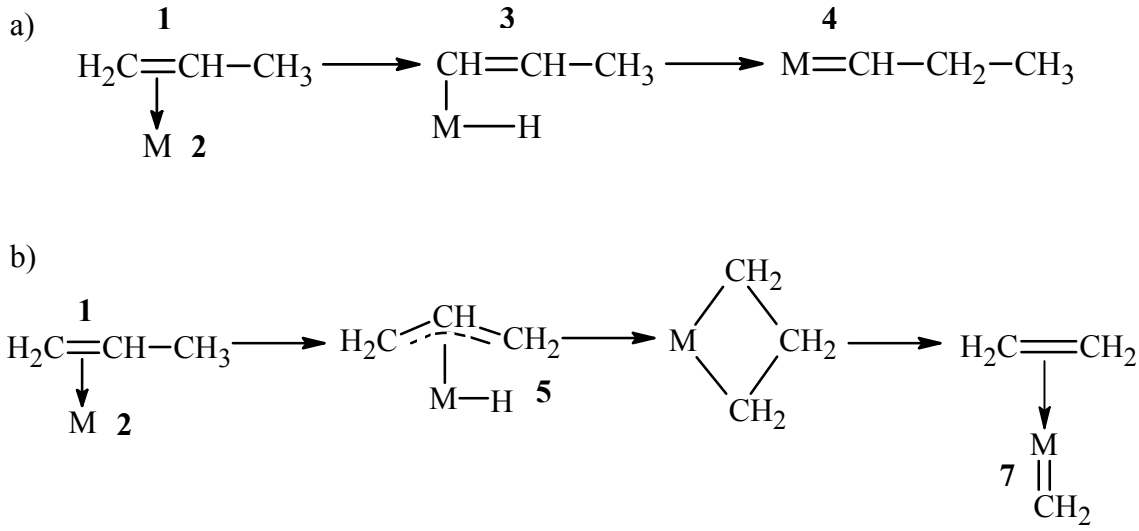

Figure 3.6

Proposed mechanisms of metal carbene formation: a) via 1,2-hydrogen shift mechanism, and b) via hydride transfer as exemplified by propene metathesis [17].

Supported MoO_3 catalysts

Supported molybdenum oxides have received much attention because they are widely used in industrial petrochemical processes incorporating alkene metathesis, such as Shell Higher Olefin Process [18]. In these applications, tungsten oxide on silica typically operates at temperatures ranging from 300 to 500 °C, whereas molybdenum oxide catalysts are usually active at temperatures from 100 to 200 °C [1]. Although rhenium oxide catalysts are active even at lower temperatures (from 20 to 100 °C), much higher price of Re in comparison with Mo represents serious disadvantage [18,19]. Therefore, molybdenum oxide catalysts are a subject of primary interest.

The structure of the MoO_3/SiO_2, MoO_3/Al_2O_3 and MoO_3/SiO_2-Al_2O_3 catalysts has been extensively studied by numerous characterization techniques, including diffuse reflectance spectroscopy in the ultraviolet-visible range (DR UV-VIS), Fourier transform infrared spectroscopy (FTIR), laser Raman spectroscopy (LRS), X-ray diffraction (XRD), magic-angle spinning nuclear magnetic resonance (MAS NMR), temperature-programmed reduction (TPR), X-ray photoelectron spectroscopy (XPS) and electron spin resonance (ESR) [1].

The catalytic activity was found to depend on:

(i) molybdenum loading,

(ii) reaction temperature,

(iii) type of the substrate,

(iv) properties of the support,

(v) catalyst preparation,

(vi) activation conditions, and

(vii) rate of deactivation.

The choice of proper Mo content, type of the support, and method of catalyst preparation and activation influence the oxidation state of Mo atoms and dispersion of molybdenum over the support. Good dispersion of Mo species and its optimum oxidation state are critical requirements to achieve highly active catalysts [1,20].

With increasing molybdenum loading the catalytic activity is increasing, reaching maximum for the Mo content approximately corresponding to the monolayer formation [1]. The critical dispersion capacity (i.e. the formation of the monolayer) of

molybdenum oxide was estimated by XPS, LRS and FTIR techniques to be about 0.8 - 1.0 Mo/nm^2 [21,22]. Below this Mo content, well-dispersed molybdenum oxide phase, which is supposed to give rise to the most active catalytic centers, was found. At higher loadings, the properties of Mo species approach the properties of bulk MoO_3 phase, which is catalytically practically inactive, and the specific catalytic activity is decreasing. In addition, generally only very small part of molybdenum present in the catalyst is transformed into catalytically active sites. According to chemisorption experiments with light alkenes, this fraction was estimated to be less than 1 % [23].

The reaction rate of alkene metathesis over supported molybdenum oxide catalysts is increasing with increasing reaction temperature. For example, the γ-Al_2O_3 supported catalyst prepared by impregnation from $MoO_2(acac)_2$ benzene solution exhibited at 100 °C about 2.8-times higher activity in propene metathesis than at 25 °C [24]. The temperature of maximum catalytic activity depends on the type of the catalyst (e.g., above-mentioned $MoO_2(acac)_2/Al_2O_3$ catalyst was the most active at 150 °C). The decrease in the catalytic activity after passing the maximum was ascribed to reversible deactivation of active sites [1].

Nevertheless, not only main metathesis reaction (Fig. 3.7a) proceeds in the reaction mixture. Typically, also double-bond shift isomerization of starting alkene followed by subsequent cross-metathesis with the substrate molecule takes place (Fig. 3.7b). In addition, dimerization and/or oligomerization of alkenes can proceed as well. All these side reactions are catalyzed by Brønsted acid sites and/or metallohydride centers on the surface of the catalyst [25].

a) $2\ CH_3(CH_2)_5CH{=}CH_2 \leftrightarrows CH_3(CH_2)_5CH{=}CH(CH_2)_5CH_3 + CH_2{=}CH_2$

b) $CH_3(CH_2)_5CH{=}CH_2 + CH_3(CH_2)_mCH{=}CH(CH_2)_{4-m}CH_3 \leftrightarrows$

$\leftrightarrows CH_3(CH_2)_5CH{=}CH(CH_2)_{4-m}CH_3 + CH_3(CH_2)_5CH{=}CH(CH_2)_mCH_3 +$

$+ CH_2{=}CH(CH_2)_{4-m}CH_3 + CH_2{=}CH(CH_2)_mCH_3$

Figure 3.7

Metathesis of 1-octene: a) the main metathesis reaction (self-metathesis of 1-octene) and b) cross-metathesis of 1-octene with its isomers (m = 0, 1, 2).

The reaction rate of side reactions is increasing with increasing temperature. Therefore, a lower selectivity to main metathesis product (7-tetradecene in the case of metathesis of 1-octene) is observed at elevated temperatures [17].

In most cases, supported molybdenum oxide catalysts are more active in metathesis of alkenes than in metathesis of unsaturated carboxylic esters, ethers etc. Water and oxygen are catalytic poisons for heterogeneous metathesis catalysts, because they can react with metallocarbene active sites, causing thus their destruction or deactivation [26]. Therefore, when oxygen-containing unsaturated substrates have to undergo the metathesis reaction, the activity of heterogeneous catalyst is often improved by the addition of cocatalyst (e.g. SnR_4, R = methyl, ethyl, butyl). The alkyl group from the cocatalyst reacts with molybdenum atom to form the metallocarbene active site.

Generally, silica, silica-alumina or alumina have been used as supports for the preparation of molybdenum catalysts as well as in their industrial applications [1,18,27]. Catalytic properties of heterogeneous molybdenum catalysts strongly depend on the type of the support. The following order is observed for the rate of propene metathesis: silica-alumina > alumina > silica, i.e. the order of decreasing Brønsted acidity of the support [28]. However, a high acidity of silica-alumina and alumina causes that double-bond shift isomerization of the substrate is running on Brønsted acid sites of the support (Lewis acid sites are too weak to catalyze this reaction). The following cross-metathesis of the isomers with substrate molecules results in lower selectivity to main metathesis product. For example, the first catalyst employed in metathesis of 1-octene ($CoO/MoO_3/Al_2O_3$) operated at 163 °C exhibited more than 70 % conversion, but only 3 % selectivity to 7-tetradecene [29]. Nevertheless, the selectivity can be improved by introducing the alkali metal ions to the catalyst surface, poisoning thus the acid sites [30].

The discoveries of mesoporous silica [31] and organized mesoporous alumina (OMA) [32] allow to design new types of the catalysts [33,34]. However, only one example of the utilization of mesoporous support in the preparation of molybdenum metathesis catalyst was reported so far [35]; these catalysts were prepared by the impregnation of HMS-type silicas with ammonium heptamolybdate solution. In this work, the application of MCM-41, MCM-48 and SBA-15 based MoO_3 catalysts in metathesis is reported for the first time.

Many experimental findings indicate that the structure of supported molybdenum catalysts - and thus their catalytic activity - is strongly influenced by the preparation method [36]. They can be prepared in the following ways:

(i) by impregnation of the support with molybdate solution,

(ii) by impregnation of the support with the solution of organomolybdenum compound and its subsequent decomposition,

(iii) by treatment of the support with $MoCl_5$ or $Mo(CO)_6$, and

(iv) by thermal spreading of molybdenum compound over the support surface.

Catalysts prepared from organometallic complexes as $(\pi\text{-}C_3H_5)_4Mo$ and $MoO_2(acac)_2$ exhibited high activity in metathesis of alkenes (even at ambient temperature) thanks to good dispersion of Mo species over the support and/or the presence of Mo in optimum oxidation state [37,38]. The activities of the catalysts obtained by anchoring Mo precursors are usually higher than those prepared by traditional impregnation [20]. It was reported for Al_2O_3 supported systems that the catalyst prepared using $MoO_2(acac)_2$ exhibited better molybdenum dispersion and significantly higher activity in metathesis compared to the catalyst prepared by impregnation of the support with ammonium heptamolybdate solution [20]. In addition, it is known also for MoO_3/SiO_2 catalysts that by applying organometallic precursors one can prevent formation of molybdenum crystalline phases [39,40].

Nevertheless, for industrial applications the cost of the organomolybdenum complexes is too high. Therefore, the most common method for the preparation of supported molybdenum oxide catalysts is the impregnation of the support with water solution of ammonium heptamolybdate [27]. In large-scale technologies, however, the necessary treatment of wastewater after the preparation of the catalyst is serious disadvantage. Moreover, the impregnation of MCM-41 was reported to cause the destruction of mesoporous structure [41].

Recently, thermal spreading method has been successfully used for the preparation of various types of supported molybdenum-based catalysts [36,42,43]. In this case, support and Mo compound are mixed together in the solid state and then

calcined at temperatures above 500 °C. This method represents easy, low-cost and environmentally friendly possibility for the preparation of molybdenum-based catalysts.

During the preparation of the catalysts, which always includes calcination at high temperature (~ 500 °C), the chemical reaction between Mo compound and surface OH groups of the support takes place. Molybdenum is dispersed on the support via the Si-O-Mo (Al-O-Mo) bridge bonds formation. Monomeric Mo species that arise on the surface of the catalyst are supposed to be the precursors of the metallocarbene active sites in metathesis reaction (Fig. 3.8) [44].

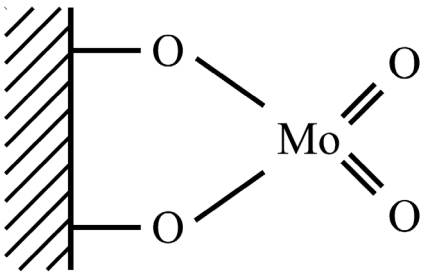

Figure 3.8
Proposed structure of the precursor of the active site for supported MoO_3 catalyst [1,45].

The oxidation state of Mo species that are the precursors of active centers is still a matter of discussion. One of the reasons is that only a small fraction of Mo atoms is active in metathesis reaction. Therefore, the oxidation state of the active sites may be different from the average oxidation state of molybdenum. Generally, neither Mo(II) nor Mo(VI) is active in metathesis; in addition, catalysts that contain a few % of Mo(V) do not exhibit any relationship between catalytic activity and intensity of ESR signal of pentavalent molybdenum [1]. However, the majority of papers [46-48] concluded that the slight reduction of molybdenum(VI) to formal oxidation state between Mo(V) and Mo(VI) is necessary to obtain an active catalyst. This reduction is achieved by proper activation of the catalyst and/or by the reduction of Mo species upon the contact with the substrate [1]. Typically, activation proceeds at high temperature (500 or 550 °C) in a stream of air and/or inert gas (argon, nitrogen) [49].

The deactivation of the catalyst is caused by the decay of metallocarbene active sites; this can proceed in several ways:

(i) by the reaction of metallocarbene with trace impurities in the reaction mixture (water, oxygen, polar compounds),

(ii) by reduction or oxidation of the metal atom to inactive oxidation state,

(iii) by blocking of the active sites with high molecular weight deposits, and

(iv) by reductive elimination of metallacyclobutane intermediate to form cyclopropane or alkene (an intrinsic deactivation mechanism) [50].

The activity of the catalyst can be restored by regeneration in a stream of oxygen (or air) at high temperature (typically 500 - 550 °C) and/or by the addition of cocatalyst [17].

3.1.3 Industrial applications

The first industrial application of alkene metathesis has been operating since 1966 as so-called Phillips Triolefin Process, where propene was converted to high-purity ethene and 2-butene. The reaction was carried out in a fixed-bed reactor with a WO_3/SiO_2 catalyst, doped with sodium to prevent double-bond shift reactions, at a reaction temperature of 350 – 425 °C [17]. Due to a high demand for propene, the reverse process called Olefin conversion technology® is employed at present by Lyondell Petrochemical Co., BASF FINA Petrochemicals and others to convert mixture of ethene and 2-butene into propene [18]. After mixing fresh C_4's and C_4 recycle with ethene feed and recycle ethene the mixed feed is heated. The metathesis reaction takes place in a fixed-bed reactor over a mixture of WO_3/SiO_2 (metathesis catalyst) and MgO (an isomerization catalyst) at more than 260 °C and 3.0 – 3.5 MPa. 1-butene in the feedstock is isomerized to 2-butene as the original 2-butene is consumed in the metathesis reaction. The conversion of butene is above 60 % per pass and the selectivity to propene is higher than 90 %. Metathesis units with this technology are often integrated in naphtha steam crackers in order to increase the production of propene [51,52].

The Institut Français du Pétrole and the Chinese Petroleum Corporation (Kaoshiang, Taiwan) have jointly developed a process for the production of propene via Meta-4 process by metathesis of ethene and 2-butene in the liquid phase. The reaction proceeds at 35 °C and 6 MPa over Re_2O_7/Al_2O_3 catalyst, the conversion is 63 % per pass. However, the process is not yet commercialized, mainly because of the cost of the catalyst and the requirement of a high-purity feed stream [18].

A large-scale industrial process incorporating alkene metathesis is the Shell Higher Olefin Process for the production of detergent-range alkenes from ethene. The process takes place in three stages (Fig. 3.4) [18].

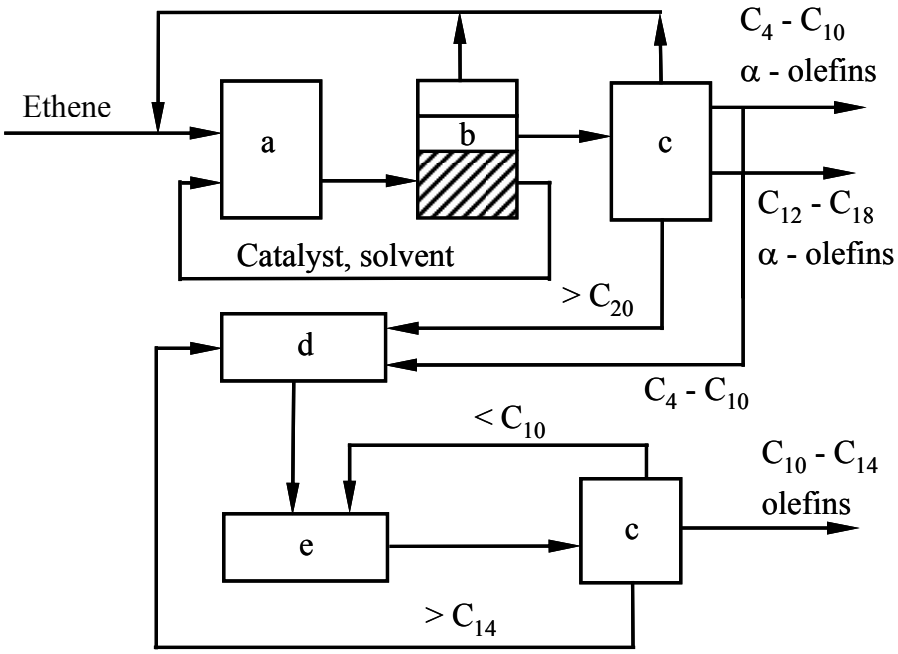

Figure 3.4

The Shell Higher Olefin Process: a) oligomerization reactor, b) phase separator, c) distillation columns, d) isomerization reactor, e) metathesis reactor [53].

In the first step, ethene is oligomerized in the presence of a homogeneous nickel–phosphine catalyst (at 90 – 100 °C and 10 – 11 MPa) in 1,4-butanediol to give a mixture of linear even-numbered 1-alkenes ranging from C_4 to C_{40}. The alkenes formed are immiscible with the solvent so that the catalyst can be easily separated and reused. The C_6–C_{18} 1-alkenes are separated from the product mixture by distillation. This fraction can be further fractionated into individual compounds, which can be used as comonomers in polyethylene production or converted into products such as synthetic lubricants, plasticizer alcohols, detergent alcohols, synthetic fatty acids, etc. The remaining lighter (< C_6) and heavier (> C_{18}) alkenes go to purification beds, which remove catalyst and solvent residues that would otherwise deactivate the isomerization catalyst [18].

In the second step, these lighter and heavier alkenes undergo the double-bond shift isomerization over a solid potassium metal catalyst to give an equilibrium mixture of internal alkenes.

In the third step, this mixture is passed over an alumina-supported molybdate metathesis catalyst and statistical distribution of linear alkenes with both odd and even number is obtained via cross-metathesis reactions. The isomerization and metathesis catalysts work at 100 – 125 °C and 1 MPa. The yield of desired $C_{11} – C_{14}$ linear alkenes is about 10 – 15 wt. % per pass. The individual products are separated by distillation and are further used for the production of detergent alcohols or detergent alkylates. The remaining lower and higher alkenes are recycled [18].

Sasol Ltd. operates heterogeneous catalyst based on molybdenum or tungsten oxide for the conversion of low value alkene feedstocks into useful $C_{11} – C_{15}$ linear internal alkenes. These can be converted to surfactants and detergent alcohols or detergent alkylates [49].

Neohexene process is employed to produce 3,3-dimethyl-1-butene (neohexene) that is an important intermediate in the production of perfumes and anti-fungal agents. Neohexene is obtained via cross-metathesis of 2,4,4-trimethyl-2-pentene and ethene. As the feed, commercial di-isobutene (mixture of 2,4,4-trimethyl-2-pentene and 2,4,4-trimethyl-1-pentene) is used. The latter can be transformed to the former one by isomerization over bifunctional catalyst (mixture of WO_3/SiO_2 and MgO). Conversion of di-isobutene 65 – 70 % and selectivity to neohexene 85 % is achieved at 370 °C and 3 MPa (molar ratio ethene/di-isobutene = 2) [18]. The catalyst is reactivated from time to time, using a mixture of air and inert gas to control the temperature of the coke burn-off. The separation of reactants and products is achieved by stripping and fractionation. The coproduct isobutene is recycled to isobutene dimerization reactor.

The metathesis of functionalized alkenes is an attractive reaction for the conversion of low value feedstocks into specialty chemicals. Metathesis of unsaturated fatty acid esters, the oleochemical raw materials obtained from renewable resources, provides a convenient route to unsaturated diesters, which can be used as intermediates for the production of polymers and agrochemicals, pheromones, fragrances and pharmaceuticals [54]. Both heterogeneous (based on MoO_3 or Re_2O_7) and homogeneous (ruthenium complexes) metathesis catalysts are expected to be employed in new processes in oleochemical industry [55].

3.2 Alkyne metathesis and polymerization

Alkyne metathesis is a reaction closely related to alkene metathesis. There are two groups of metathesis-type alkyne reactions:

(i) true metathesis, in which the triple bond is completely broken and new alkynes are formed (Fig. 3.9a), and

(ii) alkene-type metathesis, in which only two of three bonds are broken; the latter leads to the formation of conjugated polymers (Fig. 3.10) [1].

The first type of reaction is similar to alkene metathesis: it is the exchange of alkylidyne fragments around the carbon-carbon triple bond. Reaction mechanism involves the reaction of metal alkylidyne **1** with an alkyne **2** via metallacyclobutadiene intermediate to give new alkylidene **3** and new alkyne **4** (Fig. 3.9b).

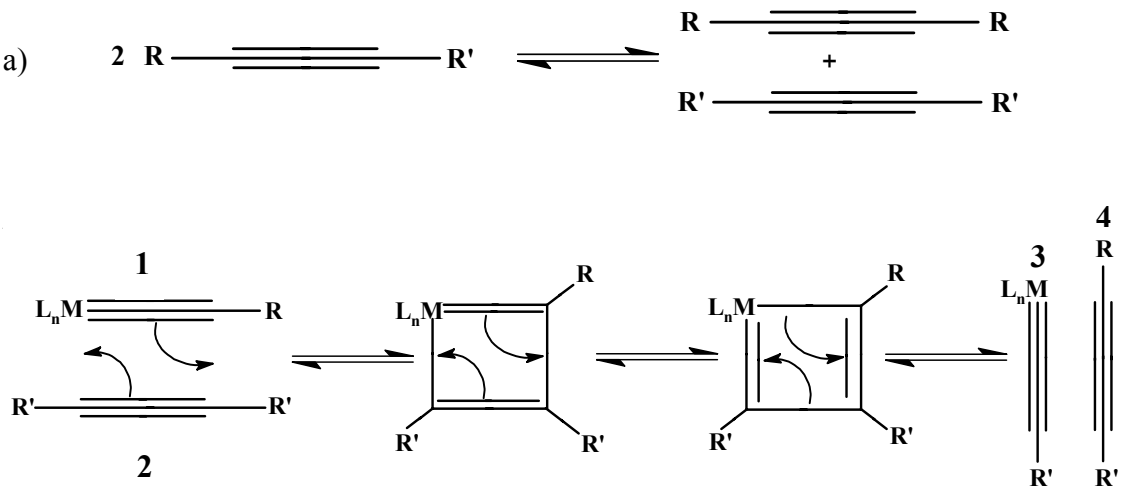

Figure 3.9
Alkyne metathesis: a) overall reaction and b) the reaction mechanism [56].

Alkyne metathesis proceeds via metal carbyne complexes. On the other hand, when an alkyne is contacted with metal carbene complex, polymerization of alkynes may proceed. In this case, metal alkylidene **1** reacts with alkyne **2** via intermediate **3** and oligomer **4** with m = 1 is formed (Fig. 3.10). This oligomer than can then react in the same way with new alkyne, and the repetition of this process provides the conjugated polymer ($m \approx 10^4 \div 10^6$).

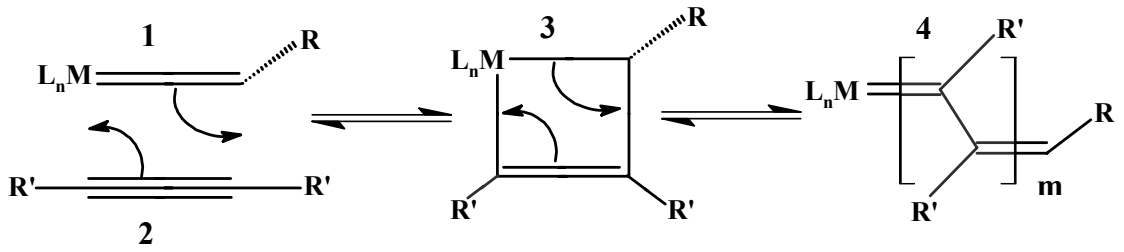

Figure 3.10
Propagation of alkyne polymerization initiated by metal carbene; m = 1 [56].

In the late 1960s, a heterogeneous mixture of tungsten trioxide and silica was found to be able to catalyze alkyne metathesis at a very high temperature (200 – 450 °C) [57]. Few years later, Mortreux reported the first homogeneous catalyst system generated from $Mo(CO)_6$ and resorcinol, which can catalyze the metathesis of p-tolylphenylacetylene at 160 °C [58].

The mechanism of alkyne metathesis was later experimentally established by Schrock using well-defined tungsten(VI) neopentylidyne complex $(Me_3CO)_3W{\equiv}CCMe_3$, which was active in the metathesis of internal alkynes under mild conditions (room temperature to 90 °C) [59].

In 2001, Basset et al. reported a silica-supported rhenium catalyst, which represents the first example of heterogeneous catalyst for alkyne metathesis. It can catalyze the metathesis of 2-pentyne to 3-hexyne at room temperature with equilibrium reached in 20 min [60]. Recently developed catalyst, $EtCMo[NAr(t\text{-}Bu)]_3$ on silica, is also tolerant to alkynes with alkyl, thienyl, benzoate and anisole substituents [61].

Alkyne metathesis is not commonly performed and is not used in industry because acetylene can be easily produced using other methods and the demand for higher alkynes is low. The catalysts, mostly based on molybdenum or tungsten complexes with alkoxide or phenoxide ligands, are used in organic synthesis (synthesis of large cycles via ring-closing alkyne metathesis, and synthesis of analogues of cyclic natural products such as musks and prostaglandins via ring closing metathesis of acyclic dienes) and in the preparation of arylene-ethynylene polymers via ring-opening alkyne metathesis polymerization [62].

In contrast, polymerization of alkynes has been extensively studied in order to develop new polymers with π-conjugated backbone. Great variety of transition-metal-based catalysts has been employed [63], mainly:

(i) Ziegler-Natta catalysts (titanium chlorides combined with alkyl aluminum cocatalyst),

(ii) alkene metathesis catalysts based on molybdenum and tungsten (e.g. $WOCl_4$, $MoCl_5$, $MoOCl_4$) in combination with cocatalysts (e.g. Bu_4Sn, Et_3Al),

(iii) Rh(I) diene complexes (e.g. $[Rh(cod)X]_2$, where cod = η^4-cyclooctadiene, X = halide), and

(iv) Schrock and Grubbs alkylidene complexes.

Organometallic catalysts (iii) and (iv) contain the well-defined active sites for the reaction directly in their structure. Thanks to the uniformity of the active sites, they enable a controlled character of polymerization with respect to the molecular weight ("living polymerization") and to the microstructure characteristics of polymers formed. Conjugated polyalkynes possess large number of potential applications as electrical (semi)conductors, membranes for separation processes, nonlinear optical devices and liquid crystals, etc. Because of these applications, polymers free of catalyst residues are often demanded. Therefore, new heterogeneous catalysts are desirable. Recently, Rh diene complexes supported on MCM-41 exhibited good results in polymerization of phenylacetylene and its derivatives [64].

3.3 Mesoporous molecular sieves

Mesoporous molecular sieves are porous inorganic solids (mainly SiO_2 and Al_2O_3) possessing uniform pores with dimensions ranging from 2 to about 30 nm, long-range ordering and large surface areas (often higher than 1 000 m^2/g). The first synthesis of an ordered mesoporous material was described in the patent literature in 1969 [65]. However, due to a lack of analysis, the remarkable features of this product were not recognized [66]. In 1992, similar materials were prepared by scientist in Mobil Oil Corporation. The new family of mesoporous siliceous materials designated as M41S possesses well-defined pores, whose diameters can be varied in the range of approximately 1.5 – 10 nm. Three members of the M41S family of materials were introduced, namely MCM-41, MCM-48 and MCM-50. MCM-41, which stands for Mobil Composition of Matter No. 41, shows a highly ordered hexagonal array of one-dimensional pores with a very narrow pore size distribution (Fig. 3.11a,b), MCM-48 has

three-dimensional array of intersecting channels with cubic geometry (Fig. 3.11c), and MCM-50 exhibits lamellar structure [31,67]. These first mesoporous silicas were prepared using sodium silicate as a silicon source and quaternary ammonium ions as structure-directing agents (templates). After the synthesis (144 h at 100 °C under static conditions), the template was removed by calcination under nitrogen and air flow at 540 °C [67], which provided open structure with accessible mesopores.

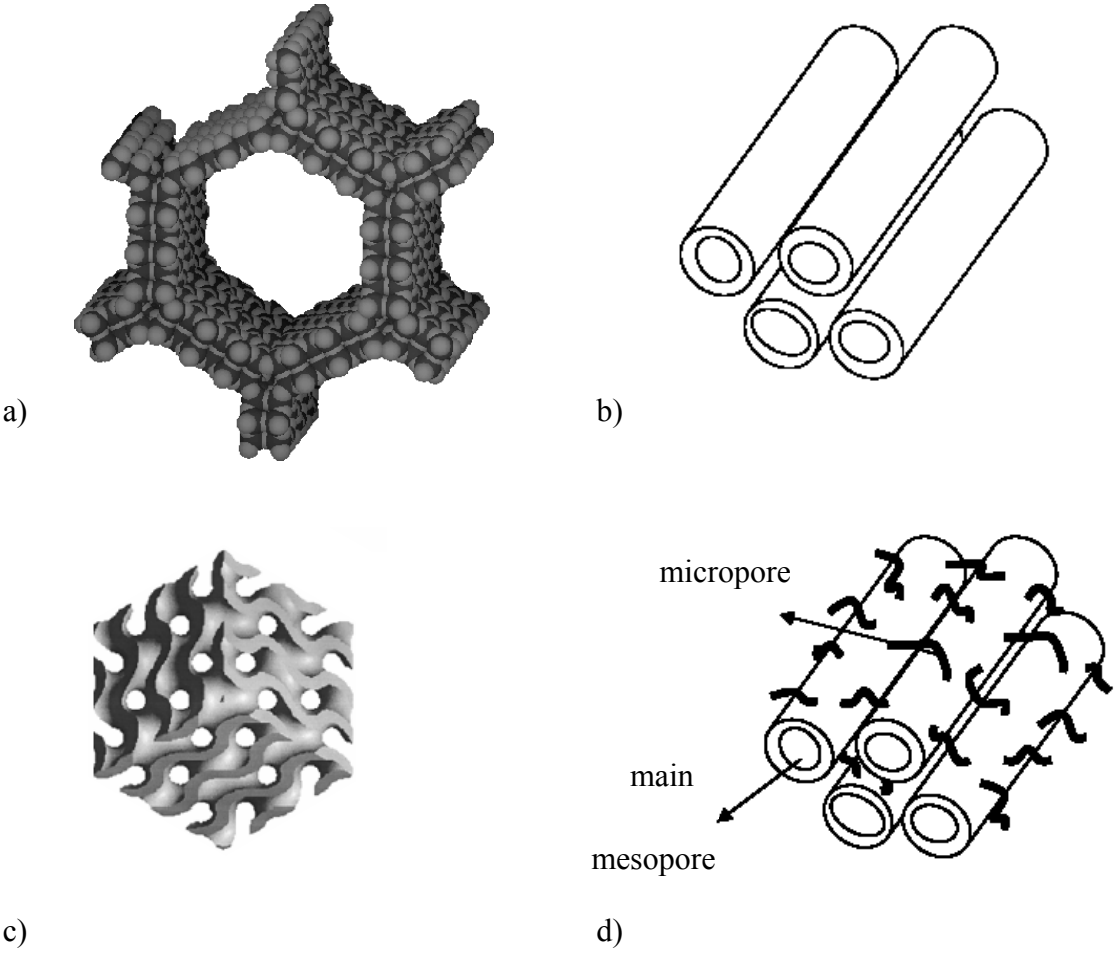

Figure 3.11

Models of mesoporous materials: a) the hexagonal pore of MCM-41 [68], b) the cylinders representing the pore structure of MCM-41 [69], c) three dimensional structure of cubic MCM-48 [70], d) SBA-15 (the dark curves represent the micropores within the pore walls) [69].

Since these early discoveries, a large research effort has been invested in the synthesis and characterization of a variety of different mesoporous materials.

Mesoporous molecular sieves are prepared using self-assembled ordered aggregates of surfactants as templates (Fig. 3.12). Accordingly, mesoporous solids occur in lamellar, hexagonal and cubic forms, just as the surfactant aggregates [71].

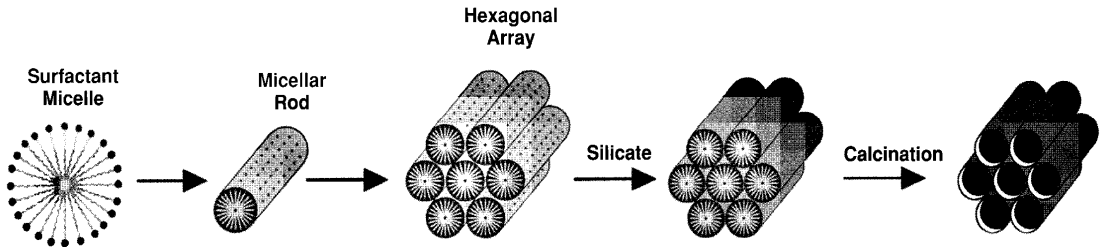

Figure 3.12

Scheme of the synthesis of mesoporous molecular sieves using surfactant micelles as a structure-directing agents (templates) [67].

The structure of resulting mesoporous sieve is influenced by the surfactant-to-silica ratio, temperature, ageing, pH of the medium, presence of counter ions, etc. [72]. The formation of the inorganic-organic assemblies is based on electrostatic interactions between the positively charged surfactants and the negatively charged silicate species in water solution. Silica precursors surround the positively charged surface of micelles, which results in the condensation of silica (Fig. 3.13) [34].

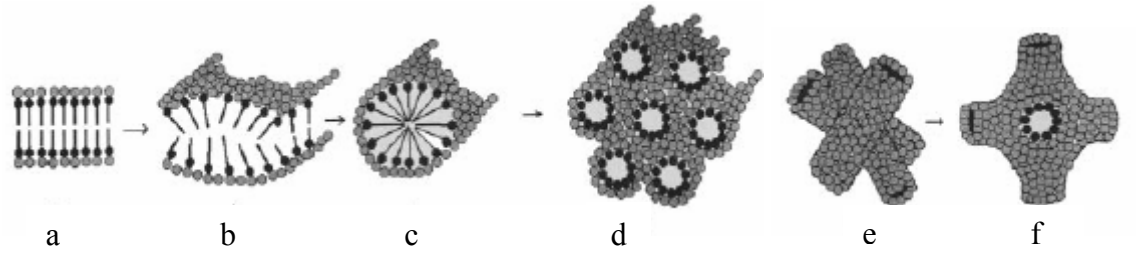

Figure 3.13

Schematic representation of lamellar to hexagonal phase transformation (a through d) and the hexagonal to cubic transformation (e and f). The shaded circles around the surfactant aggregates represent the inorganic species (generally metal alkoxides or other metal-oxo species) [73].

The individual pores are obtained from silicate condensation about separate cylindrical micelles, whereas the ordering of structure results from the appropriate arrangement of the micellar array. This "co-operative assembly pathway" is also called "liquid crystal templating", which indicates that the creating of mesoporous structure is controlled by large assemblies of organic molecules instead of individual molecules or ions. Although the resulting mesoporous sieve exhibits a long-range ordering, it is not a crystalline material – the silicate wall of the pores is amorphous, as it was shown by XRD and ^{29}Si MAS NMR [34].

Depending on the synthesis conditions, the silica source or the type of surfactant used, different mesoporous materials can be synthesized following the co-operative assembly pathway. The initial application of cationic surfactants like quaternary ammonium ions has been extended to neutral and cationic structure-directing agents. Thus, three types of synthesis can be distinguished with respect to the template used:

(i) "cationic" approach – surfactants are tetraalkylammonium cations with long chain or di-N-quarternary cations; leads to the formation of MCM-41, MCM-48, MCM-50 [31,67], FSM-16 [74], SBA-1 [75], etc.,

(ii) "anionic" approach – long-chain alkyl carboxylic acids are used for the synthesis of organized mesoporous aluminas (OMA) [32], and

(iii) "neutral" route – various higher amines, triblock copolymers, and alkyl-ethylene oxides are used for the preparation of different hexagonal mesoporous sieves as SBA-15, SBA-16 [76].

The pore size of materials ad (i) is primarily controlled by the length of the alkyl chain of the surfactant used. However, addition of auxiliary organic molecules such as aromatics [77], n-alkanes [78], or fatty acid [79] can lead to an expansion of the mesopore size.

The triblock co-polymers (e.g. poly(ethylene oxide)$_x$–poly(propylene oxide)$_y$–poly(ethylene oxide)$_x$, trade name: Pluronic®), which show the ability to form liquid–crystal structures, were used to synthesize a variety of different ordered mesoporous materials with rather large pores in various framework compositions under strongly acidic conditions. Typical material of this group, SBA-15 (Santa Barbara No. 15), exhibit walls of 3 – 7 nm thickness and large pore sizes adjustable between 6 and about 15 nm (Fig. 3.11d) [80]. The thick walls of this material substantially improve the thermal and hydrothermal stability in comparison with MCM-41 and related silicas.

Recently, a novel synthetic route for mesoporous silica by the use of anionic surfactants has been reported by Che et al. (named AMS-n, Anionic surfactant templated Mesoporous Silica). In this case, the negatively charged head groups of the anionic surfactant, such as palmitic acid or N-lauroyl-L-glutamic acid, interact with the positively charged amine or ammonium groups of 3-aminopropyltrimethoxysilane or

N-trimethyoxysilylpropyl-N,N,N-trimethylammonium, which are used as additives for co-condensation of tetraethyl orthosilicate [81].

In 1990, an alternative, but less versatile approach to mesoporous materials was described by Yanagisawa et al. [82]. Kanemite, a layered silicate, served as a silica source; the pathway leading to the ordered mesoporous material is thought to proceed via surfactant intercalation into the silicate sheets and transformation to the hexagonally packed material. Optimization of the reaction conditions yielded highly ordered mesoporous silicates and aluminosilicates designated as FSM-n, Folded Sheet mesoporous Materials-n, where n is the number of carbon atoms in the surfactant alkyl chain used to synthesize this material [74].

All methods discussed so far rely on a cooperative interaction between the surfactant and the inorganic species by which an organic/inorganic mesostructured composite is formed. However, one can also use a preformed surfactant liquid crystalline phase that is subsequently loaded with the precursor for the inorganic material. This pathway, later labeled “true liquid crystal templating” [83], had already been suggested as one possible mechanism for the formation of MCM-41 in the original publication by the Mobil group [31].

A different method is the nanocasting first reported by Ryoo and coworkers in 1999 [84]. Here no surfactant template is used, but instead the pore system of ordered mesoporous silica is used as a hard template. The pores are infiltrated with a carbon precursor such as sucrose or furfuryl alcohol, which is subsequently converted to carbon by high temperature treatment in inert gas. After leaching of the silica with HF or NaOH, a negative of the original mold is obtained (denoted as CMK-n) [84].

The discovery of mesoporous molecular sieves opened new possibilities in many areas of chemistry and material science. Due to high surface areas and large pores with narrow pore size distribution, the mesoporous molecular sieves attracted much attention as sorption materials, catalysts and catalyst supports [34]. Catalytic activity of purely siliceous sieves can be enhanced by introducing metal cations. These metal centers can than act as acid or redox active sites. The advantage of using ordered mesoporous solids in catalysis is high surface area, which allows a high concentration of active sites per mass of material. Modification of the framework composition is possible by the direct synthesis or by post-synthesis treatment of an initially prepared silica mesoporous material – it can serve as excellent support for transition metal oxides and grafted

molecular species as organometallic complexes or enzymes, offering the possibility of high dispersion of the active phase [34].

Initially, it was believed that mesoporous silicates as Al-MCM-41 could replace zeolites in Fluid Catalytical Cracking, one of the most important catalytical processes. Here, in the processing of bulky carbon molecules, the mesoporous molecular sieves could take the advantage of relatively large pores that facilitate mass transfer compared to zeolites. However, due to low hydrothermal stability and relatively low acidity of mesoporous materials the perspectives in this field are limited. In other reactions that require milder acidity and also involve bulky reactants and products, such as mild hydrocracking reactions or Friedel-Crafts alkylation of electron-rich aromatic compounds, however, mesoporous materials exhibit great potential [85].

For example, MCM-41 catalysts showed substantial cracking activity for bulky substances such as palm oil and asphaltene [86]. Al-MCM-41 was much more active in the alkylation of 2,4-di-tert-butylphenol with cinnamyl alcohol than conventional catalysts, e.g. H_2SO_4. The following acid catalyzed intramolecular ring closing reaction of cinnamylphenol gave dihydrobenzopyran (yield 35 % and 12 % for Al-MCM-41 and H_2SO_4, respectively) [87]. Aluminum substituted mesoporous silica (e.g. aluminum isopropoxide grafted MCM-41) exhibited higher activity in Diels-Alder reactions with large organic molecules compared to conventional microporous zeolites (ZSM-5, HY) or ion exchange resins [88]. The weak or intermediate-strength acid sites are also effective for the Beckmann rearrangement of cyclohexanone oxime to give ε-caprolactam (catalyst Al-MCM-41) [89], Prins condensation of β-pinene and paraformaldehyde to nopol (catalyst Sn-MCM-41) [90], and Meerwein-Ponndorf-Verley reaction (e.g. reduction of 4-tert-butylcyclohexanone with 2-propanol) over zirconium 1-propoxide grafted SBA-15 [91].

Typical process with a need for converting large molecules is hydrotreatment of petroleum fractions (i.e. hydrodesulfurization, hydrodenitrogenation, etc.). MCM-41 supported MoS_2 showed a higher rate constant for hydrodesulfurization of dibenzothiophene than MoS_2 supported on amorphous SiO_2 [92]. SBA-15 supported Ni-WS_2 exhibited 1.4 and 7.3 times higher catalytic activities than a commercial Co-Mo/Al_2O_3 catalyst for hydrodesulfurization of dibenzothiophene and hydrogenation of toluene, respectively [93].

For large substrates, there is also the possibility to take the advantage of shape selectivity of mesoporous catalysts. For example, in benzene alkylation with linear

1-alkenes with a chain length from C_6 to C_{16} by $AlCl_3$-grafted MCM-41 (pore diameter of 3.3 nm), at 100 % conversion, selectivity to mono-substituted alkyl benzene was much higher in comparison with $AlCl_3$ as homogeneous catalyst. Moreover, this selectivity increased and the formation of multi-substituted products was decreased with increasing alkyl chain length of the alkene [94].

As for redox reactions, Ti-MCM-41 can be used for selective oxidations with hydrogen peroxide or organic hydroperoxides as oxidants (e.g. oxidation of α-terpineol with *tert*-butyl hydroperoxide) [95]; Mn-MCM-41 showed high activity for the epoxidation of stilbene [96]; Nb- or NbCo-substituted mesoporous MCM-41 catalysts were active in liquid phase oxidation of aromatic hydrocarbons such as styrene, benzene or toluene to benzaldehyde, phenol or benzalcohol, respectively, with H_2O_2 [97]; Sn(IV) containing MCM-41 with H_2O_2 had a good activity in the catalytic Bayer-Villiger oxidation, which is normally carried out stoichiometrically with correspondingly high production of waste [98]; homogeneously dispersed gold particles on Ti-MCM-41 and Ti-MCM-48 catalyzed the vapor-phase epoxidation of propene using H_2/O_2-mixtures [99]; V-MCM-41 was active in oxidative dehydrogenation of alkanes [100] and methane partial oxidation by air [101]; iron oxide supported on MCM-41 had substantially higher catalytic activity in the oxidation of SO_2 than iron oxide supported on a commercial high surface area amorphous silica support [102], etc.

MCM-41 supported Ru-Pt catalysts were active in the hydrogenation of benzoic acid to cyclohexane carboxylic acid [103]. Highly dispersed Co metal supported on MCM-41 showed significant increase of CO hydrogenation activity in comparison with an amorphous SiO_2 supported catalyst [104]. Palladium grafted mesoporous silica exhibited remarkable activity in carbon-carbon coupling (Heck reaction) [105].

The MCM-41 grafted $[Mo_2(\mu\text{-}O_2CCH_3)_2(CH_3CN)_{10}](BF)_4$ had a comparable polymerization activity as in the homogeneous case; polymethylcyclopentadiene with a molecular mass of 96 000 g/mol and polydispersity index of 1.9 was obtained [106]. Weckhuysen et al. showed that the chromium acetyl acetonate complex, $[Cr(acac)_3]$, grafted onto Si-MCM-41 or Al-MCM-41 was an effective catalyst for the gas-phase and slurry phase polymerization of ethene [107].

Thus, mesoporous molecular sieves based catalysts were successfully used in a variety of reactions, especially acid-base and redox catalysis, C-C bond formation reactions, polymerization, and in the area of fine chemicals synthesis. However, in the field of metathesis, only very little was known at the time of the beginning of this

study (2003). The only publication reporting the application of the mesoporous support in the preparation of molybdenum metathesis catalyst was a preliminary communication published in 1998 by Ookoshi et al. [35]. In this two-page paper, the authors described the activity of the catalysts prepared by impregnation of several types of hexagonal mesoporous silica (HMS) with molybdate solution in metathesis of 1-octene. Nevertheless, the detailed characterization of the catalysts and HMS-type supports was missing in this work.

4 EXPERIMENTAL PART

The first part of the Chapter is centered on the synthesis of mesoporous molecular sieves. Three types of supports were prepared via hydrothermal synthesis: hexagonal MCM-41 with one-dimensional array of channels and pore size about 3 nm, SBA-15 with the same geometry but approximately two times larger pores, and cubic MCM-48 with three-dimensional array of intersecting channels and roughly the same pore diameter as MCM-41 (see Tab. 5.1). As the reference support, conventional silica Merck was used for the preparation of the catalysts. SiO_2 Merck (Silica gel 40) had surface area 559 m^2/g and very broad pore size distribution centered at 4.5 nm. The supports were modified with molybdenum oxide using the thermal spreading method as it is explained in Chapter 4.2. For comparison, some catalysts were prepared via impregnation from ammonium heptamolybdate or molybdenum acetylacetonate solution and via direct incorporation of Mo during the synthesis of mesoporous silica. Except the above-mentioned supports, zeolite Beta was also used for the preparation of molybdenum catalysts using different methods. The catalysts were characterized by numerous spectroscopic and physico-chemical techniques as mentioned in Chapter 4.3. All prepared catalysts were tested in metathesis of 1-octene and the most active catalysts were investigated in metathesis of unsaturated ethers and esters and in polymerization of alkynes (Chapter 4.4). Evaluation of catalytic data is described in Chapter 4.5. The chemicals employed in the preparation of supports and catalysts are shown in Tab. 4.1.

4.1 Synthesis of the supports

MCM-41 was synthesized by the homogeneous precipitation method, described in detail in ref. [108]. In a typical synthesis, 9.80 g of hexadecyltrimethylammonium bromide (CTMABr, Fluka) was dissolved in 500 mL of distilled water under vigorous stirring. After that, 10.00 g of Na_2SiO_3 (Aldrich) was added, and the mixture was stirred until a clear solution was obtained. After adding 450 mL of distilled water, 15 mL of ethyl acetate (Fluka) were quickly added, the mixture was homogenized and the stirring was stopped. Initial molar composition of the reaction mixture was 1 Na_2SiO_3 : 0.33 CTMABr : 644 H_2O : 1.87 ethyl acetate. The reaction mixture was allowed to stand at ambient temperature for 5 h and then heated at 90 °C for 72 h in a polypropylene bottle.

Table 4.1

Chemicals used for the preparation of supports and catalysts.

Chemical	CAS Number	Source	Purity
Hexadecyltrimethylammonium bromide	57-09-0	Fluka	purum, ≥ 96.0 %
Sodium metasilicate	6834-92-0	Aldrich	44 – 47 % SiO_2
Ethyl acetate	141-78-6	Fluka	purum, ≥ 99.0 %
Aluminum isopropoxide	555-31-7	Aldrich	≥ 98 %
Cab-O-Sil M5	112945-52-5	Cabot GmbH	> 99.8 % SiO_2
Sodium trisilicate	1344-09-8	Riedel-de Haën	purum
Tetramethylammonium hydroxide solution (25 wt. % in H_2O)	75-59-2	Aldrich	purum
Hexadecyltrimethylammonium hydroxide solution (25 wt. % in H_2O)	505-86-2	Fluka	purum
Pluronic PE 9400	9003-11-6	BASF	-
Hydrochloric acid 35 %	7647-01-0	Lach-Ner, Czech Republic	p. a.
Tetraethyl orthosilicate	78-10-4	Aldrich	98 %
Molybdenum oxide	1313-27-5	Lachema, Czech Republic	purum
Molybdenum(VI) dioxide bis(acetylacetonate)	17524-05-9	Strem Chemicals	≥ 95 %
Ammonium heptamolybdate	12054-85-2	Lachema, Czech Republic	p. a .

N,N-Dimethylformamide	68-12-2	Fluka	purum, ≥ 98.0 %
2,6-Diisopropylphenylimidoneophylidene molybdenum(VI) bis(hexafluoro-*tert*-butoxide)	139220-25-0	Strem Chemicals	-
Benzene	71-43-2	Lachema, Czech Republic	p. a.
Argon	7440-37-1	Linde Gas, Czech Republic	99.998 %
Calcium hydride	7789-78-8	Sigma-Aldrich	95 %

After the synthesis, the solid product was recovered by filtration, thoroughly washed out with distilled water and dried overnight in air. The structure-directing agent was removed by calcination in air carried out at 500 °C for 8 h with a temperature ramp of 1 °C/min.

Al-MCM-41 with Si/Al = 30 was synthesized by the same procedure using Na_2SiO_3 as silicon source, $(iPrO)_3Al$ as aluminum source and CTMABr as structure-directing agent.

Synthesis of siliceous mesoporous MCM-48 based on the modification of the method described in ref. [109] was carried out in the following way: 2.50 g of Cab-O-Sil M5 (Cabot GmbH) together with 3.20 g of $Na_2Si_3O_7$ (Riedel-de Haën) and 3.30 g of tetramethylammonium hydroxide (TMAOH) water solution (25 %, Aldrich) were dissolved in 20 mL of distilled water under vigorous stirring, resulting in a formation of a clear solution. After that, 17.30 g of hexadecyltrimethylammonium hydroxide (CTMAOH) water solution (25 %, Fluka) and 10 mL of distilled water were added and the mixture was homogenized for another 70 min. Initial molar composition of the reaction mixture was 1 $Na_2Si_3O_7$: 3.11 SiO_2 : 0.90 CTMAOH : 0.69 TMAOH : 126 H_2O. Finally, the reaction mixture was heated in a Teflon-lined stainless-steel autoclave at 130 °C for 24 h. After the synthesis, the solid product was recovered by filtration, thoroughly washed out with distilled water and dried overnight in air. The structure-directing agent was removed by calcination in air carried out at 500 °C for 8 h with a temperature ramp of 1 °C/min.

Synthesis of siliceous SBA-15 was carried out according to the procedure described in detail in ref. [110]. 4.00 g of Pluronic PE 9400 (BASF) was dissolved in the solution of 30 mL of distilled water and 120.00 g of 2 M hydrochloric acid. The reaction mixture was stirred for 15 min and then 8.50 g of tetraethyl orthosilicate (TEOS, Aldrich) was added. Initial molar composition of the reaction mixture was 1 TEOS : $2.165 \cdot 10^{-5}$ PE 9400 : 5.69 HCl : 193 H_2O. After stirring for 5 min the reaction mixture was allowed to stand at 100 °C for 43 h. After the synthesis, the solid product was recovered by filtration, thoroughly washed out with distilled water and dried overnight in air. The structure-directing agent was removed by calcination in air carried out at 500 °C for 8 h with a temperature ramp of 1 °C/min.

The sample of organized mesoporous alumina (OMA) with pore size 3.5 nm was kindly provided by N. Žilková, J. Heyrovský Institute. Zeolite H-Beta with Si/Al = 38 was purchased from Zeolyst.

4.2 Preparation of the catalysts

The thermal spreading method was utilized for the modification of mesoporous molecular sieves with molybdenum oxide in this study (Chapter 4.2.1). For comparison, catalysts were also prepared via incipient wetness method, as described in Chapter 4.2.2. In addition, $MoO_2(acac)_2$ was used for the preparation of the catalysts via both incipient wetness method and thermal spreading. Finally, direct synthesis of Mo-MCM-41 was performed as well (Chapter 4.2.3). For the polymerization experiments, Schrock carbene was grafted on MCM-41 and SBA-15 from benzene solution (Chapter 4.2.4). The overview of all prepared catalysts is given in Tab. 4.2.

4.2.1 Thermal spreading method

Typically, molybdenum oxide (Lachema, Czech Republic) was used as the source of molybdenum. Support and molybdenum oxide were carefully mixed together by hand grinding in the following weight ratios: 4, 6, 8, 12, and 16 wt. % of molybdenum. It was reported in the literature that complete dispersion of MoO_3 over MCM-41 was attained after heating for 8 h at 500 °C [111]. Thus, the physical mixtures were thermally treated in air at 500 °C for 8 h in a temperature-programmed furnace with a temperature ramp of 1 °C/min.

It is known for MoO_3/SiO_2 systems that by applying organometallic precursors one can prevent formation of molybdenum crystalline phases [39,40]. Therefore, molybdenum(VI) dioxide bis(acetylacetonate), $MoO_2(acac)_2$ (Strem Chemicals) was used as a precursor compound in order to obtain reference catalyst with very good dispersion of molybdenum. The catalyst was prepared in the same way as that one with molybdenum oxide.

4.2.2 Incipient wetness method

The supports were impregnated by using the incipient wetness method with an aqueous solution of ammonium heptamolybdate (Lachema, Czech Republic) or with dimethylformamide solution of $MoO_2(acac)_2$ (Strem Chemicals), respectively. Calculated amount of the support (previously dehydrated at 90 °C) was contacted with a dimethylformamide solution of $MoO_2(acac)_2$ for 18 h or with an aqueous solution of ammonium heptamolybdate for 1 h, respectively. Amount of Mo compound used for catalyst preparation corresponded to desired Mo loading.

Table 4.2 Overview of prepared heterogeneous catalysts; Mo loading was calculated from amount of Mo used for catalysts preparation; * = impregnation from DMF solution, ** = impregnation from water solution, † = according to Higashimoto et al. [112], ‡ = modification of the homogeneous precipitation method (see Chapter 4.2.3), § = $Mo(=CHCMe_2Ph)(=N\text{-}2,6\text{-}i\text{-}Pr_2C_6H_3)[OCMe(CF_3)_2]_2$.

Support	Mo Source	Preparation Method	Mo Loading (wt. % Mo)	Abbreviation
MCM-41	MoO_3	thermal spreading	4, 6, 8, 12, 16	4, 6, 8, 12, 16MoO_3/MCM-41
MCM-41	$MoO_2(acac)_2$	thermal spreading	6	6Mo(acac)/MCM-41
MCM-41	$MoO_2(acac)_2$	incipient wetness *	6	4.7impMo(acac)/MCM-41
MCM-41	$(NH_4)_6Mo_7O_{24}$	incipient wetness **	6	2.3impAHM/MCM-41
MCM-41	$(NH_4)_6Mo_7O_{24}$	direct synthesis of Mo-MCM-41 †	4, 7	1.4, 3.1Hi-Mo-MCM-41
MCM-41	$(NH_4)_6Mo_7O_{24}$	direct synthesis of Mo-MCM-41 ‡	6	0.8DS-Mo-MCM-41
MCM-41	Mo^{carb} §	grafting	1	1Mo^{carb}/MCM-41
Al-MCM-41	MoO_3	thermal spreading	8	8MoO_3/Al-MCM-41
OMA	MoO_3	thermal spreading	8	8MoO_3/OMA
SiO_2	MoO_3	thermal spreading	6, 8, 12	6, 8, 12MoO_3/SiO_2
H-Beta	$(NH_4)_6Mo_7O_{24}$	incipient wetness **	6	1.5impAHM/H-Beta
H-Beta	MoO_3	thermal spreading	6	6MoO_3/H-Beta
Na-Beta	MoO_3	thermal spreading	6	2.1MoO_3/Na-Beta
MCM-48	MoO_3	thermal spreading	4, 8, 12, 16	4, 8, 12, 16MoO_3/MCM-48
SBA-15	MoO_3	thermal spreading	4, 8, 12, 16	4, 8, 12, 16MoO_3/SBA-15
SBA-15	Mo^{carb} §	grafting	1	1Mo^{carb}/SBA-15

The solution was then evaporated with a rotary evaporator at 60 °C. After the impregnation, the catalysts were calcined in air at 500 °C for 8 h with a temperature ramp of 1 °C/min.

4.2.3 Direct synthesis of Mo-MCM-41

Mo-MCM-41 was synthesized by the method described in detail in ref. [112]. Mo-MCM-41 mesoporous molecular sieves with initial Si/Mo molar ratios of 40 and 23 were synthesized using tetraethyl orthosilicate (TEOS) and ammonium heptamolybdate as the starting materials and hexadecyltrimethylammonium bromide (CTMABr) as the structure-directing agent. 8.30 g of TEOS (Aldrich) together with 2.90 g of CTMABr (Fluka) was dissolved in 115 mL of distilled water under vigorous stirring. After that, calculated amount of ammonium heptamolybdate (Lachema, Czech Republic) was added and the mixture was homogenized. The molar composition of the synthesis mixture was 1.0 SiO_2 : x MoO_3 : 0.20 CTMABr : 160 H_2O (x = 0.025 and 0.044 for Mo loadings 4 and 7 wt. % Mo, respectively). The pH was adjusted to 0.5 with the HCl solution, and the reaction mixtures were stirred for 5 days at room temperature. After that, the products were recovered by filtration, washed with distilled water, and dried at 60 °C overnight. The samples were calcined in air at 500 °C for 8 h with a temperature ramp of 1 °C/min to remove any organic compounds.

For comparison, Mo-MCM-41 with initial Si/Mo molar ratio 34 was also synthesized by the homogeneous precipitation method, described in detail in Chapter 4.1. Typically, 9.80 g of hexadecyltrimethylammonium bromide (CTMABr, Fluka) was dissolved in 500 mL of distilled water under vigorous stirring. After that, 10.00 g of Na_2SiO_3 (Aldrich) was added, and the mixture was stirred until a clear solution was obtained. After adding 450 mL of distilled water, 2.98 g of ammonium heptamolybdate tetrahydrate (Lachema, Czech Republic), and 15 mL of ethyl acetate (Fluka) were quickly added, the mixture was homogenized and the stirring was stopped. Initial molar composition of the reaction mixture was 1 Na_2SiO_3 : 0.33 CTMABr : 644 H_2O : 1.87 ethyl acetate : 0.03 Mo. The reaction mixture was allowed to stand at ambient temperature for 5 h and then heated at 90 °C for 72 h in a polypropylene bottle. After the synthesis, the solid product was recovered by filtration, thoroughly washed out with distilled water and dried overnight in air. The structure-directing agent was removed by calcination in air carried out at 500 °C for 8 h with a temperature ramp of 1 °C/min.

4.2.4 Grafting of Schrock carbene

Schrock carbene 2,6-Diisopropylphenylimidoneophylidene molybdenum(VI) bis(hexafluoro-*tert*-butoxide), $Mo(=CHCMe_2Ph)(=N\text{-}2,6\text{-}i\text{-}Pr_2C_6H_3)[OCMe(CF_3)_2]_2$ (Strem Chemicals) was grafted on MCM-41 and SBA-15. 1 g of parent mesoporous silica was dried in vacuum at 300 °C for 6 h. After that, it was cooled to room temperature and suspended in a benzene solution of Schrock carbene (78 mg of the complex in 10 mL of benzene) under Ar. The suspension was stirred at room temperature until the solution became colorless (15 min). The solid phase was then separated by decantation, washed three times with 5 mL of benzene and dried in vacuum at room temperature. The catalysts were stored in sealed ampoules in vacuum.

4.3 Characterization of the catalysts

X-ray powder diffraction patterns were obtained on a Bruker AXS D8 diffractometer in the Bragg-Brentano geometry arrangement using Cu Kα radiation with a graphite monochromator and a position sensitive detector (Vantec-1).

Adsorption isotherms of nitrogen at -196 °C were taken on a Micromeritics ASAP 2020 instrument. Prior to the adsorption measurement, all samples were degassed at 300 °C until a pressure of 0.1 Pa was attained (~ 12 h).

The morphology of catalyst particles was checked using a scanning electron microscope JEOL JSM-5500LV.

UV-VIS diffuse reflectance (DR UV-VIS) spectra were measured under ambient conditions using a Perkin-Elmer UV-VIS-NIR spectrometer Lambda 19 equipped with a diffuse reflectance attachment with an integrating sphere coated by $BaSO_4$. Samples were placed in 5 mm thick silica cell. The absorption intensity was calculated from the Schuster-Kubelka-Munk equation $F(R_\infty) = (1 - R_\infty)^2/2\ R_\infty$, where R_∞ is the diffuse reflectance of a semi-infinite layer and $F(R_\infty)$ is proportional to the absorption coefficient.

The Laser Raman spectroscopy (LRS) of unactivated catalysts was performed at the Department of Inorganic and Physical Chemistry of the Ghent University, Belgium, on a Bruker FRA 106/S spectrometer equipped with an Nd-YAG-laser (λ = 1 064 nm), reference HeNe laser and a Ge-detector. The samples were measured in air at ambient temperature using aluminum sample holder. Spectra were recorded with resolution 3.5 cm^{-1} by collecting 20 000 scans for a single spectrum, using laser power 50 mW.

The Raman measurements of activated catalysts sealed in evacuated glass tubes as well as of their unactivated analogues in air were done in the Laboratoire de Réactivité de Surface, Université Pierre et Marie Curie - Paris 6, France. In this case, HoloLab Series 5000 Modular Raman Spectrometer (HL5R) from Kaiser Optical Systems Inc. equipped with a microscope, an optic fiber and a CCD detector was employed. Spectra resolution was 4 cm^{-1} and 30 acquisitions (20 s each) were collected for a single spectrum; laser power was 50 mW (10 mW on the sample) at λ = 785 nm.

FTIR spectra were recorded on FTIR spectrometer Nicolet Avatar 320 with DTGS-KBr detector and a cell with NaCl windows connected to vacuum apparatus. Spectra were recorded at room temperature with resolution of 1 cm^{-1} by collecting 64 scans for a single spectrum. Catalyst samples, equilibrated with water vapor at room temperature, were pressed in self-supporting wafers of thickness approximately 5 mg/cm^2, having a surface area of 3.0 cm^2 on each face. Before pyridine adsorption, the wafer was heated in the in-situ cell at 450 °C for 30 min in vacuum. After recording the reference spectrum, the sample was heated at 150 °C and contacted with 2.0 kPa pyridine for 15 min. Then the pyridine was pumped off for 30 min at the same temperature and a spectrum was recorded. After the measurement, the wafer was weighted in air. Difference spectra, obtained by subtracting the absorbance reference spectrum from the absorbance spectra recorded after pyridine adsorption, were normalized on the sample weight. The normalized difference spectra were used to obtain the integrated absorbance values of the Brønsted and Lewis bands (integration regions approximately 1515 – 1565 cm^{-1} and 1435 – 1470 cm^{-1}, respectively). The values of integrated absorbance of the bands corresponding to hydroxyl groups (integration region from 3 770 cm^{-1} to 3 350 cm^{-1}) were obtained from the reference spectra normalized on the sample weight. The concentration of Brønsted and Lewis acid sites were determined by a method based on the molar extinction coefficients published by Emeis [113], i.e. 1.67 cm/μmol for the band at 1 545 cm^{-1} corresponding to Brønsted acid sites, and 2.22 cm/μmol for the band at 1 455 cm^{-1} corresponding to Lewis acid sites. When two types of Lewis acid sites were present (bands at 1452 and 1449 cm^{-1}), the peak areas of individual bands were obtained by decomposition of FTIR spectra to the Gaussian bands. The DR FTIR spectra of the spent catalysts were recorded on the same apparatus. The catalyst after the reaction was washed with hexane and dried at room temperature in air. After that, the catalyst was mixed with KBr and the spectra of

resulting powder mixture were taken with the help of diffuse reflectance accessory in air.

Single pulse and cross-polarization ^{29}Si MAS NMR spectra were acquired on a Bruker Avance 500 MHz (11.7 T) Wide Bore spectrometer operating at Larmor frequency 99.35 MHz using 4 mm o.d. ZrO_2 rotors rotated at 5 kHz. The ^{29}Si chemical shifts are referenced to liquid tetramethylsilane. The measurements were performed at the Institute of Macromolecular Chemistry of the ASCR, v. v. i. in Prague, Czech Republic.

The XPS measurements were carried out using ESCA 310 (Gammadata Scienta) spectrometer equipped with monochromatic Al Kα X-ray source and hemispherical electron analyzer. The pressure of residual gases in the spectrometer chamber was below 10^{-7} Pa. The activated catalyst and the catalyst after the reaction were transported into the spectrometer chamber under inert gas. Binding energies determined with the accuracy ± 0.2 eV were referenced by the Si 2p line at 103.5 eV.

Catalyst loading was determined by chemical analysis using X-ray fluorescence spectrometer Philips PW 1404 (Research Institute of Inorganic Chemistry, a. s., Ústí nad Labem, Czech Republic) or an ICP-AES analysis (Ecochem, a. s., Prague, Czech Republic). The standard deviation of the result of chemical analysis was less than 10 %.

4.4 Catalytic testing

4.4.1 Substrates

The overview of chemicals used for catalytic testing is given in Tab. 4.3. For metathesis of linear alkenes, 2-pentene, 1-octene, 2-octene, and 1-decene were used as substrates.

4-allylanisole and diethyl diallylmalonate served as testing compounds in metathesis of unsaturated ethers and esters.

As to the monomers for alkyne polymerization, 1-hexyne, 2-hexyne, 1-decyne, 1-tetradecyne, *tert*-butylacetylene, phenylacetylene, 1-ethynyl-4-fluorobenzene, and 1-ethynyl-2,4-difluorobenzene were employed.

4.4.2 Metathesis of linear alkenes

Metathesis of neat linear alkenes was performed in a liquid phase under argon atmosphere using a glass batch reactor equipped with a magnetic stirrer.

Table 4.3

Chemicals employed in catalytic testing.

Chemical	CAS Number	Source	Purity
Benzene	71-43-2	Lachema, Czech Republic	p. a.
Toluene	108-88-3	Lach-Ner, Czech Republic	≥ 99 %
2-pentene	109-68-2	Fluka	98 %
1-octene	111-66-0	Aldrich	98 %
2-octene	111-67-1	Alfa Aesar	98 %
1-decene	872-05-9	Spolana, Czech Republic	96 %
4-allylanisole	140-67-0	Fluka	95 %
Diethyl diallylmalonate	3195-24-2	Aldrich	98 %
1-hexyne	693-02-7	Fluka	97 %
2-hexyne	764-35-2	Alfa Aesar	98 %
1-decyne	764-93-2	Aldrich	98 %
1-tetradecyne	765-10-6	Fluka	purum
Tert-butylacetylene	917-92-0	Aldrich	98 %
Phenylacetylene	536-74-3	Fluka	97 %
1-ethynyl-4-fluorobenzene	766-98-3	Aldrich	98 %
1-ethynyl-2,4-difluorobenzene	302912-34-1	Aldrich	97 %

Tetramethyltin	594-27-4	Fluka	≥ 99.0 %
Argon	7440-37-1	Linde Gas, Czech Republic	99.998 %
Sodium	7440-23-5	Fluka	purum
Calcium hydride	7789-78-8	Sigma-Aldrich	95 %
Tetrahydrofuran	109-99-9	Aldrich	≥ 99.9 %
Methanol	67-56-1	Lach-Ner, Czech Republic	≥ 99.5 %

In a typical experiment, 50 mg of catalyst was placed into the reactor and activated at 500 °C in a stream of air dried with silica gel for 0.5 h and in a stream of dried argon for 10 min. After activation, the catalyst was cooled down to the reaction temperature in a stream of dried argon and degassed until the pressure of 0.1 Pa was attained. The substrate was passed through a column of activated alumina and then purified with metallic sodium. 1.5 mL of purified substrate was injected into the stirred reactor placed in thermostated bath and filled with argon. The initial substrate-to-catalyst molar ratio was approximately 350. At given reaction times, 20 μL of liquid phase was sampled for GC analysis.

A high-resolution gas chromatograph Agilent 6890 equipped with an autosampler Agilent 7683, a DB-5 capillary column (length: 50 m, inner diameter: 320 μm, stationary phase thickness: 1 μm) and a FID detector was used for the product analysis.

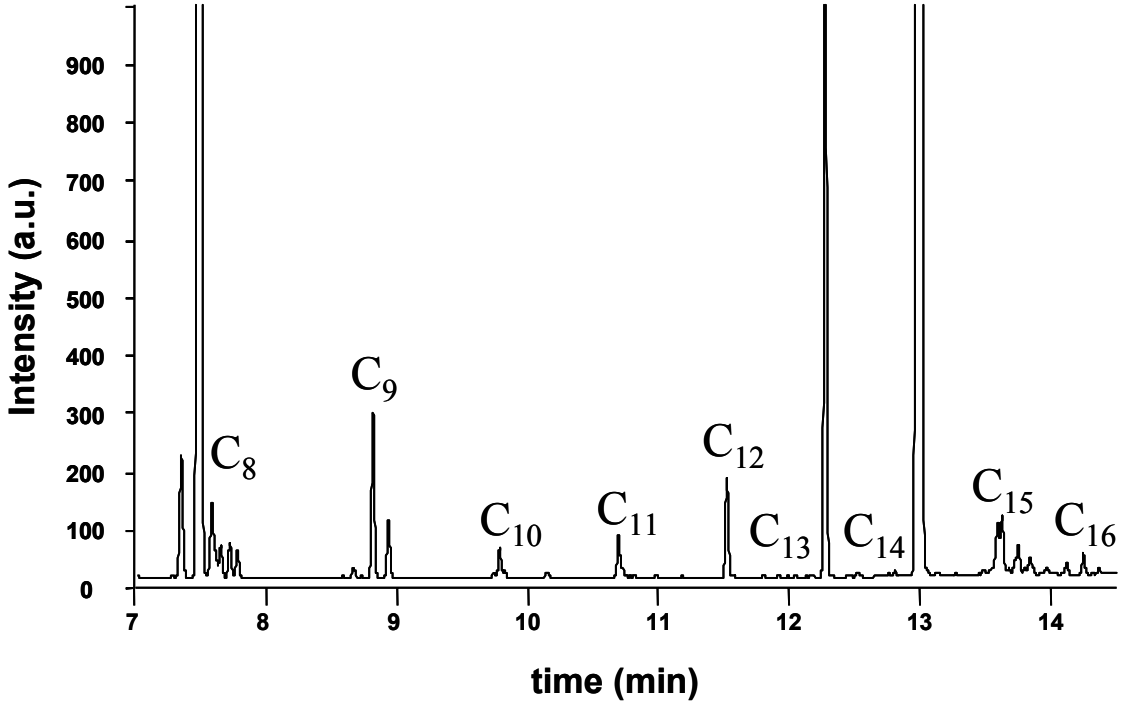

Figure 4.1

Gas chromatogram of the reaction mixture; metathesis of 1-octene. Peaks of the products (C_9 – C_{16}) were identified using GC-MS.

1 μL of the sample was injected at the inlet temperature 280 °C with helium as a mobile phase. The column temperature was increased from 80 °C to 260 °C with a temperature ramp 12 °C/min. Individual products were identified with the help of GC-MS analysis (ThermoFinnigan, FOCUS DSQ II Single Quadrupole). Typical gas chromatogram of

the reaction mixture in the case of metathesis of 1-octene is shown in Fig. 4.1. The substrate, 1-octene, and its isomers are denoted as C_8. The main metathesis product, 7-tetradecene (C_{14}), results from self-metathesis of 1-octene, whereas the cross-metathesis between 1-octene and its isomers gives the other products (C_9 – C_{13}). The C_{15} fraction are the products of cross-metathesis of 6-tetradecene (which arises from double-bond shift isomerization of 7-tetradecene) with 1-octene and its isomers. The C_{16} fraction are the products of dimerization of 1-octene and its isomers.

The determination of Mo concentration in the products was made by Research Institute of Inorganic Chemistry, a. s., Ústí nad Labem, Czech Republic using ETA AAS spectrometer equipped with a graphite cuvette.

4.4.3 Metathesis of unsaturated ethers and esters

For metathesis of unsaturated ethers and esters, toluene was used as a solvent and tetramethyltin as a cocatalyst. Toluene was purified by distillation and dried with metallic sodium. The substrate was passed through a column of activated alumina and then dried with calcium hydride. 50 mg of the catalyst was activated using the same procedure as described earlier (Chapter 4.4.2). After activation, 1 mL of toluene and calculated amount of tetramethyltin were injected into the stirred thermostated reactor filled with argon and mixed with the catalyst for 10 min. After that, the substrate was added. The initial substrate-to-catalyst molar ratio was varied between 8 and 24; the tin-to-molybdenum molar ratio was varied between 0 and 0.9. The initial substrate-to-toluene volume ratio was 0.1.

The samples of the reaction mixture were analyzed as described in Chapter 4.4.2; toluene was used as an internal standard. For the product of metathesis of 4-allylanisole, 1,4-bis(4-methoxyphenyl)-2-butene, the cis-to-trans ratio was determined from the peaks of olefinic carbon in the ^{13}C NMR spectra of the product recorded on Varian Unity Inova 400 instrument. The measurements were done in the Laboratory of Specialty Polymers, Department of Physical and Macromolecular Chemistry at the Faculty of Science of the Charles University in Prague, Czech Republic. ^{13}C NMR chemical shifts obtained from the spectra measured in deuteriochloroform were referenced to solvent signal ($\delta\{CDCl_3\} = 77.00$ ppm).

4.4.4 Polymerization of alkynes

In polymerization experiments, toluene or benzene was used as a solvent. The solvents were purified by distillation and dried with metallic sodium (toluene) or calcium hydride (benzene).

In a typical experiment, 50 mg of catalyst was activated as described in Chapter 4.4.2. Monomers were passed through a column of activated alumina and then dried with calcium hydride. In the case of 1-ethynyl-4-fluorobenzene and 1-ethynyl-2,4-difluorobenzene, the monomer was dissolved in distilled toluene and dried with calcium hydride. 2.5 mL of toluene and 0.25 mL of purified monomer (or corresponding amount of the monomer solution in toluene) were injected into the stirred thermostated reactor filled with argon. When 1-octene should be added to the reaction mixture, it was passed through activated alumina and then dried with metallic Na. After 180 min of the reaction at 40 °C, the catalyst was separated by centrifugation. If the reaction mixture was too viscous, small amount (~ 1 mL) of tetrahydrofuran was added. The polymer was isolated by precipitation into methanol and dried in vacuum at 60 °C to the constant weight. Supernatant after polymer isolation was concentrated by evaporation of volatile components at room temperature and the residue was dried in vacuum at 60 °C.

In the case of grafted Schrock catalyst ($1Mo^{carb}$/MCM-41 and $1Mo^{carb}$/SBA-15), in a typical experiment, weighted amount of catalyst (about 40 mg) was put into the reactor under argon atmosphere. After that, the reactor was evacuated and calculated amount of benzene was added by distillation under vacuum. Finally, the reactor was filled with argon and calculated amount of purified 1-hexyne was added with syringe. Initial 1-hexyne to benzene volume ratio was 0.03; initial substrate-to-catalyst molar ratio (1-hexyne to Mo) was 100. Reaction proceeded at 25 °C under vigorous stirring for 180 min. The polymer was isolated as in the previous case.

GC-MS (ThermoFinnigan, FOCUS DSQ II Single Quadrupole) was utilized for identification of low molecular weight products. The analysis of polymers was done in the Laboratory of Specialty Polymers, Department of Physical and Macromolecular Chemistry at the Faculty of Science of the Charles University in Prague, Czech Republic. SEC analyses were carried out on a Watrex Chromatograph fitted with a differential refractometer Shodex RI 101. A series of two PL-gel columns (Mixed-B and Mixed-C, Polymer Laboratories Bristol, United Kingdom) and tetrahydrofuran (flow rate 0.7 ml/min) was employed. Weight-average molecular weight, M_w, and number-average molecular weight, M_n, relative to polystyrene standards are reported. ^{1}H NMR

spectra of the polymers were recorded on Varian Unity Inova 400 instrument (proton frequency 400 MHz) in tetrahydrofuran-d8, tetramethylsilane was used as internal standard. Chemical shifts (δ scale, ppm) were obtained by first-order analysis. Number of transients was 128 and relaxation time was 5 s.

The determination of Mo concentration in polymers was made by Research Institute of Inorganic Chemistry, a. s., Ústí nad Labem, Czech Republic, using ETA AAS spectrometer equipped with a graphite cuvette.

4.5 Catalytic data evaluation

Conversion of the substrate, *C*, and selectivity to the self-metathesis product, *S*, expressed in % were calculated based on the material balance according to equations (1) and (2):

$$C = [2(n_P + n_D + \Sigma n_C)/(n_S + 2n_D + 2n_P + 2\Sigma n_C)] \cdot 100 \quad (1)$$

$$S = [n_P/(n_P + n_D + \Sigma n_C)] \cdot 100 \quad (2)$$

where n_S, n_P, n_C, n_D are the molar amounts of the substrate including its isomers (n_S), self-metathesis product (n_P), cross-metathesis products higher than the substrate (n_C) and dimer of the substrate (n_D), respectively. The molar amounts of the reactants and products were determined from the integrated areas of corresponding peaks in GC chromatogram under the assumption that ratios of weight amounts are equal to ratios of peak areas.

The turn-over frequency after τ min of the reaction (TOF_τ) expressed in s^{-1} was estimated from the conversion of the substrate according to equation (3):

$$TOF_\tau = (n_S^0 \cdot C_\tau/100)/(n_{Mo} \cdot \tau \cdot 60) \quad (3)$$

where n_S^0 is the molar amount of the substrate at the beginning of the reaction ($\tau = 0$ min), n_{Mo} is the molar amount of molybdenum atoms in the catalyst, C_τ is the conversion of the substrate after τ min of the reaction expressed in %, and τ is reaction time in min. If the experimental points did not match the time τ where conversion, selectivity or turn-over frequency should be computed, the evolution of conversion and

selectivity with time was estimated in terms of linear interpolation (or linear extrapolation, exceptionally). The initial turn-over frequency was estimated as TOF_{120}.

Polymer yield in % was computed as follows: the weight of dry reaction product was divided by the weight of the monomer used for the reaction and multiplied by 100.

5 RESULTS AND DISCUSSION

5.1 Properties of the supports and catalysts

The structural and textural properties of prepared mesoporous molecular sieves and catalysts were checked by X-ray diffraction, nitrogen adsorption and scanning electron microscopy. The content of molybdenum in the catalysts was determined by chemical analysis.

5.1.1 X-ray diffractograms

The structure of prepared mesoporous silicas was confirmed by X-ray powder diffraction at low angles. The diffractograms of pure siliceous mesoporous molecular sieves MCM-41, MCM-48, and SBA-15 are displayed in Fig. 5.1.

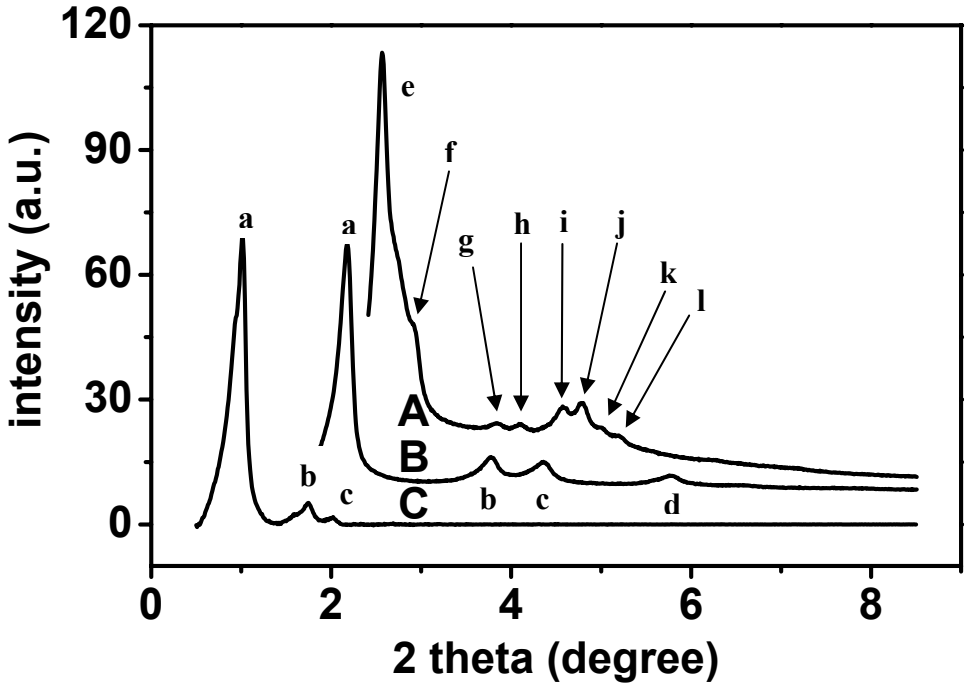

Figure 5.1

X-ray powder diffraction patterns of MCM-48 (A), MCM-41 (B) and SBA-15 (C) [114]. Individual reflections are assigned as follows: a) (100), b) (110), c) (200), d) (210), e) (211), f) (220), g) (321), h) (400), i) (420), j) (332), k) (422), l) (431) [67,71,115]. For clarity, individual diffractograms are vertically shifted.

The X-ray powder diffraction patterns of MCM-41 and SBA-15 correspond to the hexagonal structure of mesoporous silicas [67,115]. The peaks of SBA-15 are shifted to

lower 2 theta angles, and an increased correlation distance is observed in comparison with MCM-41 (a_0 determined from a (100) reflection is 8.7 nm for SBA-15 and 4.1 nm for MCM-41, respectively). On the other hand, the diffractogram of MCM-48 corresponds to the cubic structure of prepared material with diffraction lines shifted to higher 2 theta angles (a_0 determined from a (211) reflection is 3.4 nm) [71]. Well-developed diffraction lines confirm the ordered mesoporous structure of synthesized materials. After the modification of mesoporous silica with molybdenum oxide, the intensity of individual diffraction lines decreased, the character of the diffractogram, however, remained unchanged (Fig. 5.2). This indicates that the thermal spreading of MoO_3 did not cause the collapse of mesoporous structure and is therefore a suitable method for the preparation of molybdenum catalysts supported on mesoporous silicas.

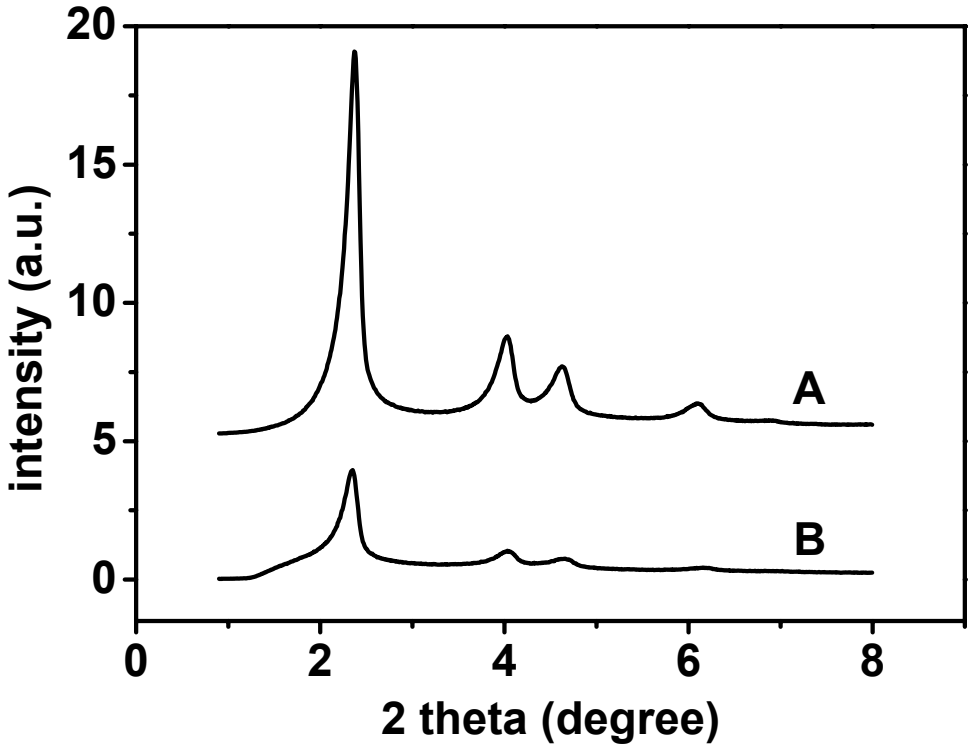

Figure 5.2

X-ray diffraction patterns of MCM-41 (A) and 16MoO_3/MCM-41 (B). For clarity, individual diffractograms are vertically shifted.

For comparison, two types of direct synthesis of MCM-41 modified with molybdenum were performed. In addition, siliceous MCM-41 was impregnated with ammonium heptamolybdate aqueous solution. The diffractograms of 0.8DS-Mo-MCM-41, 1.4Hi-

Mo-MCM-41, and 2.3impAHM/MCM-41 are shown in Fig. 5.3. In contrast to the results published in literature [41], from XRD data it seems that the impregnation of MCM-41 with an aqueous solution of ammonium heptamolybdate did not cause the collapse of the mesoporous structure (Fig. 5.3C). Similarly, also after the impregnation of MCM-41 with dimethylformamide solution of $MoO_2(acac)_2$ as well as in the case of thermal spreading of $MoO_2(acac)_2$ over MCM-41, the mesoporous structure of the support was preserved (not shown in Fig.).

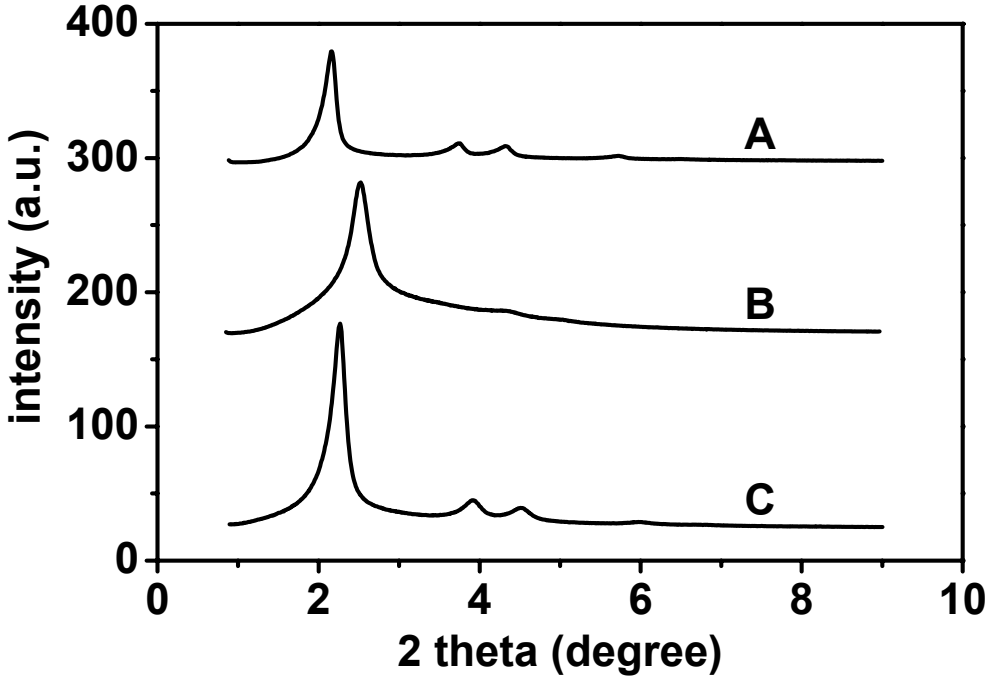

Figure 5.3

X-ray diffraction patterns of 0.8DS-Mo-MCM-41 (A), 1.4Hi-Mo-MCM-41 (B), and 2.3impAHM/MCM-41 (C). For clarity, individual diffractograms are vertically shifted.

When ammonium heptamolybdate was added to the synthesis gel during the preparation of MCM-41, ordered structure of Mo-MCM-41 with four discernible diffraction lines was observed after the synthesis (Fig. 5.3A). On the other hand, both 1.4Hi-Mo-MCM-41 (Fig. 5.3B) and 3.1Hi-Mo-MCM-41 (not shown in Fig.) exhibited only a low degree of ordering of the mesoporous structure. Therefore, it seems that the method according to Higashimoto et al. [112] is not valuable for the direct synthesis of molybdenum-containing MCM-41 catalysts.

The dispersion of molybdenum over the supports was investigated using X-ray powder diffraction at higher angles. The diffractograms of physical mixture of MoO_3 with MCM-41 and MoO_3/MCM-41 catalysts with different loadings is provided in Fig. 5.4. In the diffractogram of the physical mixture of the support with molybdenum oxide, diffraction lines corresponding to crystalline MoO_3 are clearly visible. On the other hand, these diffraction lines are not present in the diffractograms of MoO_3/MCM-41 catalysts with loadings up to 8 wt. % Mo (Fig. 5.4B), which indicates good dispersion of molybdenum oxide for these samples.

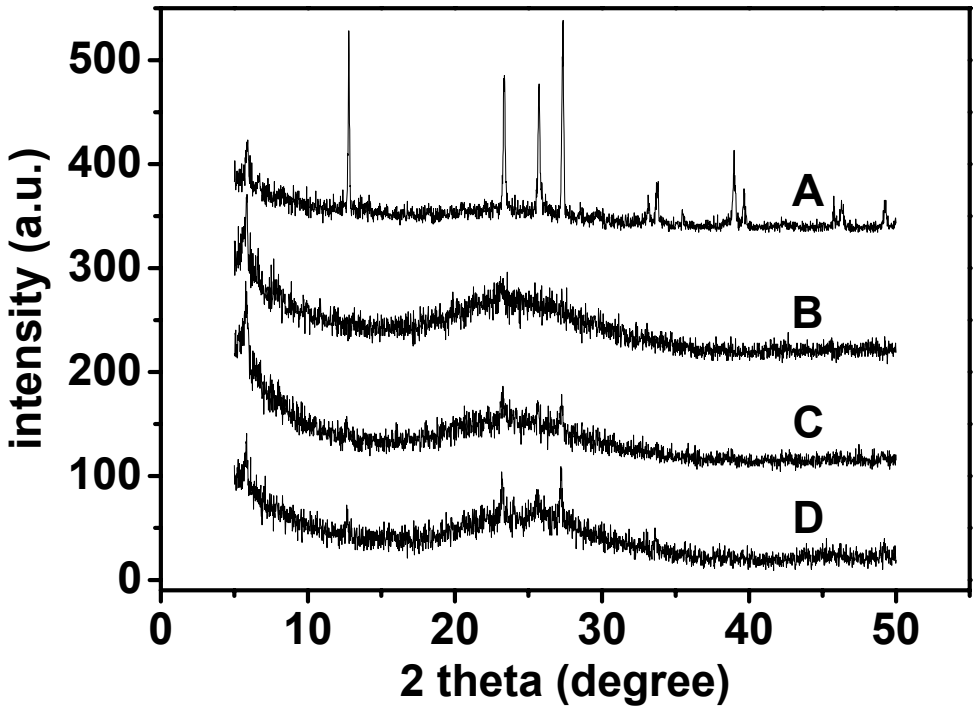

Figure 5.4

X-ray diffraction patterns of physical mixture of MCM-41 and MoO_3 with 16 wt. % Mo (A), and 8MoO_3/MCM-41 (B), 12MoO_3/MCM-41 (C) and 16MoO_3/MCM-41 (D). For clarity, individual diffractograms are vertically shifted.

However, at higher loadings, the diffraction lines of bulk molybdenum oxide appear and their intensity is increasing with increasing molybdenum loading (Fig. 5.4C, D). Thus, in the case of catalysts with 12 and 16 wt. % Mo, some part of molybdenum is present in the form of crystalline molybdenum oxide. The average particle size of molybdenum oxide crystallites was estimated using the Scherrer equation (4) [116]:

$$\Delta = \frac{K\lambda}{\beta \cos \Theta_0} \tag{4}$$

where Δ is the mean crystallite size, K is the constant (K = 0.9), λ is the wavelength of the X-ray radiation, β is the corrected broadening of the diffraction line in 2 theta units, and Θ_0 is the diffraction angle of the maximum of the diffraction line. Variable β can be calculated according to equation (5),

$$\beta = B - b \tag{5}$$

where B is full width at half maximum of the peak of molybdenum oxide in the diffractogram of investigated material and b is full width at half maximum of the reference peak (diffractogram of standard sample with particle size larger than 100 nm). Crystalline molybdenum oxide (Lachema, Czech Republic) served as a reference. Applying the Scherrer method, the average particle size of molybdenum oxide crystallites was estimated to be about 5 nm for 16MoO_3/MCM-41 and 16MoO_3/SBA-15, being about 3 nm for 16MoO_3/MCM-48. For other catalysts, the diffraction lines of molybdenum oxide crystals were not visible or were of too low intensity to apply the Scherrer equation. The only exception was 12MoO_3/SBA-15, where the estimated size of MoO_3 crystallites was about 2.5 nm. These differences in the dispersion of the active phase over the supports were further studied by DR UV-VIS spectroscopy (Chapter 5.3.1), Raman spectroscopy (Chapter 5.3.2), and X-ray photoelectron spectroscopy (Chapter 5.3.5). The correlation between surface area of the support and the size of molybdenum oxide crystallites is discussed in Chapter 5.1.2.

To check the influence of molybdenum compound used for the preparation of the catalysts on their activity and selectivity, water solution of ammonium heptamolybdate and DMF solution of molybdenum(VI) dioxide bis(acetylacetonate) were also used for the preparation of the catalysts supported on MCM-41 via the incipient wetness method. However, according to the results of chemical analysis (Chapter 5.1.4), the Mo content in the catalysts was lower than desired 6 wt. % Mo loading (2.3 and 4.7 wt. % Mo for 2.3impAHM/MCM-41 and 4.7impMo(acac)/MCM-41, respectively, see Tab. 5.4). No diffraction lines of molybdenum oxide were present in the diffractograms of these samples (Fig. 5.5), as well as in the case of MCM-41 supported catalyst prepared by

thermal spreading of $MoO_2(acac)_2$ (not shown in Fig.). Therefore, no differences in the dispersion of molybdenum can be observed in this case using X-ray diffraction.

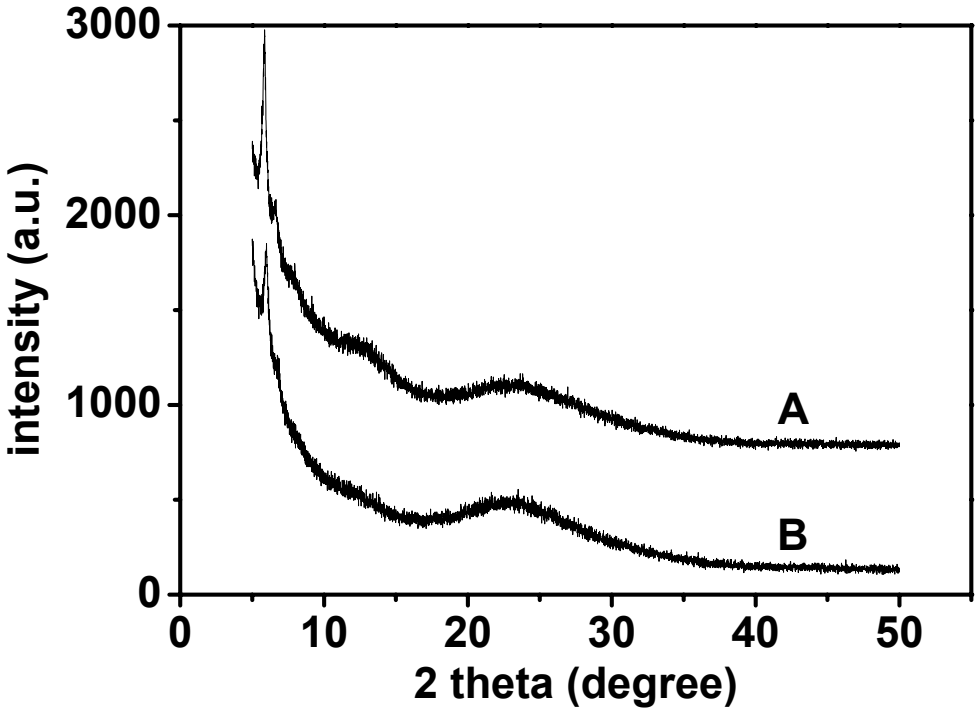

Figure 5.5

X-ray diffraction patterns of 2.3impAHM/MCM-41 (A) and 4.7impMo(acac)/MCM-41 (B). For clarity, individual diffractograms are vertically shifted.

In the diffractograms of 1.4Hi-Mo-MCM-41, 3.1Hi-Mo-MCM-41 and 0.8DS-Mo-MCM-41, no diffraction lines corresponding to crystalline molybdenum oxide were observed as well.

5.1.2 Texture characteristics

Textural properties of prepared supports and catalysts were examined using nitrogen adsorption at -196 °C. Nitrogen adsorption isotherms of pure siliceous MCM-41, MCM-48 and SBA-15 are given in Fig. 5.6. All isotherms are of type IV according to the IUPAC classification and are typical for mesoporous materials [117]. The steep increase in the adsorbed amount in the region of 0.3 – 0.4 p/p_0 for MCM-41 and MCM-48 is caused by reversible capillary condensation within the mesopores of these materials and indicates their narrow pore size distribution. The broad hysteresis in

the adsorption isotherm of MCM-41 at p/p_0 0.5 – 1 can be explained by the presence of some secondary pores in the material.

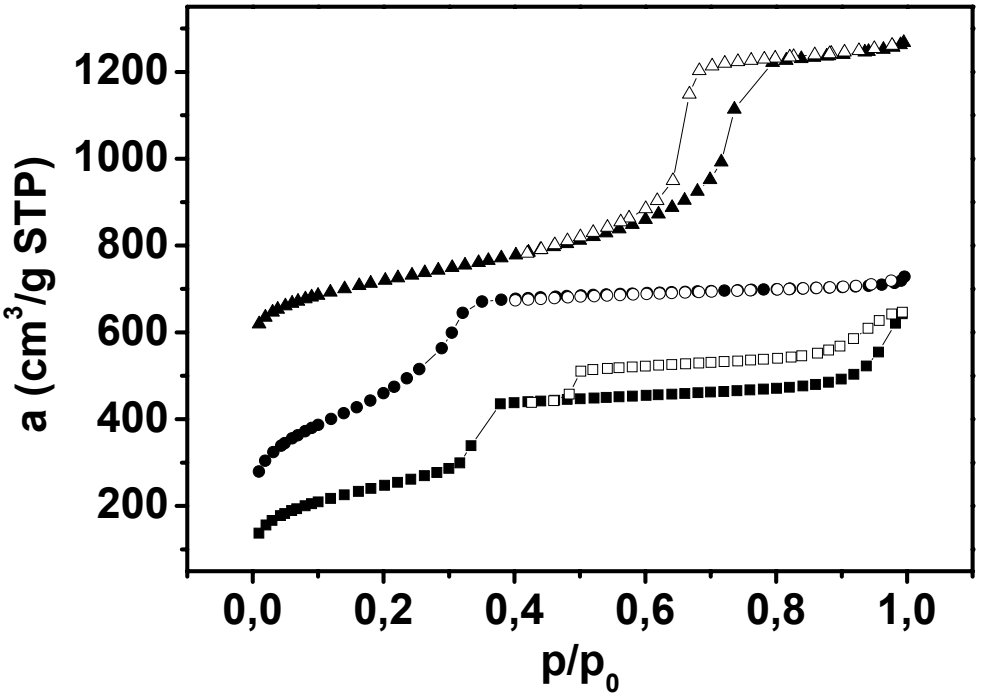

Figure 5.6

Adsorption isotherms of nitrogen at -196 °C on MCM-41 (■), MCM-48 (●) and SBA-15 (▲); desorption branches are depicted using open symbols. For clarity, 100 and 500 cm^3/g (STP) was added to the adsorption isotherms of MCM-48 and SBA-15, respectively.

The position of the steep increase in adsorbed amount depends on pore size (see Tab. 5.1). Therefore, the shift to higher p/p_0 is observed for MCM-41 in comparison with MCM-48 (pore diameter 3.1 nm for MCM-41 and 2.8 nm for MCM-48, respectively). In the case of SBA-15 with approximately two times larger pores than MCM-41 and MCM-48 (Tab. 5.1), this shift is much more pronounced and occurs at p/p_0 0.6 – 0.7. The hysteresis loop on the adsorption isotherm of SBA-15 corresponds to the well-defined cylindrical pores with pore diameter 6.1 nm (Tab. 5.1).

BET surface area, S_{BET}, pore diameter, d, mesopore volume, V_{meso}, and external surface area, S_{ext}, of the supports and catalysts prepared by thermal spreading of MoO_3 on mesoporous MCM-41, MCM-48 and SBA-15 are shown in Tab. 5.1.

Table 5.1

Texture characteristics of the supports and catalysts prepared by thermal spreading of MoO_3 determined from nitrogen adsorption isotherms.

Sample	S_{BET} (m^2/g)	S_{BET} (m^2/g SiO_2)	d (nm)	V_{meso} (cm^3/g)	S_{ext} (m^2/g)
MoO_3/MCM-41					
0 wt. % Mo	1 071	1 071	3.1	0.841	167
4 wt. % Mo	874	929	3.0	0.658	132
6 wt. % Mo	811	891	2.9	0.590	150
8 wt. % Mo	875	994	2.9	0.635	125
12 wt. % Mo	831	1 013	2.7	0.568	125
16 wt. % Mo	754	992	2.7	0.511	98
MoO_3/MCM-48					
0 wt. % Mo	1 334	1 334	2.8	0.927	53
4 wt. % Mo	1 128	1 200	2.7	0.769	53
8 wt. % Mo	829	942	2.6	0.549	36
12 wt. % Mo	961	1 172	2.5	0.591	37
16 wt. % Mo	884	1 163	2.3	0.518	33
MoO_3/SBA-15					
0 wt. % Mo	777	777	6.1	1.258	73
4 wt. % Mo	489	520	6.0	0.649	50
8 wt. % Mo	606	689	6.0	0.865	67
12 wt. % Mo	458	559	6.0	0.825	56
16 wt. % Mo	455	599	5.8	0.715	65
MoO_3/SiO_2					
0 wt. % Mo	559	559	4.5	0.473	-
8 wt. % Mo	298	339	5.7	0.457	-
12 wt. % Mo	300	366	5.4	0.447	-

As the reference support, conventional SiO_2 (Merck, Silica gel 40) with relatively very high surface area (S_{BET} = 559 m^2/g) and very broad pore size distribution centered at 4.5 nm was used for the preparation of the catalysts.

From Tab. 5.1 it is visible that with increasing molybdenum loading the surface area and pore volume of the catalysts are decreasing, but the pore size remains nearly the same. Similar dependence was observed by Li et al. for MoO_3/MCM-41 catalysts prepared by thermal spreading of MoO_3 (calcination at 500 °C for 24 h) [44]. From only a small reduction of the pore size in comparison with parent MCM-41, it was concluded that MoO_3 is inside the channels in dispersed state. In ref. [44], the steep decrease in the surface area and pore volume connected with an increase in pore diameter at loadings higher than 15.4 wt. % Mo was observed. This sharp decrease in the surface area was ascribed to a partial structural collapse of the support. In contrast to study [44], this is not observed in Tab. 5.1.

To check the structural stability of the support, the surface areas of the samples in m^2 per gram of the catalyst were recalculated to m^2 per gram of SiO_2. As pure MoO_3 has surface area lower than 1 m^2/g [118], it practically does not contribute to the surface area of the catalyst. Therefore, with increasing MoO_3 loading the surface area of the catalysts would decrease even if the structure of the support remains unaffected. As shown in Tab. 5.1, there are no significant differences in the surface area expressed in m^2/g SiO_2 among the catalysts with the same support but different Mo content. Thus, it was confirmed that the mesoporous structure of the support is preserved during the preparation of the catalyst. Some decrease in the external surface area at the highest loadings is probably connected with the presence of MoO_3 crystallites, which were found also by X-ray diffraction (Chapter 5.1.1). It can be inferred that the thermal spreading method is suitable for supporting of molybdenum oxide on mesoporous molecular sieves in studied range of loadings (up to 16 wt. % Mo).

The pore diameters obtained from nitrogen adsorption isotherms were compared with correlation distances determined from X-ray diffraction patterns (Tab. 5.2). The wall thickness of mesoporous silica was estimated as a difference between the correlation distance and corresponding pore diameter. It is seen that the estimated wall thickness is increasing in the order MCM-48 < MCM-41 < SBA-15. This is not surprising, as it is known that SBA-15 usually possess thicker pore walls in comparison with molecular sieves of M41S family, where the wall thickness is typically less than 1.5 nm [119]; the estimated wall thickness for SBA-15 (2.6 nm) is in agreement with the literature [110].

Table 5.2

Wall thickness of MCM-41, MCM-48 and SBA-15 estimated from the comparison of correlation distances (as determined from X-ray diffraction patterns) with pore diameters (as determined from nitrogen adsorption isotherms).

Sample	a_0 (nm)	d (nm)	Wall Thickness (nm)
MCM-41	4.1	3.1	1.0
MCM-48	3.4	2.8	0.6
SBA-15	8.7	6.1	2.6

In order to check the presence of micropores, the samples of mesoporous silica were examined by the α_s-analysis, which uses the method of comparison plots [117]. The adsorption on the studied sample, a, was compared with the adsorption on the reference adsorbent not containing micropores, a_{ref}. As a reference, macroporous silica gel Davisil 663XWP (Supelco, S_{BET} = 82 m^2/g) was used. Comparison plots for MCM-41, MCM-48 and SBA-15 are shown in Fig. 5.7.

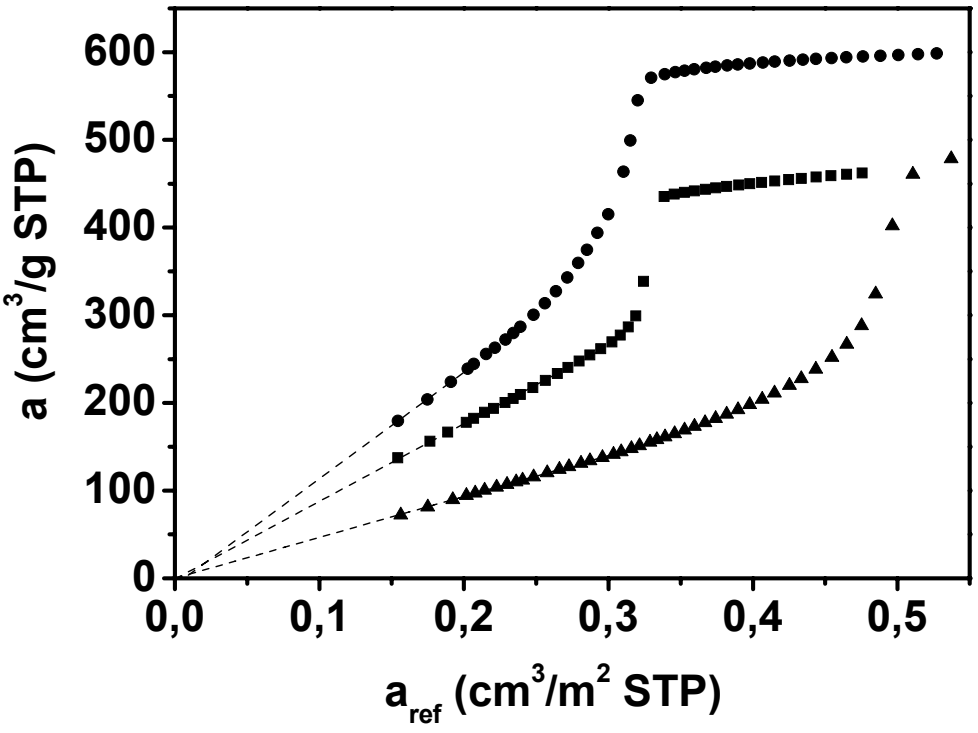

Figure 5.7

Comparison plots for MCM-41 (■), MCM-48 (●) and SBA-15 (▲).

It is seen that after back extrapolation of the linear part of comparison plots to a_{ref} equal to zero (dotted line), practically no intercepts on y-axis are obtained. In the case of MCM-41 and SBA-15, the intercept on y-axis is 0.1 cm^3/g, whereas for MCM-48 it is -8.1 cm^3/g. The values obtained for MCM-41 and SBA-15 are negligible; on the other hand, for MCM-48 a negative adsorbed amount is obtained, which makes no sense from a physical point of view. However, because of the limited amount of data points, the obtained value is satisfactory, since the absolute value of adsorbed amount is very small compared with the total adsorbed amount, which is close to a value of 600 cm^3/g. Thus, the results of α_s-analysis indicate that the adsorption on mesoporous silicas MCM-41, MCM-48 and SBA-15 is proportional to the adsorption on reference macroporous silica and therefore practically no micropores are present in investigated materials. It is interesting especially in the case of SBA-15, which usually contains micropores connecting the main mesopores in its structure [110]. The absence of micropores is advantageous for catalytic applications of mesoporous silicas, as the presence of micropores may decline the catalytic activity of the final catalysts due to the location of molybdenum species in micropores, which are less accessible for the molecules of substrate and products, etc.

To check the repeatability of the catalyst preparation, three samples of $8MoO_3$/MCM-41 were prepared independently using the same parent support. The same pore diameter was determined for all the samples; the standard deviation of the surface area was 39 m^2/g, and the standard deviation of the pore volume was 0.028 cm^3/g. This indicates a good reproducibility of the textural properties of prepared catalysts.

In order to study the influence of the precursor compound, molybdenum(VI) dioxide bis(acetylacetonate), $MoO_2(acac)_2$, and ammonium heptamolybdate (AHM) were also employed in the preparation of MCM-41 supported catalysts. Their texture characteristics are displayed in Tab. 5.3. The amount of Mo used for the preparation of the catalysts corresponded to desired 6 wt. % Mo loading; however, except when thermal spreading method was used, the Mo content according to chemical analysis was lower (4.7 wt. % Mo for 4.7impMo(acac)/MCM-41 and 2.3 wt. % Mo for 2.3impAHM/MCM-41, see Chapter 5.1.4).

The modification of parent MCM-41 with $MoO_2(acac)_2$ via both thermal spreading and impregnation from DMF solution did not cause the complete destruction of mesoporous structure of the support (Chapter 5.1.1).

Table 5.3

Sorption characteristics of the support and catalysts determined from nitrogen adsorption isotherms.

Sample	S_{BET} (m^2/g)	d (nm)	V_{meso} (cm^3/g)
MCM-41	1 424	5.0	1.766
6Mo(acac)/MCM-41	846	5.0	1.053
4.7impMo(acac)/MCM-41	883	5.0	1.106
2.3impAHM/MCM-41	680	4.6	0.783

However, significant decrease (~ 40 %) in both the surface area and the pore volume was detected, while the pore size remained practically the same. This might indicate that part of the support collapsed during the preparation of the catalyst.

When MCM-41 support was impregnated using ammonium heptamolybdate water solution, the decrease in the surface area and pore volume was even higher (more than 50 %) and was accompanied by the reduction in the pore size (from 5.0 to 4.6 nm). It is in agreement with the literature, where the impregnation of MCM-41 with AHM water solution was reported to lead to the diminishing of the surface area [41]. On the other hand, we cannot speak about complete destruction of mesoporous structure, as it is mentioned in ref. [41], when the surface area is still 680 m^2/g and fully developed X-ray diffraction pattern corresponding to mesoporous structure of MCM-41 is observed (Chapter 5.1.1, Fig. 5.3C).

5.1.3 Morphology of the particles

The morphology of the support particles was investigated using scanning electron microscopy (SEM). Estimated average particle size of the supports was between 1 and 3 μm (Fig. 5.8 – 5.10).

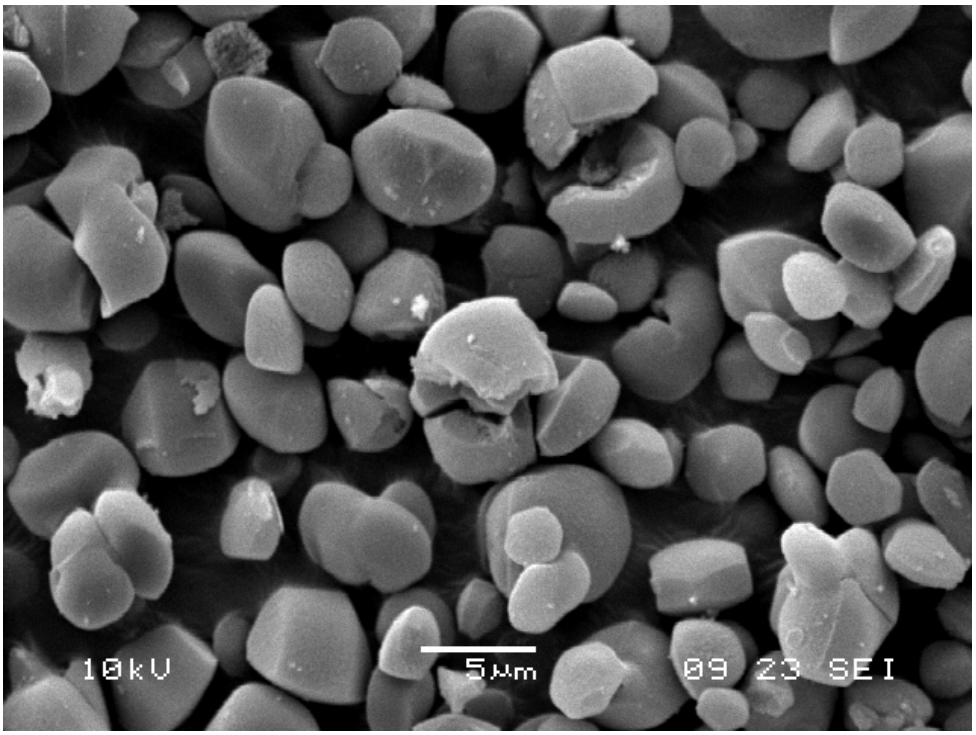

Figure 5.8

SEM image of parent MCM-41.

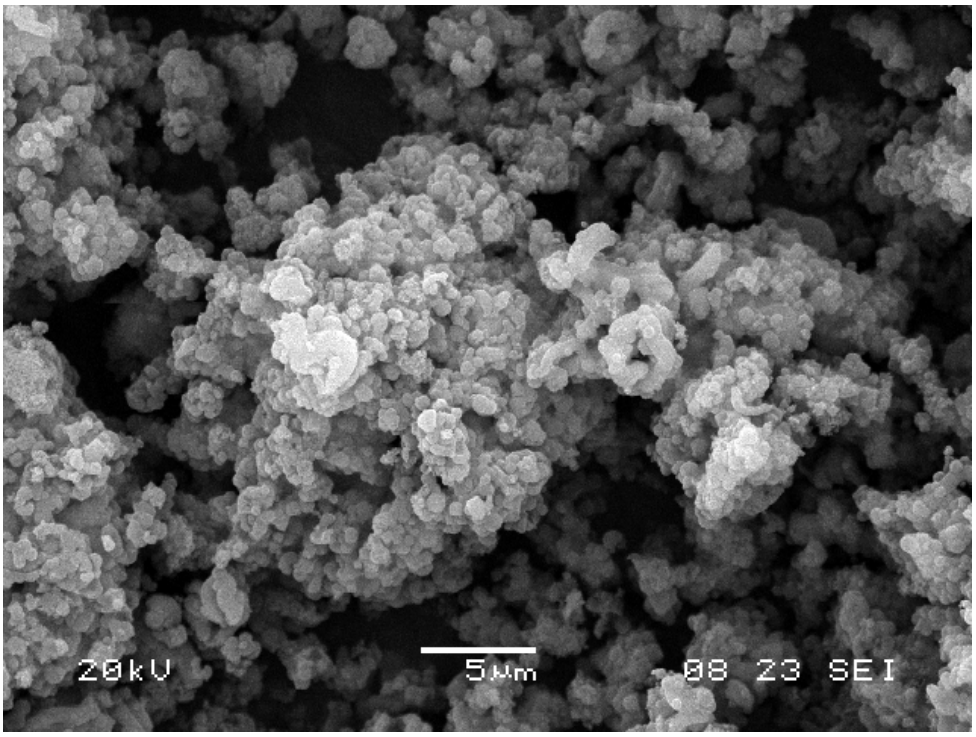

Figure 5.9

SEM image of parent MCM-48.

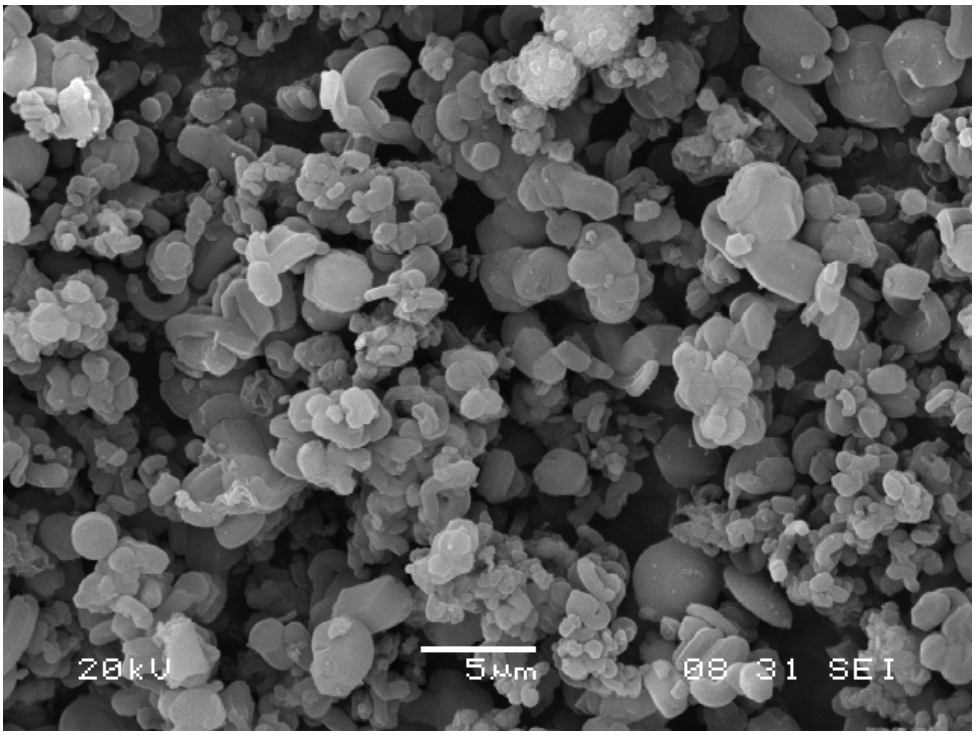

Figure 5.10
SEM image of parent SBA-15.

5.1.4 Chemical analysis

The Mo content in the catalysts was analyzed by X-ray fluorescence spectroscopy. All catalysts prepared by thermal spreading (except that supported on Na-Beta) exhibited Mo content corresponding to amount of Mo that was used for the preparation of the catalysts.

From Tab. 5.4 it is seen that when the incipient wetness method was used for the impregnation of MCM-41 with ammonium heptamolybdate water solution, less than 40 % of Mo used for the preparation was present in the catalyst. Better results were achieved when dimethylformamide solution of $MoO_2(acac)_2$ was employed for the preparation of the catalyst using the same method (about 80 % of Mo remained in the catalyst). The difference between target and actual loading might be connected with residues of counter anions and ligands still present on the surface of the catalysts and/or with the presence of residual amount of water on the surface of the support before the impregnation. In the case of H-Beta zeolite impregnated with ammonium heptamolybdate water solution, the Mo content was even much lower than the desired Mo loading (1.5 vs. 6 wt. % Mo, i.e. 25 %).

Table 5.4

Comparison of Mo loading calculated from amount of Mo used for catalysts preparation with Mo loading according to XRF chemical analysis. * = impregnation from DMF solution, ** = impregnation from water solution, † = according to Higashimoto et al. [112], ‡ = modification of the homogeneous precipitation method.

Catalyst	Preparation Method	Mo Loading Calculated (wt. % Mo)	Mo Loading Found (wt. % Mo)
4.7impMo(acac)/MCM-41	incipient wetness *	6	4.7
2.3impAHM/MCM-41	incipient wetness **	6	2.3
1.4, 3.1Hi-Mo-MCM-41	direct synthesis of Mo-MCM-41 †	4, 7	1.4, 3.1
0.8DS-Mo-MCM-41	direct synthesis of Mo-MCM-41 ‡	6	0.8
1.5impAHM/H-Beta	incipient wetness **	6	1.5
2.1MoO_3/Na-Beta	thermal spreading	6	2.1

As for the direct synthesis of Mo-MCM-41, the procedure according to Higashimoto et al. [112] led to higher Mo content in the catalyst (35 – 45 % of Mo amount used for the synthesis) in comparison with modified homogeneous precipitation method (13 % of Mo amount used for the synthesis). However, in both cases the Mo content is substantially lower than desired 6 wt. % Mo loading (Tab. 5.4). Therefore, it is assumed that not all molybdenum atoms incorporate into the structure of MCM-41 during the synthesis. Thus, it was shown that the thermal spreading of MoO_3 or $MoO_2(acac)_2$ over MCM-41 was the only method that did not lead to loss of Mo content during catalyst preparation.

In the case of Schrock carbene grafted on MCM-41 and SBA-15, the Mo content as determined by ICP AES was in accordance with amount of Mo used for catalysts preparation (loading 1 wt. % Mo).

5.2 Metathesis of linear alkenes

Generally, C_2 – C_{18} alkenes are used as a feed in industrial processes utilizing alkene metathesis [18]. The metathesis of 1-alkenes over heterogeneous catalysts is a subject of primary interest, since it yields simultaneously ethylene, which is a valuable monomer, and internal alkenes with long chain that can be easily separated from the

reaction mixture [120]. Therefore, 1-octene and 1-decene were chosen as model compounds in this study.

For the preparation of the catalysts, thermal spreading of MoO_3 was used. With MoO_3/MCM-41 catalyst, the optimization of catalyst activation (Chapter 5.2.1), reaction temperature (Chapter 5.2.2), and molybdenum loading (Chapter 5.2.3) was done; moreover, deactivation and reusability of this catalyst was investigated (Chapter 5.2.4).

In addition, the influence of Mo compound and method used for catalyst preparation on its catalytic properties was described for MCM-41 based catalysts (Chapter 5.2.5). Finally, different types of supports were used for the preparation of the catalysts (Chapter 5.2.6).

As for the repeatability of the catalytic testing, the standard deviation of conversion and selectivity determined from three experiments conducted under the same conditions was lower than 2 %.

5.2.1 Effect of catalyst activation

As moisture (water) and oxygen are catalytic poisons for heterogeneous metathesis catalysts [26], it is necessary to dehydrate the catalyst before the metathesis reaction and to put it under the inert atmosphere. During the pretreatment, the catalysts are usually activated in a stream of dry air or argon and/or in vacuum at temperatures between 500 and 600 °C for several hours, and placed under the atmosphere of dry nitrogen or argon [35,36,49,121,122].

In order to optimize the activation procedure, several catalytic experiments with activation differing in temperature, duration, and atmosphere used were performed. After activation, the catalyst was treated with dried Ar for 10 min at given temperature, cooled down to the reaction temperature in a stream of argon and degassed until the pressure of 0.1 Pa was attained. The reaction proceeded under Ar atmosphere. The activity of the catalysts is compared in terms of turn-over frequency (*TOF*). The *TOF* after 200 min of the reaction (TOF_{200}) was estimated from the conversion of 1-decene achieved at the same time according to Eq. 3.

Fig. 5.11 shows the activities and selectivities reached in metathesis of 1-decene at 60 °C with 12MoO_3/MCM-41 catalyst after different activation procedures. It is seen that (i) with increasing time of the activation at 500 °C the activity was increasing, (ii) the shortening of the activation time to 10 min led to decrease in both activity and

selectivity, (iii) similar activity was reached after activation at 300 °C and at 500 °C for 30 min; however, the selectivity to 9-octadecene was higher in latter case, (iv) neither activation under Ar or O_2 nor the elevated activation temperature (600 °C) led to increase in activity or selectivity in comparison with activation at 500 °C in a stream of air.

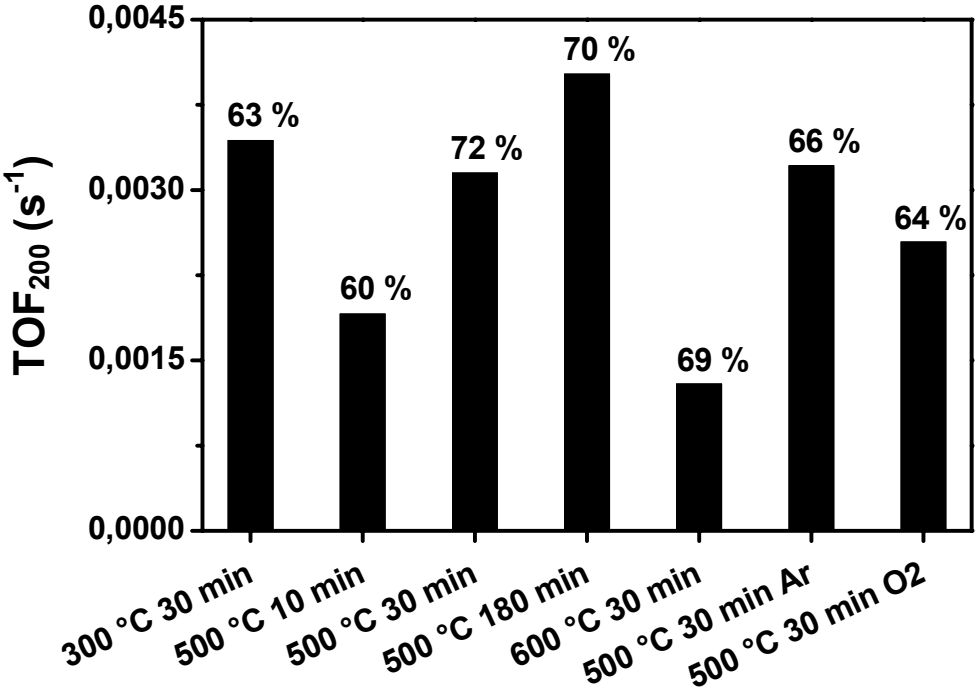

Figure 5.11

Dependence of specific activity (expressed as TOF_{200}) on the method of catalyst activation. Activation proceeded in a stream of dry air (not indicated), argon (Ar) or oxygen (O_2). Catalyst $12MoO_3$/MCM-41, metathesis of 1-decene at 60 °C. Selectivity to 9-octadecene is shown in %.

In order to obtain an efficient catalyst within reasonable activation time, treatment of the catalyst in a stream of air at 500 °C for 30 min was chosen as the standard activation procedure from above-mentioned possibilities.

5.2.2 Effect of the reaction temperature

Molybdenum oxide catalysts are usually active at temperatures from 100 to 200 °C [1,18]. Nevertheless, the utilizing of mesoporous silica as a support allowed us designing new type of molybdenum catalyst that is highly active under mild reaction conditions. Conversions and selectivities achieved with MoO_3/MCM-41 catalyst in

1-octene metathesis in the temperature range from 30 to 60 °C are shown in Fig. 5.12. The conversion achieved after 360 min of the reaction was increasing with increasing reaction temperature (33, 40, and 48 % for 30, 40, and 60 °C, respectively). However, selectivity was slightly decreasing in the same order (93, 86, and 78 %, respectively). This indicates that the rate of parallel isomerization reactions increased with temperature more steeply than the rate of metathesis.

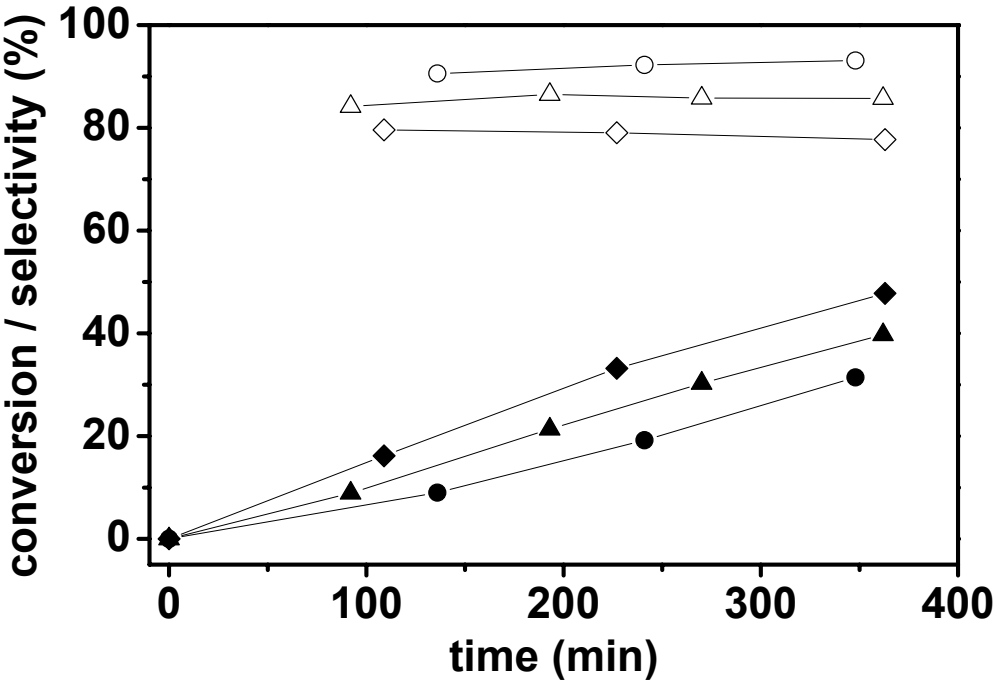

Figure 5.12

Conversion of 1-octene (solid symbols) and selectivity to 7-tetradecene (open symbols) dependence on time for reaction temperature 30 (●), 40 (▲), and 60 °C (◆). Metathesis of 1-octene over 12MoO_3/MCM-41.

With respect to both activity and selectivity of the catalyst, 40 °C seems to be the optimum reaction temperature. This temperature is much lower than that usually used in both academia and industry for molybdenum metathesis catalysts, what may be of great advantage.

5.2.3 Effect of molybdenum content

Conversions and selectivities achieved with MoO_3/MCM-41 catalysts with different Mo loading are shown in Fig. 5.13.

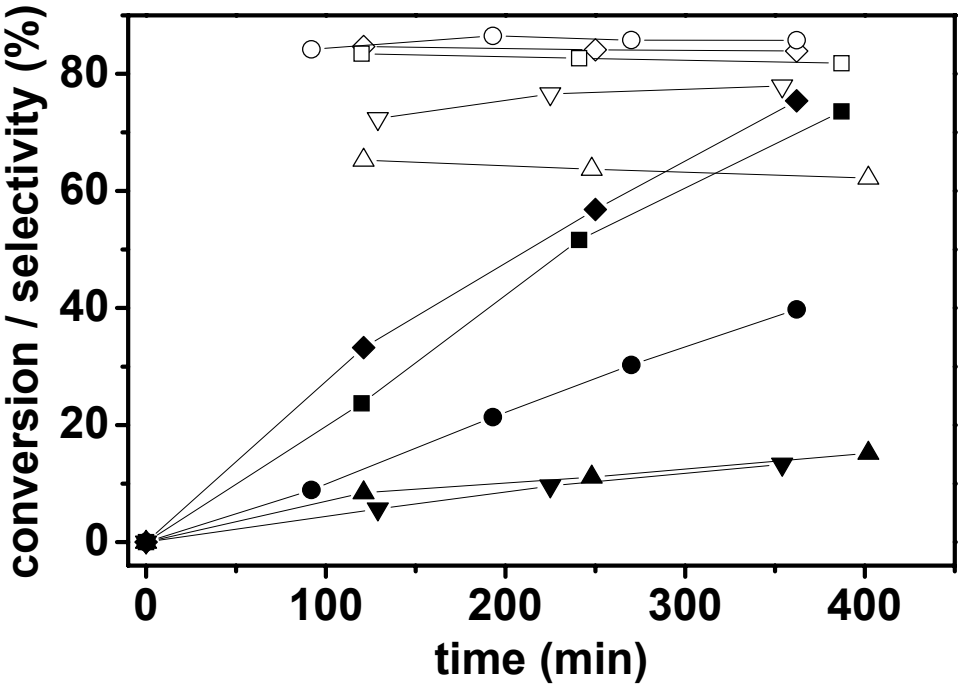

Figure 5.13

Conversion of 1-octene (solid symbols) and selectivity to 7-tetradecene (open symbols) dependence on time for: $4MoO_3$/MCM-41 (▲), $6MoO_3$/MCM-41 (◆), $8MoO_3$/MCM-41 (■), $12MoO_3$/MCM-41 (●) and $16MoO_3$/MCM-41 (▼); metathesis of 1-octene at 40 °C [114].

It is clearly seen that highest conversion was accomplished with $6MoO_3$/MCM-41, followed by $8MoO_3$/MCM-41 and $12MoO_3$/MCM-41 (75, 70, and 40 % in 360 min, respectively). The catalysts with the lowest and the highest loading reached only low conversion (14 and 13 % for $4MoO_3$/MCM-41 and $16MoO_3$/MCM-41, respectively).

The low conversion achieved with $4MoO_3$/MCM-41 may be explained by low concentration of the active sites, especially if we take into account that generally only very small part (less than 1 %) of molybdenum atoms present in the catalyst is transformed into metallocarbene active sites [23]. On the other hand, in the case of $16MoO_3$/MCM-41, the presence of molybdenum in the form of MoO_3 crystallites (Chapter 5.1.1) that are catalytically practically inactive may deteriorate the catalytic activity.

The low selectivity of $4MoO_3$/MCM-41 and $16MoO_3$/MCM-41 catalysts (63 and 78 %, respectively) is in contrast to high selectivities achieved with all other catalysts

(84, 82, and 86 % for $6MoO_3$/MCM-41, $8MoO_3$/MCM-41, and $12MoO_3$/MCM-41, respectively). This lower selectivity may be caused by low rate of metathesis in contrast to the rate of double-bond shift isomerization, which results in a higher amount of C_9 – C_{13} and C_{15} by-products.

5.2.4 Deactivation and reusability

In order to investigate the deactivation of the catalysts, following test was performed with $12MoO_3$/MCM-41 in metathesis of 1-octene at 40 °C: after the steady-state conversion (approximately 90 %) was reached, a new portion of the substrate (50 % of the initial amount) was added to the reaction mixture (Fig. 5.14).

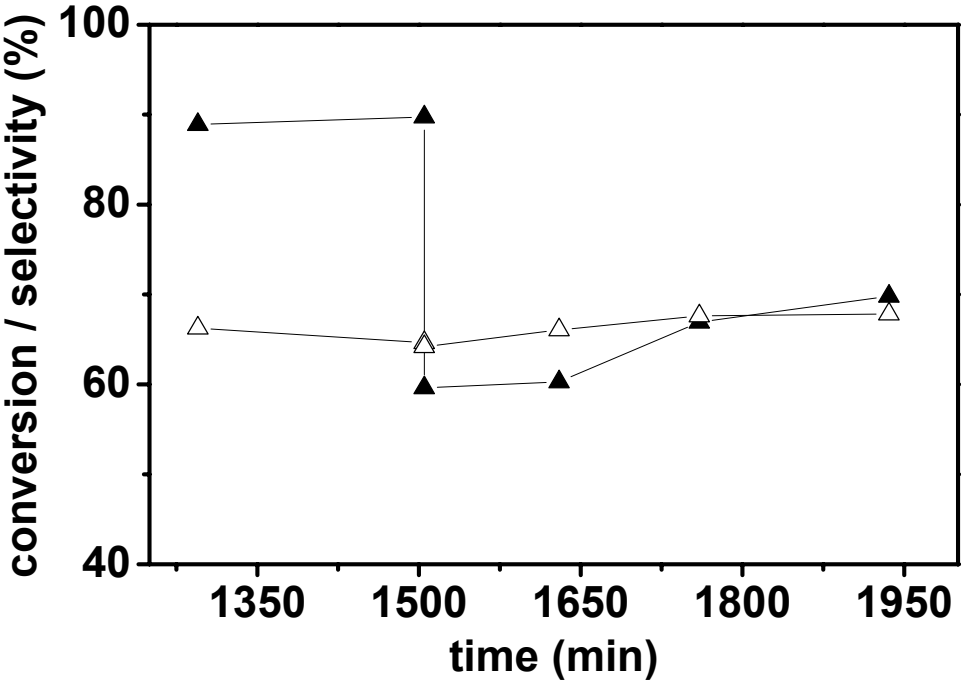

Figure 5.14

Conversion of 1-octene (solid symbols) and selectivity to 7-tetradecene (open symbols) dependence on time for $12MoO_3$/MCM-41; at τ = 1 505 min new portion of substrate was added. Reaction temperature 40 °C.

The activity of the catalyst after the addition was considerably lower (~ 20 %) as compared with the activity at the beginning of the catalytic test, whereas the selectivity was not substantially changed. This decrease in the catalyst activity indicates the partial deactivation of the catalyst. In order to find the possible reasons that caused the catalyst

deactivation, the catalyst after the reaction was characterized using several methods as described below.

To check the structural stability of the catalyst during the reaction, X-ray diffraction patterns of $12MoO_3$/MCM-41 catalyst before and after the reaction were recorded (Fig. 5.15). The spent catalyst was separated by decantation and transferred to X-ray diffractometer in air.

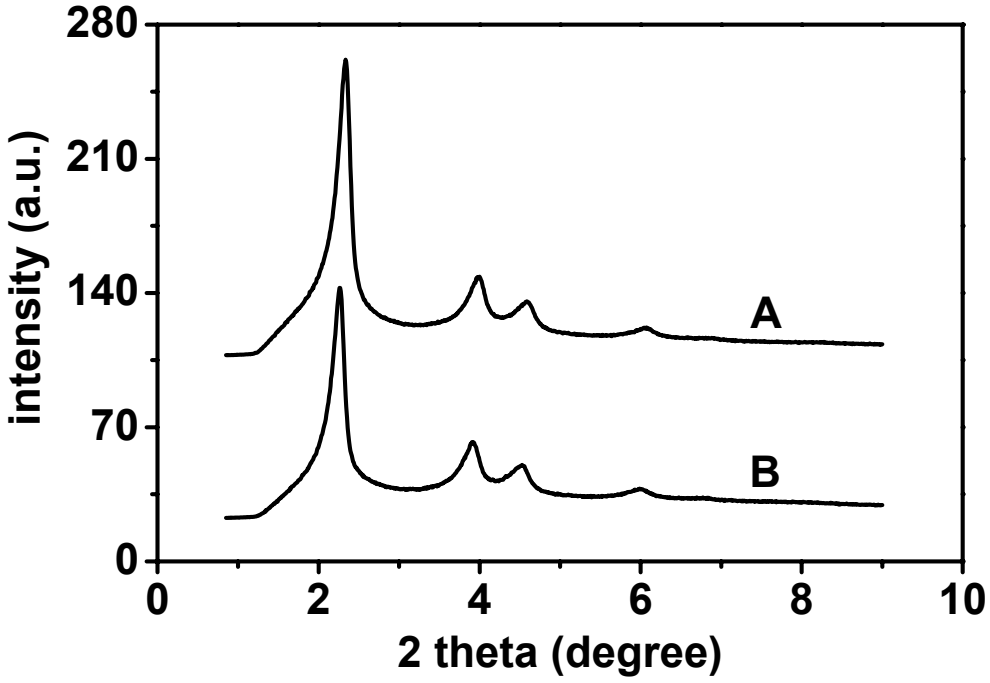

Figure 5.15

X-ray diffraction patterns of $12MoO_3$/MCM-41 before the reaction (A) and after 375 min of the metathesis of 1-octene at 40 °C (B). For clarity, individual diffractograms are vertically shifted.

From Fig. 5.15B, it is clearly seen that after 375 min of the metathesis of 1-octene at 40 °C the mesoporous structure was preserved. However, a slight shift to lower 2 theta angles is observed for all diffraction lines.

To verify possible changes in dispersion of molybdenum during the catalytic reaction, X-ray diffraction patterns of $12MoO_3$/MCM-41 catalyst before the reaction (unactivated sample) and at different reaction times were measured (Fig. 5.16). The reaction was stopped at given reaction time and the catalyst separated by decantation was transferred to X-ray diffractometer in air. It is evident that there are some changes

in the dispersion of Mo. The intensity of diffraction lines corresponding to crystalline molybdenum oxide is higher in the case of the catalyst involved in the reaction as compared with the catalyst before the reaction. As the activation of the catalyst (heating at 500 °C) can hardly contribute to the creation of MoO_3 crystallites, it indicates that some aggregation of Mo species takes place during the reaction and that the amount of crystalline molybdenum oxide on the surface of the catalyst increased after the beginning of the reaction. As the crystalline molybdenum oxide is catalytically practically inactive (Chapter 5.2.6), the redispersion of molybdenum in the course of the reaction might be responsible for the decrease in catalytic activity. On the other hand, practically no evolution of the intensity of diffraction lines of MoO_3 was observed with increasing reaction time.

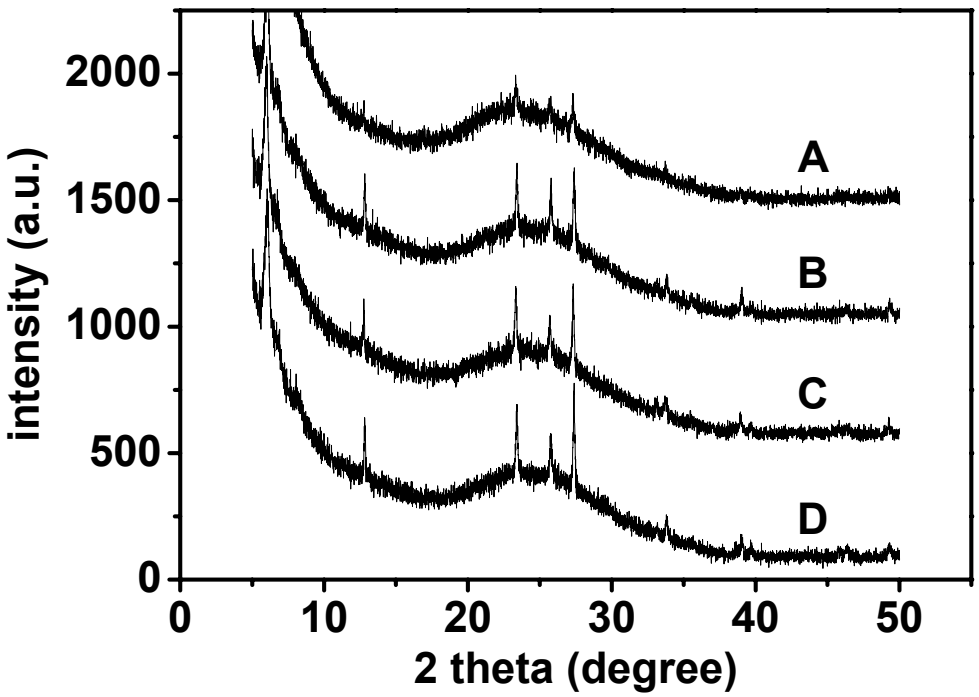

Figure 5.16

X-ray diffraction patterns of $12MoO_3$/MCM-41 before the reaction (A) and after 120 (B), 240 (C), and 375 min of the metathesis of 1-octene at 40 °C (D). For clarity, individual diffractograms are vertically shifted.

In order to understand the deactivation processes, nitrogen adsorption isotherms of spent catalysts were also measured. MoO_3/MCM-41 catalysts with different loadings were employed in metathesis of 1-octene at 40 °C. At given reaction time, the reaction

was stopped and the catalyst separated by decantation was washed three times with 5 mL of pentane and dried at ambient temperature in air. The adsorption data are compared with that of fresh catalysts before activation (Tab. 5.5).

Table 5.5

Texture characteristics of MCM-41 supported catalysts prepared by thermal spreading of MoO_3 determined from nitrogen adsorption isotherms. The catalysts were analyzed before the reaction (unactivated) and after the reaction (reaction time indicated in min).

Sample	S_{BET} (m^2/g)	d (nm)	V_{meso} (cm^3/g)
4MoO_3/MCM-41 before	874	3.0	0.658
4MoO_3/MCM-41 (120 min)	541	3.0	0.401
8MoO_3/MCM-41 before	875	2.9	0.635
8MoO_3/MCM-41 (120 min)	724	3.0	0.542
12MoO_3/MCM-41 before	831	2.7	0.568
12MoO_3/MCM-41 (120 min)	709	3.0	0.527
12MoO_3/MCM-41 (240 min)	723	3.0	0.534
12MoO_3/MCM-41 (375 min)	735	2.9	0.541
16MoO_3/MCM-41 before	754	2.7	0.511
16MoO_3/MCM-41 (120 min)	578	2.8	0.398

For all spent catalysts, a decrease in the pore volume and the surface area was observed in comparison with fresh catalysts. These changes might indicate the presence of some organic deposits adsorbed on the walls of the MCM-41 support that are responsible for the decreased activity of the catalysts.

Similarly, the loss in the surface area and pore volume after the reaction (especially when spiked feed was used) was observed for CoO/MoO_3/Al_2O_3 catalyst employed in metathesis of 1-octene [49]. In ref. [49], the decrease in the catalytic activity was explained as a result of the adsorption of heavy molecular weight compounds on the surface of the catalyst. Moreover, the results of carbon content analysis showed that spent CoO/MoO_3/Al_2O_3 catalysts contained considerably higher amount of carbon in comparison with fresh catalyst. Finally, an exothermal peak at a temperature between 400 and 430 °C was observed in the differential thermogravimetrical pattern of the spent CoO/MoO_3/Al_2O_3 catalysts. This weight loss was ascribed to burn-off of the carbon from the heavy molecular weight compounds

[49]. The mechanism of deactivation was described in ref. [123], where the polymerization of alkenes on acidic sites of the catalyst was shown to lead to the formation of high molecular weight polynuclear aromatics that condense as carbonaceous material on the catalyst surface.

Nevertheless, in our case, only C–H stretching vibrations corresponding to CH_3– and CH_2– groups were observed in the DR FTIR spectra of spent $12MoO_3$/MCM-41 catalyst. As the catalyst was washed three times with 5 mL of pentane and dried at ambient temperature in air before the measurement, the C–H stretching bands in the FTIR spectra of the spent catalyst can be explained by the presence of residual amounts of pentane. On the other hand, the absence of any other bands indicates that no high molecular weight polyaromatics were present on the surface of the catalyst.

A lower tendency to deactivation due to the formation of aromatic by-products may be caused by lower acidity of the MCM-41 (i.e. silica) supported catalyst in comparison with an alumina-supported one. On the other hand, the deactivation might be connected with the presence of trace amounts of water in the reaction mixture. Water can act as a catalytic poison, causing the deactivation of the catalyst via destruction of metallocarbene active sites (e.g. oxidation of carbenes to carbonyl compounds) or by bonding strongly to the metal centre, preventing thus the coordination of the alkene [124]. In the case of $CoO/MoO_3/Al_2O_3$ catalyst employed in metathesis of 1-octene [49], the deactivation by water seemed to be mainly related to molecular structural changes of the catalyst rather than accumulation of carbonaceous deposits as well.

It can be concluded that the structural changes of Mo species are probably more critical for the deactivation of MoO_3/MCM-41 catalysts than the formation of polyaromatic by-products on the surface of the catalyst. Thus, preserving proper oxidation state and dispersion of molybdenum is crucial to maintain high catalytic activity.

In metathesis of 1-octene over $12MoO_3$/MCM-41 catalyst, no leaching of molybdenum species was observed and the concentration of Mo in the products determined by ETA AAS was lower than 0.005 ppm. Typically, supported molybdenum metathesis catalysts are regenerated at 500 - 550 °C in a stream of oxygen or air, enabling both combustion of heavy molecular weight compounds responsible for deactivation and reoxidation of reduced Mo species [17,49]. If the spent $12MoO_3$/MCM-41 catalyst was washed with hexane and reactivated at 500 °C for 0.5 h

under the stream of dry air, practically the same conversion and selectivity was achieved as with fresh catalyst (Fig. 5.17).

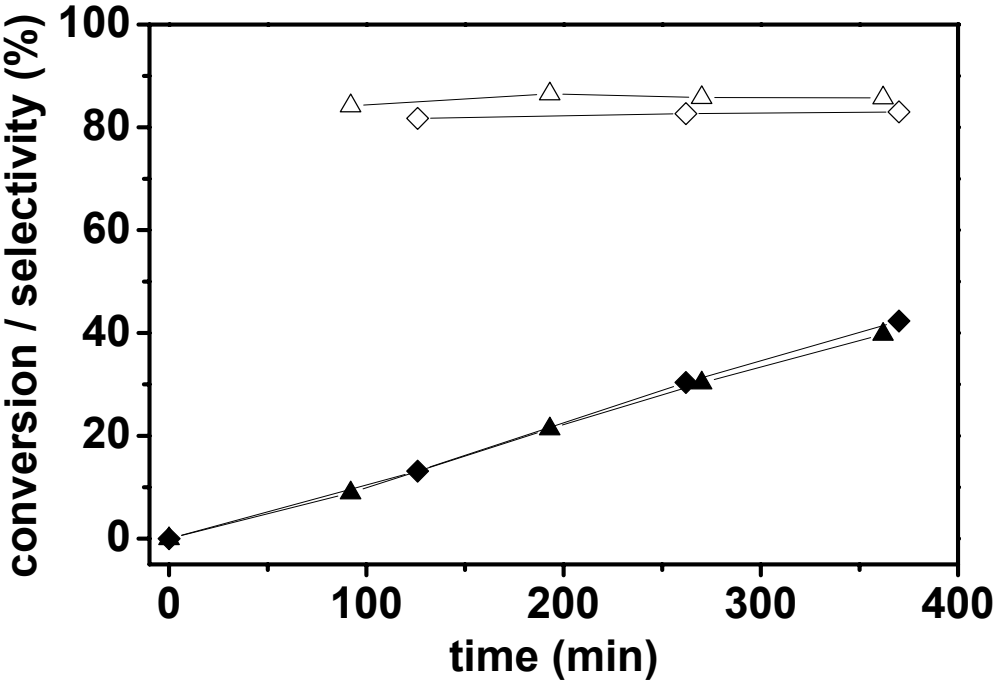

Figure 5.17

Conversion of 1-octene (solid symbols) and selectivity to 7-tetradecene (open symbols) dependence on time for $12MoO_3$/MCM-41: first (▲), and second (◆) run; metathesis of 1-octene at 40 °C.

It may indicate that during reactivation, possible polymeric deposits are burned out and/or the structure of surface Mo species is restored while the mesoporous structure of the catalyst is preserved.

5.2.5 Effect of catalyst preparation

The activity and selectivity of MCM-41 supported catalyst prepared by thermal spreading of MoO_3 was compared with that of the catalysts prepared by different methods: thermal spreading of $MoO_2(acac)_2$ over MCM-41, impregnation of MCM-41 with $MoO_2(acac)_2$ dimethylformamide solution, and impregnation of MCM-41 with ammonium heptamolybdate water solution. The amount of Mo compound used for the preparation of the catalysts corresponded to desired 6 wt. % Mo loading. However, except the thermal spreading method, the Mo content according to the chemical analysis was lower (2.3 wt. % Mo for 2.3impAHM/MCM-41 and 4.7 wt. % Mo in the case of

4.7impMo(acac)/MCM-41, Chapter 5.1.4). The conversions of 1-octene and selectivities to 7-tetradecene achieved with individual catalysts are displayed in Fig. 5.18.

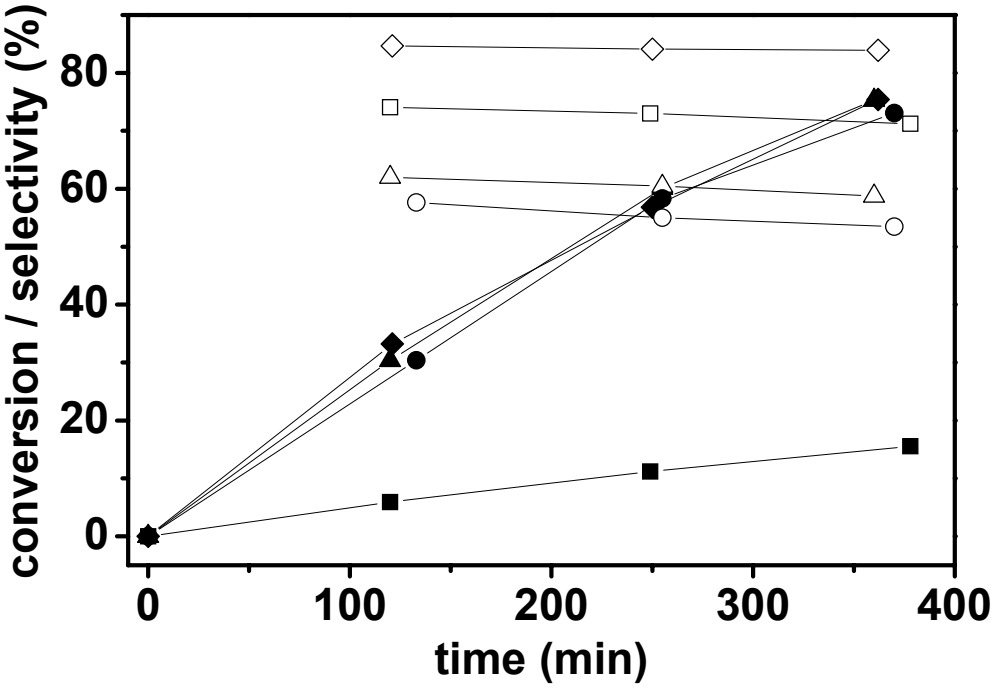

Figure 5.18

Conversion of 1-octene (solid symbols) and selectivity to 7-tetradecene (open symbols) dependence on time for 2.3impAHM/MCM-41 (■), 4.7impMo(acac)/MCM-41 (●), 6Mo(acac)/MCM-41 (▲), and 6MoO_3/MCM-41 (◆). Reaction temperature 40 °C.

It is clearly seen that the lowest conversion was reached with 2.3impAHM/MCM-41 (15 % after 360 min of the reaction). This may be caused by low Mo content due to the preparation procedure. On the other hand, the conversions achieved with all other catalysts are much higher, but comparable (75 % after 360 min of the reaction).

This high conversion was achieved with both $MoO_2(acac)_2$ catalysts despite the fact that significant decrease (~ 40 %) in both surface area and pore volume was detected during their preparation from MCM-41 (Chapter 5.1.2). Moreover, the catalyst prepared by impregnation had lower Mo content (4.7 wt. % Mo). On the other hand, the catalytic activity of 2.3impAHM/MCM-41 was even lower than it would correspond to the difference in Mo content in comparison with other catalysts in Fig. 5.18. This might be connected with the fact that in this case the decrease in the surface area and the pore

volume in comparison with parent MCM-41 was higher (more than 50 %) and in contrary to 4.7impMo(acac)/MCM-41 it was also accompanied with the reduction in the pore size (Chapter 5.1.2).

Surprisingly, the conversion achieved with the catalyst prepared by thermal spreading of MoO_3 is practically the same as that one reached with both $MoO_2(acac)_2$ catalysts, which are known to possess highly dispersed Mo species and thus supreme catalytic activity [20,39,40]. What is more, the selectivity to main metathesis product, 7-tetradecene, is the highest in the case of $6MoO_3$/MCM-41 (85 % after 360 min of the reaction), but substantially lower in the case of both $MoO_2(acac)_2$ catalysts (62 % and 58 % for 6Mo(acac)/MCM-41 and 4.7impMo(acac)/MCM-41, respectively), being 74 % for 2.3impAHM/MCM-41. Thus, we can conclude that the highest conversion and the highest selectivity at the same time were accomplished with $6MoO_3$/MCM-41. By employing the thermal spreading of MoO_3, one can achieve low-cost (in comparison with expensive organometallic precursors) and environmentally friendly (in comparison with impregnation methods) preparation of highly active and selective catalyst.

In addition to the thermal spreading and the incipient wetness method, molybdenum catalysts supported on mesoporous silica can be also obtained via direct incorporation of Mo atoms during the synthesis of mesoporous molecular sieve. The Mo-MCM-41 catalysts were synthesized according to recently reported method of Higashimoto et al. [112] and via modified homogeneous precipitation method as described in Chapter 4.2.3. The amount of Mo used for the preparation of the catalysts corresponded to the target loading 6 wt. % Mo; however, the Mo content according to the chemical analysis was lower (see Chapter 5.1.4).

Although there are substantial differences in Mo content, from Fig. 5.19 it is visible that high conversions were achieved with two types of Mo-MCM-41 catalysts: 45 % after 360 min of the reaction with the 3.1Hi-Mo-MCM-41 and 56 % at the same time with 0.8DS-Mo-MCM-41. It is remarkable that with the catalyst synthesized via modified homogeneous precipitation method possessing only 0.8 wt. % Mo content it was possible to achieve such high conversion. However, this conversion is still lower in comparison with that one accomplished with $6MoO_3$/MCM-41 catalyst prepared by thermal spreading (75 % after 360 min of the reaction). Moreover, there is significant difference in selectivity: whereas 3.1Hi-Mo-MCM-41 exhibited high selectivity (97 % after 360 min of the reaction), with 0.8DS-Mo-MCM-41 the selectivity was rather low (44 % at the same time).

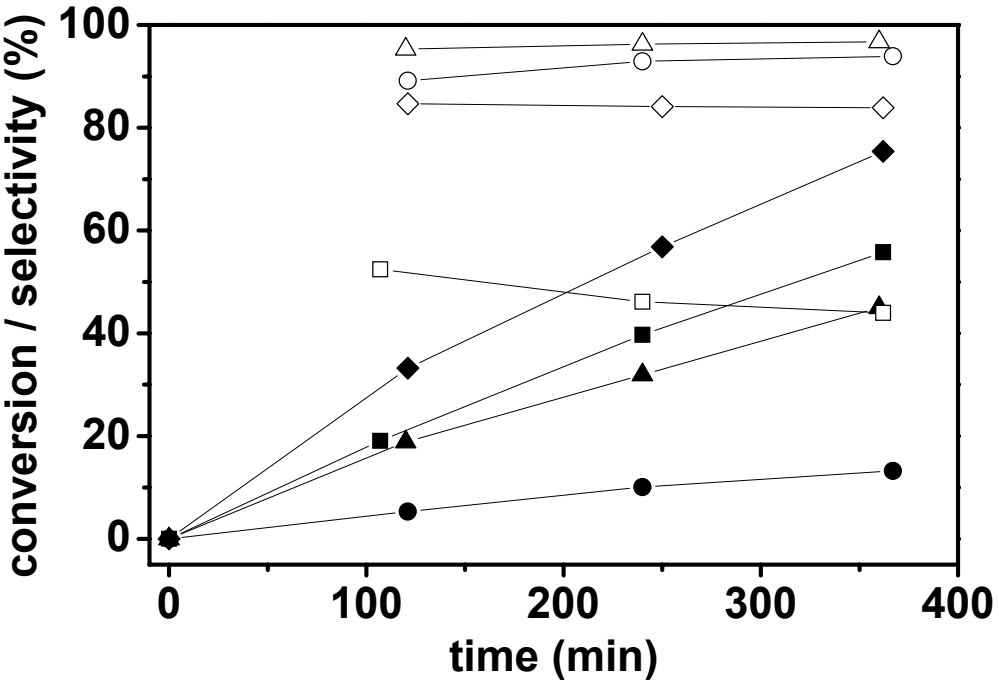

Figure 5.19

Conversion of 1-octene (solid symbols) and selectivity to 7-tetradecene (open symbols) dependence on time for: 1.4Hi-Mo-MCM-41 (●), 3.1Hi-Mo-MCM-41 (▲), 0.8DS-Mo-MCM-41 (■), and $6MoO_3$/MCM-41 (◆). Reaction temperature 40 °C.

Finally, with 1.4Hi-Mo-MCM-41, which was the highest loaded catalyst used in ref. [112], the conversion achieved after 360 min of the reaction was much lower in comparison with other catalysts (13 %).

Thus, we can conclude that although 3.1Hi-Mo-MCM-41 allowed achieving very high selectivity (97 %) and, with respect to low Mo content, surprisingly high conversion (45 % after 360 min), $6MoO_3$/MCM-41 still represents more valuable alternative (75 % conversion with 85 % selectivity after 360 min of the reaction). Therefore, the thermal spreading of MoO_3 represents favorable method for the preparation of supported molybdenum catalysts.

5.2.6 Effect of the support

Negligible activity in metathesis was found for parent siliceous supports. For example, with pure siliceous MCM-41, only 0.7 % conversion of 1-octene (mainly to its isomers and dimers) was achieved after 360 min of the reaction at 40 °C. In addition, when unsupported, bulk molybdenum oxide was used as a catalyst in metathesis of

1-octene at 40 °C, only 0.1 % conversion was reached in 360 min. Thus, both parent supports and MoO_3 are practically inactive in investigated reaction.

Fig. 5.20 shows the conversions of 1-octene and selectivities to 7-tetradecene achieved with catalysts prepared by thermal spreading of MoO_3 over conventional silica (Merck, Silica gel 40), MCM-41, Al-MCM-41 (Si/Al = 30) and organized mesoporous alumina (OMA). It is seen that (i) the conversion reached with $8MoO_3$/MCM-41 (70 % in 360 min) is about 9 times higher than that one accomplished with $8MoO_3/SiO_2$ and $8MoO_3$/OMA, (ii) with $8MoO_3$/Al-MCM-41 the reaction proceeds even faster than with $8MoO_3$/MCM-41, but the selectivity is much lower (20 %), (iii) the highest selectivity exhibited $8MoO_3/SiO_2$ (92 %) followed by $8MoO_3$/MCM-41 (82 %).

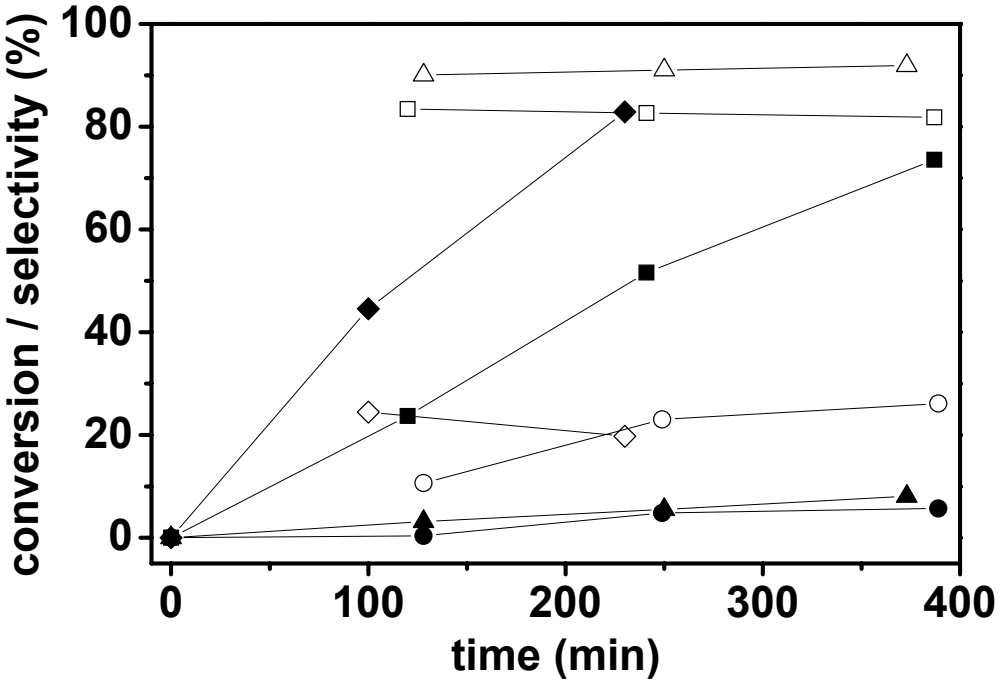

Figure 5.20

Conversion of 1-octene (solid symbols) and selectivity to 7-tetradecene (open symbols) dependence on time for: $8MoO_3$/OMA (●), $8MoO_3/SiO_2$ (▲), $8MoO_3$/MCM-41 (■), and $8MoO_3$/Al-MCM-41 with Si/Al = 30 (◆). Metathesis of 1-octene at 40 °C.

The low selectivities achieved with $8MoO_3$/Al-MCM-41 and $8MoO_3$/OMA in comparison with $8MoO_3/SiO_2$ and $8MoO_3$/MCM-41 are probably connected with high acidity of the Al-containing supports, which increased the rate of double-bond shift isomerization of 1-octene in comparison with fully siliceous supports. Thus, the most

suitable catalyst is MoO_3 supported on pure mesoporous silica, which allows achieving high conversion of 1-octene together with high selectivity to 7-tetradecene at the same time.

Catalysts prepared by thermal spreading of molybdenum oxide over different types of mesoporous silicas and over conventional silica (Merck, Silica gel 40) are compared in Fig. 5.21. It is clearly seen that the conversion of 1-octene achieved after 360 min of the reaction is decreasing in order $8MoO_3$/MCM-41 > $8MoO_3$/MCM-48 > $8MoO_3$/SBA-15 > $8MoO_3/SiO_2$ (70, 32, 18 and 8 %, respectively). All catalysts supported on mesoporous silica reached higher conversions than $8MoO_3/SiO_2$.

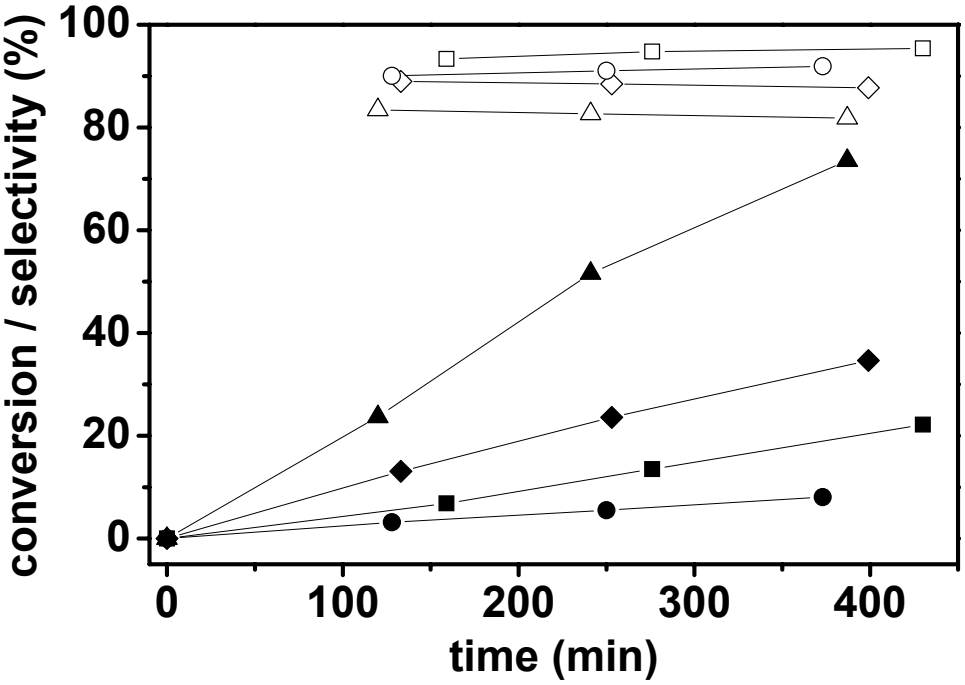

Figure 5.21

Conversion of 1-octene (solid symbols) and selectivity to 7-tetradecene (open symbols) dependence on time for: $8MoO_3/SiO_2$ (●), $8MoO_3$/SBA-15 (■), $8MoO_3$/MCM-48 (◆), and $8MoO_3$/MCM-41 (▲). Metathesis of 1-octene at 40 °C.

For $8MoO_3$/MCM-41, the conversion achieved after 360 min of the reaction was more than eight times higher in comparison with $8MoO_3/SiO_2$. Lower difference in 1-octene conversion was found between $6MoO_3$/MCM-41, the most active MoO_3/MCM-41 catalyst, and $6MoO_3/SiO_2$ (1-octene conversions 75 and 20 % after 360 min of the reaction, respectively, with selectivity to 7-tetradecene 84 and 93 %; not shown in Fig.).

Thus, in terms of turn-over frequency (TOF_{120}), $6MoO_3$/MCM-41 was about four times more active than $6MoO_3/SiO_2$ (TOF_{120} 0.0141 and 0.0034 s^{-1}, respectively).

Surprisingly, $8MoO_3$/MCM-41 exhibited higher 1-octene conversion than $8MoO_3$/SBA-15, although the latter possessed about two times larger pores (Chapter 5.1.2). In addition, the same was the truth for $8MoO_3$/MCM-41 in comparison with $8MoO_3$/MCM-48 possessing approximately the same pore diameter, but three-dimensional array of intersecting channels. Therefore, it seems that diffusion limitations do not play the decisive role in catalytic activity.

In contrast, in metathesis of 1-octene over molybdenum catalysts supported on hexagonal mesoporous silica (HMS) Ookoshi and Onaka [35] observed an increase in the initial reaction rate with increasing alkyl chain of the amine used in HMS preparation (i.e. probably with increasing pore size; pore diameter determined from nitrogen adsorption isotherms was not mentioned in this paper). However, these HMS supported catalysts with larger pores suffered from a high rate of deactivation. As a result, higher final yield of 7-tetradecene was reported for the catalyst with lower pore size. The authors ascribed the rapid deactivation to different particle size of the catalysts. They supposed that shorter channels in smaller particles caused lower rate of deactivation of Mo sites or less blockage of the pores by polymeric side products. In our case, however, the average particle size of the supports was between 1 and 3 μm (Chapter 5.1.3), i.e. much higher than that of all HMS supports (50 – 700 nm). Nevertheless, rapid deactivation of the catalysts as in ref. [35] was not observed in any case. For example, with $8MoO_3$/MCM-41 the conversion of 1-octene gradually increased up to 89 % at 1 075 min with selectivity to 7-tetradecene being 75 % at the same time (not shown in Fig. 5.21). Therefore, there must be another reason for lower conversions achieved with $8MoO_3$/MCM-48 and $8MoO_3$/SBA-15 in comparison with $8MoO_3$/MCM-41.

The selectivity of individual catalysts to 7-tetradecene practically did not change with conversion (Fig. 5.21). An increase in the selectivity was observed in order $8MoO_3$/MCM-41 < $8MoO_3$/MCM-48 < $8MoO_3/SiO_2$ < $8MoO_3$/SBA-15 (82, 88, 92 and 95 %, respectively), i.e. in the order of decreasing activity of the catalysts (with the exception of MoO_3/SiO_2). Although the selectivity of $8MoO_3$/MCM-41 was lower in comparison with $8MoO_3$/MCM-48 and $8MoO_3$/SBA-15, its supreme catalytic activity turns it into the most interesting system. Moreover, majority of side products (namely

$C_{11} - C_{15}$ alkenes) can be utilized in further industrial processes following metathesis [49].

In order to check the effect of molybdenum loading, a series of MCM-48 and SBA-15 supported catalysts with Mo content in the range from 4 to 16 wt. % Mo was prepared by thermal spreading of MoO_3. With MoO_3/MCM-48, the achieved conversions are generally lower and differences among individual catalysts are less pronounced in comparison with MoO_3/MCM-41 (Fig. 5.22).

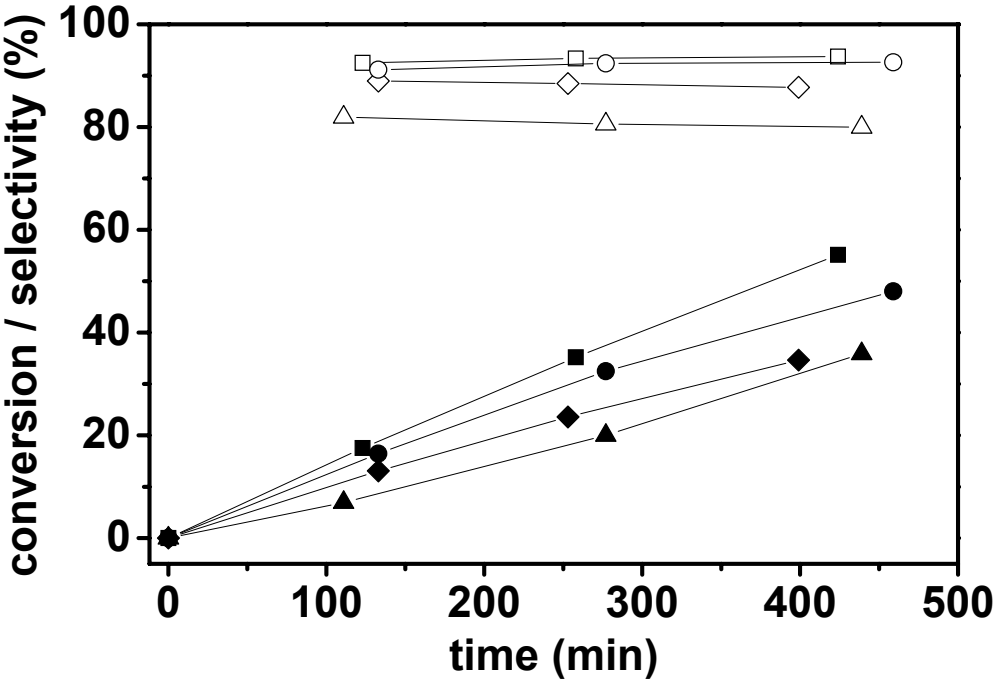

Figure 5.22

Conversion of 1-octene (solid symbols) and selectivity to 7-tetradecene (open symbols) dependence on time for: 4MoO_3/MCM-48 (▲), 8MoO_3/MCM-48 (◆), 12MoO_3/MCM-48 (■), and 16MoO_3/MCM-48 (●); metathesis of 1-octene at 40 °C [114].

The highest conversion of 1-octene was achieved with 12MoO_3/MCM-48 followed by 16MoO_3/MCM-48 (48 and 40 % conversion after 360 min of the reaction, respectively), whereas 8MoO_3/MCM-48 and 4MoO_3/MCM-48 exhibited lower conversions (32 and 28 % in 360 min, respectively). Thus, surprisingly, the highest conversion was accomplished with Mo loading two times higher than in the case of MoO_3/MCM-41.

Generally, the selectivity to 7-tetradecene is evolving only slightly with time and is a little bit higher than in the case of MoO_3/MCM-41 catalysts. The highest selectivity

was achieved with the most active $12MoO_3$/MCM-48 and $16MoO_3$/MCM-48 catalysts (94 and 92 %, respectively), being lower for $8MoO_3$/MCM-48 and especially for $4MoO_3$/MCM-48 (88 and 80 %, respectively). This lower selectivity may be caused by low rate of metathesis in contrast to the rate of double-bond shift isomerization.

Catalysts prepared by thermal spreading of MoO_3 over SBA-15 exhibited even lower conversions of 1-octene than their MoO_3/MCM-48 analogues (Fig. 5.23). Nevertheless, the conversion reached with the most active $12MoO_3$/SBA-15 (26 % in 360 min) was still higher than that achieved with MoO_3 supported on conventional silica with the same loading (21 % in 360 min, not shown in Fig.).

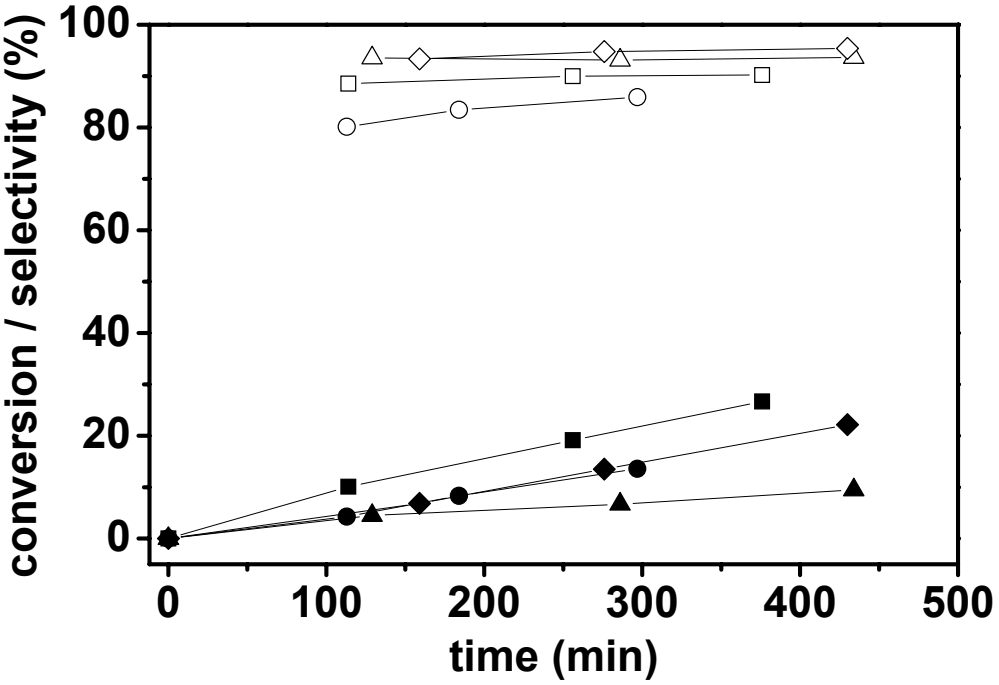

Figure 5.23

Conversion of 1-octene (solid symbols) and selectivity to 7-tetradecene (open symbols) dependence on time for: $4MoO_3$/SBA-15 (▲), $8MoO_3$/SBA-15 (◆), $12MoO_3$/SBA-15 (■), and $16MoO_3$/SBA-15 (●); metathesis of 1-octene at 40 °C [114].

As in the case of MoO_3/MCM-48 catalysts, the highest conversion over MoO_3/SBA-15 was reached with the 12 wt. % Mo loaded catalyst. The conversion of 1-octene achieved after 360 min of the reaction was decreasing in the order $12MoO_3$/SBA-15 > $8MoO_3$/SBA-15 ≈ $16MoO_3$/SBA-15 > $4MoO_3$/SBA-15 (26, 18, 17, and 8 %, respectively). The selectivity to 7-tetradecene was decreasing in the order

$8MoO_3$/SBA-15 ≈ $4MoO_3$/SBA-15 > $12MoO_3$/SBA-15 > $16MoO_3$/SBA-15 (95, 93, 90, and 87 %, respectively).

Recently, the use of zeolite Beta as a support for molybdenum metathesis catalyst was reported [125]. The catalysts prepared by impregnation of H-Beta with ammonium heptamolybdate water solution exhibited good activity in metathesis of ethene and 2-butene to propene. The highest activity was reported for the catalyst with 1 wt. % Mo; however, the selectivity to propene was low (27 %). In our case, the zeolite Beta supported catalysts were prepared by the same method as in ref. [125] and by thermal spreading of MoO_3.

The conversion reached with $6MoO_3$/H-Beta was much higher than any achieved with H-Beta supported catalysts prepared by impregnation (Fig. 5.24). This is not surprising, because although amount of Mo used for catalysts preparation corresponded to 6 wt. % Mo, in the case of the catalyst prepared by impregnation the Mo content as determined by chemical analysis (Chapter 5.1.4) was much lower (1.5 wt. % Mo).

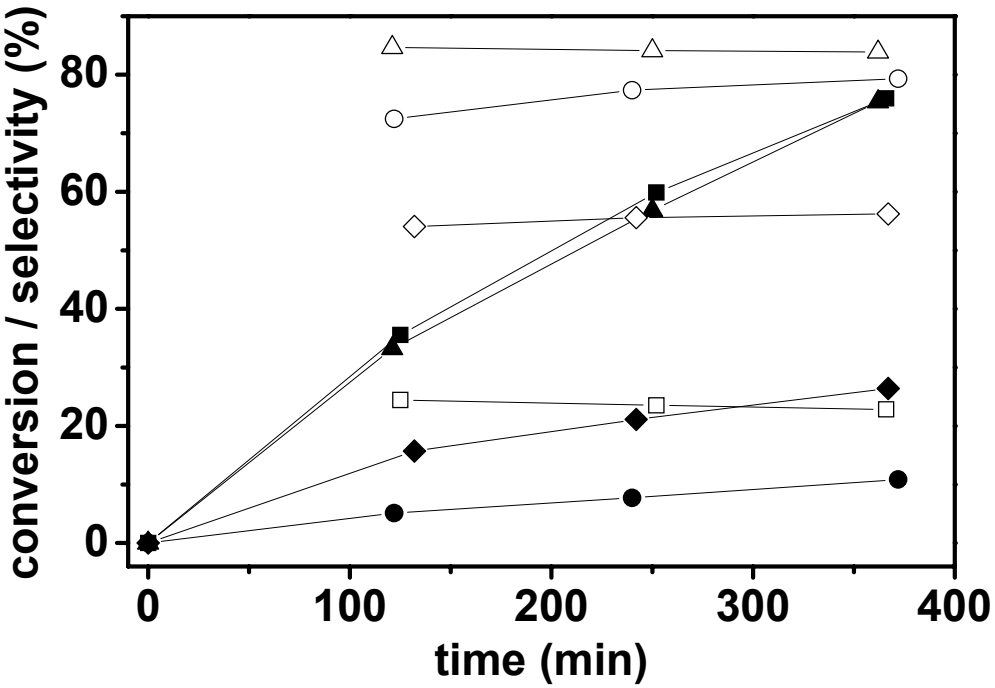

Figure 5.24

Conversion of 1-octene (solid symbols) and selectivity to 7-tetradecene (open symbols) dependence on time for: $2.1MoO_3$/Na-Beta (●), 1.5impAHM/H-Beta (◆), $6MoO_3$/MCM-41 (▲), and $6MoO_3$/H-Beta (■). Metathesis of 1-octene at 40 °C.

The conversion of 1-octene achieved with $6MoO_3$/H-Beta was even the same as the conversion accomplished with $6MoO_3$/MCM-41 catalyst (75 % after 360 min of the reaction). Nevertheless, the selectivity to 7-tetradecene achieved with $6MoO_3$/H-Beta was much lower than that of $6MoO_3$/MCM-41 (23 and 84 %, respectively).

The lower selectivity of $6MoO_3$/H-Beta was probably caused by high acidity of the support, which led to increased rate of double-bond shift isomerization. Therefore, an attempt was made to enhance the selectivity of this catalyst using Na-Beta instead H-Beta as a support. Na-Beta was obtained by ion exchange of H-Beta with 0.5 M aqueous solution of sodium nitrate at 25 °C for four times, followed by drying at 50 °C.

Indeed, the selectivity of $2.1MoO_3$/Na-Beta catalyst was much higher than that of $6MoO_3$/H-Beta (Fig. 5.24). However, the conversion of 1-octene achieved with $2.1MoO_3$/Na-Beta catalyst was low (11 % in 360 min). It can be explained by the fact that although the amount of MoO_3 used for catalysts preparation corresponded to 6 wt. % Mo loading, the Mo content in $2.1MoO_3$/Na-Beta according to the chemical analysis (Chapter 5.1.4) was only 2.1 wt. % Mo.

It was shown that there is a strong interaction between Mo species and H-Beta support and that the proper acidity and interaction of Mo species with the support are crucial for the activity in metathesis [125]. Therefore, the lower content of Mo in the catalyst and thus the low catalytic activity of $2.1MoO_3$/Na-Beta can be caused by insufficient acidity of Na-Beta, which did not allow the proper interaction of MoO_3 with the support during the preparation of the catalyst.

It can be summarized that although the $6MoO_3$/H-Beta catalyst exhibited high activity, its selectivity to 7-tetradecene was very low. Therefore, the MoO_3/MCM-41 system remains the most usable due to its high selectivity. This selectivity is very good especially if we take into account that in many industrial applications both self-metathesis and cross-metathesis products may be utilized in further processes; the selectivity of MoO_3/MCM-41 catalysts to metathesis products was always higher than 97 %.

5.3 Structure – activity relationships

Molybdenum species, which are formed on the surface of the catalyst during the thermal spreading of MoO_3, are only the precursors of the active sites. The metallocarbene active sites are formed by the interaction of these precursors with the substrate [16]. However, typically only less than 1 % of total Mo content undergoes

such transformation [23]. Therefore, the estimation of the relationships between the structure and catalytic activity is in the case of supported MoO_3 metathesis catalyst rather difficult. The small amount of metallocarbene active sites practically disables their in-situ characterization. Therefore, ex-situ spectroscopic techniques were employed in order to characterize the precursors of active sites and to estimate the relationships between the structure of the catalysts before the reaction and their catalytic properties in metathesis of 1-octene (Chapter 5.2).

Good dispersion of Mo species and optimum oxidation state of Mo atoms (i. e. lower than Mo(VI), Chapter 3.1.2) are critical requirements to achieve a highly active catalyst [1,20]. As the reducibility of Mo atoms is influenced by the dispersion of Mo species [126], the dispersion of Mo is the key factor determining the catalytic activity.

Diffuse reflectance spectroscopy in the ultraviolet-visible range (DR UV-VIS spectroscopy) and Laser Raman spectroscopy (LRS) were used to check the dispersion of Mo species. Oxidation state of Mo atoms as well as dispersion of Mo were determined by X-ray photoelectron spectroscopy (XPS). Number of surface OH groups and the acidity of the catalysts were investigated by ^{29}Si magic-angle spinning nuclear magnetic resonance (^{29}Si MAS NMR) and by Fourier-transform infrared spectroscopy (FTIR).

5.3.1 DR UV-VIS spectra

Fig. 5.25 presents the UV-visible diffuse reflectance spectra of pure MoO_3 and MoO_3/MCM-41 catalysts with different loadings recorded under ambient conditions in air. The spectra show only one broad absorption band corresponding to Mo(VI) ion with d^0 electronic configuration. This absorption bands was ascribed to ligand-metal charge transfer $O^{2-} \rightarrow Mo^{6+}$. It can be attributed to the coexistence of two species: isolated molybdate species (MoO_4^{2-}, $Mo_2O_7^{2-}$), and polymolybdates (heptamolybdate, octamolybdate) [27,121].

It is known that the diffuse reflectance UV-VIS spectrum may distinguish a dispersed monolayer or sub-monolayer from a crystalline oxide [44]. When the spectra of MoO_3 are compared with those of MoO_3/MCM-41 catalysts, there is a shift of the absorption edge to higher wavelengths in the sequence MoO_3 < 16MoO_3/MCM-41 < 12MoO_3/MCM-41 < 8MoO_3/MCM-41 (25 250 cm^{-1}, 27 470 cm^{-1}, 27 700 cm^{-1} and 27 780 cm^{-1}, respectively). The large difference in the wavelength of the absorption edge

between supported and unsupported MoO_3 confirms the presence of dispersed Mo species on the surface of MoO_3/MCM-41 catalysts.

Nevertheless, there are also slight differences among individual MoO_3/MCM-41 catalysts. The shift of the absorption edge indicates that the catalysts exhibit different dispersion of Mo. The higher is molybdenum loading, the lower is dispersion of molybdenum species and therefore the presence of the crystalline phase is to be expected. This is in agreement with the results of the X-ray analysis (Chapter 5.1.1), where diffraction lines indicating the presence of MoO_3 crystals occur at loadings higher than 12 wt. % Mo for all the supports. This conclusion is also supported by ref. [44], where the critical dispersion capacity of MoO_3 on the surface of MCM-41 was estimated to be about 13.7 wt. % Mo.

Finally, from Fig. 5.25 it is clearly visible that the MoO_3/MCM-41 catalysts exhibited higher intensity of the absorption bands in comparison with pure MoO_3. This increase in the intensity confirms the presence of dispersed Mo species, as it is a result of the multiple reflection effects between light and dispersed species [27].

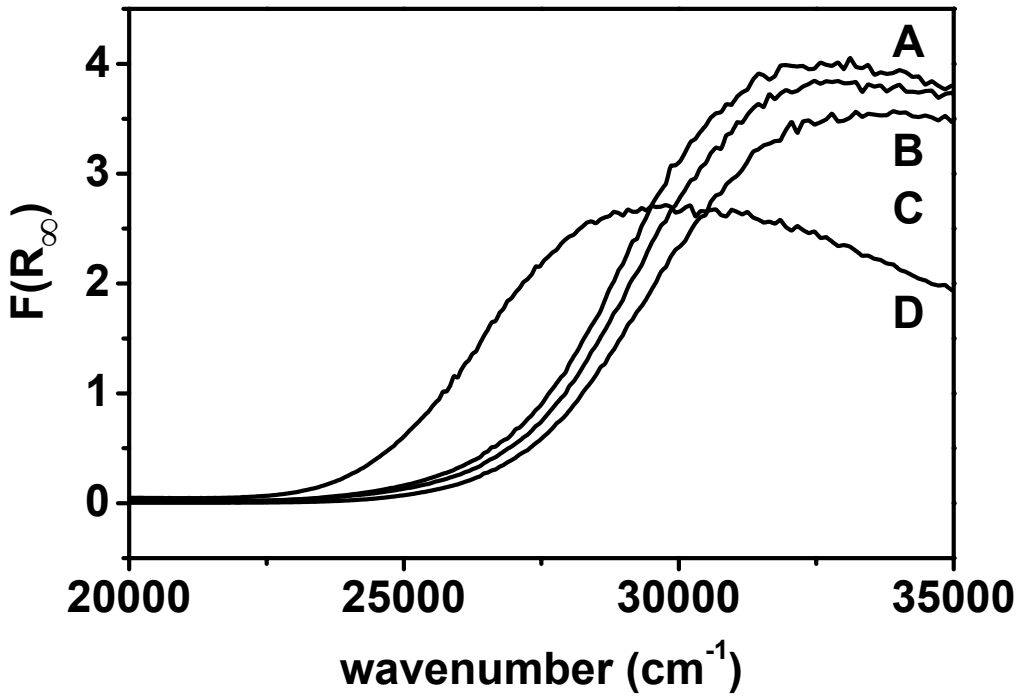

Figure 5.25

DR UV-VIS spectra of MoO_3 (D) and unactivated $16MoO_3$/MCM-41 (A), $12MoO_3$/MCM-41 (B) and $8MoO_3$/MCM-41 (C) measured in air.

To summarize, it was shown that MoO_3 disperses onto the surface of MCM-41 support. The degree of dispersion depends on molybdenum loading. However, the local structures of Mo species could not be clearly identified by electronic transition because they exhibit a similar energy gap between the HOMO and LUMO levels [127].

5.3.2 Raman spectra

In order to further investigate the differences in the dispersion of Mo among individual supported MoO_3 catalysts and to identify Mo species present on the surface of the catalysts, the samples of the catalysts before the reaction (unactivated and activated) were studied using Raman spectroscopy.

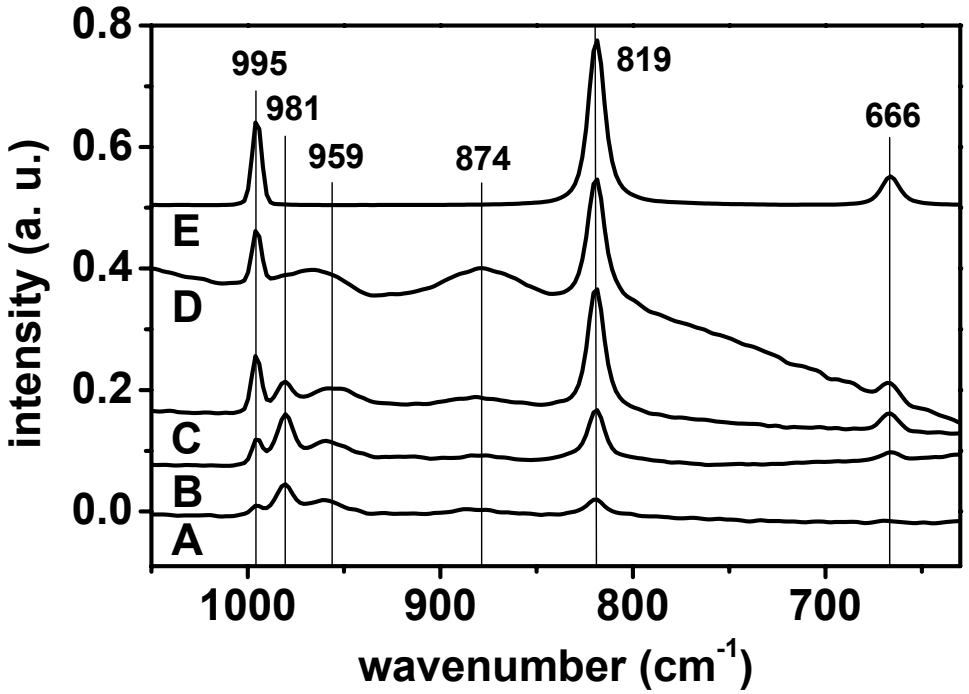

Figure 5.26

Laser Raman spectra of unactivated $4MoO_3$/MCM-41 (A), $8MoO_3$/MCM-41 (B), $12MoO_3$/MCM-41 (C), $16MoO_3$/MCM-41 (D), and MoO_3 (E) [114] measured in air on a Bruker spectrometer.

Fig. 5.26 shows the Raman spectra of MoO_3 and MoO_3/MCM-41 catalysts with different Mo loading recorded under ambient conditions in air. The Raman spectrum of bulk MoO_3 exhibits typical bands at 995 cm^{-1} (stretching vibration of the terminal Mo=O group) and 819 cm^{-1} together with 666 cm^{-1} (Mo-O-Mo bridge bonds vibrations)

[27,107]. In the spectra of MoO_3/MCM-41 catalysts, three different types of Mo species are present: (i) crystalline MoO_3 with corresponding bands as mentioned above, (ii) surface polymolybdates characterized by Mo=O stretching vibration at 959 cm^{-1} and by antisymmetric Mo-O-Mo bridge bond vibration at 874 cm^{-1} [107], and (iii) Mo species that possess stretching vibration of the terminal Mo=O group at 981 cm^{-1}. In the literature, this band was ascribed to isolated surface monomeric molybdenum oxide species (with the band at 980 – 982 cm^{-1}) [128,129]. However, such species were observed only under dehydrated conditions. Thus, it is possible that although relatively low laser power (50 mW) was used for the acquisition of the spectra, the laser irradiation led to a partial dehydration of the sample. Nevertheless, significant differences in the nature of the spectra of MoO_3/MCM-41 catalysts with different loadings indicate that the character of the samples was not substantially changed even upon laser irradiation. Thus, the band at 981 cm^{-1} will be referred to as isolated monomeric Mo species.

Fig. 5.26 clearly shows that with increasing molybdenum loading the population of different Mo species is changing. However, as the dependence of band intensity on the concentration of Mo species is not known and may differ for individual Mo species (e.g. Raman cross section for bulk MoO_3 is higher than for small Mo clusters and dispersed Mo species [27]), only qualitative conclusions can be drawn from the spectra. At low loadings between 4 and 8 wt. % Mo, the band corresponding to isolated monomeric Mo species is the most intensive one. With increasing Mo content, the intensity of the bands corresponding to crystalline MoO_3 is rising. Finally, for 16MoO_3/MCM-41 the bands at 981 cm^{-1} and 959 cm^{-1} overlap and additional band of surface polymolybdates at 874 cm^{-1} appears. It indicates that the dominating Mo species are surface polymolybdates and bulk MoO_3. This in agreement with X-ray diffraction data (Chapter 5.1.1) and confirms the results obtained by DR UV-VIS spectroscopy (Chapter 5.3.1), where decreasing dispersion of Mo species was observed with increasing Mo loading. Moreover, these data correlate well with the conversions achieved with MoO_3/MCM-41 catalysts in metathesis of 1-octene (Chapter 5.2.3): assuming that isolated monomeric Mo species are giving rise to the catalytically most active structures [107], the high conversions reached with the catalysts possessing loading between 4 and 8 wt. % Mo can be explained as a result of a high relative concentration of isolated monomeric Mo species. On the other hand, bulk MoO_3 is

catalytically practically inactive (Chapter 5.2.6), and surface polymolybdates are supposed to be less efficient precursors of the active sites in comparison with isolated monomeric Mo species. Therefore, lower conversions of 1-octene accomplished with the catalysts with higher Mo loadings are not surprising.

The spectra shown in Fig. 5.26 were obtained on Bruker FRA 106/S FT spectrometer equipped with Ge-detector and Nd-YAG-laser (λ = 1 064 nm). The high wavelength of laser radiation allowed avoiding the problems with fluorescence. However, it could cause the overheating of the sample leading to its partial dehydration as mentioned above. To be sure that the data obtained under such experimental conditions are correct, additional measurements were performed with another type of Raman spectrometer, HL5R from Kaiser Optical Systems Inc. With this spectrometer equipped with a laser working at λ = 785 nm and a CCD detector, it was possible to record the spectra with laser power on the sample only 10 mW.

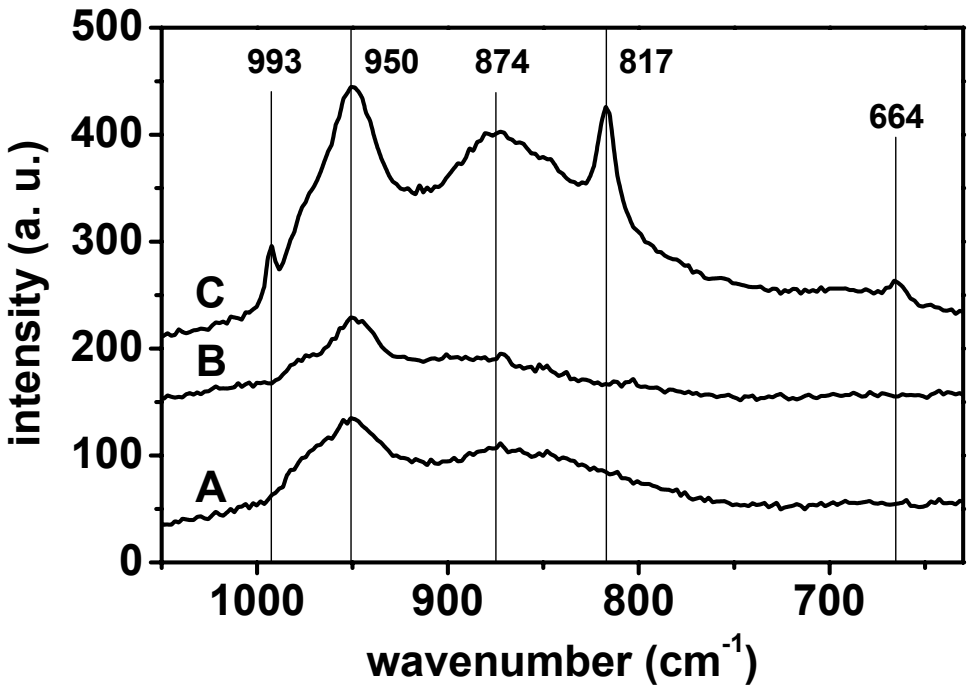

Figure 5.27

Laser Raman spectra of unactivated $4MoO_3$/MCM-41 (A), $6MoO_3$/MCM-41 (B), and $12MoO_3$/MCM-41 (C) measured in air on a HL5R spectrometer.

Although the spectra are not as well developed as that taken on a Bruker spectrometer, it is seen that at least two types of Mo species can be recognized (Fig. 5.27): a broad

band at ~ 950 cm^{-1} with a shoulder on the high-energy side that corresponds to surface polymolybdates, and the bands at 993, 817, and 664 cm^{-1} corresponding to crystalline MoO_3 (the difference in the position of the bands in comparison with Fig. 5.26, e.g. 993 cm^{-1} vs. 995 cm^{-1}, is within the experimental error). A small shoulder at ~ 980 cm^{-1} that could be ascribed to isolated monomeric Mo species is hardly visible; this might indicate that lower power of laser irradiation used resulted in a lower extent of dehydration of the samples.

With increasing Mo loading, the intensity of the band at ~ 950 cm^{-1} is relatively increasing with respect to the shoulder at ~ 980 cm^{-1} (Fig. 5.27). In another words, with increasing Mo loading there is an increasing amount of surface polymolybdates. Finally, at 12 wt. % Mo loading, the bands at 993, 817, and 664 cm^{-1} corresponding to crystalline MoO_3 appear. These results are consistent with that obtained from the spectra in Fig. 5.26. On the other hand, it is known that the wavelength of the laser used for acquiring Raman spectra influences the character of resulting spectra; e.g. the penetration depth of laser radiation depends on its wavelength [130]. Therefore, the different relative intensity of the individual bands in comparison with Fig. 5.26 can be caused by different wavelength of the laser source used. Thus, it seems that the irradiation of the samples during the measurements caused their partial dehydration, the extent of which depended on the laser power used. However, as the Bruker FRA 106/S spectrometer enabled to obtain spectra with better resolution of the bands of individual Mo species than in the latter case, it was used for the characterization of supported MoO_3 catalysts under ambient conditions.

The Raman spectra of MoO_3/MCM-48 obtained on Bruker FRA 106/S spectrometer are shown in Fig. 5.28. It is seen that there are some differences between MoO_3/MCM-48 and MoO_3/MCM-41 catalysts. At the lowest loading, the band at 981 cm^{-1} corresponding to isolated monomeric Mo species has the highest intensity as well. However, for $8MoO_3$/MCM-48 and $12MoO_3$/MCM-48 the band at 959 cm^{-1} corresponding to surface polymolybdates is strongly rising. Finally, at the highest loading, the spectrum is similar to that of $16MoO_3$/MCM-41, i.e. the bands of surface polymolybdates and crystalline MoO_3 are dominating.

The different dependence of Mo dispersion on Mo loading in the case of MoO_3/MCM-48 catalysts in comparison with MoO_3/MCM-41 can explain the lower conversions of 1-octene achieved with MoO_3/MCM-48 catalysts (Chapter 5.2.6).

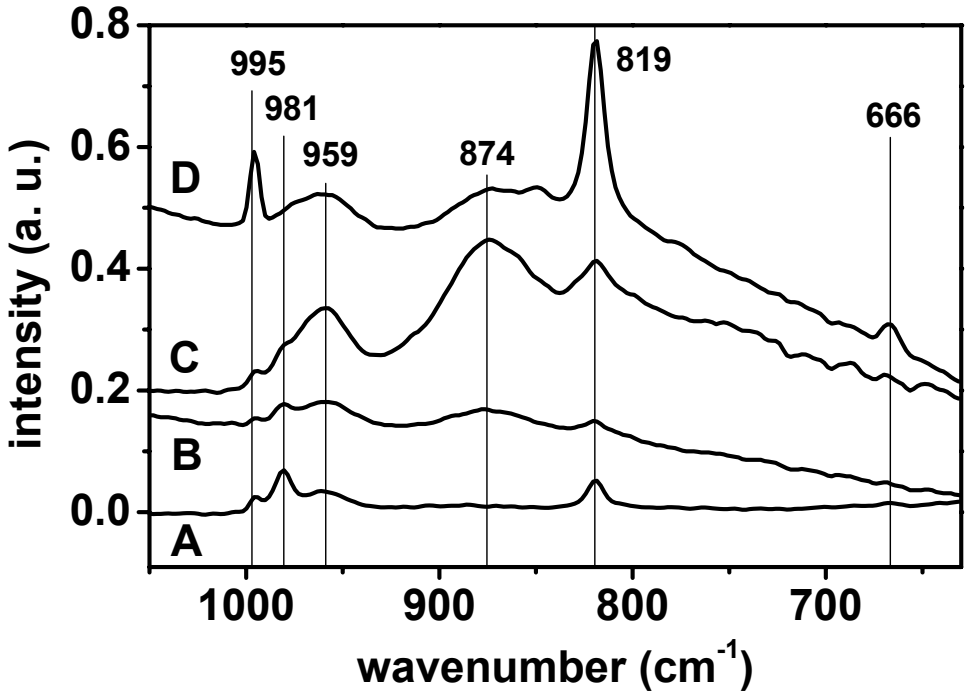

Figure 5.28

Laser Raman spectra of unactivated $4MoO_3$/MCM-48 (A), $8MoO_3$/MCM-48 (B), $12MoO_3$/MCM-48 (C), and $16MoO_3$/MCM-48 (D) [114] measured in air on a Bruker spectrometer.

Whereas in the case of MoO_3/MCM-41, a high intensity of the bands corresponding to isolated monomeric Mo species was observed from 4 to 8 wt. % Mo, with MCM-48 supported catalysts, this was the case only for $4MoO_3$/MCM-48. At 8 wt. % Mo loading, the dispersion changed and the intensity of the band corresponding to surface polymolybdates was similar to that of isolated monomeric Mo species. Consequently, decreased conversion of 1-octene over $8MoO_3$/MCM-48 as compared to $8MoO_3$/MCM-41 was observed (Chapter 5.2.6). On the other hand, high intensity of the bands corresponding to surface polymolybdates in the spectra of $12MoO_3$/MCM-48 correlates with higher conversion of 1-octene reached in comparison with $12MoO_3$/MCM-41, where the bands corresponding to crystalline MoO_3 were the most intensive one. Finally, similar Raman spectra of $4MoO_3$/MCM-48 and $4MoO_3$/MCM-41 are in accord with similar conversions of 1-octene accomplished with these catalysts.

The Raman spectra of MoO_3/SBA-15 (acquired also on Bruker FRA 106/S spectrometer) differ significantly from that of MoO_3/MCM-41 and MoO_3/MCM-48

(Fig. 5.29). In the spectra of $4MoO_3$/SBA-15, the bands at 959 cm^{-1} and 874 cm^{-1} corresponding to surface polymolybdates together with the band at 819 cm^{-1} corresponding to MoO_3 are present. For all other samples, the bands corresponding to crystalline MoO_3 (995, 819, and 666 cm^{-1}) are prevailing. Therefore, in comparison with both MoO_3/MCM-41 and MoO_3/MCM-48 catalysts, MoO_3 supported on SBA-15 exhibited much lower dispersion of Mo species.

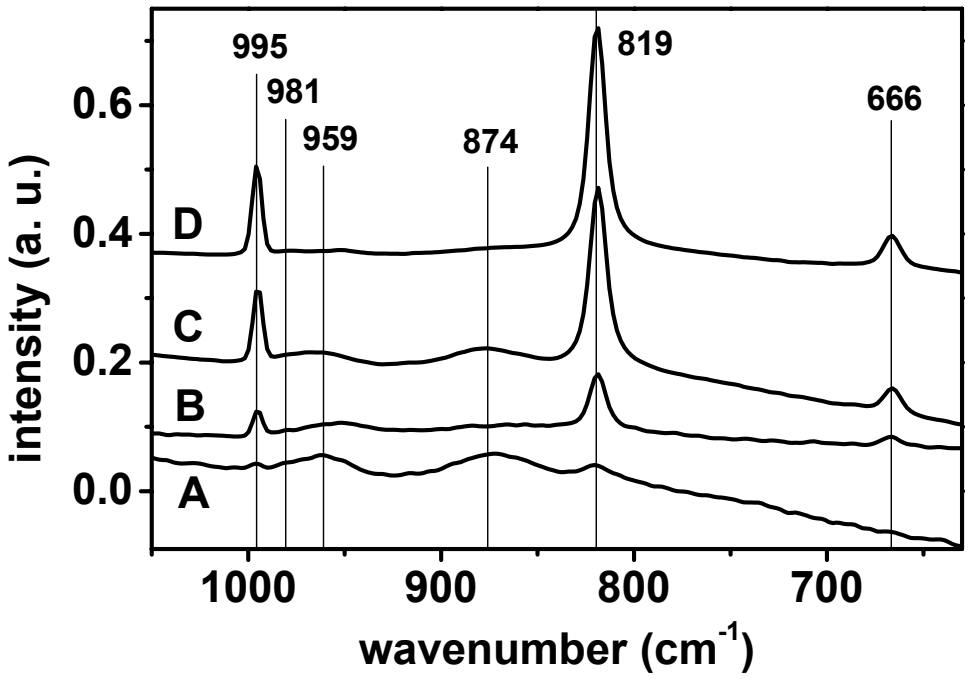

Figure 5.29

Laser Raman spectra of unactivated $4MoO_3$/SBA-15 (A), $8MoO_3$/SBA-15 (B), $12MoO_3$/SBA-15 (C), and $16MoO_3$/SBA-15 (D) [114] measured in air on a Bruker spectrometer. Spectra (A) and (B) were four times magnified.

A high intensity of the band corresponding to crystalline MoO_3 in comparison with MoO_3/MCM-41 and MoO_3/MCM-48 catalysts with the same loading explains the lower conversions of 1-octene achieved with MoO_3/SBA-15 in comparison with MoO_3/MCM-41 and MoO_3/MCM-48 (Chapter 5.2.6). Low dispersion of Mo species in the case of MoO_3/SBA-15 catalysts was also indicated by X-ray diffraction (Chapter 5.1.1), where MoO_3 crystallites of average size 2.5 nm were detected for $12MoO_3$/SBA-15 but not for $12MoO_3$/MCM-41 and $12MoO_3$/MCM-48.

In Raman spectra of $8MoO_3/SiO_2$ taken on Bruker FRA 106/S spectrometer, only one broad band between 1 000 and 940 cm^{-1} was observed (not shown in Fig.). On the other hand, with Kaiser HL5R spectrometer, good spectrum of $6MoO_3/SiO_2$ was gained. The spectra of $6MoO_3/SiO_2$ and $6MoO_3$/MCM-41 are compared in Fig. 5.30. It is evident that the dispersion of Mo is substantially different. The spectrum of $6MoO_3$/MCM-41 catalyst is characterized by a broad band at ~ 950 cm^{-1} with a shoulder on the high-energy side (~ 980 cm^{-1}) that correspond to surface polymolybdates and isolated monomeric Mo species, respectively; no crystalline MoO_3 is observed. On the other hand, in the spectrum of $6MoO_3/SiO_2$, surface polymolybdates (with additional band at 636 cm^{-1} [128]) and bulk MoO_3 are prevailing.

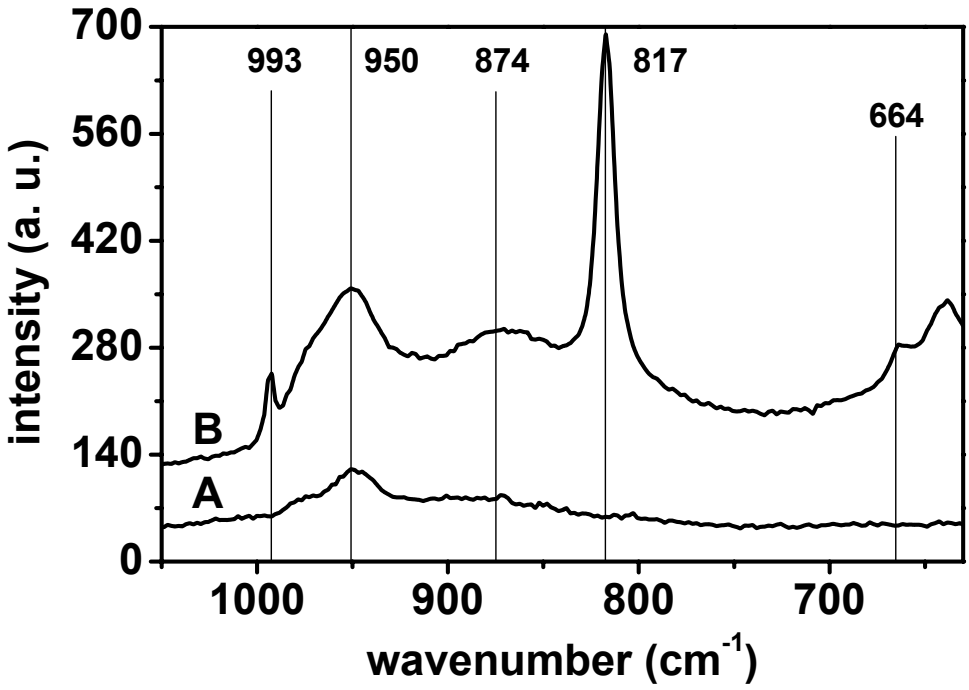

Figure 5.30

Laser Raman spectra of unactivated $6MoO_3$/MCM-41 (A) and unactivated $6MoO_3/SiO_2$ (B) measured in air on a HL5R spectrometer.

These results clearly show that the ability to possess highly dispersed Mo species is much higher in the case of MCM-41 support than for conventional silica. Consequently, a large difference was observed between the conversions of 1-octene reached with $6MoO_3/SiO_2$ and $6MoO_3$/MCM-41 catalysts (Chapter 5.2.6). The different

dispersion of Mo species over MCM-41 and SiO_2 might be connected with different concentration of OH groups per gram of the support (cf. Chapter 5.3.3).

To check the structural changes of the catalyst during the activation process, samples of activated catalysts (standard activation at 500 °C for 30 min in a stream of air) were sealed into glass tubes and measured on Kaiser HL5R spectrometer equipped with an optic fiber and a microscope. Raman spectra of $6MoO_3$/MCM-41 before and after activation are compared in Fig. 5.31.

Before the activation, a broad band at ~ 950 cm^{-1} with a shoulder on the high-energy side (~ 980 cm^{-1}) corresponding to surface polymolybdates and isolated monomeric Mo species, respectively, was present. After the activation, the band at ~ 950 cm^{-1} disappeared and new band at ~ 988 cm^{-1} together with broad shoulder on the low-energy side (~ 980 cm^{-1}) was formed.

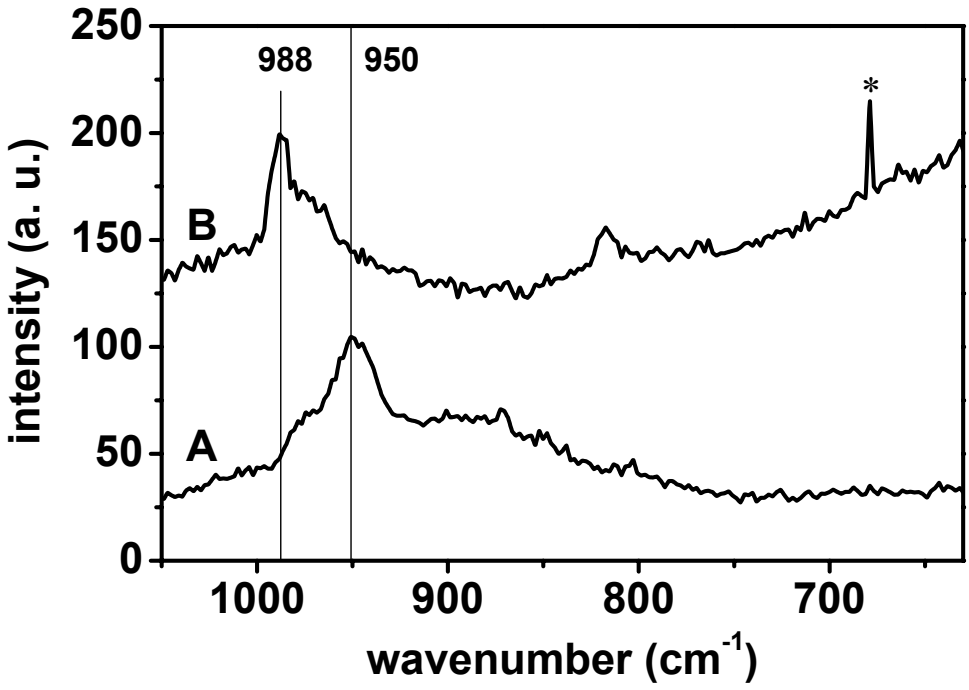

Figure 5.31

Laser Raman spectra of unactivated $6MoO_3$/MCM-41 measured in air (A) and activated $6MoO_3$/MCM-41 sealed in evacuated glass tube (B) taken on a HL5R spectrometer; * = cosmic rays.

It is known that upon dehydration, the polymolybdate structures are unstable and spread over the silica surface to form isolated surface monomeric molybdenum species

[128,131]. Thus, it seems that during activation, the surface polymolybdates (partially) decompose and isolated monomeric Mo species are formed. It was shown that degree of hydration affects the nature of the Mo species present on silica surface [131]. Therefore, the new band at ~ 988 cm^{-1} might correspond to dehydrated isolated monomeric Mo species (or "highly dispersed species" under anhydrous conditions [131]), whereas the shoulder at ~ 980 cm^{-1} might correspond to only partially dehydrated isolated monomeric Mo species.

5.3.3 Infrared spectra

The differences in the conversion of 1-octene reached with MoO_3 catalysts supported on different types of mesoporous molecular sieves were correlated with different dispersion of Mo (Chapter 5.3.2). However, as all types of mesoporous molecular sieves used (MCM-41, MCM-48, and SBA-15) have the same chemical composition (i.e. SiO_2), a question may arise, what is the reason for such significant differences in the dispersion of Mo over individual types of mesoporous silica. Whereas the conversion of 1-octene (Chapter 5.2.6) as well as the dispersion of Mo species (Chapter 5.3.2) was found to decrease in the order MCM-41 > MCM-48 > SBA-15, the surface area of the support was decreasing in the order MCM-48 > MCM-41 > SBA-15 (Chapter 5.1.2). Therefore, there must be another factor besides the surface area of the support that influences the dispersion of molybdenum oxide.

It is known that MoO_3 disperses over the surface of the catalyst thanks to the chemical reaction with surface OH groups of the support. When physical mixture of molybdenum oxide and siliceous support was calcined at 500 °C on air, new Si-O-Mo bonds were formed [44]. Therefore, it may be interesting to compare the concentration of surface OH groups of individual supports and catalysts.

Infrared spectra of mesoporous silica exhibit two types of OH stretching vibrations of silanol groups: a sharp band at 3 745 cm^{-1} and a broad band around 3 530 cm^{-1} corresponding to free and hydrogen-bonded SiOH groups, respectively (cf. Fig. 5.37) [76,132]. From Fig. 5.32 it is seen that both bands corresponding to OH stretching vibrations of silanol groups decreased after the modification of the support with MoO_3.

By ^1H MAS NMR experiments with deuterated pyridine, it was shown for MCM-41 and SBA-15 that most silanol groups arise from the surface of mesoporous silica, but not from walls or small pores that are not accessible to pyridine [133].

Therefore, it is reasonable to estimate the concentration of surface OH groups from FTIR spectra, omitting thus the negligible amount of OH groups that may be hidden inside the pore walls. In order to compare the concentration of surface OH groups of different types of catalysts, the area of infrared bands corresponding to OH stretching vibrations was calculated for parent supports and MoO_3 supported on MCM-41, MCM-48, and SBA-15.

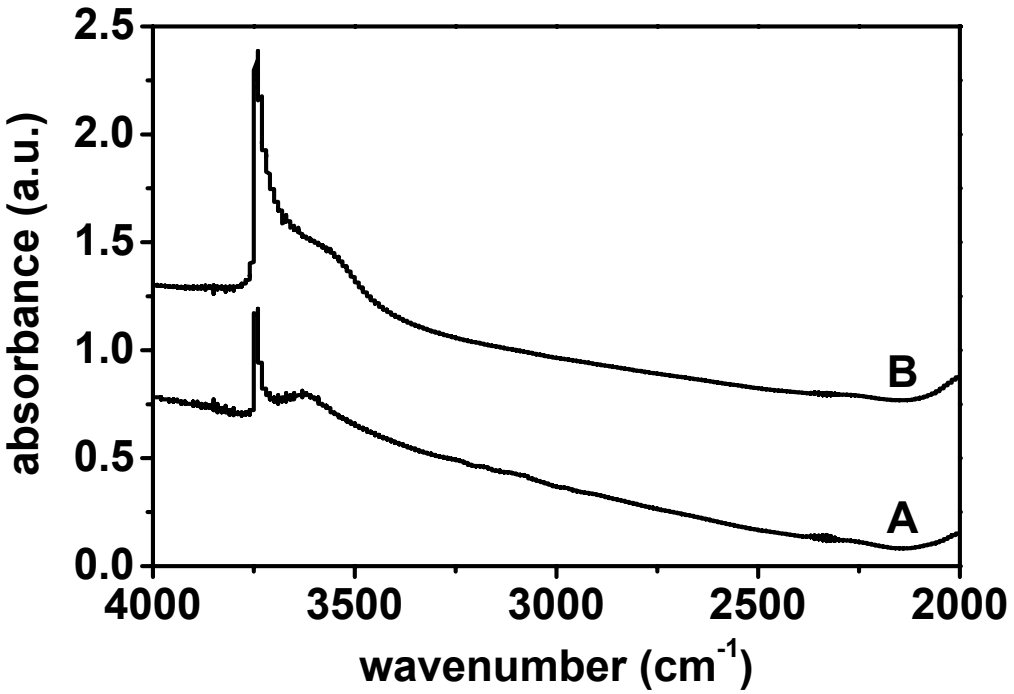

Figure 5.32

FTIR spectra of $16MoO_3$/MCM-41 (A) and MCM-41 (B). For clarity, the spectra are vertically shifted.

Integrated absorbances normalized on the sample weight (integration region from 3 770 cm^{-1} to 3 350 cm^{-1}) determined from FTIR spectra of above-mentioned catalysts are shown in Fig. 5.33. In order to remove water adsorbed on the surface of the catalysts, samples were treated at 450 °C for 30 min in vacuum prior to the measurement.

If we compare the concentrations of surface OH groups for parent supports, it is seen that MCM-41 exhibited the highest concentration of surface OH groups expressed per gram of the support, followed by MCM-48 and SBA-15. The differences in the population of OH groups for parent supports correlate well with differences in

conversion of 1-octene that were achieved with corresponding molybdenum oxide catalysts (Chapter 5.2.6). Taking into account that molybdenum oxide is dispersed onto the siliceous support via the Si-O-Mo bridge-bonds formation [44], it is not surprising that the support with the highest concentration of surface OH groups is able to possess the highest dispersity of Mo species and, consequently, the highest conversion of 1-octene.

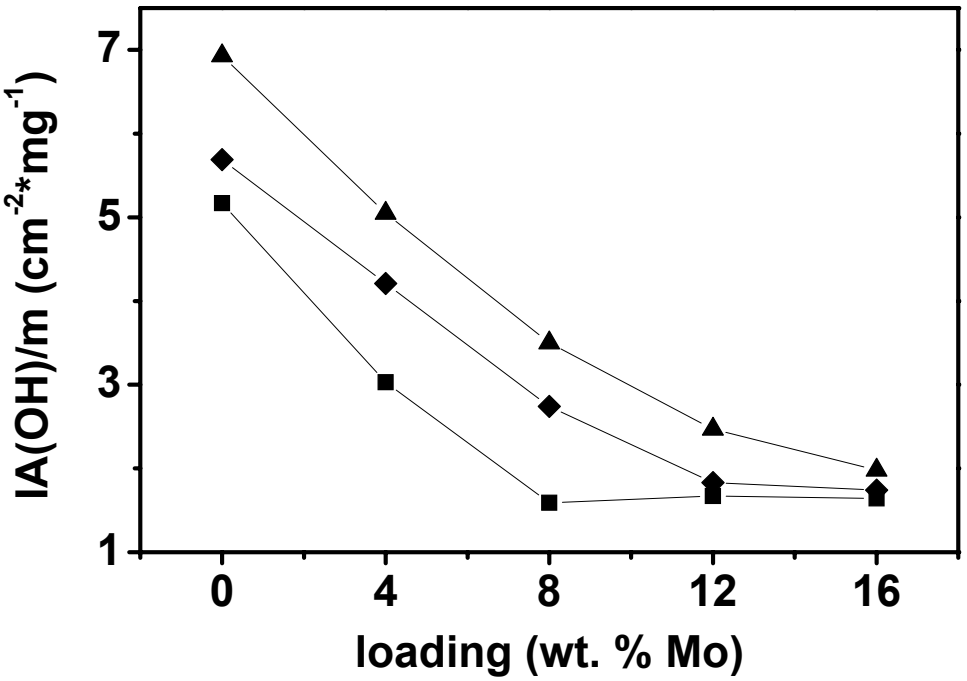

Figure 5.33

Dependence of integrated absorbance of OH stretching vibration bands normalized on sample weight on Mo loading as calculated from FTIR spectra of molybdenum oxide supported on MCM-41 (▲), MCM-48 (◆) and SBA-15 (■). Lines are intended as visual aids.

This conclusion is in agreement with the results obtained by Raman spectroscopy (Chapter 5.3.2), where for the same Mo loading the superior dispersion of Mo species was observed for MoO_3/MCM-41 catalysts, whereas in the case of MoO_3/MCM-48 lower amount of dispersed Mo species was detected, and for MoO_3/SBA-15 typically crystalline molybdenum oxide was prevailing.

With increasing molybdenum loading, the concentration of surface OH groups (expressed per gram of the sample) was decreasing for all the supports (Fig. 5.33). This

trend remained the same also when the concentration of surface OH groups was recalculated per gram of the support (not shown in Fig.). The decrease in the concentration of surface OH groups with increasing molybdenum loading is caused by the reaction of increasing amount of surface silanols with MoO_3 [111]. Finally, at higher loadings, all silanols that can be utilized for the dispersion of molybdenum oxide were consumed and their concentration remained constant. This situation appeared at first in the case of MoO_3 supported on SBA-15, which possessed the lowest concentration of surface OH groups. Consequently, large part of Mo was in the form of crystalline MoO_3 (Chapter 5.3.2) and low conversion of 1-octene was accomplished (Chapter 5.2.6).

The acidities of the catalysts were characterized by FTIR spectra of adsorbed pyridine (Fig. 5.34). Because of the pretreatment procedure, the measured samples corresponded approximately to an activated catalyst (samples were heated at 450 °C for 30 min in vacuum prior to the measurement).

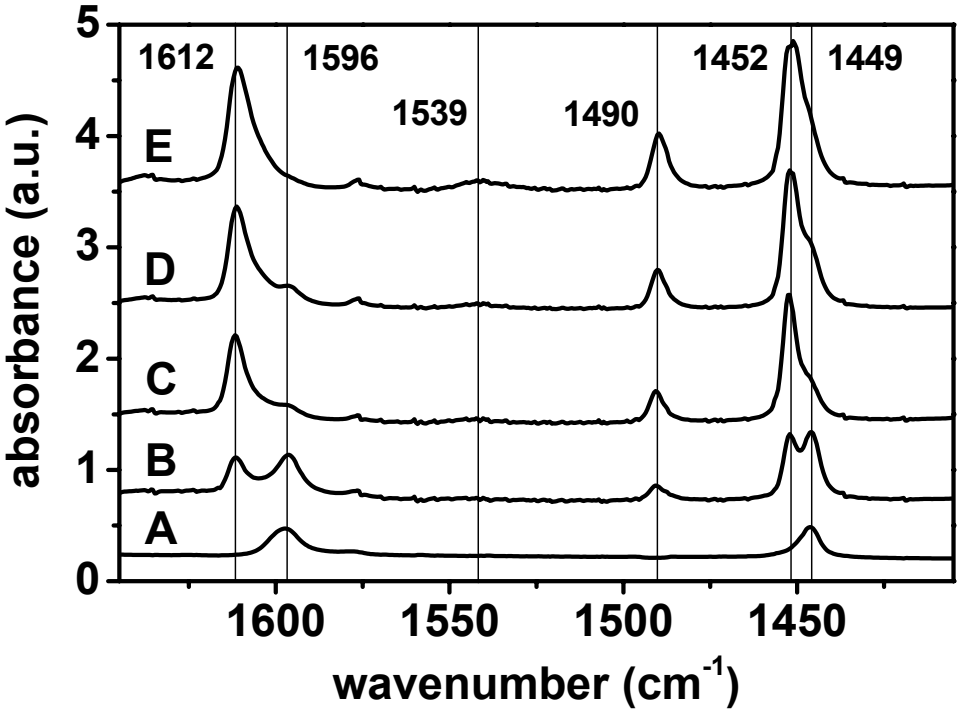

Figure 5.34

FTIR subtracted spectra of chemisorbed pyridine over MCM-41 (A), $4MoO_3$/MCM-41 (B), $8MoO_3$/MCM-41 (C), $12MoO_3$/MCM-41 (D), and $16MoO_3$/MCM-41 (E). For clarity, individual spectra are vertically shifted.

The samples of the parent supports and corresponding MoO_3 based catalysts showed the expected bands due to Lewis-bound pyridine (1449 + 1452 cm^{-1}, 1596 + 1612 cm^{-1} and 1576 cm^{-1}), negligible amount of pyridine bound on Brønsted acid sites (1539 cm^{-1}) and a band at 1490 cm^{-1} attributed to pyridine associated with both Lewis and Brønsted acid sites [113].

Only Lewis type acidity (bands at 1449 and 1596 cm^{-1}) was observed for parent siliceous MCM-41, MCM-48, and SBA-15. When molybdenum oxide was introduced, small amount of Brønsted acid sites and a new type of Lewis acid sites at 1452 and 1612 cm^{-1} appeared on the surface of all types of the catalysts (Fig. 5.35). Although the amount of Brønsted acid sites was practically negligible, from Fig. 5.35 it is seen that their concentration was slightly increasing with increasing molybdenum loading. A new type of Lewis acid sites appeared when molybdenum oxide was introduced on siliceous supports. These Lewis acid sites were stronger than that one observed on pure silica.

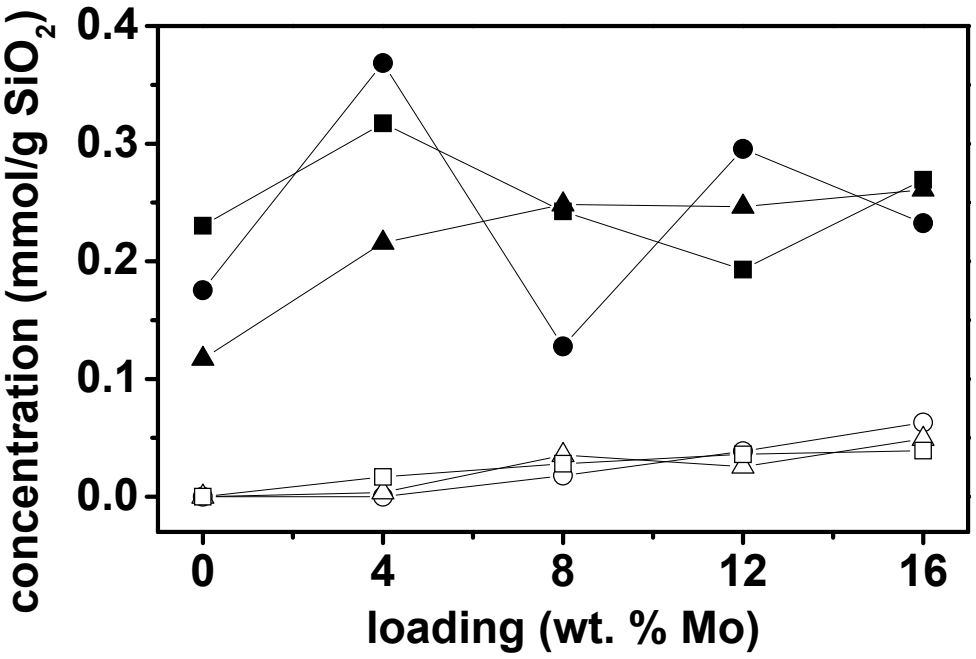

Figure 5.35

Concentration of Brønsted (open symbols) and Lewis acid sites corresponding to the band at 1449 cm^{-1} (solid symbols) over molybdenum oxide supported on MCM-41 (●), MCM-48 (▲), and SBA-15 (■) according to FTIR spectra of chemisorbed pyridine. Lines are intended as visual aid.

Whereas the first type of Lewis acid sites at 1449 cm^{-1} correspond to weakly acidic OH groups of siliceous support [132,134], the second type at 1452 cm^{-1} might be tentatively ascribed to reduced molybdenum atoms. The presence of reduced Mo species is necessary to obtain an active catalyst [46-48].

Comparing the data obtained by decomposition of FTIR spectra to the Gaussian bands (Fig. 5.35 and 5.36), we can see that whereas the number of 1449 cm^{-1} Lewis acid sites depends non-monotonously on Mo loading, the number of 1452 cm^{-1} Lewis acid sites is increasing with molybdenum loading for all the supports. However, it is not possible to establish direct correlation between the number of reduced molybdenum atoms and activity of the catalyst in metathesis reaction. The reason may lie in fact that except the pre-reduction of Mo atoms during the activation procedure, reduced Mo species may be formed also upon the contact of the catalyst with the substrate [1]. Moreover, the proper oxidation state of Mo atoms is only one of the conditions that are essential for obtaining an active catalyst. The presence of highly dispersed Mo species is crucial as well [20].

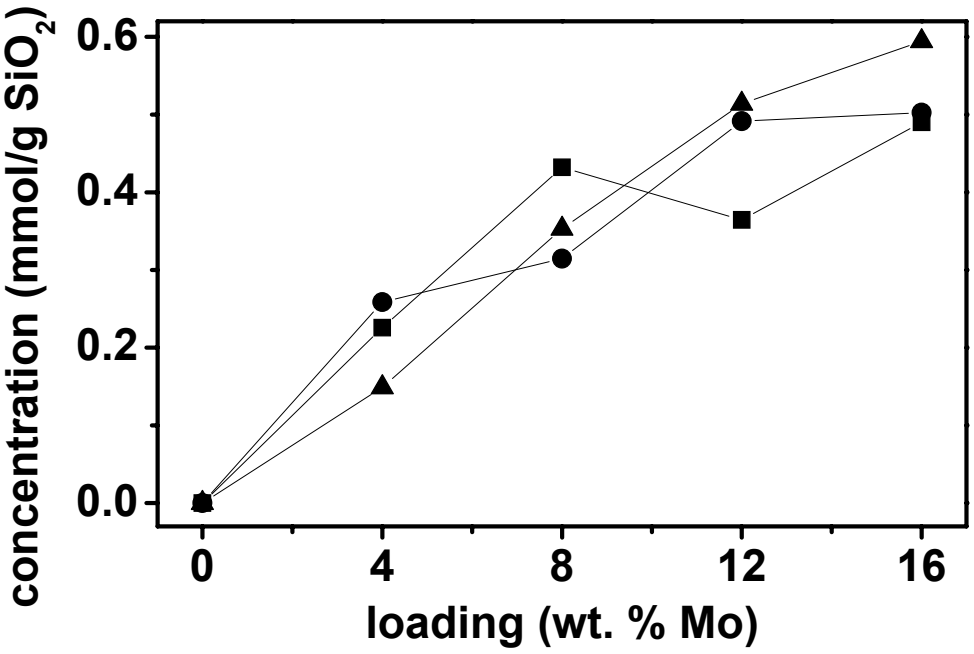

Figure 5.36

Concentration of Lewis acid sites corresponding to the band at 1452 cm^{-1} over molybdenum oxide supported on MCM-41 (●), MCM-48 (▲), and SBA-15 (■) according to FTIR spectra of chemisorbed pyridine. Lines are intended as visual aid.

As for weakly acidic OH groups (Lewis acid sites at 1449 cm^{-1}), higher densities of silanols than that indicated in Fig. 5.35 were determined in the literature by FTIR spectroscopy of adsorbed pyridine (e.g. ~ 0.8 mmol/g for MCM-41 [132]). However, in our case, the low amount of OH groups on the surface of MCM-41 can be caused by higher partial dehydroxylation of the silica surface (samples were heated at 450 °C for 30 min in vacuum prior to the measurement) in comparison with literature data (e.g. pretreatment at 400 °C in ref. [132]).

5.3.4 Nuclear magnetic resonance spectra

Although widely used, FTIR cannot discriminate between single and geminal SiOH groups. On the other hand, with the aid of the solid-state ^{29}Si nuclear magnetic resonance experiments employing magic-angle spinning (^{29}Si MAS NMR), silicon atoms to which OH groups are directly connected and silicon atoms without OH groups can be recognized. As the chemical shielding of ^{29}Si nuclei depends on the number of attached OH groups, geminal and single SiOH groups can be discerned as Q^2 and Q^3 silicon sites, respectively, and can be measured quantitatively (Fig. 5.37) [76].

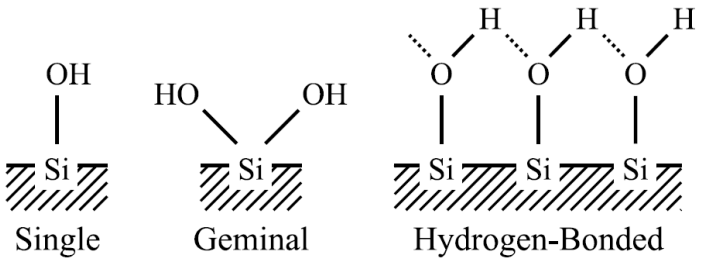

Figure 5.37

Schematic representation of the three types of SiOH groups in siliceous mesoporous molecular sieves [45].

In addition, the intensities of silicon atoms that are used for quantitative analysis are not affected by the presence of water molecules, and therefore the preparation of anhydrous samples and problems with different extent of sample dehydroxylation can be avoided.

^{29}Si MAS NMR spectra of parent MCM-48 are shown in Fig. 5.38. The low intensity peak at -92 ppm corresponds to surface silicon atoms with two siloxane bonds and two silanol groups, i.e. geminal silanol sites $(SiO)_2*Si(OH)_2$ (Q^2), which may be either single or hydrogen bonded (Fig. 5.37). The resonance at -100 ppm is attributed to surface silicon atoms with three siloxane bonds and one silanol group, i.e. isolated

silanol sites, $(SiO)_3$*Si(OH) (Q^3), while the resonance at -109 ppm is ascribed to surface silicon atoms with four siloxane bonds, i.e. $(SiO)_4$*Si (Q^4) [135]. Similar spectra were obtained for all parent supports and MoO_3 based catalysts. The relative peak areas after curve fitting the spectra with a series of Gaussian peaks are listed in Tab. 5.6. Populations of Q^2, Q^3, and Q^4 silicon atoms were determined from ^{29}Si MAS NMR spectra of parent supports and MoO_3 based catalysts with 8 wt. % Mo.

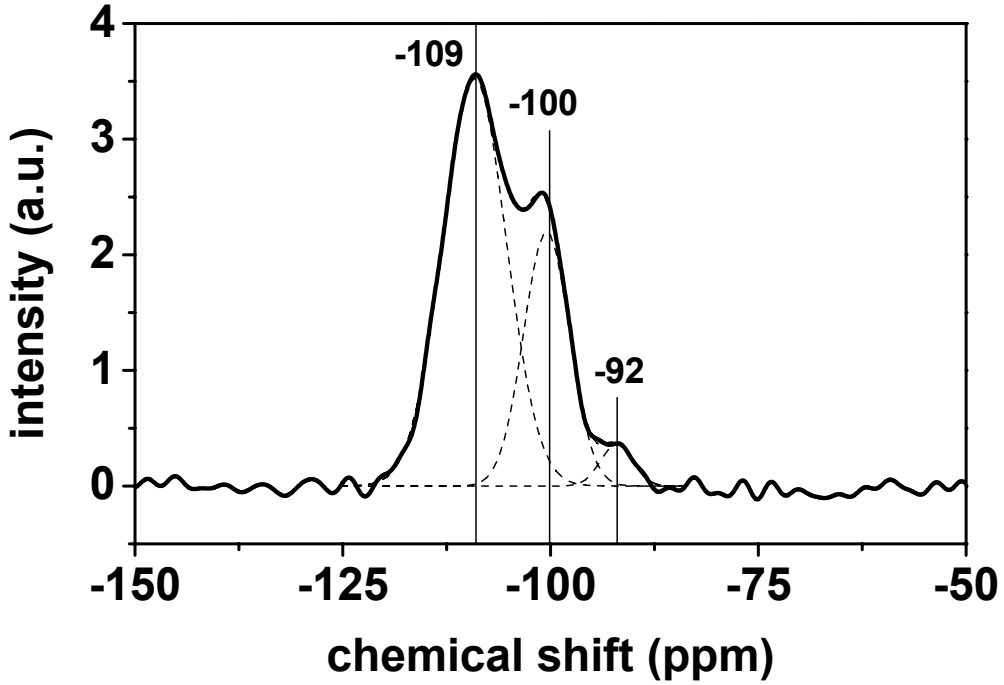

Figure 5.38

^{29}Si MAS NMR spectra of MCM-48. The decomposition of the spectra to the Gaussian peaks is indicated by dashed lines.

^{1}H → ^{29}Si cross-polarization (CP) experiment restricts detection of an NMR signal to silicon nuclei to which OH groups are directly connected [76]. The ^{29}Si CP MAS NMR spectra of all samples showed substantial increase in the relative intensity of the Q^2 and Q^3 peaks in comparison with their ^{29}Si MAS NMR spectra (e.g. relative peak areas 11.4 % and 72.6 % for Q^2 and Q^3, respectively, in the case of parent MCM-41; not shown in Fig.). This confirms that these silicon atoms are attached to hydroxyl groups [106]. The decrease in the number of Q^3 silicon atoms after the modification of parent support with MoO_3 is expressed as CP Q^3 ratio (Tab. 5.6). This was calculated as the ratio of relative peak areas of Q^3 silicon atoms in the ^{29}Si CP MAS

NMR spectra of the parent support and corresponding MoO_3 based catalyst with 8 wt. % Mo.

By the ^{1}H MAS NMR experiments with deuterated pyridine, it was shown for MCM-41 and SBA-15 that large majority of silanol hydroxyl groups arise from the surface of mesoporous silica but not from walls or small pores, which are not accessible to pyridine [133].

Table 5.6

Relative peak areas of Q^2, Q^3, and Q^4 silicons in the ^{29}Si MAS NMR spectra of parent supports and MoO_3 based catalysts, CP Q^3 ratio, and number of surface OH groups per nm^2 of the support estimated from relative peak areas of Q^2 and Q^3 silicons in the ^{29}Si MAS NMR spectra of the support according to Eq. (6).

Sample	Q^2 (%)	Q^3 (%)	Q^4 (%)	CP Q^3 Ratio	S_{BET} (m^2/g)	α (nm^{-2})
MCM-41	1.8	28.8	69.4	0.756	1 003	3.2
8MoO_3/MCM-41	2.3	25.9	71.8		-	-
MCM-48	4.1	35.9	59.9	0.685	1 334	4.4
8MoO_3/MCM-48	3.4	30.0	66.6		-	-
SBA-15	3.0	35.0	62.0	0.589	777	4.1
8MoO_3/SBA-15	3.2	28.1	68.7		-	-

Thus, if we assume that only negligible amount of SiOH and $Si(OH)_2$ groups is hidden inside the pore walls of mesoporous silica, the number of surface OH groups of the support can be estimated from the relative peak area of Q^2 and Q^3 silicon atoms in the ^{29}Si MAS NMR spectra of the support using the surface area of the support determined by nitrogen adsorption (S_{BET}) as indicated in the equation (6):

$$\alpha = [n(\mathrm{Si}) * 0.01 * (Q^3 + 2Q^2) * N_A] / [S_{BET} * 10^{18}] \quad (6)$$

where α is number of surface OH groups per nm^2 of the support, n(Si) is molar amount of Si atoms per gram of the support (i.e. 0.01664 mol), Q^3 and Q^2 are relative peak areas of Q^3 and Q^2 silicon atoms in the ^{29}Si MAS NMR spectra of the support, respectively, N_A is Avogadro's number, and S_{BET} is the BET surface area of the support expressed in m^2/g. The results for siliceous MCM-41, MCM-48, and SBA-15 are given in Tab. 5.6.

From Tab. 5.6 it is seen that:

(i) the number of surface OH groups estimated from ^{29}Si MAS NMR spectra of the support according to Eq. (6) is in reasonable agreement with the literature data (the number of surface OH groups estimated by NMR was between 2 and 3 OH groups/nm^2 for MCM-41 [76,133] as well as for MCM-48 [34], and about 3.7 OH groups/nm^2 for SBA-15 [133]),

(ii) the estimated number of surface OH groups per nm^2 is increasing in the order MCM-41 < MCM-48 ≈ SBA-15,

(iii) CP Q^3 ratios indicate that the relatively highest amount of surface OH groups was consumed during the thermal spreading of MoO_3 in the case of SBA-15 supported catalyst, followed by MCM-48 and MCM-41 supported one, and

(iv) the population of Q^3 silanols is slightly higher, and in the case of Q^2 silanols even much higher for SBA-15 and especially for MCM-48 in comparison with MCM-41; substantially higher amount of $Si(OH)_2$ groups in SBA-15 as compared with MCM-41 was also mentioned in the literature [133].

To compare the results obtained from NMR with that revealed from FTIR spectra, it is necessary to recalculate the number of surface OH groups α per gram of the support. In this case, the concentration of surface OH groups according to NMR is decreasing in the order MCM-48 > MCM-41 ~ SBA-15 ($5.9 \cdot 10^{21}$, $3.2 \cdot 10^{21}$, and $3.2 \cdot 10^{21}$ g^{-1}, respectively). This is in contradiction with FTIR results, where the concentration of surface OH groups was found to decrease in the order MCM-41 > MCM-48 > SBA-15 (Chapter 5.3.3), i.e. in the same order as decreased the ability of the support to possess dispersed of Mo species (Chapter 5.3.2).

Because of good correlation between the concentrations of surface OH groups as determined from FTIR spectra with the dispersion of Mo species, the FTIR results seem to be more reliable in this case. The discrepancy between the results obtained by FTIR spectroscopy of adsorbed pyridine and ^{29}Si MAS NMR spectra was also observed in the literature (e.g. for MCM-41 from 2 to 3 OH groups/nm^2 was estimated by ^{29}Si CP MAS NMR, but much smaller values around 1 OH group/nm^2 were obtained by FTIR spectroscopy of adsorbed pyridine [133]).

5.3.5 X-ray photoelectron spectra

In order to determine the oxidation state of molybdenum atoms, $12MoO_3$/MCM-41 catalyst was analyzed by X-ray photoelectron spectroscopy before and after standard activation at 500 °C for 30 min in a stream of air (Fig. 5.39). The binding energy of the Mo $3d_{5/2}$ peak for the unactivated sample was found to be 233.2 eV and corresponds to that one reported for the supported molybdenum oxo-species in the highest oxidation state, i.e. Mo(VI) [111]. Two components are present in the spectrum of the activated sample. They correspond to Mo(V) (39 % of total Mo amount) and Mo(VI) (61 % of total Mo amount). This finding is in accord with the literature, where the slight reduction of molybdenum(VI) to formal oxidation state between Mo(V) and Mo(VI) was found to be essential for obtaining an active metathesis catalyst [46-48]. Moreover, the amount of Mo(V) determined by XPS is in good agreement with the results obtained by FTIR spectroscopy (Chapter 5.3.3).

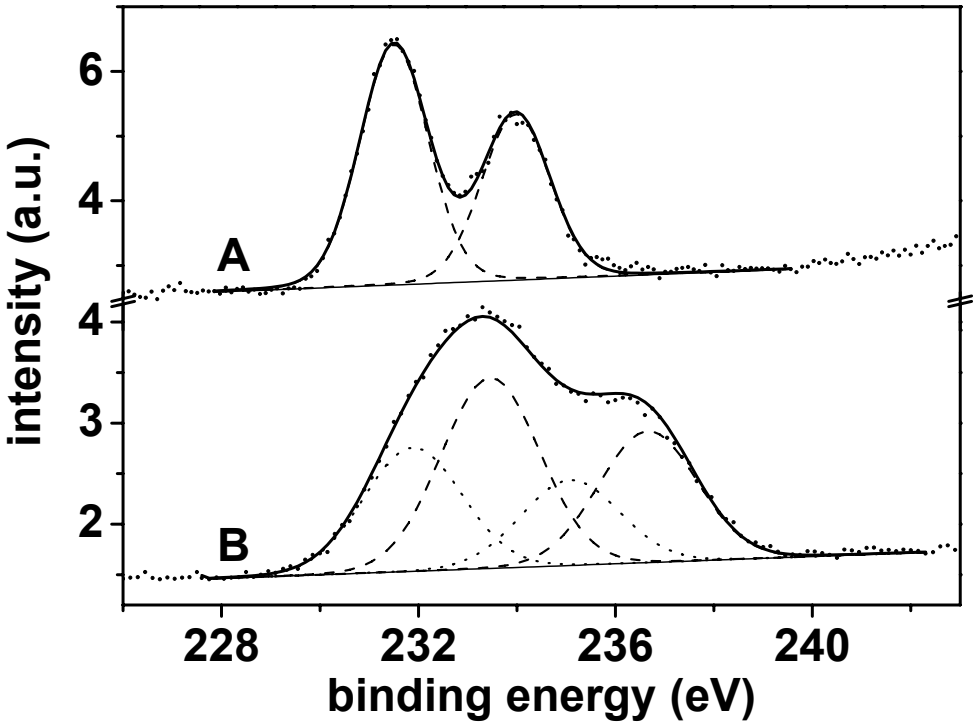

Figure 5.39

XPS spectra of 3d photoelectrons of Mo for unactivated (A) and activated (B) $12MoO_3$/MCM-41 catalyst. The decomposition of the spectra to individual peaks is indicated in dotted lines for Mo(V) and dashed lines for Mo(VI). The spectra are normalized on the same height of Mo doublet.

Thanks to the pretreatment procedure applied in FTIR measurements, the measured samples corresponded approximately to an activated catalyst (samples were treated at 450 °C for 30 min in vacuum prior to the measurement). From FTIR spectra of adsorbed pyridine, the concentration of reduced molybdenum atoms in activated $12MoO_3$/MCM-41 catalyst was estimated to be 0.5 mmol/g SiO_2 (Fig. 5.36). This corresponds to 33 % of total Mo content, which is similar to the value obtained by XPS (39 %).

For activated $12MoO_3$/MCM-41 catalyst, the Mo $3d_{5/2}$ binding energy is shifted to higher values (233.6 eV) in comparison with unactivated one (Fig. 5.39). It is probably caused by a stronger interaction of the highly dispersed molybdenum species with the MCM-41 support [44]. The increase in the dispersion of Mo is also indicated by an increased XPS surface Mo3d:Si2p ratio [20,27,80,111]. For $12MoO_3$/MCM-41, this ratio increased from 0.053 for unactivated catalyst to 0.065 in the case of an activated catalyst. The increase in the dispersion of Mo as shown by XPS measurements is in accord with Raman spectra (Chapter 5.3.2), where the activation of the MoO_3/MCM-41 catalyst was supposed to lead to the transformation of low-dispersed surface polymolybdates to highly dispersed isolated monomeric Mo species.

Fig. 5.40 shows the XPS spectra of $6MoO_3$/MCM-41 catalyst after the metathesis reaction. The catalyst was activated and employed in metathesis of 1-hexene at 40 °C. After that, the spent catalyst was dried by evacuation and transported into the spectrometer chamber under argon, without any contact with air. In the unactivated catalyst before the reaction, only Mo(VI) was present (not shown in Fig. 5.40). The XPS spectrum of the $6MoO_3$/MCM-41 catalyst after the reaction corresponds to the superposition of two spectral components with Mo $3d_{5/2}$ binding energies 232.3 and 233.7 eV (Fig. 5.40A). Both values of binding energies are slightly higher than those reported in the literature for Mo oxides in corresponding oxidation state (Fig. 5.41) but practically the same as that of activated $12MoO_3$/MCM-41 catalyst (Mo $3d_{5/2}$ binding energy 233.6 eV). Similarly to $12MoO_3$/MCM-41 catalyst, this difference is probably caused by the presence of highly dispersed Mo species and by their interaction with the support.

75 % of Mo(V) and 25 % of Mo(VI) was revealed from the deconvolution of the XPS spectra of the spent $6MoO_3$/MCM-41 catalyst (Fig. 5.40A).

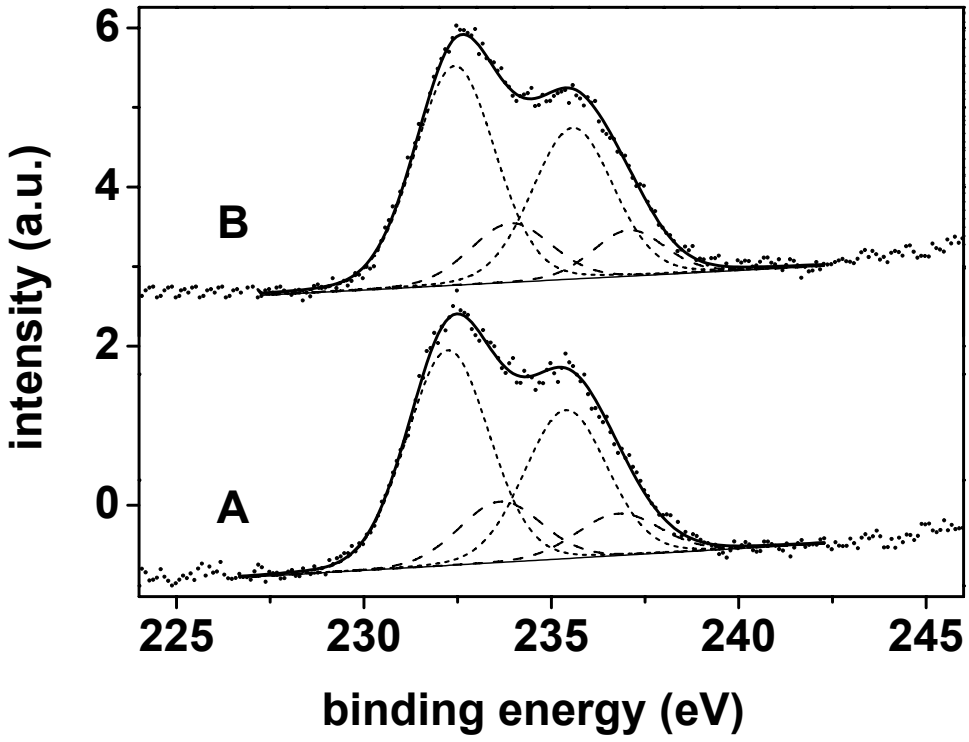

Figure 5.40

The evolution of the XPS spectra of 3d photoelectrons of Mo for the $6MoO_3$/MCM-41 catalyst after the metathesis reaction with time: measured as received (A), and after 60 min of the irradiation with monochromatic X-ray source (B). The decomposition of the spectra to individual peaks is indicated in dotted lines for Mo(V) and dashed lines for Mo(VI). The spectra are normalized on the same height of Mo doublet.

It might be speculated that the catalyst with such high content of Mo(V) is below the optimum oxidation state (Chapter 3.1.2) and, therefore, the reduction of Mo atoms during the reaction might be connected with catalyst deactivation (Chapter 5.2.4). The changes in the oxidation state of Mo atoms in the course of the reaction may result from the interaction of the catalyst with the substrate (it was shown that supported molybdenum catalysts undergo reduction of Mo atoms upon the contact with an alkene [1]).

After the spectrum shown in Fig. 5.40A was taken, the measurement was prolonged for another 60 min in order to check if the monochromatic Al Kα X-ray source used for the measurements could change the nature of the sample as reported in the literature (the effect of photoinduced reduction [44]).

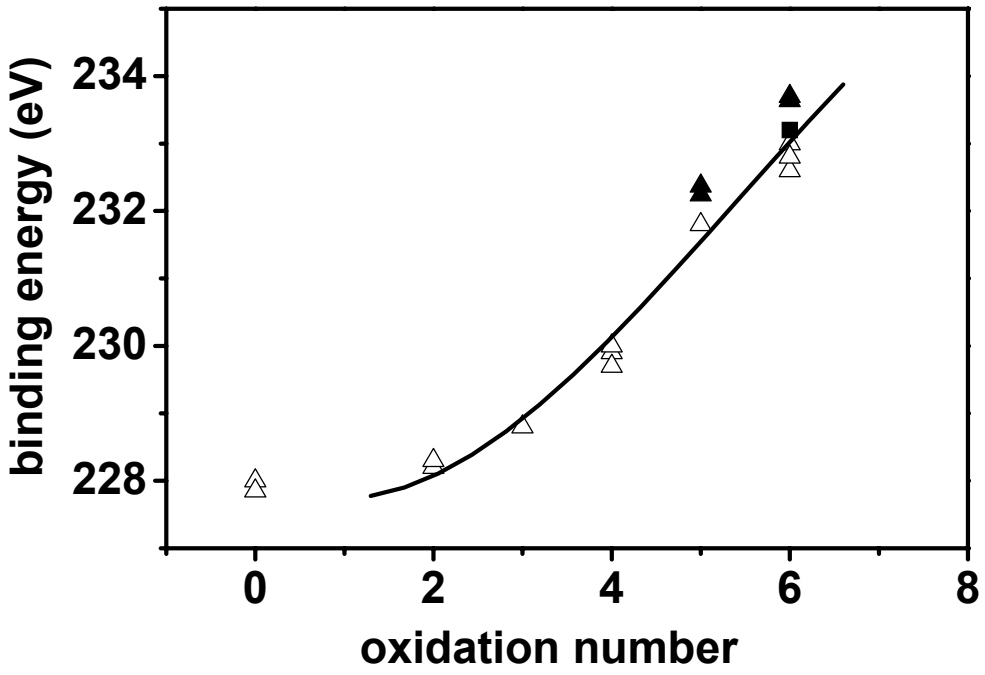

Figure 5.41

Dependence of binding energy of Mo $3d_{5/2}$ electrons on formal oxidation state of Mo atoms. Literature data [136,137] are indicated by open symbols; solid symbols show the results obtained for $6MoO_3$/MCM-41 catalyst after the metathesis reaction (▲) and unactivated $12MoO_3$/MCM-41 catalyst before the reaction (■).

As it is seen from Fig. 5.40B, practically identical spectrum was acquired after 60 min of the irradiation. Thus, it was confirmed that the monochromatic Al Kα X-ray radiation employed in the XPS measurements did not cause the changes in the oxidation state of Mo atoms.

5.3.6 Summary

Using Raman spectroscopy it was shown that the population of different types of Mo species and MoO_3 depends on the type of the support and molybdenum loading (Chapter 5.3.2). The dispersion of Mo was decreasing in the order MoO_3/MCM-41 > MoO_3/MCM-48 > MoO_3/SBA-15 ≈ MoO_3/SiO_2, i.e. in the order of decreasing conversion of 1-octene (Chapter 5.2.6). For all types of catalysts, decreasing dispersion of Mo species was observed with increasing molybdenum loading. Whereas for low loadings (from 4 to 8 wt. % Mo), the bands corresponding to isolated monomeric molybdenum species prevailed, with higher Mo content the intensity of the bands of

surface polymolybdates increased and finally at 16 wt. % Mo loading the bands of crystalline MoO_3 were dominating. However, because the dependences of band intensity on the concentration of individual Mo species are not known, their amount cannot be quantitatively determined.

The differences in conversion of 1-octene may be explained as follows: whereas isolated monomeric Mo species are supposed to give rise to high amount of catalytically active sites [107], bulk MoO_3 is catalytically practically inactive (Chapter 5.2.6), and surface polymolybdates are supposed to be less efficient precursors of the active sites in comparison with isolated monomeric Mo species. Thus, the conversions of 1-octene reached with the catalysts having loading between 4 and 8 wt. % Mo (Chapter 5.2.6) can be correlated with higher relative concentration of isolated monomeric Mo species than in other cases. Similarly, the superior catalytic activity of MoO_3/MCM-41 catalyst may be connected with excellent dispersion of Mo over this support.

Moreover, by Raman spectroscopy it was shown that the dispersion of Mo species on the surface of MoO_3/MCM-41 changed during the activation of the catalyst. The increase in the dispersion of Mo accompanied with the reduction of Mo atoms in the course of the activation was also indicated by XPS.

The large difference in conversion of 1-octene achieved with MoO_3/MCM-41 and MoO_3/SiO_2 can be explained by high surface area of mesoporous support, which enables better dispersion of Mo species together with easier reduction of Mo atoms. Therefore, higher conversions of 1-octene over MoO_3/MCM-41 might be expected. On the other hand, the differences in the dispersion of Mo and thus the reached 1-octene conversion among MoO_3 catalysts supported on MCM-41, MCM-48, and SBA-15 do not correlate neither with surface area nor with pore size of the parent support. Therefore, there should be other factors influencing the dispersion of Mo.

It is known that the spreading of MoO_3 over the siliceous support proceeds via formation of Si-O-Mo bonds with the surface OH groups of the support [44]. When the concentrations of surface OH groups per gram of parent support were estimated from the bands corresponding to OH stretching vibrations in FTIR spectra of the supports, it was found that the concentration of surface OH groups was decreasing in the order MCM-41 > MCM-48 > SBA-15, i.e. in the same order as the dispersion of Mo as determined by Raman spectroscopy (Chapter 5.3.2). Thus, the differences in the dispersion of Mo among MoO_3/MCM-41, MoO_3/MCM-48, and MoO_3/SBA-15 may be assigned to different concentration of OH groups per gram of the support. However, it

should be mentioned that this finding is in contradiction with the concentration of weekly acidic OH groups per gram of the support as determined by FTIR spectroscopy of adsorbed pyridine, which was decreasing in the order SBA-15 > MCM-41 > MCM-48. In contrary, the concentration of OH groups per gram of the support estimated from ^{29}Si MAS NMR spectra of parent supports was decreasing in the order MCM-48 > MCM-41 ~ SBA-15. However, the discrepancy between results obtained by FTIR spectroscopy of adsorbed pyridine and ^{29}Si MAS NMR spectra was also observed in the literature [133].

According to the XPS measurements, only Mo(VI) was found in unactivated 12MoO_3/MCM-41 catalyst (Chapter 5.3.5). After activation, the catalyst contained 39 % of Mo(V) and 61 % of Mo(VI). This finding is in accord with the literature [46-48], where the slight reduction of molybdenum(VI) to formal oxidation state between Mo(V) and Mo(VI) was found to be essential for obtaining an active metathesis catalyst.

In agreement with Raman spectroscopy (Chapter 5.3.2), the increase in the dispersion of Mo species during the activation of the catalyst was confirmed by increased Mo3d:Si2p ratio and shifted Mo $3d_{5/2}$ binding energy.

75 % of Mo(V) and 25 % of Mo(VI) was revealed from the XPS spectra of the spent 6MoO_3/MCM-41 catalyst involved in the metathesis reaction. It might be speculated that such high content of Mo(V) could be detrimental for catalytic activity.

5.4 Metathesis of unsaturated ethers and esters

In order to check the activity of MoO_3/MCM-41 catalysts in metathesis of unsaturated ethers and esters, 4-allylanisole and diethyl diallylmalonate were tested as substrates; toluene was used as a solvent.

When 4-allylanisole underwent the metathesis over 8MoO_3/MCM-41 catalyst, practically zero conversion was observed after 360 min of the reaction (Fig. 5.42), even though the initial substrate-to-catalyst molar ratio (*S:C*) was low (*S:C* = 24).

It is known that heterogeneous metathesis catalysts can be effectively promoted with tetraalkyltins [138]. These cocatalysts are responsible for the alkylation of metal sites, which is probably followed by transformation of part of them into active metal alkylidenes [20]. It was shown that treating alumina supported molybdenum catalysts with tetramethyltin caused an increase in the number of the metathesis active sites [23].

Therefore, tetramethyltin was used in order to increase the activity of MoO_3/MCM-41 catalyst in metathesis of unsaturated ethers and esters.

From Fig. 5.42 it is seen that the higher was tin-to-molybdenum molar ratio (*Sn:Mo*), the higher was the conversion achieved after 360 min of the reaction (17 and 33 % for *Sn:Mo* = 0.35 and 0.9, respectively). In contrast, the optimal *Sn:Mo* = 0.05 was reported for alumina supported molybdenum catalyst in metathesis of propene [138].

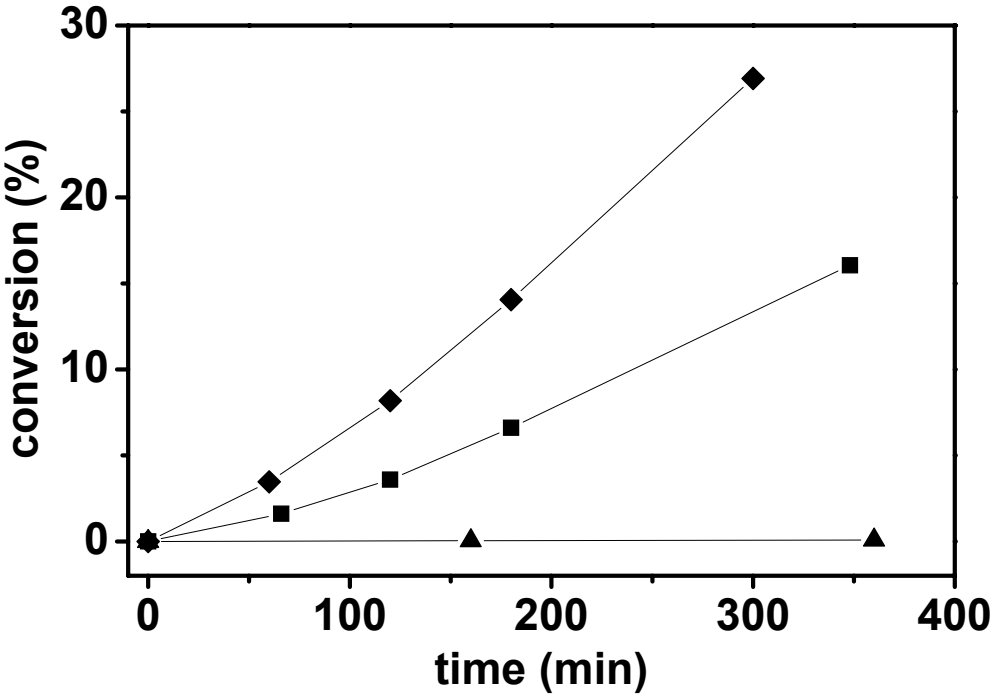

Figure 5.42

Conversion of 4-allylanisole dependence on time for $8MoO_3$/MCM-41 with *S:C* = 24: not promoted (▲), and promoted with tetramethyltin, *Sn:Mo* = 0.35 (■) and 0.9 (◆); reaction temperature 40 °C, initial substrate-to-toluene volume ratio 0.1.

No side products were observed; the selectivity to main metathesis product, 1,4-bis(4-methoxyphenyl)-2-butene, was 100 % and the cis-to-trans ratio determined from ^{13}C NMR spectra of the product was about 0.25 in all cases.

When *S:C* was decreased from 24 to 8, even without the presence of cocatalyst some conversion of 4-allylanisole was reached over $8MoO_3$/MCM-41 catalyst (6 % after 360 min of the reaction; Fig. 5.43). Nevertheless, when tetramethyltin was used as a cocatalyst (*Sn:Mo* = 0.9), the conversion of 4-allylanisole increased dramatically (81 % after 180 min of the reaction). This corresponds to an increase in the activity of

about 29 times (TOF_{120} was $2.38 \cdot 10^{-5}$ and $6.79 \cdot 10^{-4}$ s^{-1} for *Sn:Mo* = 0 and *Sn:Mo* = 0.9, respectively). Similar increase in activity (about 20 times) was reported for alumina supported molybdenum catalyst in metathesis of propene [138]. However, in ref. [138], *Sn:Mo* was only 0.05. Finally, when *Sn:Mo* was 0.9 and *S:C* was increased about three times (*S:C* = 24), the conversion achieved over $8MoO_3$/MCM-41 was rather small (14 % after 180 min of the reaction; Fig. 5.43).

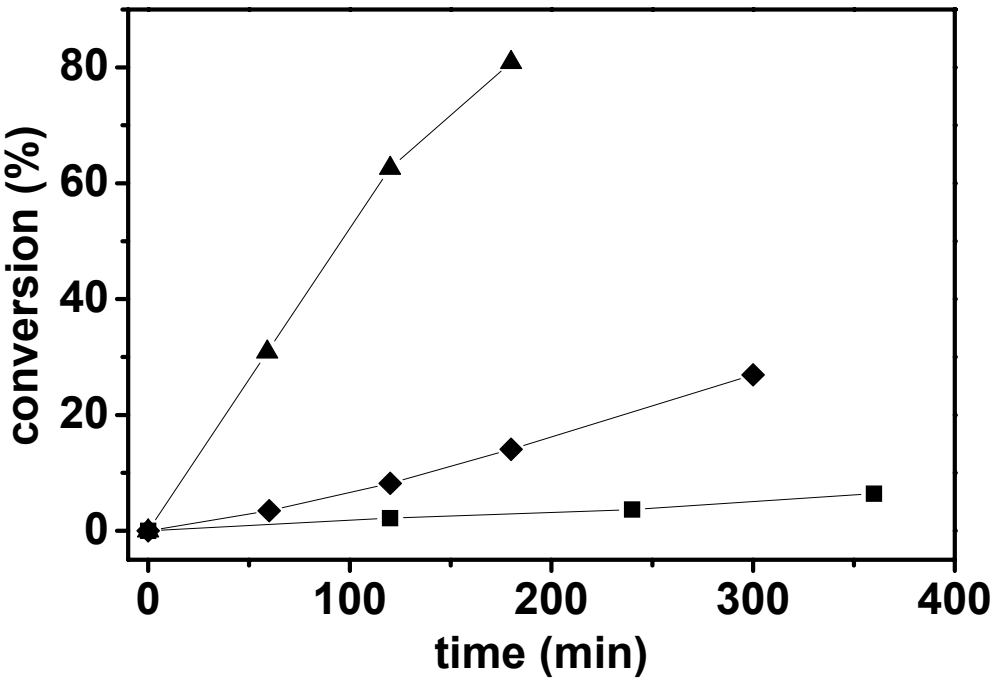

Figure 5.43

Conversion of 4-allylanisole dependence on time for $8MoO_3$/MCM-41 with different *S:C*: not promoted, *S:C* = 8 (■), and promoted with tetramethyltin (*Sn:Mo* = 0.9) with *S:C* = 24 (◆) and *S:C* = 8 (▲). Reaction temperature 40 °C, initial substrate-to-toluene volume ratio 0.1.

The conversions of 4-allylanisole achieved with $8MoO_3$/MCM-41 catalyst seemed to be insufficiently low even with the aid of tetramethyltin as a cocatalyst. However, in the case of 4-allylanisole, the oxygen-containing group causing the decay of the metallocarbene active sites was far from the double bond, where the reaction proceeded. On the other hand, the presence of the functional group in the proximity of the double bond, as in the case of diethyl diallylmalonate, caused a further decrease in catalytic activity (Fig. 5.44). Only negligible conversion of diethyl diallylmalonate (2 % after

360 min of the reaction) was achieved over $8MoO_3$/MCM-41 promoted with tetramethyltin (*Sn:Mo* = 0.9) when *S:C* was 21. With other substrates such as allyl phenyl ether, hexenyl acetate, methyl undecenoate, and chlorostyrene even lower conversion than with diethyl diallylmalonate (13 % after 360 min of the reaction) under the same reaction conditions (*S:C* = 8, *Sn:Mo* = 0.9) were achieved (not shown in Fig.).

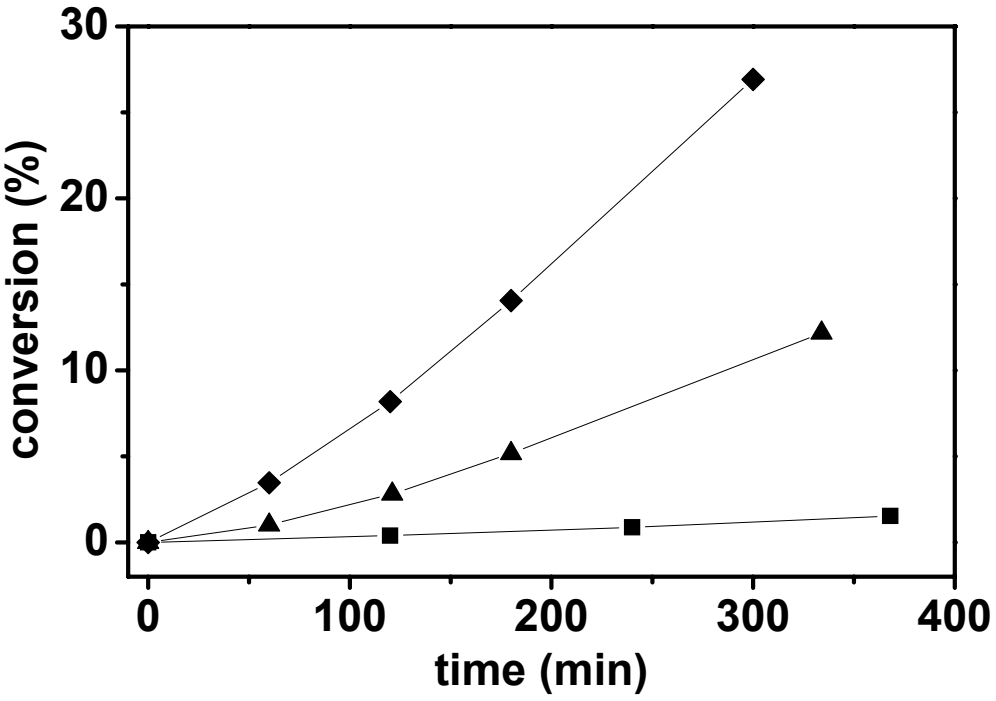

Figure 5.44

Conversion of 4-allylanisole and diethyl diallylmalonate dependence on time for $8MoO_3$/MCM-41 promoted with tetramethyltin (*Sn:Mo* = 0.9): diethyl diallylmalonate with *S:C* = 21 (■), diethyl diallylmalonate with *S:C* = 8 (▲), and 4-allylanisole with *S:C* = 24 (◆); reaction temperature 40 °C, substrate-to-toluene volume ratio 0.1.

Thus, it seems that other types of catalysts are to be preferred in metathesis of unsaturated ethers and esters. Recently, good results were achieved with rhenium oxide supported on organized mesoporous alumina [139].

5.5 Polymerization of alkynes

Molybdenum oxide supported on mesoporous molecular sieves MCM-41, MCM-48 and SBA-15 was also tested in metathesis of alkynes; 1-hexyne was chosen as a model substrate. However, in the presence of above-mentioned catalysts, the products of metathesis were not found and only polymerization reaction took place.

With $6MoO_3$/MCM-41, the most active catalyst in metathesis of alkenes, the polymerization of 1-hexyne proceeded rapidly and the polymer was continuously released to the liquid phase. Toluene was used as a solvent, initial substrate-to-catalyst molar ratio *S:C* (1-hexyne to Mo) was 70. After 15 min of the reaction, a slightly yellow polymer of M_w = 19 000 was isolated in 7 % yield; after 90 min the yield of polymer increased to 34 % (Tab. 5.7). With increasing polymer yield the viscosity of the reaction mixture increased and the reaction rate decreased. After 180 min of the reaction, 38 % yield of the polymer with M_w = 23 000 was achieved. Evaporation residue of grease consistence (22 % yield) consisted mainly of higher oligomers (SEC peak area = 43 %, M_w = 2 700) and cyclotrimers (SEC peak area = 54 %). Cyclotrimers (1,3,5-tributylbenzene and 1,2,4-tributylbenzene) were found in roughly equimolar amounts by GC-MS.

Table 5.7

Polymerization of 1-hexyne over MoO_3 based catalysts with 6 wt. % Mo; solvent: toluene, reaction time 180 min, reaction temperature 40 °C, initial substrate-to-catalyst molar ratio *(S:C)* = 70. * = reaction time 15 min, ** = reaction time 90 min, † = 1-octene was added in equimolar amount to 1-hexyne, ‡ = 1-octene was added in excess to 1-hexyne (initial molar ratio 1-octene:1-hexyne = 5), § = reactivated catalyst; M_w, M_n = weight-average molecular weight and number-average molecular weight, respectively; n.d. = not determined.

Catalyst	Polymer Yield (%)	Evaporation Residue Yield (%)	Polymer Molecular Weight	
			M_w	M_n
$6MoO_3$/MCM-41 *	7	6	19 000	7 500
$6MoO_3$/MCM-41 **	34	n.d.	n.d.	n.d.
$6MoO_3$/MCM-41	38	22	23 000	10 000
$6MoO_3$/MCM-48	22	n.d.	8 800	2 700
$6MoO_3$/SBA-15	64	n.d.	30 000	7 500
$6MoO_3/SiO_2$	4	3	6 800	2 200
$6MoO_3$/MCM-41 †	3	12	13 000	7 000
$6MoO_3$/MCM-41 ‡	0	18	n.d.	n.d.
$6MoO_3$/MCM-41 §	18	n.d.	6 100	1 600

Catalyst $6MoO_3$/SBA-15 appeared to be even more active in polymerization of 1-hexyne than $6MoO_3$/MCM-41. Polymer with M_w = 30 000 was obtained in 64 % yield

after 180 min of the reaction. On the other hand, with $6MoO_3$/MCM-48, only 22 % yield was afforded at the same time. Both polymer yield and M_w increased in the order MoO_3/MCM-48 < MoO_3/MCM-41 < MoO_3/SBA-15.

As shown in Chapter 5.1, MCM-48 has in comparison with MCM-41 only slightly lower pore size, but possesses a three-dimensional array of intersecting channels. On the other hand, MCM-41 and SBA-15 have the same structure with one-dimensional array of channels, but differ in pore size. Therefore, it should be expected that the increasing pore size plays the decisive role in the catalytic activity. However, other factors as dispersion of molybdenum oxide (Chapter 5.3) may influence the catalytic activity in polymerization of 1-hexyne as well.

Only 4 % yield of polymer, together with 3 % yield of oligomeric fraction, was reached with $6MoO_3/SiO_2$ catalyst. Thus, in comparison with MoO_3 supported on mesoporous silicas, its activity in polymerization of 1-hexyne was substantially lower (similar difference in activity was observed in metathesis of 1-octene as well, Chapter 5.2.6).

When the spent MoO_3/MCM-41 catalyst was regenerated by calcination in air at 500 °C for 3 h, only 18 % polymer yield of poly(1-hexyne) was achieved after 180 min of the reaction. Thus, in contrast to the results obtained in metathesis of 1-octene (Chapter 5.2.4), the activity of the catalyst after the regeneration was significantly reduced. However, no leaching was observed and Mo concentration in the polymers determined by ETA AAS was only 8 ppm, which indicates a high purity of obtained polyalkynes. In a blank experiment with pure MCM-41, no polymer was formed even after 20 h of the reaction (not given in Tab. 5.7).

Generally, two reaction mechanisms of polymerization of alkynes over transition metal catalysts must be taken into account: (i) insertion (metal vinyl) mechanism, and (ii) metathesis (metal carbene) mechanism (Fig. 5.45). As the supported MoO_3 catalysts are highly active in metathesis of alkenes (Chapter 5.2), it is supposed that also in polymerization of alkynes they possess the same type of active sites, i.e. metal carbenes.

In order to check whether the $6MoO_3$/MCM-41 catalyst operates in metathesis mode during the polymerization of 1-hexyne, following experiment was made: on the beginning of the polymerization experiment, 1-octene was added to the reaction mixture. If the polymerization proceeds via metal carbene mechanism, 1-octene present in the reaction mixture will cause the chain transfer reaction, which will result in a

lower polymer molecular weight. In contrast, if the polymerization mechanism is a metal vinyl one, the molecular weight of the polymer will be not affected.

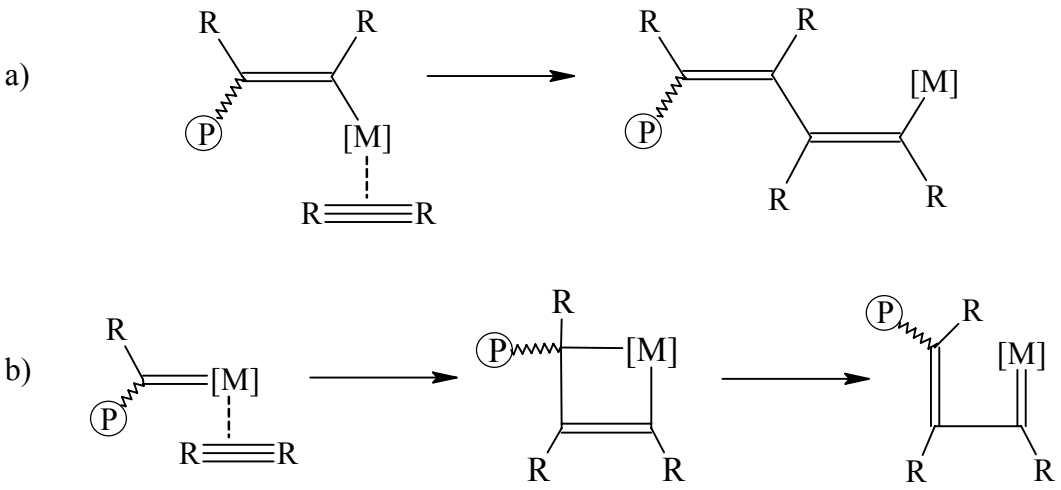

Figure 5.45

Insertion (metal vinyl) mechanism (a) and metathesis (metal carbene) mechanism (b) of alkyne polymerization [63]; (P) = polymer chain, R = alkyl.

As it is seen from Tab. 5.7, when 1-octene was added in equimolar amount to 1-hexyne, polymer yield was reduced from 38 to 3 % and M_w decreased from 23 000 to 13 000 in comparison with the same experiment performed without 1-octene. At initial 1-octene:1-hexyne ratio = 5, only oligomers were formed (higher oligomers of M_w = 2 600 with 12 % yield, and cyclotrimers with 6 % yield). These results clearly show that 1-octene acted as a chain transfer agent, which supports the assumption that the polymerization of 1-hexyne over $6MoO_3$/MCM-41 catalyst proceeds via metal carbene mechanism.

Surprisingly, the products of metathesis of 1-octene were not found in the reaction mixture. This might be explained by different affinity of the substrates to metallocarbenes, which are supposed to be the active sites in both types of reactions. Alkynes exhibit on the C≡C bond higher electron density than alkenes on their C=C bond; therefore, higher affinity of alkynes to electrophilic metallocarbenes may be expected as compared with alkynes. Consequently, a polymerization reaction occurs, whereas the reaction rate of metathesis is practically zero. This statement is in accord with the results reported for homogeneous $Mo(NAr)(CHR)(OR')_2$ Schrock catalyst (R,

R' = alkyls), where relative electron-withdrawing OR' ligands favor high catalytic activity [7,140].

Series of different alkynes was polymerized with $6MoO_3$/MCM-41 catalyst. Linear 1-alkynes with longer chains (1-decyne and 1-tetradecyne) were polymerized with similar yields as in the case of 1-hexyne (from 35 to 38 %), and polymers with molecular weights close to that of poly(1-hexyne) were obtained (Tab. 5.8). In the case of poly(tetradecyne), only a part of the polymer was soluble in THF after its isolation. Therefore, molecular weight characteristics are referred to the soluble part only.

On the other hand, poly(*tert*-butylacetylene) was obtained in 11 % yield only and in the polymerization of 2-hexyne, negligible 1 % yield of polymer was reached. In both cases, the low yield is probably caused by limited release of high molecular weight polymer from the catalyst pores. In the polymerization of phenylacetylene, only 1 % yield of polymer was achieved together with 0.2 % yield of cyclotrimers. The introduction of electron-withdrawing fluorine substituents on the phenyl ring (monomers: 4-fluoro-, and 2,4-difluorophenylacetylene) led to only a slight increase in the polymer yield (10 and 8 %, respectively).

Table 5.8

Polymerization of different alkynes with $6MoO_3$/MCM-41 catalyst; solvent: toluene, reaction time 180 min, reaction temperature 40 °C, *S:C* = 70. * = THF soluble part, ** = MeOH soluble product; M_w, M_n = weight-average molecular weight and number-average molecular weight, respectively.

Monomer	Polymer Yield (%)	M_w	M_n
1-hexyne	38	23 000	10 000
1-decyne	38	18 000	8 400
1-tetradecyne	35	20 000 *	13 000 *
tert-butylacetylene	11	300 000	39 000
2-hexyne	1	199 000 *	22 000 *
phenylacetylene	1	16 000	4 700
4-fluorophenylacetylene	10	5 200	2 800
2,4-difluorophenylacetylene	8 **	1 900	1 500

Recently, Schrock carbene complexes anchored on MCM-41 by alkoxy ligand exchange reaction were successfully employed in ring opening metathesis

polymerization of norbornene and cyclooctene [141]. With these new catalysts, high molecular weight polymers of high purity (about 6 ppm of Mo) were obtained in good yields. Therefore, Mo(=CHCMe$_2$Ph)(=N-2,6-*i*-Pr$_2$C$_6$H$_3$)[OCMe(CF$_3$)$_2$]$_2$ (Mo^{carb}) grafted on MCM-41 and SBA-15 (catalysts denoted as 1Mo^{carb}/MCM-41 and 1Mo^{carb}/SBA-15, respectively) was tested in polymerization of 1-hexyne as well (Tab. 5.9).

The polymer yields achieved with 1Mo^{carb}/MCM-41 and 1Mo^{carb}/SBA-15 were slightly lower in comparison with corresponding MoO_3 based catalysts (cf. Tab. 5.7). In addition, the molecular weights of resulting poly(1-hexyne) were significantly lower (e.g. M_w = 4 900 for 1Mo^{carb}/SBA-15 vs. M_w = 30 000 for 6MoO_3/SBA-15). To check the intrinsic catalytic activity of Mo^{carb} complex, the experiment with Mo^{carb} as homogeneous catalyst was conducted as well (Tab. 5.9).

Table 5.9

Polymerization of 1-hexyne over Schrock-type Mo carbene based catalysts with 1 wt. % Mo; solvent: benzene, reaction time 180 min, reaction temperature 25 °C, *S:C* = 100, initial 1-hexyne-to-benzene volume ratio = 0.03. * = Mo^{carb} in benzene as homogeneous catalyst; M_w, M_n = weight-average molecular weight and number-average molecular weight, respectively.

Catalyst	Polymer Yield (%)	M_w	M_n
1Mo^{carb}/MCM-41	34	7 500	2 800
1Mo^{carb}/SBA-15	59	4 900	1 900
Mo^{carb} *	98	17 000	10 000

In this case, poly(1-hexyne) was obtained in nearly quantitative yield (98 %), however, the molecular weight of the polymer (M_w = 17 000) was also lower in comparison with MoO_3 based catalysts (cf. Tab. 5.7). Nevertheless, the relatively low molecular weight of the polymer is not surprising. In the heterogeneous catalyst, not all Mo atoms are easily accessible due to diffusion limitations and sterical hindrances arising from the location on the surface of the support. On the other hand, in the case of a homogeneous one, practically every Mo atom takes part in the polymerization reaction. The high number of active sites then leads to lower molecular weight of the polymer in comparison with that obtained over heterogeneous catalyst.

Whereas with homogeneous Mo^{carb} a polymer with reasonably low polydispersity index was prepared (M_w/M_n = 1.7), in the case of both anchored Mo^{carb} catalysts M_w/M_n

was about 2.6. Such high polydispersity index indicates that the polymerization is very far from a "living" one. This increase in the polydispersity may be caused by limited diffusion rate of monomer and polymer molecules in the catalyst channels as well as by chain transfer processes, which are responsible for polymer releasing from the catalyst into the reaction mixture. Diffusion limitations and chain transfer processes may be responsible for the decrease in polymer molecular weight as well.

The structure of polymers prepared was checked by nuclear magnetic resonance. ^{1}H NMR spectrum of poly(1-hexyne) prepared with $6MoO_3$/MCM-41 catalyst is shown in Fig. 5.46b. It corresponds to a typical polyacetylene structure of the polymer consisting of conjugated main chain with n-butyl pendant groups, which give rise the signal with chemical shift 1.3 ppm (-CH_2- groups) and 0.9 ppm (-CH_3 group) [142]. Similar spectra, but with properly increased intensity of methylene proton signals at δ = 1.3 ppm, were also observed in the case of poly(1-decyne) and poly(1-tetradecyne) prepared with the same catalyst (Fig. 5.46c, d). The broad signal of the olefinic proton on the main chain (δ from 5.0 to 6.5 ppm) indicates irregular structure of the polymers, i.e. random distribution of cis and trans double bonds along the main chain and randomness in head-to-head and head-to-tail monomer linkage.

In contrast, ^{1}H NMR spectra of poly(1-hexyne)s prepared with $1Mo^{carb}$/MCM-41 (Fig. 5.46a) and $1Mo^{carb}$/SBA-15 (not shown in Fig.) possessed a narrow signal at δ = 5.9 ppm. This sharp signal of main-chain olefinic proton indicates increased polymer regularity. The same signal was observed for poly(1-hexyne)s prepared with Rh complexes [143], which are well known for their cis-transoidal stereoselectivity [144]. Therefore, this signal was ascribed to the main-chain olefinic proton on double bonds with cis configuration, although it is in disagreement with some other literature data [145]. Thus, according to ^{1}H NMR spectra the polymers prepared with heterogenized Schrock-type Mo catalysts had higher content of cis double bonds in comparison with polymers obtained with MoO_3 based catalysts. In addition, also in the case of Mo^{carb} employed as homogeneous catalyst, similar sharp signal of olefinic proton at 5.9 ppm was observed in ^{1}H NMR spectrum of poly(1-hexyne). Therefore, it seems that the polymerization selectivity leading to high content of cis- double bonds and increased regularity of the polymer is an inherent property of Mo^{carb} catalyst, which is preserved also after immobilization.

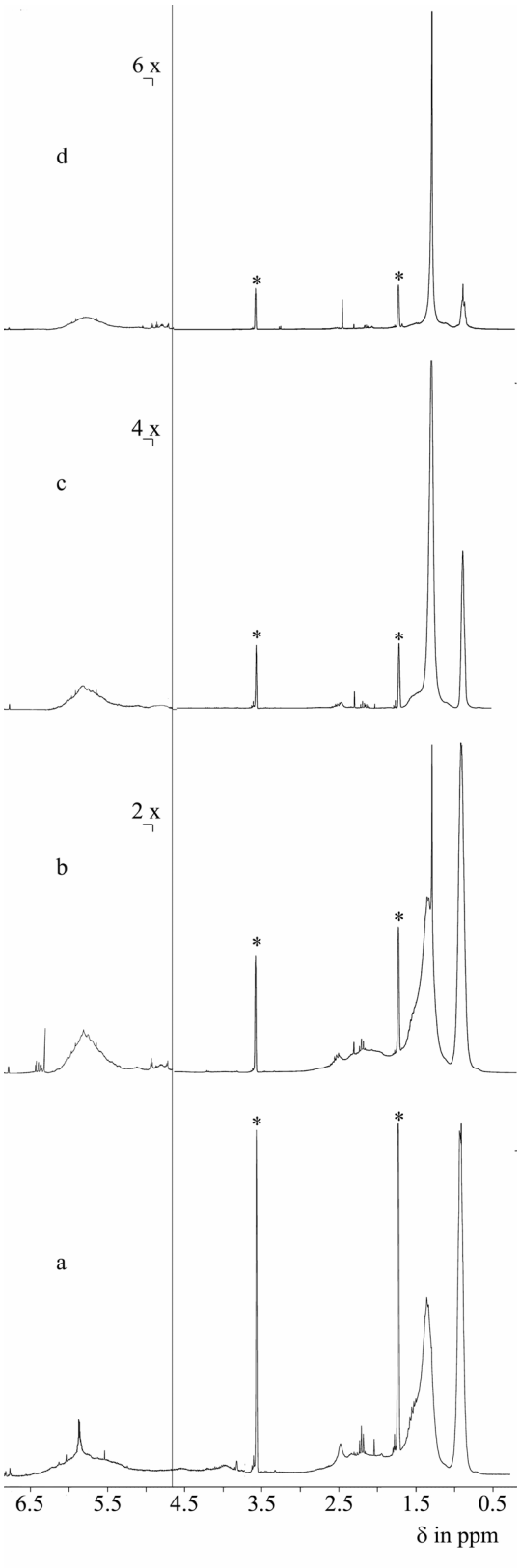

Figure 5.46

^{1}H NMR spectra of polyalkynes: a) poly(1-hexyne) prepared with 1Mo^{carb}/MCM-41, and b) poly(1-hexyne), c) poly(1-decyne), and d) THF soluble part of poly(1-tetradecyne) prepared with 6MoO_3/MCM-41. Recorded in THF-d8 at room temperature; * signal of THF.

This selectivity can be associated with the structure of Mo^{carb}: the presence of bulky ligands in coordination sphere of Mo leads to an uniform type of addition of 1-hexyne to the propagating carbene, which results in the uniform head-to-tail linkage of monomeric units in the polymer chain [146].

6 CONCLUSIONS

New type of heterogeneous catalysts for metathesis of alkenes and polymerization of alkynes based on molybdenum oxide supported on siliceous mesoporous molecular sieves MCM-41, MCM-48, and SBA-15 was developed. For the preparation of the catalysts, environmentally friendly thermal spreading method (calcination at 500 °C) was successfully used.

These new systems represent inexpensive, easy-to-prepare and highly active and selective heterogeneous catalysts for metathesis of linear alkenes that operate without the necessity of solvent or cocatalyst presence in the reaction mixture, which makes the separation of the products much easier. In contrast to commercial catalysts, they work under mild reaction conditions. At 40 °C, the most active MoO_3/MCM-41 catalyst with 6 wt. % of Mo allowed reaching 75 % conversion of 1-octene after 360 min of the reaction with selectivity to 7-tetradecene being 84 %. The initial turn-over frequency of MoO_3/MCM-41 catalyst (loading 6 wt. % Mo) at 40 °C was 0.014 s^{-1}, i.e. more than four times higher in comparison with conventional MoO_3/SiO_2 catalyst with the same loading operating under the same reaction conditions.

Neither catalysts prepared from organometallic precursors as $MoO_2(acac)_2$ nor that prepared by direct synthesis of Mo-MCM-41 or by impregnation from ammonium heptamolybdate solution exhibited higher activity than MoO_3/MCM-41 catalyst. The activity of MoO_3 based catalysts loaded with 8 wt. % Mo decreased in the order MoO_3/MCM-41 > MoO_3/MCM-48 > MoO_3/SBA-15 > MoO_3/SiO_2, while the selectivity was slightly increasing (from 82 to 95 %). Catalysts with lower loadings (from 4 to 8 wt. % Mo) exhibited higher specific activity than catalysts with the highest loading (16 wt. % Mo).

The differences in catalytic activity were correlated with the results of XRD, DR UV-VIS, XPS and Raman spectroscopy. It was shown that dispersion of molybdenum depends on Mo loading and kind of support used. Whereas for low loadings, isolated monomeric molybdenum species were prevailing, with higher Mo content the amount of surface polymolybdates increased and finally for the highest loaded catalysts 2.5 - 5 nm crystallites of MoO_3 appeared on the surface of the support. The relative amount of undispersed (bulky) MoO_3 was the highest for SBA-15 supported catalysts. No experimental evidences of the collapse of mesoporous structure of the catalysts were

observed, neither at the highest loading (16 wt. % Mo). The differences in the dispersion of Mo are probably connected with different number of surface OH groups of individual supports, as determined by FTIR spectroscopy.

No leaching of molybdenum species was observed and the concentration of Mo in the products was lower than 0.005 ppm. After reactivation, the catalyst fully recovered to its original activity and selectivity.

In metathesis of unsaturated ethers and esters, the activity of the catalysts was much lower than in metathesis of linear alkenes, even when tetramethyltin was employed as a cocatalalyst. The highest conversion was achieved in metathesis of 4-allylanisole (33 % conversion after 360 min of the reaction over MoO_3/MCM-41 catalyst with 8 wt. % Mo at 40 °C; toluene was used as a solvent, the initial substrate-to-catalyst molar ratio was 24 and the tin-to-molybdenum molar ratio was 0.9). No side products were observed; the selectivity to main metathesis product was 100 % in all cases.

In polymerization of alkynes, good results were achieved for aliphatic 1-alkynes. At 40 °C, poly(1-hexyne) with M_w = 30 000 was obtained in 64 % yield after 180 min of the reaction over the most active MoO_3/SBA-15 catalyst with 6 wt. % Mo. Both yield of poly(1-hexyne) and its molecular weight increased in the order MoO_3/SiO_2 < MoO_3/MCM-48 < MoO_3/MCM-41 < MoO_3/SBA-15 (loading 6 wt. % Mo). Polymers easy separable from the catalysts and of high purity were provided. The polyacetylene-like structure of the polymers (conjugated main chain with alkyl pendant groups) was confirmed by ^{1}H NMR. Polymerization via metathesis mechanism was proposed. In contrast to aliphatic 1-alkynes, the yields of internal alkynes and phenylacetylenes were low.

In comparison with corresponding MoO_3 based catalysts, Schrock carbene complexes anchored on MCM-41 and SBA-15 exhibited slightly lower polymer yields and significantly lower molecular weights of poly(1-hexyne)s. On the other hand, polymers prepared with these catalysts exhibited more regular microstructure and an increased content of cis double bonds.

7 REFERENCES

[1] K.J. Ivin, J.C. Mol, *Olefin Metathesis and Metathesis Polymerization*, Academic Press, London, 1997.

[2] *Olefin Metathesis/Grubbs Reaction*. Available from: http://www.organic-chemistry.org/namedreactions/olefin-metathesis.shtm.

[3] J.-L. Hérisson, Y. Chauvin, Makromol. Chem. 141 (1971) 161.

[4] K. Tanaka, Appl. Catal. A 188 (1999) 37.

[5] K.C. Nicolaou, P.G. Bulger, D. Sarlah, Angew. Chem. Int. Ed. 44 (2005) 4490.

[6] E.L. Dias, S.T. Nguyen, R.H. Grubbs, J. Am. Chem. Soc. 119 (1997) 3887.

[7] R.R. Schrock, J.S. Murdzek, G.C. Bazan, J. Robbins, M. Dimare, M. Oregan, J. Am. Chem. Soc. 112 (1990) 3875.

[8] A.M. Rouhi, Chem. Eng. News 80 (2002) 29.

[9] M.M. Kirk, *Ruthenium based homogeneous olefin metathesis (dissertation)*, University of the Free State, 2005.

[10] C. Coperet, J.M. Basset, Adv. Synth. Catal. 349 (2007) 78.

[11] R.H. Grubbs, Angew. Chem. Int. Ed. 45 (2006) 3760.

[12] R.R. Schrock, Angew. Chem. Int. Ed. 45 (2006) 3748.

[13] Y. Schrodi, R.L. Pederson, Aldrichim. Acta 40 (2007) 45.

[14] K.A. Burdett, L.D. Harris, P. Margl, B.R. Maughon, T. Mokhtar-Zadeh, P.C. Saucier, E.P. Wasserman, Organometallics 23 (2004) 2027.

[15] H. Balcar, N. Žilková, J. Sedláček, J. Zedník, J. Mol. Catal. A 232 (2005) 53.

[16] B.N. Shelimov, I.V. Elev, V.B. Kazansky, J. Mol. Catal. 46 (1988) 187.

[17] J.C. Mol, Catal. Today 51 (1999) 289.

[18] J.C. Mol, J. Mol. Catal. A 213 (2004) 39.

[19] J. Kopečný, L. Kurc, L. Červený, Chem. Listy 98 (2004) 246.

[20] J. Handzlik, J. Ogonowski, J. Stoch, M. Mikolajczyk, Appl. Catal. A 273 (2004) 99.

[21] M.A. Banares, I. Rodriguezramos, A. Guerreroruiz, J.L.G. Fierro, B.R. Hodnett, A. Parmaliana, K. Klier, U.S. Ozkan, O.V. Krylov, J.B. Moffat, C. Li, I.E. Wachs, Stud. Surf. Sci. Catal. 75 (1993) 1131.

[22] M.A. Banares, J.L.G. Fierro, Catal. Lett. 17 (1993) 205.

[23] J. Handzlik, J. Ogonowski, Catal. Lett. 88 (2003) 119.

[24] A.N. Startsev, O.V. Klimov, E.A. Khomyakova, J. Catal. 139 (1993) 134.

[25] D.T. Laverty, J.J. Rooney, A. Stewart, J. Catal. 45 (1976) 110.

[26] P. Amigues, Y. Chauvin, D. Commereuc, C.T. Hong, C.C. Lai, Y.H. Liu, J. Mol. Catal. 65 (1991) 39.

[27] S. Braun, L.G. Appel, V.L. Camorim, M. Schmal, J. Phys. Chem. B 104 (2000) 6584.

[28] Y. Iwasawa, H. Ichinose, S. Ogasawara, M. Soma, J. Chem. Soc., Faraday Trans. I 77 (1981) 1763.

[29] R.L. Banks, G.C. Bailey, Ind. Eng. Chem., Prod. Des. Rev. 3 (1964) 170.

[30] D.L. Crain, J. Catal. 13 (1969) 110.

[31] C.T. Kresge, M.E. Leonowicz, W.J. Roth, J.C. Vartuli, J.S. Beck, Nature 359 (1992) 710.

[32] J. Čejka, Appl. Catal. A 254 (2003) 327.

[33] R. Hamtil, N. Žilková, H. Balcar, J. Čejka, Appl. Catal. A 302 (2006) 193.

[34] A. Taguchi, F. Schüth, Microporous Mesoporous Mater. 77 (2005) 1.

[35] T. Ookoshi, M. Onaka, Chem. Commun. (1998) 2399.

[36] J. Handzlik, J. Ogonowski, J. Stoch, M. Mikolajczyk, P. Michorczyk, Appl. Catal. A 312 (2006) 213.

[37] J. Handzlik, J. Ogonowski, J. Stoch, M. Mikolajczyk, Catal. Lett. 101 (2005) 65.

[38] M. Ichikawa, Q. Zhuang, G.J. Li, K. Tanaka, T. Fujimoto, A. Fukuoka, A.A. Tsyganenko, J.C. Mol, W. Grunert, W.K. Hall, J.C. Conesa, D.C. Koningsberger, J. Vedrine, J.J. Rooney, Stud. Surf. Sci. Catal. 75 (1993) 529.

[39] C.C. Williams, J.G. Ekerdt, J.-M. Jehng, F.D. Hardcastle, A.M. Turek, I.E. Wachs, J. Phys. Chem. 95 (1991) 8781.

[40] N.C. Ramani, D.L. Sullivan, J.G. Ekerdt, J.-M. Jehng, I.E. Wachs, J. Catal. 176 (1998) 143.

[41] N. Ichikuni, T. Eguchi, H. Murayama, K.K. Bando, S. Shimazu, T. Uematsu, Stud. Surf. Sci. Catal. 146 (2003) 359.

[42] A. Sampieri, S. Pronier, J. Blanchard, M. Breysse, S. Brunet, K. Fajerwerg, C. Louis, G. Perot, Catal. Today 107-08 (2005) 537.

[43] L. Kaluža, M. Zdražil, N. Žilková, J. Čejka, Catal. Commun. 3 (2002) 151.

[44] Z.P. Li, L. Gao, S. Zheng, Appl. Catal. A 236 (2002) 163.

[45] D. Bruhwiler, G. Calzaferri, Microporous Mesoporous Mater. 72 (2004) 1.

[46] V. Indovina, A. Cimino, D. Cordischi, S. Dellabella, S. Derossi, G. Ferraris, D. Gazzoli, M. Occhiuzzi, M. Valigi, W. Grunert, M. Ichikawa, J. Goldwasser, C. Li, J.C. Mol, I.E. Wachs, W.K. Hall, Stud. Surf. Sci. Catal. 75 (1993) 875.

[47] B.A. Zhang, N.S. Liu, Q.S. Lin, D. Jin, J. Mol. Catal. 65 (1991) 15.

[48] B.N. Shelimov, I.V. Elev, V.B. Kazansky, J. Catal. 98 (1986) 70.

[49] M.N. Kwini, J.M. Botha, Appl. Catal. A 280 (2005) 199.

[50] R. Spronk, A. Andreini, J.C. Mol, J. Mol. Catal. 65 (1991) 219.

[51] European Chemical News, 25 March 2002, p. 20.

[52] A. Scott, Chemical Week, 3 November 1999, p. 41.

[53] *Ullmann's Encyclopedia of Industrial Chemistry*, Wiley-VCH, Weinheim, 2003.

[54] J.C. Mol, Top. Catal. 27 (2004) 97.

[55] J.C. Mol, Green Chem. 4 (2002) 5.

[56] R. Toreki. Available from: http://www.ilpi.com/organomet/index.html.

[57] F. Pennella, R.L. Banks, G.C. Bailey, Chem. Commun. (1968) 1548.

[58] A. Mortreux, M. Blanchar, J. Chem. Soc., Chem. Commun. (1974) 786.

[59] R.R. Schrock, Polyhedron 14 (1995) 3177.

[60] M. Chabanas, A. Baudouin, C. Coperet, J.M. Basset, J. Am. Chem. Soc. 123 (2001) 2062.

[61] H. Weissman, K.N. Plunkett, J.S. Moore, Angew. Chem. Int. Ed. 45 (2006) 585.

[62] W. Zhang, J.S. Moore, Adv. Synth. Catal. 349 (2007) 93.

[63] M.G. Mayershofer, O. Nuyken, J. Polym. Sci. A 43 (2005) 5723.

[64] H. Balcar, J. Čejka, J. Sedláček, J. Svoboda, J. Zedník, Z. Bastl, V. Bosáček, J. Vohlídal, J. Mol. Catal. A 203 (2003) 287.

[65] V. Chiola, J.E. Ritsko, C.D. Vanderpool, U.S. Patent No. 3 556 725, 1971.

[66] F. DiRenzo, H. Cambon, R. Dutartre, Microporous Mater. 10 (1997) 283.

[67] J.S. Beck, J.C. Vartuli, W.J. Roth, M.E. Leonowicz, C.T. Kresge, K.D. Schmitt, C.T.W. Chu, D.H. Olson, E.W. Sheppard, S.B. McCullen, J.B. Higgins, J.L. Schlenker, J. Am. Chem. Soc. 114 (1992) 10834.

[68] V. Gusev. Available from: http://www.chm.bris.ac.uk/motm/mcm41/mcm41.htm.

[69] S. Bhattacharya, *Molecular Models for Templated Mesoporous Materials: Mimetic Simulation and Gas Adsorption (dissertation)*, North Carolina State University, Raleigh, 2006.

[70] M. Kaneda, T. Tsubakiyama, A. Carlsson, Y. Sakamoto, T. Ohsuna, O. Terasaki, S.H. Joo, R. Ryoo, J. Phys. Chem. B 106 (2002) 1256.

[71] J.C. Vartuli, K.D. Schmitt, C.T. Kresge, W.J. Roth, M.E. Leonowicz, S.B. McCullen, S.D. Hellring, J.S. Beck, J.L. Schlenker, D.H. Olson, E.W. Sheppard, Chem. Mater. 6 (1994) 2317.

[72] A. Monnier, F. Schüth, Q. Huo, D. Kumar, D. Margolese, R.S. Maxwell, G.D. Stucky, M. Krishnamurthy, P. Petroff, A. Firouzi, M. Janicke, B.F. Chmelka, Science 261 (1993) 1299.

[73] Neeraj, C.N.R. Rao, J. Mater. Chem. 8 (1998) 1631.

[74] S. Inagaki, A. Koiwai, N. Suzuki, Y. Fukushima, K. Kuroda, Bull. Chem. Soc. Jpn. 69 (1996) 1449.

[75] Q.S. Huo, R. Leon, P.M. Petroff, G.D. Stucky, Science 268 (1995) 1324.

[76] X.S. Zhao, G.Q. Lu, A.K. Whittaker, G.J. Millar, H.Y. Zhu, J. Phys. Chem. B 101 (1997) 6525.

[77] M. Linden, P. Agren, S. Karlsson, P. Bussain, H. Amenitsch, Langmuir 16 (2000) 5831.

[78] N. Ulagappan, C.N.R. Rao, Chem. Commun. (1996) 2759.

[79] A. Lind, J. Andersson, S. Karlsson, P. Agren, P. Bussian, H. Amenitsch, M. Linden, Langmuir 18 (2002) 1380.

[80] X. Ma, J. Gong, S. Wang, N. Gao, D. Wang, X. Yang, F. He, Catal. Commun. 5 (2004) 101.

[81] A.E. Garcia-Bennett, O. Terasaki, S. Che, T. Tatsumi, Chem. Mater. 16 (2004) 813.

[82] T. Yanagisawa, T. Shimizu, K. Kuroda, C. Kato, Bull. Chem. Soc. Jpn. 63 (1990) 988.

[83] G.S. Attard, J.C. Glyde, C.G. Goltner, Nature 378 (1995) 366.

[84] R. Ryoo, S.H. Joo, S. Jun, J. Phys. Chem. B 103 (1999) 7743.

[85] A. Corma, Chem. Rev. 97 (1997) 2373.

[86] F.A. Twaiq, A.R. Mohamed, S. Bhatia, Microporous Mesoporous Mater. 64 (2003) 95.

[87] E. Armengol, M.L. Cano, A. Corma, H. Garcia, M.T. Navarro, J. Chem. Soc. Chem. Commun. (1995) 519.

[88] T. Kugita, S.K. Jana, T. Owada, N. Hashimoto, M. Onaka, S. Namba, Appl. Catal. A 245 (2003) 353.

[89] L.-X. Dai, K. Koyama, T. Tatsumi, Catal. Lett. 53 (1998) 211.

[90] A.L. Villade, P.E. Alarcon, C.M. Correa, Chem. Commun. (2002) 2654.

[91] Y. Zhu, S. Jaenicke, G.K. Chuah, J. Catal. 218 (2003) 396.

[92] E. Rivera-Munoz, D. Lardizabal, G. Alonso, A. Aguilar, M.H. Siadati, R.R. Chianelli, Catal. Lett. 85 (2003) 147.

[93] L. Vradman, M.V. Landau, M. Herskowitz, V. Ezersky, M. Talianker, S. Nikitenko, Y. Koltypin, A. Gedanken, J. Catal. 213 (2003) 163.

[94] X. Hu, M.L. Foo, G.K. Chuah, S. Jaenicke, J. Catal. 195 (2000) 412.

[95] T. Blasco, A. Corma, M.T. Navarro, J. Perez-Pariente, J. Catal. 156 (1995) 65.

[96] M. Yonemitsu, Y. Tanaka, M. Iwamoto, J. Catal. 178 (1998) 207.

[97] V. Parvulescu, C. Constantin, B.L. Su, J. Mol. Catal. A 202 (2003) 171.

[98] A. Corma, M.T. Navarro, M. Renz, J. Catal. 219 (2003) 242.

[99] A.K. Sinha, S. Seelan, T. Akita, S. Tsubota, M. Haruta, Catal. Lett. 85 (2003) 223.

[100] B. Sulikowski, Z. Olejniczak, E. Włoch, J. Rakoczy, R.X. Valenzuela, V.C. Corberan, Appl. Catal. A 232 (2002) 189.

[101] H. Berndt, A. Martin, A. Bruckner, E. Schreier, D. Muller, H. Kosslick, G.U. Wolf, B. Lucke, J. Catal. 191 (2000) 384.

[102] A. Wingen, N. Anastasievic, A. Hollnagel, D. Werner, F. Schuth, J. Catal. 193 (2000) 248.

[103] R. Raja, T. Khimyak, J.M. Thomas, S. Hermans, B.F.G. Johnson, Angew. Chem. Int. Ed. 40 (2001) 4638.

[104] E. Iglesia, S.L. Soled, R.A. Fiato, J. Catal. 137 (1992) 212.

[105] C.P. Mehnert, D.W. Weaver, J.Y. Ying, J. Am. Chem. Soc. 120 (1998) 12289.

[106] C.D. Nunes, A.A. Valente, M. Pillinger, J. Rocha, I.S. Goncalves, Chem. Eur. J. 9 (2003) 4380.

[107] O. Collart, P. Van Der Voort, E.F. Vansant, E. Gustin, A. Bouwen, D. Schoemaker, R. Ramachandra Rao, B.M. Weckhuysen, R.A. Schoonheydt, Phys. Chem. Chem. Phys. 1 (1999) 4099.

[108] G. Schulz-Ekloff, J. Rathouský, A. Zukal, Int. J. Inorg. Mater. 1 (1999) 97.

[109] S. Hitz, R. Prins, J. Catal. 168 (1997) 194.

[110] M. Kruk, M. Jaroniec, C.H. Ko, R. Ryoo, Chem. Mater. 12 (2000) 1961.

[111] Z. Li, L. Gao, S. Zheng, Mater. Lett. 57 (2003) 4605.

[112] S. Higashimoto, Y. Hu, R. Tsumura, K. Iino, M. Matsuoka, H. Yamashita, Y.G. Shul, M. Che, M. Anpo, J. Catal. 235 (2005) 272.

[113] C.A. Emeis, J. Catal. 141 (1993) 347.

[114] P. Topka, H. Balcar, J. Rathouský, N. Žilková, F. Verpoort, J. Čejka, Microporous Mesoporous Mater. 96 (2006) 44.

[115] D.Y. Zhao, J.L. Feng, Q.S. Huo, N. Melosh, G.H. Fredrickson, B.F. Chmelka, G.D. Stucky, Science 279 (1998) 548.

[116] A. Klug, P. Harold, E. Leroy, *X-Ray Diffraction Procedures For Polycrystalline and Amorphous Materials*, J. Wiley & Sons, New York, 1954.

[117] S.J. Gregg, K.S.W. Sing, *Adsorption, Surface Area and Porosity*, Academic Press, New York, 1982.

[118] R.F. de Farias, J. Phys. Chem. Solids 64 (2003) 1241.

[119] T. Klimova, A. Esquivel, J. Reyes, M. Rubio, X. Bokhimi, J. Aracil, Microporous Mesoporous Mater. 93 (2006) 331.

[120] R. Zavoianu, A.P.V.S. Dias, O.D. Pavel, E. Angelescu, M.F. Portela, Catal. Commun. 6 (2005) 321.

[121] H. Aritani, O. Fukuda, T. Yamamoto, T. Tanaka, S. Imamura, Chem. Lett. (2000) 66.

[122] J. Aguado, J.M. Escola, M.C. Castro, B. Paredes, Appl. Catal. A 284 (2005) 47.

[123] C.H. Bartholomew, Appl. Catal. A 212 (2001) 17.

[124] R.L. Banks, Appl. Ind. Catal. 3 (1984) 215.

[125] X. Li, W. Zhang, S. Liu, X. Han, L. Xu, X. Bao, J. Mol. Catal. A 250 (2006) 94.

[126] J. Sarrin, O. Noguera, H. Royo, M.J.P. Zurita, C. Scott, M.R. Goldwasser, J. Goldwasser, M. Houalla, J. Mol. Catal. A 144 (1999) 441.

[127] H. Jeziorowski, H. Knozinger, J. Phys. Chem. 83 (1979) 1166.

[128] M.A. Banares, I.E. Wachs, J. Raman Spectrosc. 33 (2002) 359.

[129] M. Faraldos, M.A. Banares, J.A. Anderson, H. Hu, I.E. Wachs, J.L.G. Fierro, J. Catal. 160 (1996) 214.

[130] L. Cao, L. Laim, P.D. Valenzuela, B. Nabet, J.E. Spanier, J. Raman Spectrosc. 38 (2007) 697.

[131] G. Mestl, T.K.K. Srinivasan, Cat. Rev. - Sci. Eng. 40 (1998) 451.

[132] A. Jentys, K. Kleestorfer, H. Vinek, Microporous Mesoporous Mater. 27 (1999) 321.

[133] I.G. Shenderovich, G. Buntkowsky, A. Schreiber, E. Gedat, S. Sharif, J. Albrecht, N.S. Golubev, G.H. Findenegg, H.H. Limbach, J. Phys. Chem. B 107 (2003) 11924.

[134] A.V. Biradar, S.B. Umbarkar, M.K. Dongare, Appl. Catal. A 285 (2005) 190.

[135] D.W. Sindorf, G.E. Maciel, J. Am. Chem. Soc. 103 (1981) 4263.

[136] M. Yamada, J. Yasumaru, M. Houalla, D.M. Hercules, J. Phys. Chem. 95 (1991) 7037.

[137] *Database NIST*. Available from: http://srdata.nist.gov/xps/index.htm.

[138] J. Handzlik, J. Ogonowski, Catal. Lett. 83 (2002) 287.

[139] H. Balcar, R. Hamtil, N. Žilková, Z. Zhang, T.J. Pinnavaia, J. Čejka, Appl. Catal. A 320 (2007) 56.

[140] R.R. Schrock, A.H. Hoveyda, Angew. Chem. Int. Ed. 42 (2003) 4592.

[141] H. Balcar, J. Čejka, in: *New Frontiers in Metathesis Chemistry: From Nanostructure Design to Sustainable Technologies for Synthesis of Advanced Materials*, ed. Y. Imamoglu and V. Dragutan, 2007, Springer, Dordrecht, p. 151.

[142] A. Petit, S. Moulay, T. Aouak, Eur. Polym. J. 35 (1999) 953.

[143] J. Sedláček, J. Vohlídal, Collect. Czech. Chem. Commun. 68 (2003) 1745.

[144] A. Furlani, S. Licoccia, M.V. Russo, A. Camus, N. Marsich, J. Polym. Sci. A 24 (2003) 991.

[145] M. Leclerc, R.E. Prud'homme, A. Soum, M. Fontanille, J. Polym. Sci. B 23 (1985) 2031.

[146] R.R. Schrock, S. Luo, J.C. Lee, N.C. Zanetti, W.M. Davis, J. Am. Chem. Soc. 118 (1996) 3883.

8 LIST OF USED SYMBOLS AND ABBREVIATIONS

A	relative area
a	adsorbed amount (cm^3/g STP)
a_0	correlation distance (nm)
α	number of surface OH groups (nm^{-2})
AHM	ammonium heptamolybdate
B	full width at half maximum of the peak (°, 2Θ)
b	full width at half maximum of the reference peak (°, 2Θ)
β	corrected broadening of the diffraction line (°, 2Θ)
BET	Brunauer-Emmett-Teller theory
C	conversion (%)
CP	cross polarization
CTMABr	hexadecyltrimethylammonium bromide
CTMAOH	hexadecyltrimethylammonium hydroxide
d	pore diameter (nm)
δ	chemical shift (ppm)
Δ	mean crystallite size (nm)
DMF	dimethylformamide
DR UV-VIS	diffuse reflectance spectroscopy in the ultraviolet-visible range
DR FTIR	diffuse reflectance Fourier transform infrared spectroscopy
ESR	electron spin resonance
ETA AAS	atomic absorption spectrometry with electrothermal atomization
FID	flame ionization detector
FTIR	Fourier transform infrared spectroscopy
GC	gas chromatography
GC-MS	gas chromatograph coupled with mass spectrometer
Θ	diffraction angle (°)
Θ_0	diffraction angle of the maximum of the diffraction line (°, 2Θ)
HMS	hexagonal mesoporous silica
HOMO	highest occupied molecular orbital
IA	integrated absorbance (cm^{-1})
ICP AES	inductively coupled plasma - atomic emission spectroscopy

K	constant
λ	wavelength (nm)
LRS	laser Raman spectroscopy
LUMO	lowest unoccupied molecular orbital
M_n	number-average molecular weight
M_w	weight-average molecular weight
m	weight (mg)
MAS NMR	magic-angle spinning nuclear magnetic resonance
MeOH	methanol
Mo^{carb}	$Mo(=CHCMe_2Ph)(=N\text{-}2,6\text{-}i\text{-}Pr_2C_6H_3)[OCMe(CF_3)_2]_2$
$MoO_2(acac)_2$	molybdenum(VI) dioxide bis(acetylacetonate)
n	molar amount (mol)
NMR	nuclear magnetic resonance
OMA	organized mesoporous alumina
p/p_0	relative pressure
ppm	parts per million (= mg/kg)
Q^2	geminal silanol sites, $(SiO)_2*Si(OH)_2$
Q^2	relative peak area of Q^2 atoms in ^{29}Si MAS NMR spectra (%)
Q^3	isolated silanol sites, $(SiO)_3*Si(OH)$
Q^3	relative peak area of Q^3 atoms in ^{29}Si MAS NMR spectra (%)
Q^4	silicon atoms with four siloxane bonds, $(SiO)_4*Si$
Q^4	relative peak area of Q^4 atoms in ^{29}Si MAS NMR spectra (%)
R	alkyl
S	selectivity (%)
S_{BET}	surface area according to Brunauer-Emmett-Teller theory (m^2/g)
S_{ext}	external surface area (m^2/g)
$S:C$	initial substrate-to-catalyst molar ratio
SEC	size exclusion chromatography
SEM	scanning electron microscopy
$Sn:Mo$	tin-to-molybdenum molar ratio
STP	standard temperature and pressure (273.15 K, 101.325 kPa)
τ	reaction time (min)
TEOS	tetraethyl orthosilicate
THF	tetrahydrofuran

TMAOH	tetramethylammonium hydroxide
TOF	turn-over frequency (s^{-1})
TOF_τ	turn-over frequency after τ min of the reaction (s^{-1})
TPR	temperature-programmed reduction
V_{meso}	mesopore volume (cm^3/g)
x	relative molar amount of Mo in the synthesis mixture
XPS	X-ray photoelectron spectroscopy
XRD	X-ray diffraction
XRF	X-ray fluorescence
y	molybdenum loading (wt. % Mo)

9 ENCLOSURES

Enclosure I

H. Balcar, P. Topka, N. Žilková, J. Pérez-Pariente, J. Čejka
Metathesis of linear α-olefins with MoO_3 supported on MCM-41 catalyst
Stud. Surf. Sci. Catal. 156 (2005) 795

Enclosure II

P. Topka, H. Balcar, J. Rathouský, N. Žilková, F. Verpoort, J. Čejka
Metathesis of 1-octene over MoO_3 supported on mesoporous molecular sieves: The influence of the support architecture
Microporous Mesoporous Mater. 96 (2006) 44

Enclosure III

H. Balcar, P. Topka, J. Sedláček, J. Zedník, J. Čejka
Polymerization of aliphatic alkynes with heterogeneous Mo catalysts supported on mesoporous molecular sieves
J. Polym. Sci. A 46 (2008) 2593

Enclosure I

H. Balcar, P. Topka, N. Žilková, J. Pérez-Pariente, J. Čejka

Metathesis of linear α-olefins with MoO_3 supported on MCM-41 catalyst

Stud. Surf. Sci. Catal. 156 (2005) 795

Metathesis of linear α-olefins with MoO_3 supported on MCM-41 catalyst

Hynek Balcar[a], Pavel Topka[a], Naděžda Žilková[a], Joaquín Pérez-Pariente[b] and Jiří Čejka[a]

[a]J. Heyrovský Institute of Physical Chemistry, Academy of Sciences of the Czech Republic, Dolejškova 3, CZ-182 23 Prague 8, Czech Republic, e-mail: jiri.cejka@jh-inst.cas.cz

[b]Instituto de Catálisis y Petroleoquímica (CSIC), c/ Marie Curie s/n, 28049 Cantoblanco, Madrid, Spain

New type of heterogeneous catalysts based on mesoporous molecular sieve MCM-41 modified with molybdenum oxide was proposed for the application in metathesis of linear 1-olefins. This catalyst prepared via „thermal spreading method" operates in a liquid phase under ambient or slightly higher reaction temperature without the presence of solvent. The optimum loading of molybdenum oxide was 8 wt. % of Mo. For 1-octene, the conversion achieved in 390 min. at 40 °C was 74 %, and the selectivity to 14-tetradecene was 82 %.

1. INTRODUCTION

Olefin metathesis represents an important reaction in upgrading of less valuable olefins into desired ones and has numerous industrial applications (e.g. Phillips triolefin process, Shell higher olefin process, neohexene process [1,2]. Heterogeneous catalysts used for these applications are based on tungsten, molybdenum and rhenium oxides supported on silica or alumina. Tungsten and molybdenum oxide catalysts require higher temperatures, where side reactions decreasing metathesis selectivity can occur. Only rhenium oxide catalysts exhibit a high activity and selectivity at temperatures below 100 °C [1,3].

Modern homogeneous catalysts for metathesis reactions are based on stable carbene complexes especially of Ru, Mo and W [4,5,6]. In the case of heterogeneous catalysts, typical examples are MoO_3/SiO_2, WO_3/SiO_2 and Re_2O_7/Al_2O_3, without or with cocatalyst (usually tetraalkyltin). Recently, we have shown that mesoporous molecular sieves, particularly of organized alumina type [7], can be successfully used as a support for rhenium oxide active species to catalyze 1-olefin metathesis at low reaction temperatures [8]. The activity of this new type of catalyst was found to be about 1 order of magnitude higher compared to the Re catalyst of the same loading using conventional alumina support. It was reported that the optimum loading of Re was between 9 and 15 wt. % and the catalyst activity increased with increasing pore size diameter. This high activity of Re_2O_7 spread on organized mesoporous alumina was explained by the absence of micropores in the alumina support.

According to our best knowledge, there is only one short communication in the literature dealing with the application of mesoporous sieves as a support for MoO_3 based metathesis catalyst [9]. The authors reported in it, that hexagonal mesoporous silica prepared using octylamine as templating agent and impregnated with aqueous molybdate solution exhibited considerable catalytic activity in 1-octene metathesis at 60

°C contrary to the practically negligible activity of MoO_3 on normal silica. This study lacks, however, detailed characterization of catalysts.

The objective of this contribution was to synthesize a new type of metathesis catalyst based on molybdenum oxide supported on siliceous mesoporous molecular sieves MCM-41. As the impregnation of MCM-41 with ammonium heptamolybdate aqueous solution was reported to cause the destruction of hexagonal mesoporous structure and to lead to a severe decrease in the surface area [10], we used the "thermal spreading method" for the support impregnation with MoO_3. This approach should improve the activity of molybdenum oxide catalyst in alkene metathesis utilizing high surface area and narrow pore size distribution of MCM-41 material.

2. EXPERIMENTAL

2.1. Catalyst preparation

MCM-41 was synthesized by the homogeneous precipitation method, described in a detail in refs. [11,12]. Synthesis of siliceous mesoporous MCM-41 was carried out in the following way: 9.80 g of hexadecyltrimethylammonium bromide (Fluka) together with 10.00 g of Na_2SiO_3 (Aldrich) was dissolved in 950 mL of distilled water under vigorous stirring, resulting in a clear solution. Afterwards 15 mL of ethyl acetate (Fluka) were quickly added, the mixture was homogenized and the stirring was stopped. The reaction mixture was allowed to stand at ambient temperature for 5 h and then heated at 90 °C for 72 h in a polypropylene bottle. After that, the mixture was cooled down to the ambient temperature. The solid product was collected by filtration, thoroughly washed with distilled water and dried overnight in air. The template was removed by calcination in air at 500 °C for 6 h with a temperature ramp of 1 °C/min.

The MoO_3/MCM-41 catalyst was prepared via the „thermal spreading method". Calcined MCM-41 and molybdenum oxide (Lachema, Czech Republic) were carefully mixed together by hand-grinding in the following weight ratios: 4, 8, 12, and 16 wt. % of molybdenum. The physical mixtures were then thermally treated at 500 °C for 8 h in a temperature-programmed furnace.

2.2. Characterization

The catalyst and the support were characterized by X-ray diffraction, nitrogen adsorption measurement and chemical analysis. Powder X-ray diffraction data were obtained on Bruker AXS D8 diffractometer in the Bragg-Brentano geometry arrangement using Cu Kα radiation with a graphite monochromator and a scintillation detector. Adsorption isotherms of nitrogen at –196 °C were measured with a Micromeritics ASAP 2010 instrument. Before the adsorption measurement, all samples were degassed at 300 °C until a pressure of 0.1 Pa was attained. The BET surface area, S_{BET}, was evaluated from adsorption data in the relative pressure (p/p_0) range from 0.05 to 0.25. The total mesopore volume V_{ME} was determined from the amount adsorbed at a relative pressure of about 0.9. Catalyst loading calculated from the amount of MoO_3 used for its preparation was in accordance with that based on ICP AES analysis (Ecochem, Czech Republic).

2.3. Catalytic reaction

Metathesis of neat 1-octene and 1-decene was carried out in a liquid phase using a glass batch reactor. In a typical experiment, 50 mg of MoO_3/MCM-41 catalyst was placed into the reactor and activated 0.5 h at 500 °C under the stream of dried air. After activation, the catalyst was cooled down to the reaction temperature under the stream of dried argon and degassed until a pressure of 0.1 Pa was attained. Substrates (1-octene, Aldrich, 98 % or 1-decene, Spolana, Czech Republic, 96 %) were passed through a column of activated alumina and further purified with metallic sodium. 1.5 mL of purified substrate was injected into the reactor filled with argon and placed into thermostated bath. The reaction proceeded under argon atmosphere and the reaction mixture was stirred with a magnetic stirrer. At given reaction times, 20 μL of liquid phase were sampled for GC analysis. High-resolution gas chromatograph Agilent 6890 with DB-5 column (length: 50 m, inner diameter: 320 μm, stationary phase thickness: 1 μm) was used for the product analysis. Conversion of 1-alkene, K, and selectivity to the self-metathesis product, S, were calculated based on the material balance using following formulas: $K = 2(n_P + n_D + \Sigma n_C)/(n_S + 2n_D + 2n_P + 2\Sigma n_C)$, $S = n_P/(n_P + n_D + \Sigma n_C)$, where n_S, n_P, n_C, n_D are the molar amounts of starting alkene (including its isomers), self-metathesis product, cross-metathesis products higher than starting alkene and dimer of starting alkene, respectively.

3. RESULTS AND DISCUSSION

Mesoporous MCM-41 in SiO_2 form used as a support in this study as well as the prepared catalysts were characterized by X-ray powder diffraction at low-angle degrees and by nitrogen adsorption isotherms. Fig. 1 presents the X-ray diffraction patterns of MCM-41 and MoO_3/MCM-41 showing the properly developed structure of MCM-41 with 4 well discernible diffraction lines. After the modification of MCM-41 with MoO_3 (12 wt. % of Mo) the intensity of individual diffraction lines decreased, however, the

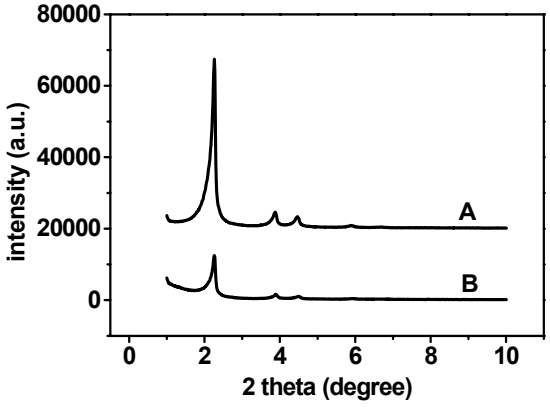

Fig. 1. X-ray diffraction patterns of MCM-41 (A) and MoO_3/MCM-41 with 12 wt. % of Mo (B).

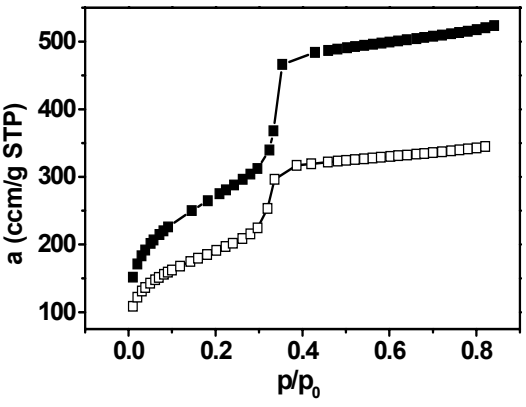

Fig. 2. Adsorption isotherms of nitrogen at 77 K on MCM-41 (■) and MoO_3/MCM-41 with 16 wt. % of Mo (□).

character of the diffractogram was not changed. Therefore, MoO_3/MCM-41 catalyst prepared by thermal spreading method exhibits the same hexagonal mesoporous structure as the support used for its preparation.

Fig. 2 provides nitrogen adsorption isotherms of MCM-41 before and after modification with 16 wt. % of Mo. The adsorption isotherms exhibited steep increase in the adsorbed amount of nitrogen at p/p_0 of about 0.4, which is typical for mesoporous molecular sieves with narrow pore size distribution. The resulting surface area according to BET analysis was 977 m^2/g, void volume 0.805 cm^3/g and pore diameter 3.3 nm. After the modification with 16 wt. % of Mo surface area decreased to 694 m^2 per 1 g of MoO_3/MCM-41 (i.e. 915 m^2 per 1 g of MCM-41 used), void volume to 0.530 cm^3/g and pore diameter was also slightly diminished (3.0 nm). This slight decrease in the pore diameter suggests that the dispersed Mo oxide was located at least partially inside the pores of MCM-41 [13].

The progress of MoO_3 thermal spreading was checked by X-ray diffraction at higher angles. From Fig. 3 and Fig. 4 it is evident that after mixing of MoO_3 with MCM-41 typical diffraction lines for crystalline MoO_3 are present in the diffractogram. The intensity of these diffraction lines continuously decreases during the thermal treatment performed at 500 °C. In the case of the MoO_3/MCM-41catalyst with 4 wt. % of Mo, the diffraction lines of MoO_3 disappeared completely after calcination at this temperature for 2 h. In contrast, for MoO_3/MCM-41 catalyst with 16 wt. % of Mo (Fig. 4, curves B and C) some of these diffraction lines remain visible even after thermal treatment in a stream of air at 500 °C for 8 h.

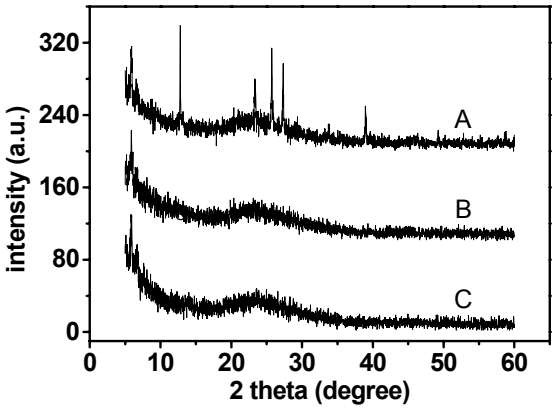

Fig. 3. X-ray diffraction patterns of MoO_3/MCM-41 with 4 wt. % of Mo: physical mixture (A), calcined 2 h (B) and 8 h (C) in a stream of air.

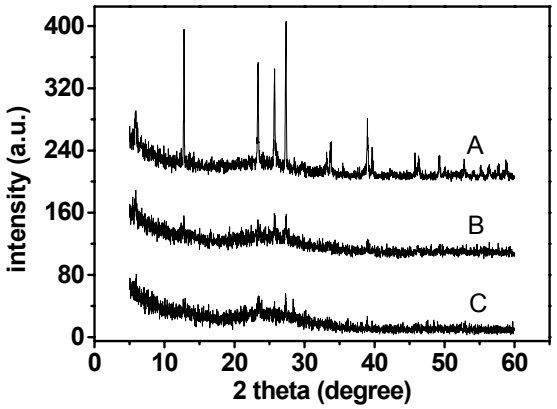

Fig. 4. X-ray diffraction patterns of MoO_3/MCM-41 with 16 wt. % of Mo: physical mixture (A), calcined 2 h (B) and 8 h (C) in a stream of air.

Activity of MoO_3/MCM-41 catalyst was tested in metathesis of 1-octene and 1-decene. The reaction proceeds according to the Eq. (1) (n = 5,7, respectively):

$$2\ CH_3(CH_2)_nCH{=}CH_2 \leftrightarrows CH_2{=}CH_2 + CH_3(CH_2)_nCH{=}CH(CH_2)_nCH_3 \quad (1)$$

In principle, reaction equilibrium is reached at 50 % conversion, however, removing ethylene from the reaction mixture can shift the equilibrium towards the reaction

products. In addition to the main reaction product (7-tetradecene, 9-octadecene, respectively) certain amounts of alkenes with shorter chain originating from the double bond shift isomerization of starting alkene and subsequent cross-metathesis - Eq. (2), m = 0,1,2,3 - were observed.

$$CH_3(CH_2)_nCH=CH_2 + CH_3(CH_2)_mCH=CH(CH_2)_{n-m-1}CH_3 \leftrightarrows$$
$$\leftrightarrows CH_2=CH(CH_2)_mCH_3 + CH_3(CH_2)_mCH=CH(CH_2)_nCH_3 +$$
$$+ CH_2=CH(CH_2)_{n-m-1}CH_3 + CH_3(CH_2)_nCH=CH(CH_2)_{n-m-1}CH_3 \quad (2)$$

Among the reaction products, dimers of starting alkene were also observed, but no oligomers were found. Alkene isomerization, dimerization and/or oligomerization frequently accompany alkene metathesis on heterogeneous catalyst. These reactions proceed simultaneously with the metathesis on surface Brønsted acid sites and/or metallohydride centres [14].

Fig. 5 depicts the time development of the total conversion of starting alkene and selectivity to the main reaction product during metathesis of 1-decene and 1-octene at 60 °C. The development of conversion was practically the same for both 1-octene and 1-decene. Nearly linear increase in the conversion with time was observed up to approximately 50 % conversion; at prolonged reaction time, the reaction rate went down as a result of reactant alkene consumption. Very high final conversion (about 90%) was observed for both 1-decene and 1-octene at prolonged reaction times. Selectivity decreases slightly with reaction time. This selectivity reduction is caused mainly by cross-metathesis. Conversion to the dimers did not exceed 3 %. The difference in selectivity between 1-octene and 1-decene is not clear. It may result from some impurities promoting formation of isomerization centres on MoO_3/MCM-41. With Re_2O_7 on mesoporous organised alumina, metathesis of 1-octene and 1-decene (of the same provenience as in this study) proceeded with similar selectivity (> 90 %) [7].

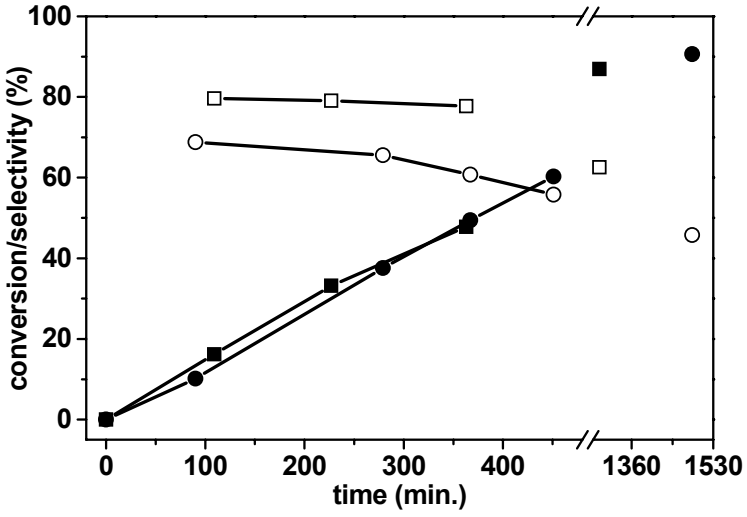

Fig. 5. Time dependence of conversion (solid symbols) and selectivity (open symbols) for metathesis of 1-decene (●) and 1-octene (■) over MoO_3/MCM-41 (12 wt. % of Mo). Reaction temperature 60 °C.

Fig. 6 shows activity dependence on the reaction temperature. At 30 ^{o}C, induction period, which may correspond to the formation of catalytically active species (Mo carbenes) from Mo oxide precursors on MCM-41 by reaction with alkene molecules [15,16], was clearly visible. At higher temperatures, this period was not observed. The maximum reaction rate increased with the increasing temperature. The selectivity, however, decreased slightly with increasing reaction temperature, indicating that the rate of parallel isomerization and dimerization reactions increased with temperature more steeply than the rate of metathesis.

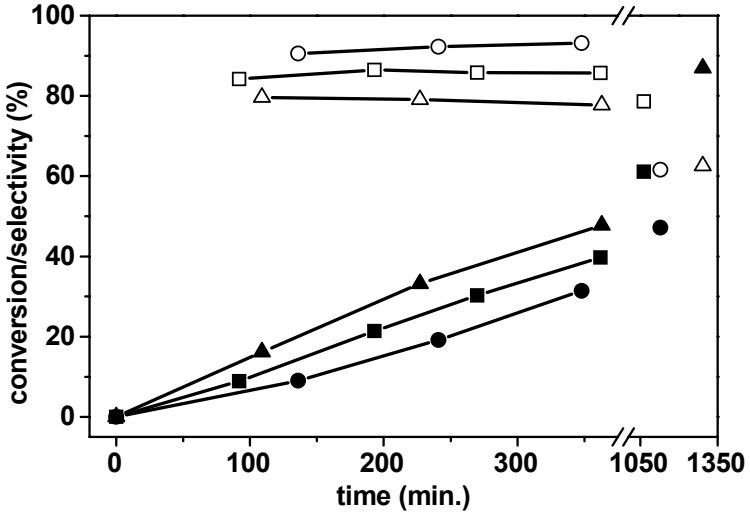

Fig. 6. Time dependence of conversion (solid symbols) and selectivity (open symbols) for metathesis of 1-octene over MoO_3/MCM-41(12 wt. % of Mo) at the reaction temperature 30 °C (●) , 40 °C (■), and 60 °C (▲).

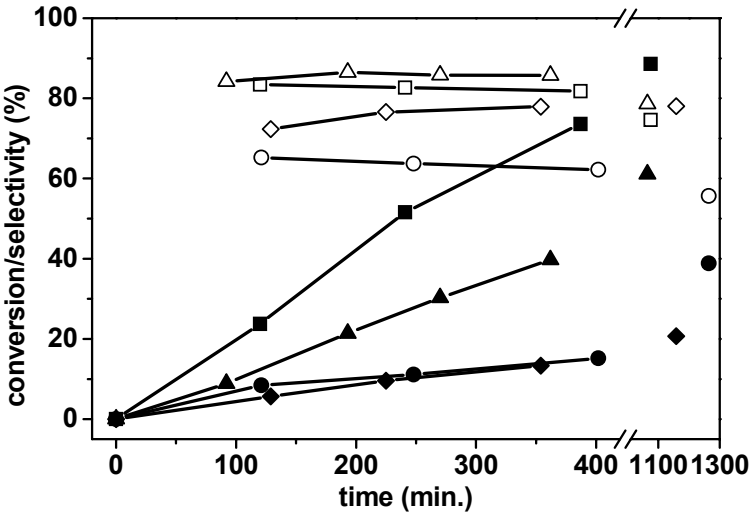

Fig. 7. The effect of catalyst loading on MoO_3/MCM-41 activity in metathesis of 1-octene. Loading in wt. % of Mo: 4 (●), 8 (■), 12 (▲) and 16 (◆); conversion (solid symbols) and selectivity (open symbols). Reaction temperature 40 °C.

The effect of the catalyst loading on MoO_3/MCM-41 activity in 1-octene metathesis is shown in Fig. 7. The activity (expressed as the conversion after 360 min of the reaction) increased in the sequence 4 wt. % ≈ 16 wt. % < 12 wt. % < 8 wt. %. It is known for all metathesis catalysts based on transition metal oxides that only a relatively small part of supported metal is converted into a metathesis active centres [17] and no direct relationship between metal content and catalytic activity exists. Moreover, the low activity of high loaded catalysts may be connected with the presence of a part of Mo in MoO_3 crystallites (see Fig. 4). The highest selectivity was reached for MoO_3/MCM-41 with 8 wt. % and 12 wt. % of Mo. As double bond shift isomerization of starting alkenes proceeds on the catalytic centres different from that involved in metathesis, the rates of metathesis and isomerization could not depend on catalyst loading in the same manner. The selectivity than simply reflects the ratio of metathesis and isomerization reaction rates.

MoO_3/MCM-41 under optimal conditions exhibited pretty good activity and high selectivity in metathesis of higher linear 1-olefins. It provided the yield of self-metathesis products higher than that obtained in ref. [9]. Moreover, in contradiction to this paper [9], our MoO_3/MCM-41 catalyst operates without any solvent, which brings the advantage of easy product separation.

The nature of the beneficial effect of the mesoporous structure of the Mo carrier on catalyst activity has yet to be elucidated. The better accessibility of Mo centres located in mesopores surely plays its role. The possibility that the regular hexagonal structure could stabilize the active Mo centres may also be taken into account. The detailed investigation of catalyst surface by spectroscopic methods is under study.

4. CONCLUSIONS

New type of heterogeneous catalyst for metathesis of linear 1-olefins was investigated. High catalytic activity of these catalysts is based on the proper combination of textural properties of all-silica mesoporous molecular sieve possessing MCM-41 structure with a high activity of molybdenum oxide.

Thermal spreading method was employed to synthesize this catalyst without the necessity of using water solutions. Physical mixing of both catalyst components followed by thermal treatment carried out at 500 °C is sufficient to prepare a highly active catalyst.

Metathesis of linear 1-olefins proceeds easily at ambient or slightly increased temperature (from 30 to 60 oC). No solvent is required, which makes the separation of reactants and products easier.

The selectivity to the main reaction product (higher symmetrical alkene) is high. The side reactions (double bond shift isomerization followed by cross-metathesis, dimerization of the starting alkene) can be minimized by proper reaction conditions.

The maximum reaction rate was found to increase with increasing temperature. However, the higher is the reaction temperature, the higher is also the rate of side reactions (isomerization, dimerization).

The best activity was found for loading 8 wt. % of Mo. The conversion of 1-octene achieved with catalyst of this loading at 40 oC was 74 % in 390 min. and the selectivity to 14-tetradecene was 82 %. Although conversions up to 89 % were achieved at prolonged reaction time, the decreased selectivity at that time (75 %) reduced the final yield of the main metathesis product.

ACKNOWLEDGEMENT

The authors thank to project of cooperation between CSIC and Academy of Sciences of the Czech Republic. J. Č. and H. B. also thank the Grant Agency of the Academy of Sciences of the Czech Republic for the grant (A4040411). P. T. thanks to the Grant Agency of the Czech Republic for a project 203/03/H140. Recording of adsorption isotherms by Dr. A. Zukal is highly appreciated.

REFERENCES

[1] K.J. Ivin and J.C. Mol, Olefin Metathesis and Metathesis Polymerization, Academic Press, London, 1997.
[2] J.C. Mol, J. Mol. Catal. A: Chem., 213 (2004) 39.
[3] J.C. Mol, Catalysis Today, 51 (1999) 289.
[4] E.L. Dias, S.T. Nguyen and R.H. Grubbs, J. Am. Chem. Soc., 119 (1997) 3887.
[5] R.R. Schrock, Polyhedron, 14 (1995) 3177.
[6] R.R. Schrock, Acc. Chem. Res., 19 (1986) 324.
[7] J. Čejka, Appl. Catal. A, 254 (2003) 327.
[8] H. Balcar, R. Hamtil, N. Žilková and J. Čejka, Catal. Lett., 97 (2004) 25.
[9] T. Ookoshi and M. Onaka, Chem. Commun., 1998, 2399.
[10] N. Ichikun, T. Eguchi, H. Murayama, K.K. Bando, S. Shimazu and T. Uematsu, Stud. Surf. Sci. Catal., 146 (2003) 359.
[11] G. Schulz-Ekloff, J. Rathouský and A. Zukal, J. Inorg. Mater., 1 (1997) 97.
[12] J. Dědeček, N. Žilková and J. Čejka, Microporous Mesoporous Mater., 44 (2001) 299.
[13] Z.P. Li, L. Gao and S. Zheng, Appl. Catal. A, 236 (2002) 163.
[14] D.T. Laverty, J.J. Rooney and A. Stewart, J. Catal., 45 (1976) 110.
[15] B.N. Shelimov, I.V. Elev and V.B. Kazansky, J. Mol. Catal., 46 (1988) 187.
[16] Y. Iwasawa, H. Kubo and H. Hamamura, J. Mol. Catal., 28 (1985) 191.
[17] A.W. Aldag, C.J. Lin and A. Clark, J. Catal., 51 (1978) 278.

Enclosure II

P. Topka, H. Balcar, J. Rathouský, N. Žilková, F. Verpoort, J. Čejka

Metathesis of 1-octene over MoO_3 supported on mesoporous molecular sieves: The influence of the support architecture

Microporous Mesoporous Mater. 96 (2006) 44

Available online at www.sciencedirect.com
ScienceDirect
Microporous and Mesoporous Materials 96 (2006) 44–54
MICROPOROUS AND MESOPOROUS MATERIALS
www.elsevier.com/locate/micromeso

Metathesis of 1-octene over MoO_3 supported on mesoporous molecular sieves: The influence of the support architecture

Pavel Topka [a], Hynek Balcar [a], Jiří Rathouský [a], Naděžda Žilková [a], Francis Verpoort [b], Jiří Čejka [a,*]

[a] J. Heyrovský Institute of Physical Chemistry, Academy of Sciences of the Czech Republic, Dolejškova 3, CZ-182 23 Prague 8, Czech Republic
[b] Department of Inorganic and Physical Chemistry, Division Organometallic Chemistry and Catalysis, Ghent University, Krijgslaan 281 (S-3), B-9000 Ghent, Belgium

Received 28 March 2006; received in revised form 8 June 2006; accepted 10 June 2006
Available online 25 July 2006

Abstract

New types of heterogeneous catalysts for alkene metathesis based on molybdenum oxide supported on mesoporous molecular sieves MCM-41, MCM-48 and SBA-15 were developed. These new systems represent inexpensive, easy-to-prepare and highly active and selective heterogeneous catalysts for metathesis of linear alkenes applicable under mild reaction conditions without the necessity of solvent or co-catalyst presence in the reaction mixture. In metathesis of 1-octene, these catalysts showed considerably higher activity compared with MoO_3 supported on conventional silica with selectivity to 7-tetradecene being in the range between 60% and 95%. The highest activity exhibited MoO_3/MCM-41 with 6 wt.% of Mo (75% conversion after 6 h at 40 °C with selectivity to 7-tetradecene 84%). The turn-over-frequency of the catalysts loaded with 8 wt.% of Mo decreased in the order MCM-41 > MCM-48 > SBA-15, while the selectivity slightly increased in the same order. Using Raman spectroscopy, the differences in the catalytic activity were elucidated as a result of different dispersion of the active phase over the supports.

Keywords: Metathesis; 1-Octene; Mesoporous molecular sieves; Molybdenum oxide; Raman spectroscopy

1. Introduction

The metathesis of alkenes is at present one of the most frequently used transformations in modern chemical synthesis. It is an attractive reaction for the conversion of low value feedstocks into useful chemical products as important petrochemicals, polymers, oleochemicals and specialty chemicals. The most important applications of alkene metathesis in the field of petrochemicals are the Olefin conversion technology process (originally the Phillips triolefin process) and the Shell higher olefins process, both upgrading less valuable alkenes into the desired products [1]. Tungsten, molybdenum and rhenium oxides supported on high surface area silica and alumina were used as catalysts in these processes and also in other industrial applications of alkene metathesis [2].

Tungsten and molybdenum oxide catalysts require higher reaction temperatures, at which side reactions (isomerization and oligomerization) decreasing metathesis selectivity occur. Tungsten oxide on silica operates at temperatures ranging from 300 to 500 °C, and molybdenum oxide on alumina or silica is active usually at temperatures from 100 to 200 °C. Only high-priced rhenium oxide catalysts exhibit a high activity and selectivity at temperatures below 100 °C [1–3].

From the practical point of view, catalysts based on molybdenum oxide have attracted the most attention and were thoroughly investigated. Their catalytic activity was

* Corresponding author. Fax: +420 286582307.
E-mail address: jiri.cejka@jh-inst.cas.cz (J. Čejka).

1387-1811/$ - see front matter © 2006 Elsevier Inc. All rights reserved.
doi:10.1016/j.micromeso.2006.06.016

found to depend particularly on (i) the properties of the support, (ii) the content of molybdenum oxide, (iii) activation conditions, and (iv) the oxidation state of molybdenum species. As concerns the support, the activity was found to decrease in the order of decreasing Brønsted acidity of the support, i.e. silica–alumina > alumina > silica [4]. Specific activity of such catalysts was found to pass a maximum for Mo content corresponding approximately to the formation of monolayer of Mo species on the surface [1]. At higher Mo concentrations specific activity decreases due to the formation of catalytically inactive bulk MoO_3 [5]. According to the well-known mechanism of alkene metathesis [1], active centers represent molybdenum carbenes bound to the support surface. High dispersity of molybdenum oxide species on the support surface and a slight reduction of Mo^{VI} to a lower oxidation state (Mo^{IV} or Mo^{V} [5,6]) are prerequisites for the formation of sufficiently active and stable Mo carbene species. The concentration of carbene species on the catalyst surface is rather low, usually only a small fraction of the total amount of molybdenum is converted into the catalytically active species (e.g. about 1% [7]). Up to now, the investigation of molybdenum oxide based metathesis catalysts has been centered on their application in low alkene metathesis in gaseous phase. However, the importance of higher linear alkene metathesis in liquid phase is growing in connection with new demands of feeds for detergent production [8]. Therefore, new efficient catalysts for metathesis of higher alkenes as 1-octene are desired and were developed [9,10]. Key improvement in increasing selectivity of molybdenum oxide catalysts was connected with the introduction of alkali metals on the catalyst surface to poison the acid sites. Thus, while the first metathesis catalyst for 1-octene metathesis ($CoO/MoO_3/Al_2O_3$) operated at 163 °C allowing to achieve more than 70% conversion but only 3% selectivity to tetradecene [11], the system $K_2O/MoO_3/Al_2O_3$ reached 82% conversion and 81% selectivity to 7-tetradecene at 178 °C [12]. The application of MoO_3/SiO_2 system in metathesis of higher alkenes was not yet reported, although low acidity of SiO_2 support promises an increased selectivity of this catalyst.

In 1992, successful synthesis of MCM-41, the first member of a new family of mesoporous molecular sieves, opened a new area in the research of porous materials [13]. These new types of silica and alumina possess high surface areas, regular structure and mesopores of narrow pore size distribution, which make them ideal for catalysts supporting [14,15]. As concerns the alkene metathesis, siliceous MCM-41 has been used as a support for anchoring of homogeneous Mo and Ru-based metathesis catalysts [16,17]. It was also recently reported that rhenium oxide supported on organized mesoporous alumina (OMA) exhibited more than one order of magnitude higher activity in metathesis of higher alkenes than similar catalysts based on conventional γ-alumina [18–20]. Pore size of OMA was found to influence both the catalyst activity and selectivity [21]. In spite of some hypotheses [19,20,22] the reason for enhanced activity of these catalysts on OMA is not yet completely understood. According to our best knowledge, only a short communication dealing with application of mesoporous silica as a support for molybdenum oxide metathesis catalyst has been published [23]. Hexagonal mesoporous silica (HMS) was prepared and impregnated with molybdate solution and tested in 1-octene metathesis at 50 °C. The catalyst activity depended strongly on the support structure. Three HMS samples were prepared using three alkylamines with different alkyl chain length (C_8, C_{12} and C_{16}) as templating agents. Nevertheless, only HMS prepared with octylamine provided the extraordinary high activity in comparison with catalyst prepared using conventional silica as a support (more than ten times higher). However, this study lacks detailed characterization of HMS support and prepared catalysts. In our preliminary communication we have shown that siliceous mesoporous molecular sieve of ordinary MCM-41 type can be effectively used as a support for molybdenum oxide to catalyze 1-alkene metathesis at low reaction temperatures [24].

The objective of this contribution was to utilize the advantages of mesoporous molecular sieves in the preparation of new types of molybdenum oxide catalysts for metathesis of higher alkenes. Three all-siliceous supports with different pore sizes and architectures have been employed in this study: (i) MCM-41 with hexagonal array of one-dimensional channels, (ii) SBA-15 also of hexagonal structure but with approximately two times larger channel diameter, and (iii) cubic MCM-48 with three-dimensional intersecting channels. By supporting MoO_3 on these supports new metathesis catalysts were prepared. As commonly used impregnation with ammonium heptamolybdate aqueous solution was reported to destroy a hexagonal mesoporous structure of MCM-41 [25], we used the thermal spreading for supporting of MoO_3. This relatively new approach represents an easy and low-cost method, which has been recently used in the preparation of various Mo oxide catalysts [26–28]. The catalysts prepared were characterized by nitrogen adsorption, X-ray diffraction, scanning electron microscopy and Raman spectroscopy and tested in the metathesis of 1-octene, which was chosen as a model substrate. The effect of support architecture and concentration of the active phase on catalyst activity and selectivity was investigated. The catalytic activity of all these catalysts was compared with that of MoO_3 supported on conventional silica.

2. Experimental

2.1. Catalyst preparation

MCM-41 was synthesized by the homogeneous precipitation method, described in a detail in Ref. [24]. Hexadecyltrimethylammonium bromide (CTABr) was used as a template and sodium silicate as a silicon source; pH of the synthesis mixture was controlled by the addition of ethyl acetate. The molar composition of the reaction

mixture was Na_2SiO_3:CTABr:H_2O:ethyl acetate = 1:0.33:644:1.87.

Synthesis of siliceous mesoporous MCM-48 based on the modification of the method described in Ref. [29] was carried out in the following way: 2.5 g of Cab-O-Sil M5 (Cabot GmbH) together with 3.2 g of $Na_2Si_3O_7$ (Riedel-de Haen) and 3.3 g of tetramethylammonium hydroxide (TMAOH) water solution (25%, Aldrich) were dissolved in 20 mL of distilled water under vigorous stirring, resulting in a formation of a clear solution. After that 17.3 g of hexadecyltrimethylammonium hydroxide (CTMAOH) water solution (25%, Fluka) and 10 mL of distilled water were added and the mixture was homogenized for further 70 min. The molar composition of the reaction mixture was SiO_2:CTMAOH:TMAOH:H_2O = 1:0.15:0.11:31. Finally, the reaction mixture was heated in a Teflon-lined stainless-steel autoclave at 130 °C for 24 h. Then, the autoclave was cooled down to the ambient temperature. The solid product was washed out with distilled water and filtered off.

Synthesis of siliceous SBA-15 was performed according to the procedure described in details in Ref. [30]. Four grams of Pluronic PE 9400 (BASF) was dissolved in the solution of 30 mL of distilled water and 120.0 g of 2 M hydrochloric acid. The reaction mixture was stirred for 15 min and then 8.5 g of tetraethyl orthosilicate (TEOS, Aldrich) was added. The molar composition of the reaction mixture was TEOS:PE 9400:HCl:H_2O = $1:2.17\times10^{-5}$:5.69:193. After stirring for 5 min the reaction mixture was allowed to stand at 100 °C for 43 h. The solid products were thoroughly washed with distilled water, collected by filtration and dried overnight in air. In all cases, the structure-directing agents were removed by calcination in air carried out at 500 °C for 6 h with a temperature ramp of 1 °C/min.

The molybdenum oxide/mesoporous molecular sieves catalysts were prepared via the thermal spreading method. Calcined molecular sieves and molybdenum oxide (Lachema Co., Czech Republic) were carefully mixed together by hand-grinding in weight ratios corresponding to catalyst loadings: 4.0, 6.0, 8.0, 12.0, and 16.0 wt.% of molybdenum, respectively. Then, the physical mixtures were thermally treated at 500 °C for 8 h in a temperature-programmed furnace (ramp 1 °C/min). Molybdenum oxide supported on conventional silica (Silica gel 40, Merck) was prepared in the same way. The catalysts were denoted as yMo/X, where y is molybdenum oxide loading in wt.% of Mo and X stands for the type of the support.

2.2. Characterization

X-ray powder diffraction data were obtained on a Bruker AXS D8 diffractometer in the Bragg–Brentano geometry arrangement using CuKα radiation with a graphite monochromator and a position sensitive detector (Vantec-1).

Adsorption isotherms of nitrogen at −196 °C were measured with a Micromeritics ASAP 2010 instrument. Prior to the adsorption measurement, all samples were degassed at 300 °C until pressure of 0.1 Pa was attained.

The Laser Raman spectroscopy (LRS) was performed on a Bruker FRA 106/S spectrometer equipped with an Nd-YAG-laser (λ = 1064 nm), reference HeNe laser and Ge-detector. The samples were measured in air at ambient temperature using aluminum sample holder. Spectra were recorded with resolution 3.5 cm^{-1} by collecting 20000 scans for a single spectrum.

The morphology of catalyst particles was analyzed using a scanning electron microscope JEOL JSM-5500LV.

Catalyst loading determined by chemical analysis using an ICP AES spectrometer (Ecochem Co., Czech Republic) was the same as that one calculated from the amount of MoO_3 used for catalyst preparation. The standard deviation of the result of chemical analysis was less than 10%.

2.3. Metathesis reaction

Metathesis of neat 1-octene was investigated in a liquid phase using a glass batch reactor filled with argon and equipped with a magnetic stirrer. In a typical experiment, 50 mg of catalyst was placed into the reactor and activated in a stream of dried air at 500 °C for 0.5 h. After activation, the catalyst was cooled down to the reaction temperature in a stream of dried argon and degassed until the pressure of 0.1 Pa was attained. 1-Octene (Aldrich, 98%) was passed through a column of activated alumina and then purified with metallic sodium. Purified substrate (1.5 mL) was injected into the reactor placed in thermostated bath. At given reaction times, 20 μL of liquid phase were sampled for GC analysis. A high-resolution gas chromatograph Agilent 6890 with DB-5 column (length: 50 m, inner diameter: 320 μm, stationary phase thickness: 1 μm) was used for the product analysis. Conversion of 1-alkene, C, and selectivity to the self-metathesis product, S, were calculated based on the material balance using following formulas: $C = 2(n_P + n_D + \sum n_C)/(n_S + 2n_D + 2n_P + 2\sum n_C)$, $S = n_P/(n_P + n_D + \sum n_C)$, where n_S, n_P, n_C, n_D are the molar amounts of starting alkene including its isomers (n_S), self-metathesis product (n_P), cross-metathesis products higher than starting alkene (n_C) and dimer of starting alkene (n_D), respectively.

3. Results and discussion

3.1. Characterization of the catalysts

Both the mesoporous SiO_2 materials and the prepared catalysts were characterized by X-ray powder diffraction and nitrogen adsorption. Fig. 1 presents the X-ray powder diffraction patterns of parent MCM-41, MCM-48 and SBA-15 at low angles showing well-discernible diffraction lines corresponding to the properly developed mesoporous structures. After the modification with MoO_3, the intensity of individual diffraction lines decreased, however, the character of the diffractogram was not changed (Fig. 2 shows

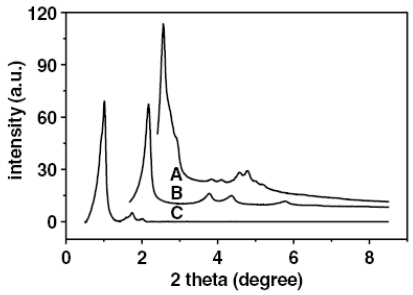

Fig. 1. X-ray diffraction patterns of MCM-48 (A), MCM-41 (B) and SBA-15 (C).

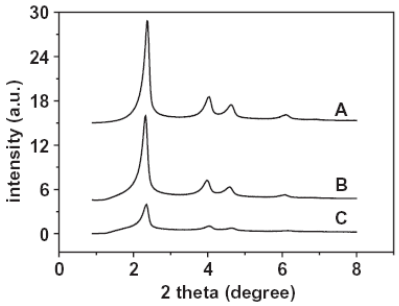

Fig. 2. X-ray diffraction patterns of parent MCM-41 (A), 8Mo/MCM-41 (B) and 16Mo/MCM-41 (C).

the diffractograms for MCM-41 supported catalysts as an example). Therefore, the catalysts prepared by thermal spreading method exhibit the same mesoporous structure as the support used for its preparation.

The MoO_3 thermal spreading was checked by X-ray diffraction at higher diffraction angles (from 5° to 50°). Fig. 3 shows the diffractograms of MoO_3/MCM-41 catalysts with different molybdenum oxide loadings. Whereas for 8Mo/MCM-41 no diffraction lines of crystalline phase of MoO_3 are visible, at higher loadings, these lines appear

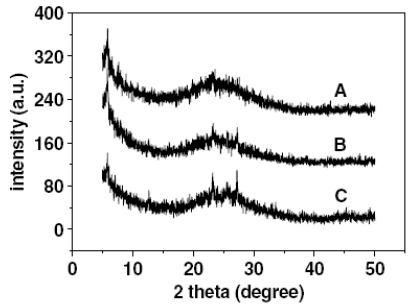

Fig. 3. X-ray diffraction patterns of 8Mo/MCM-41 (A), 12Mo/MCM-41 (B) and 16Mo/MCM-41 (C) calcined 8 h at 500 °C in air.

Table 1
MoO_3 particle size in catalysts determined by X-ray diffraction according to the Scherrer equation

Sample	MoO_3 particle size (nm)		
	MCM-41	MCM-48	SBA-15
4Mo/	*	*	*
6Mo/	*	–	–
8Mo/	*	*	*
12Mo/	*	*	2.5
16Mo/	5	3	5

Symbol "*" indicates that the diffraction line was not observed or its intensity was too low to apply the Scherrer equation, samples 6Mo/MCM-48 and 6Mo/SBA-15 were not studied.

and their intensity increases with increasing loading of the molybdenum oxide. Moreover, the MoO_3 crystalline phase remained present even when the samples were thermally treated at 500 °C for additional 16 h. Similar diffractograms were obtained for MoO_3/MCM-48 and MoO_3/SBA-15 catalysts (cf. Table 1).

The average particle size of molybdenum oxide crystallites present in the catalysts was estimated from the broadening of the MoO_3 diffraction lines using the Scherrer equation [31] (Eq. (1))

$$d = \frac{K\lambda}{\beta \cos \Theta_0} \tag{1}$$

where d is the mean crystallite size, K is the constant ($K = 0.9$), λ is the wavelength of the X-ray radiation, β is the corrected broadening of the diffraction line in 2Θ units and Θ_0 is the diffraction angle of the maximum of the diffraction line.

Variable β can be calculated according to Eq. (2),

$$\beta = B - b \tag{2}$$

where B is full width at half maximum of the peak and b is full width at half maximum of the reference peak (standard sample with particle size larger than 100 nm). In this study, pure molybdenum oxide was used as a reference sample. The average particle size of molybdenum oxide crystallites estimated from the diffractograms measured in the region from 24.8° to 26.8° (2Θ) with enhanced resolution and sensitivity (not given in the figure) using the most intensive diffraction line of pure MoO_3 at 25.7° (2Θ). The results are shown in Table 1. They indicate that at the highest loadings not all the molybdenum oxide is spread over the surface of the support and MoO_3 crystallites (2.5–5 nm large) occur in the catalysts. Comparing these results with surface area measurements (see Table 2) we can show that there is a correlation between the surface area of the support and its ability to spread the active phase. For instance, as the MCM-48 has the highest surface area, in 16Mo/MCM-48 the average size of MoO_3 crystallites was only 3 nm. On the other hand, in the case of SBA-15 possessing the lowest surface area, the crystallites of 5 nm were observed in 16Mo/SBA-15 sample. Moreover, crystallites of average size 2.5 nm were present even in the 12Mo/SBA-15

Table 2
Sorption characteristics of the supports and catalysts determined from nitrogen adsorption isotherms

Sample	S_{BET} (m^2/g)	S_{BET} (m^2/g SiO_2)	d (nm)	V_{meso} (cm^3/g)	S_{ext} (m^2/g)
MCM-41	1071	1071	3.1	0.841	167
4Mo/MCM-41	874	929	3.0	0.658	132
6Mo/MCM-41	811	891	2.9	0.590	150
8Mo/MCM-41	875	994	2.9	0.635	125
12Mo/MCM-41	831	1013	2.7	0.568	125
16Mo/MCM-41	754	992	2.7	0.511	98
MCM-48	1334	1334	2.8	0.927	53
4Mo/MCM-48	1128	1200	2.7	0.769	53
8Mo/MCM-48	829	942	2.6	0.549	36
12Mo/MCM-48	961	1172	2.5	0.591	37
16Mo/MCM-48	884	1163	2.3	0.518	33
SBA-15	777	777	6.1	1.258	73
4Mo/SBA-15	489	520	6.0	0.649	50
8Mo/SBA-15	606	689	6.0	0.865	67
12Mo/SBA-15	458	559	6.0	0.825	56
16Mo/SBA-15	455	599	5.8	0.715	65
SiO_2	559	559	4.5	0.473	–
8Mo/SiO_2	298	339	5.7	0.457	–
12Mo/SiO_2	300	366	5.4	0.447	–

catalyst. These results are not surprising, because the tendency of MoO_3 to form MoO_3 crystallites on silica surfaces is well-known [32–34].

Fig. 4 shows adsorption isotherms of nitrogen at −196 °C on all parent supports. Nitrogen adsorption isotherms recorded on MCM-41 and MCM-48 exhibit a steep increase in the adsorption at p/p_0 of 0.3–0.4, which is due to the reversible capillary condensation within the mesopores of these materials. Its steepness proves their narrow pore size distribution. A slight shift of this steep increase for MCM-41 to higher partial pressures in comparison with that for MCM-48 is due to the slightly larger pore size of the MCM-41 sample. The broad hysteresis for the adsorption isotherms on MCM-41 at p/p_0 of 0.5–1 can be explained by the presence of some imperfections. The SBA-15 exhibits a typical isotherm of the type IV with hysteresis loop of H1 type corresponding to the well-defined cylindrical pore channels with pore size equal to 6.1 nm. From this reason the steep increase in the adsorbed amount of nitrogen is shifted to p/p_0 of 0.6–0.7.

The low-pressure region of both parent and loaded samples was analyzed by the method of comparative plots. In this method the adsorption on the sample under study (a) is compared with that on a suitable reference adsorbent (a_{ref}), here on the macroporous silica gel Davisil 663XWP (Supelco, $S_{BET} = 82\ m^2/g$). The comparative plots for parent mesoporous molecular sieves are shown in Fig. 5. When extrapolating the linear parts of these dependences to zero practically no intercepts on y-axis were obtained. This indicates that the amount of micropores present in our samples is negligible. It is in contrast to Ref. [30], where micropores were observed in the case of SBA-15 prepared by the same method. The lack of micropores is of a great advantage for the catalytic application of these materials as the presence of micropores may deteriorate the catalytic performance of the final catalyst, due to the location of molybdenum species in micropores, which are less accessible for 1-octene molecules, the creation of centers of preferential coking, etc.

The surface areas of the individual catalysts were determined by both the BET and comparative plot methods. A reasonable agreement (within less than 2%) between the values obtained by both methods was achieved. The pore volume was determined from the limit adsorption at p/p_0 of ca. 0.9. The external surface areas corresponding to the surface area of particles after filling up the mesopores were determined by the t-plot method. Finally, the pore size was determined by the BJH method for SBA-15. Due to the restriction of the validity of the Kelvin's equation for pores smaller than 4–5 nm, the BJH method is not applicable for both the MCM-41 and MCM-48. Therefore the 4V/S geometrical method was used for these samples. Textural parameters of parent supports and catalysts prepared are provided in Table 2. Conventional silica (Merck) with relatively high surface area (559 m^2/g) was used for

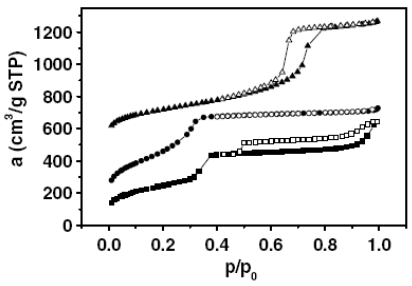

Fig. 4. Adsorption isotherms of nitrogen at −196 °C on MCM-41 (■), MCM-48 (●) and SBA-15 (▲); desorption branches are depicted using open symbols. For clarity, 100 and 500 cm^3/g (STP) was added to the adsorption isotherms of MCM-48 and SBA-15, respectively.

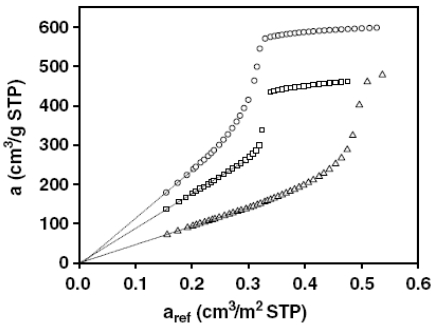

Fig. 5. The nitrogen adsorption isotherms on MCM-41 (□), MCM-48 (○) and SBA-15 (△) transformed into the comparison plots; a = adsorption on the measured sample, a_{ref} = adsorption on the reference adsorbent.

the preparation of the reference MoO_3/SiO_2 catalyst. The pore size distribution of this silica is very broad with very flat maximum centered at 4.5 nm.

To check the reproducibility of the textural parameters of the catalysts, three samples of 8Mo/MCM-41 catalyst were prepared independently using the same MCM-41 support. The same pore diameter was determined for all the samples. The standard deviation of the surface area was 39 m^2/g and the standard deviation of the pore volume was 0.028 cm^3/g. These data indicate good reproducibility of the textural properties of prepared catalysts.

As it is seen from Table 2, a decrease in the surface area and pore volume with increasing MoO_3 loading was observed for MoO_3/MCM-41 catalysts similarly to the study of Li et al. [34], made with catalyst prepared in the same way (thermal spreading, calcination at 500 °C for 24 h). In contrast to our work, for the sample with 15.4 wt.% of Mo they found much sharper decrease in the surface area and the pore volume accompanied with a simultaneous increase in the pore diameter. They ascribed these changes to a partial structural collapse of the support. In our case, only small reduction in the pore size with increasing loading was observed (especially pore diameter was the same for both 12Mo/MCM-41 and 16Mo/MCM-41). It suggests that the mesoporous structure of parent molecular sieves is not significantly affected by thermal spreading even at the highest loading applied. It may be explained taking into consideration that MoO_3 crystallites formed at this loading (see Table 1) are located mainly on the external surface of the MCM-41 particles. This conclusion is supported by a substantially lower external surface area of 16Mo/MCM-41 sample compared with all other MoO_3/MCM-41 catalysts with lower loadings (Table 2).

As the surface area of pure molybdenum oxide is only about 1 m^2/g, the surface areas of all samples were recalculated to m^2/g of siliceous support. If we compare the low loaded and high loaded catalysts (Table 2), only small differences in their surface areas are found. For example, for 16Mo/MCM-41 catalyst the content of MoO_3 is four times higher than that of 4Mo/MCM-41 but the change in the surface area (calculated per gram of SiO_2) is only 63 m^2/g (7%). From these data it is even more clearly seen that (up to 16 wt.% of Mo at least) the structure of parent mesoporous sieve remains preserved after the thermal spreading.

In principle, the same dependence of the textural characteristics on the Mo loading has been revealed for the MCM-48 and SBA-15 supported catalysts (Table 2). Thus, the textural study confirmed that the thermal spreading method is suitable for supporting MoO_3 on all mesoporous molecular sieves applied in this study. At low loadings, molybdenum oxide is well dispersed over the siliceous support, forming a sub-monolayer inside the channels. Large MoO_3 crystallites (3–5 nm) located mainly on the external surface of the catalysts are formed at loadings higher than 12 wt.% of Mo.

3.2. Metathesis of 1-octene

The metathesis of 1-octene proceeds according to Eq. (3):

$$2\ CH_3(CH_2)_5CH{=}CH_2 \leftrightarrows CH_2{=}CH_2 + CH_3(CH_2)_5CH{=}CH(CH_2)_5CH_3 \quad (3)$$

Because ethylene was released from the reaction mixture, the reaction equilibrium was shifted towards the reaction products and conversions higher than 50% were achieved. Except of the main metathesis reaction, the double bond shift isomerization of starting alkene followed by subsequent cross-metathesis reactions – Eq. (4), $m = 0, 1, 2$ – proceeded

$$CH_3(CH_2)_5CH{=}CH_2 + CH_3(CH_2)_mCH{=}CH(CH_2)_{4-m}CH_3 \leftrightarrows CH_3(CH_2)_5CH{=}CH(CH_2)_{4-m}CH_3 + CH_3(CH_2)_5CH{=}CH(CH_2)_mCH_3 + CH_2{=}CH(CH_2)_{4-m}CH_3 + CH_2{=}CH(CH_2)_mCH_3 \quad (4)$$

Products of self-metathesis (Eq. (3)), cross-metathesis (Eq. (4)) and also dimers of starting alkene were observed in the reaction mixture but no oligomers were found. Alkene isomerization, dimerization and/or oligomerization frequently accompany alkene metathesis on heterogeneous catalysts. These reactions proceed simultaneously with the metathesis on Brønsted acid sites and/or metallohydride centers [35]. Negligible activity in metathesis was found for pristine supports. Only 0.7% conversion of 1-octene was achieved for pristine MCM-41 after 360 min of the reaction.

Fig. 6a shows conversion and selectivity dependences on time for MoO_3/MCM-41 catalysts of various Mo loadings at the reaction temperature of 40 °C. It is seen that the highest initial reaction rate of 1-octene metathesis was achieved with 6Mo/MCM-41. Seventy-five percent conversion of 1-octene and 84% selectivity to 7-tetradecene were achieved over this catalyst at 360 min. The specific activity of the individual catalysts is compared in terms of the turnover-frequency at 120 min of the reaction (TOF_{120}) expressed in mol of the substrate converted per mol of Mo and per second (Fig. 7). It is seen that the specific activity increased in the following order 16Mo/MCM-41 < 12Mo/MCM-41 < 4Mo/MCM-41 < 8Mo/MCM-41 < 6Mo/MCM-41. The selectivity, S (Fig. 6a) increased from 60% to 86% in the order 4Mo/MCM-41 < 16Mo/MCM-41 < 8Mo/MCM-41 ≈ 6Mo/MCM-41 ≈ 12Mo/MCM-41. Fig. 6b shows the dependence of the conversion and selectivity achieved over MoO_3/MCM-48 catalysts on the catalyst loading. The differences in the activity among individual catalysts based on MCM-48 are lower than in the case of MCM-41 supported ones. The highest conversion was achieved with 12Mo/MCM-48 (55% at 420 min of the reaction). The selectivities S were slightly higher than those for MCM-41 supported catalysts and increased from 80% to 95% in the order 4Mo/MCM-48 < 8Mo/

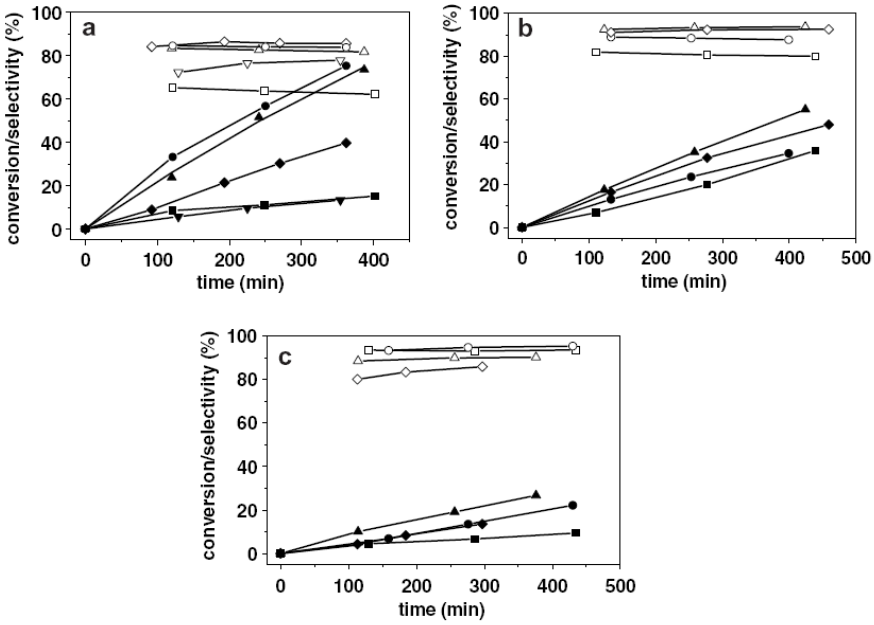

Fig. 6. Conversion of 1-octene (solid symbols) and selectivity to 7-tetradecene (open symbols) dependence on time: (a) 4Mo/MCM-41 (■), 6Mo/MCM-41 (●), 8Mo/MCM-41 (▲), 12Mo/MCM-41 (♦) and 16Mo/MCM-41 (▼); (b) 4Mo/MCM-48 (■), 8Mo/MCM-48 (●), 12Mo/MCM-48 (▲) and 16Mo/MCM-48 (◆); (c) 4Mo/SBA-15 (■), 8Mo/SBA-15 (●), 12Mo/SBA-15 (▲) and 16Mo/SBA-15 (◆) neat 1-octene at 40 °C.

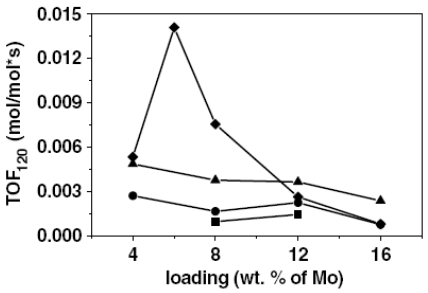

Fig. 7. Specific activity (expressed as TOF_{120}) of MoO_3 supported on: SiO_2 (■), SBA-15 (●), MCM-48 (▲) and MCM-41 (◆); neat 1-octene at 40 °C. Lines are intended as visual aids.

MCM-48 < 12Mo/MCM-48 ≈ 16Mo/MCM-48. TOF_{120} values monotonously decreased with increasing loading (Fig. 7). The dependence of the conversion and selectivity on the reaction time for the MoO_3/SBA-15 catalysts is shown in Fig. 6c. The results are similar to those of MoO_3/MCM-48 catalysts, but generally the conversions are lower. The highest conversion achieved with 12Mo/SBA-15 was only 27% at 380 min. The TOF_{120} values were also lower than that for MoO_3/MCM-48 catalysts and exhibited the similar dependence on loading (Fig. 7). However, the selectivities to 7-tetradecene were in the same range as for MoO_3/MCM-48 catalysts and increasing slightly in the order 16Mo/SBA-15 < 12Mo/SBA-15 < 4Mo/SBA-15 ≈ 8Mo/SBA-15.

The influence of the support on the activity of the catalysts is provided in Fig. 7. From this figure it is clearly seen that (i) for MoO_3/MCM-41 catalysts, the dependence of specific activities on Mo loading reaches its maximum for 6 wt.% of Mo; 6Mo/MCM-41 exhibited the highest specific activity among all catalysts investigated, (ii) for 4 and 8 wt.% of Mo loaded catalysts the activity increased according to the mesoporous support used in the order SBA-15 < MCM-48 < MCM-41, (iii) the activity of the catalysts with 16 wt.% of Mo is strongly depressed (probably due to the presence of the major part of Mo in crystallites), (iv) the activity of all catalysts based on mesoporous molecular sieves is higher in comparison with that of conventional silica supported catalyst (e.g. for 8Mo/MCM-41 about nine times higher). The trend described in (ii) is rather surprising, because larger pore diameter (SBA-15) and three-dimensional channel system (MCM-48) should enhance diffusion of the substrate and reaction products and ensure better accessibility of catalyst centers. Ookoshi and Onaka [23] observed similarly a decrease in catalyst activity of MoO_3/HMS catalysts with increasing alkyl chain of amine used in HMS preparation (i.e. with increasing pore size supposingly). However, they ascribed this decrease to the different size of

catalysts particles. For larger particle sizes, they supposed longer channels and higher extent of deactivation of catalyst sites and/or pore blockage by polymeric by-products. In our case, however, the average particle size of catalyst was between 1 and 3 μm (see Fig. 8), i.e. higher than particle size of all MoO_3/HMS (50–700 nm) and we did not observe a rapid deactivation for any of our catalysts. For example, with 8Mo/MCM-41 the conversion of 1-octene increased gradually up to 89% at 1075 min and the selectivity to main metathesis product was 75% at the same time (not shown in Fig. 6a). Therefore, in our case, there must be another reason for reduced activity of MoO_3/MCM-48 and MoO_3/SBA-15 compared with MoO_3/MCM-41 catalysts.

On the other hand, the selectivities of MoO_3/MCM-48 and MoO_3/SBA-15 catalysts are slightly higher in comparison with that of MoO_3/MCM-41 catalysts and comparable with selectivity reached with the catalysts supported on conventional silica ($S = 86$–91%). This difference, however, is too small to overweight the advantage of high activity of 6Mo/MCM-41 and 8Mo/MCM-41 catalysts in most applications. Moreover, in many industrial processes, all the side metathesis products (except dimers of starting alkenes) can be fully utilized in the subsequent steps of the process.

3.3. Raman spectra of supported MoO_3

The Raman spectra of MoO_3 and MoO_3/MCM-41 catalysts are shown in Fig. 9. There are three molybdenum species on the surface of MoO_3/MCM-41 discernable in the spectra: (i) isolated surface molybdenum oxide species, (ii) highly dispersed surface polymolybdates and (iii) bulk MoO_3. The band at 981 cm^{-1} corresponds to the stretching vibration mode of the terminal Mo=O bond of isolated

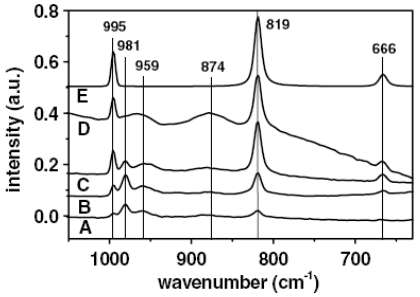

Fig. 9. Laser Raman spectra of 4Mo/MCM-41 (A), 8Mo/MCM-41 (B), 12Mo/MCM-41 (C), 16Mo/MCM-41 (D) and MoO_3 (E).

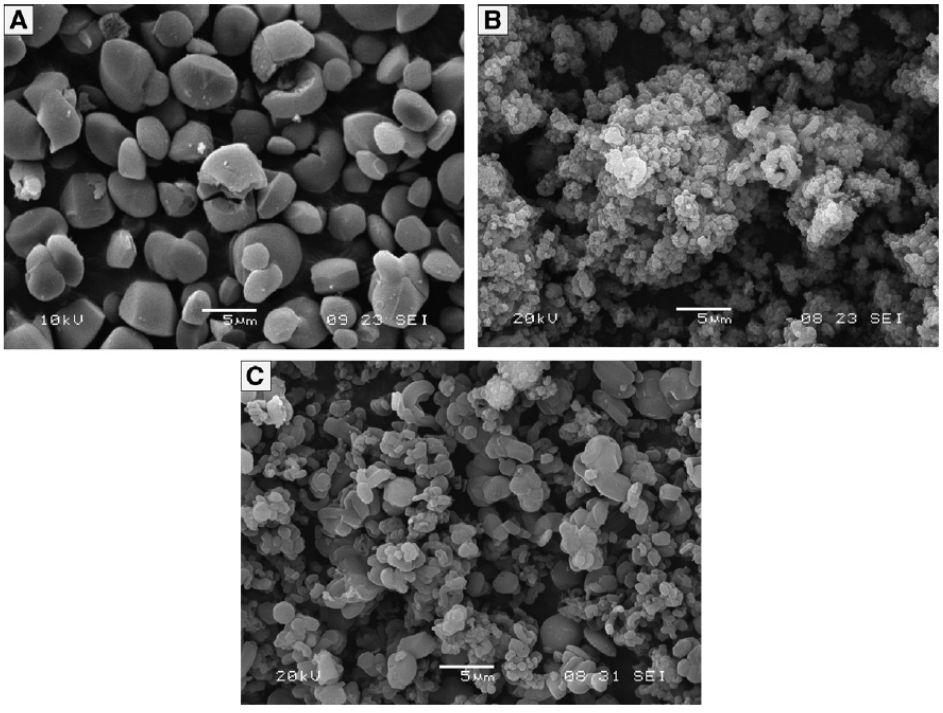

Fig. 8. SEM micrograph of MCM-41 (A), MCM-48 (B) and SBA-15 (C).

surface molybdenum oxide species [36]. The surface polymolybdates are characterized by the Mo=O stretching mode at 959 cm^{-1} and the antisymmetric stretching mode of Mo–O–Mo bridges at 874 cm^{-1} [37,38]. The Raman spectrum of bulk MoO_3 shows the stretching mode band of the terminal Mo=O groups at 995 cm^{-1} and the Mo–O–Mo bridge bond vibrations at 819 and 666 cm^{-1} [36–39]. As the relationship between the concentration of Mo species and the intensity of corresponding peaks is not known and the intensity of bands corresponding to the same concentration of different molybdenum species may differ significantly (e.g. Raman scattering for bulk MoO_3 is higher than for small Mo clusters [39]), only qualitative conclusions can be drawn from the spectra.

For MoO_3/MCM-41 catalysts, isolated surface molybdenum oxide species (see band 981 cm^{-1})are dominant at lower metal loading (4Mo/MCM-41 and 8Mo/MCM-41). With increasing molybdenum oxide loading the molybdenum surface species are approaching the bulk MoO_3 phase. For 16Mo/MCM-41 catalyst, the peaks at 981 and 958 cm^{-1} overlap; it indicates together with a broad band at 874 cm^{-1} and intensive bands at 995 cm^{-1} and 819 cm^{-1} that MoO_3 is predominantly in the form of surface polymolybdates and small crystallites of bulk MoO_3. This is in agreement with X-ray diffraction data, which showed the presence of small MoO_3 crystallites (about 5 nm) in 16Mo/MCM-41. Assuming a lower catalytic activity of surface polymolybdates compared with isolated molybdenum oxide species and the inactivity of MoO_3 bulk structure in metathesis reaction, we could explain the dependence of the specific activity on catalyst loading. The enhanced activity of catalysts with loading from 4 to 8 wt.% of Mo is then a result of a relatively high amount of isolated surface molybdenum oxide species, observed for both 4Mo/MCM-41 and 8Mo/MCM-41 catalysts.

Fig. 10 shows the Raman spectra of MoO_3/MCM-48 catalyst. The dispersion of MoO_3 is different from that of MCM-41-based catalysts. While for the 4Mo/MCM-48 sample the isolated surface molybdenum oxide species are typical, for 8Mo/MCM-48 and 12Mo/MCM-48 samples the band at 958 cm^{-1} strongly increases and hence the surface polymolybdates are prevailing. For 16Mo/MCM-48 catalyst the spectrum is in principle the same as for 16Mo/MCM-41, i.e. polymolybdate and MoO_3 crystallites strongly prevail. The different populations of Mo species in MoO_3/MCM-48 catalysts in comparison with MoO_3/MCM-41 catalysts can explain the different catalytic activity of MoO_3/MCM-48 catalysts. It seems that molybdenum is present prevailingly in the form of dispersed surface polymolybdates in both 8Mo/MCM-48 and 12Mo/MCM-48, which explain the depressed catalytic activity of 8Mo/MCM-48 but a little higher activity of 12Mo/MCM-48 both compared with MoO_3/MCM-41 catalysts with the same loading. On the other hand, the less loaded MoO_3/MCM-48 sample (4Mo/MCM-48) exhibits similar activity as 4Mo/MCM-41, which corresponds to the similar character of the spectra of both samples in question.

The Raman spectra of MoO_3/SBA-15 catalysts are shown in Fig. 11. In this case, it seems that only a small amount of MoO_3 is transformed into dispersed surface Mo species. For 4Mo/SBA-15 the surface polymolybdates are prevailing. For other samples, much larger part of Mo content is present in MoO_3 bulk phase compared with MCM-41 and MCM-48 supported catalysts. This is in a reasonable agreement with X-ray diffraction data, which showed the presence of MoO_3 crystallites even for 12Mo/SBA-15. Thus, a lower catalytic activity compared with both MoO_3/MCM-41 and MoO_3/MCM-48 catalyst series is not surprising.

In Raman spectra of conventional silica supported MoO_3 (8 wt.% of Mo), only one broad band was observed in the area from 1000 to 940 cm^{-1} (not shown in figure). The presence of a very small amount of isolated surface molybdenum oxide species could not be excluded, but the substantial part of the molybdenum oxide species is present in the form of various types of surface polymolybdates. Taking into account also a lower surface area of conventional silica, a lower catalytic activity compared with all mesoporous supports can be expected. In addition, electronic and steric properties of the surface inside the channels of highly organized mesoporous sieves may differ from those on the surface of conventional silica. These

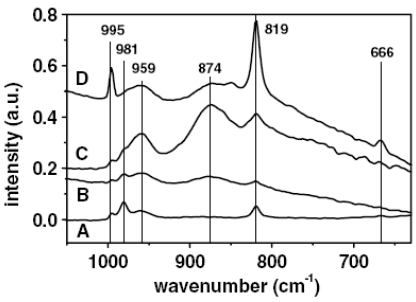

Fig. 10. Laser Raman spectra of 4Mo/MCM-48 (A), 8Mo/MCM-48 (B), 12Mo/MCM-48 (C) and 16Mo/MCM-48 (D).

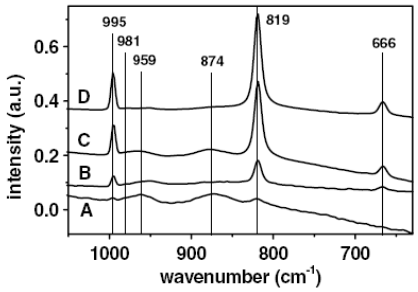

Fig. 11. Laser Raman spectra of 4Mo/SBA-15 (A), 8Mo/SBA-15 (B), 12Mo/SBA-15 (C) and 16Mo/SBA-15 (D). Spectra (A) and (B) were four times magnified.

differences may result in the easier formation and/or enhanced stabilization of catalytic centers in mesoporous channels increasing, thus, the catalytic activity of corresponding catalysts.

4. Conclusions

New types of heterogeneous catalysts for metathesis of linear alkenes based on molybdenum oxide supported on MCM-41, MCM-48 and SBA-15 were prepared and employed in metathesis of 1-octene. For MoO_3 supporting a low-cost and environmentally friendly thermal spreading method was successfully used. The XRD and Raman analysis showed that molybdenum oxide dispersion over the surface of mesoporous siliceous supports depends on loadings and type of the support used. At low Mo loadings, predominantly isolated surface molybdenum oxide species and highly dispersed surface polymolybdates were observed. At higher loadings, the properties of supported MoO_3 is close to the bulk phase and finally 2.5–5 nm crystallites of MoO_3 appeared on the external surface of the support. The relative amount of undispersed (bulky) MoO_3 was the highest for SBA-15. No experimental evidences of the collapse of mesoporous structure were observed, neither at the highest loadings (16 wt.% of Mo).

Prepared catalysts exhibited a high activity at mild reaction conditions. Moreover, neither solvent nor co-catalyst is required for the reaction, which makes the separation of the products much easier. Comparing the activity of the catalysts used, we can state that (i) the activity of all catalysts was higher than that of MoO_3 on conventional silica, (ii) catalysts of lower loadings (from 4 to 8 wt.% of Mo) exhibited higher specific activity than the catalysts with the highest loading (16 wt.% of Mo) due to the increasing amount of molybdenum oxide in the form of crystallites with increasing loading, (iii) turn-over-frequency of the catalysts loaded with 8 wt.% of Mo decreased according to the support used in the order MCM-41 > MCM-48 > SBA-15, probably due to simultaneously decreasing amount of isolated surface molybdenum oxide species, which are supposed to give rise the very active catalyst centers.

The highest specific activity was achieved with 6Mo/MCM-41. Seventy-five percent conversion of 1-octene was reached at 6 h at 40 °C. The outstanding activity of this catalyst may result from very well dispersed active phase and good accessibility of catalytically active species for substrate molecules. We can also speculate about the specific electronic and/or steric properties of the hexagonally ordered pores of MCM-41, which can contribute to the generation and/or stabilization of the active sites and/or their precursors. The selectivity to 7-tetradecene was in the range from 62% to 95%, for the most active catalyst 6Mo/MCM-41 the selectivity was 84%. This selectivity is rather high especially if we take into account that in many industrial applications both self-metathesis and cross-metathesis products may be utilized in further processes as well. For our catalysts the selectivity to all metathesis products was always higher than 97%.

Acknowledgments

J.Č. and H.B. thank the Grant Agency of the Academy of Sciences of the Czech Republic for the grant (A4040411). P.T. thanks to the Grant Agency of the Czech Republic for a project 203/03/H140 and Bilateral Scientific Cooperation Flanders – Czech Republic (Project 2004-2005-07). The authors thank Dr. L. Brabec (J. Heyrovský Institute) for recording SEM images.

References

[1] K.J. Ivin, J.C. Mol, Olefin Metathesis and Metathesis Polymerization, Academic Press, London, 1997.
[2] J.C. Mol, J. Mol. Catal. A 213 (2004) 39.
[3] J.C. Mol, Catal. Today 51 (1999) 289.
[4] Y. Iwasawa, H. Ichinose, S. Ogasawara, J. Chem. Soc. Faraday Trans. 1 77 (1981) 1763.
[5] B. Zhang, N. Liu, Q. Lin, D. Jin, J. Mol. Catal. 65 (1991) 15.
[6] B.N. Shelimov, I.V. Elev, V.B. Kazansky, J. Catal. 98 (1986) 70.
[7] J. Handzlik, J. Ogonowski, Catal. Lett. 88 (2003) 119.
[8] M.N. Kwini, J.M. Botha, Appl. Catal. A 280 (2005) 199.
[9] C. van Schalwyk, A. Spamer, D.J. Moodley, T. Dube, J. Reynhardt, J.M. Botha, Appl. Catal. A 255 (2003) 121.
[10] R. Zavoianu, A. Dias, O. Pavel, E. Angelescu, M. Portela, Catal. Commun. 6 (2005) 321.
[11] R.L. Banks, G.C. Bailey, Ind. Eng. Chem., Prod. Res. Dev. 3 (1964) 170.
[12] D.L. Crain, J. Catal. 13 (1969) 113.
[13] J.S. Beck, J.C. Vartuli, W.J. Roth, M.E. Leonowicz, C.T. Kresge, K.D. Schmitt, C.-W. Chu, D.H. Olson, E.W. Sheppard, S.B. McCullen, J.B. Higgins, J.L. Schlenker, J. Am. Chem. Soc. 114 (1992) 10834.
[14] F. Schüth, Chem. Mater. 13 (2001) 3184.
[15] J. Čejka, Appl. Catal. A 254 (2003) 327.
[16] H. Balcar, N. Žilková, J. Sedláček, J. Zedník, J. Mol. Catal. A 232 (2005) 53.
[17] K. Melis, D. de Vos, P. Jacobs, F. Verpoort, J. Mol. Catal. A 169 (2001) 47.
[18] H. Balcar, R. Hamtil, N. Žilková, J. Čejka, Catal. Lett. 97 (2004) 25.
[19] T. Oikawa, T. Ookoshi, T. Tanaka, T. Yamamoto, M. Onaka, Micropor. Mesopor. Mater. 74 (2004) 93.
[20] J. Aguado, J.M. Escola, M.C. Castro, B. Paredes, Appl. Catal. A 284 (2005) 47.
[21] R. Hamtil, N. Žilková, H. Balcar, J. Čejka, Appl. Catal. A 302 (2006) 193.
[22] Ch. Copéret, New J. Chem. 28 (2004) 1.
[23] T. Ookoshi, M. Onaka, Chem. Commun. (1998) 2399.
[24] H. Balcar, P. Topka, N. Žilková, J. Pérez-Pariente, J. Čejka, in: M. Jaroniec, A. Sayari (Eds.), Nanoporous Materials IV, Stud. Surf. Sci. Catal, 156, Elsevier, Amsterdam, 2005, p. 795.
[25] N. Ichikun, T. Eguchi, H. Murayama, K.K. Bando, S. Shimazu, T. Uematsu, in: S.-E. Park, R. Ryoo, W.-S. Ahu, Ch.W. Lee, J.-S. Chang (Eds.), Nanotechnology in Mesostructured Materials, Stud. Surf. Sci. Catal, 146, Elsevier, Amsterdam, 2003, p. 359.
[26] S.T. Wong, H.P. Lin, C.Y. Mou, Appl. Catal. A 198 (2000) 103.
[27] A. Sampieri, S. Pronier, J. Blanchard, M. Breysse, S. Brunet, K. Fajerwerg, C. Louis, G. Pérot, Catal. Today 107–108 (2005) 537.
[28] L. Kaluža, M. Zdražil, N. Žilková, J. Čejka, Catal. Commun. 3 (2002) 151.
[29] S. Hitz, R. Prins, J. Catal. 168 (1997) 194.

[30] M. Kruk, M. Jaroniec, C.H. Ko, R. Ryoo, Chem. Mater. 12 (2000) 1961.
[31] A. Klug, P. Harold, E. Leroy, X-Ray Diffraction Procedures For Polycrystalline and Amorphous Materials, J. Wiley & Sons, New York, 1954.
[32] Z. Li, L. Gao, S. Zheng, Mater. Lett. 57 (2003) 4605.
[33] M. de Boer, A.J. van Dillen, D.C. Koningsberger, J.W. Geus, M.A. Wurman, I.E. Wachs, Catal. Lett. 11 (1991) 227.
[34] Z. Li, L. Gao, S. Zheng, Appl. Catal. A 236 (2002) 163.
[35] D.T. Laverty, J.J. Rooney, A. Stewart, J. Catal. 45 (1976) 110.
[36] M. Faraldos, M.A. Bañares, J.A. Anderson, H. Hu, I.E. Wachs, J.L.G. Fierro, J. Catal. 160 (1996) 214.
[37] A.N. Desikan, L. Huang, S.T. Oyama, J. Phys. Chem. 95 (1991) 10050.
[38] H. Jeziorowski, H. Knözinger, P. Grange, P. Gajardo, J. Phys. Chem. 84 (1980) 1825.
[39] S. Braun, L.G. Appel, V.L. Camorim, M. Schmal, J. Phys. Chem. B 104 (2000) 6584.

Enclosure III

H. Balcar, P. Topka, J. Sedláček, J. Zedník, J. Čejka

Polymerization of aliphatic alkynes with heterogeneous Mo catalysts supported on mesoporous molecular sieves

J. Polym. Sci. A 46 (2008) 2593

NOTE

Polymerization of Aliphatic Alkynes with Heterogeneous Mo Catalysts Supported on Mesoporous Molecular Sieves

HYNEK BALCAR,[1] PAVEL TOPKA,[1] JAN SEDLÁČEK,[2] JIŘÍ ZEDNÍK,[2] JIŘÍ ČEJKA[1]

[1]J. Heyrovský Institute of Physical Chemistry, Academy of Sciences of the Czech Republic, v.v.i., Dolejškova 3, CZ-182 23 Prague 8, Czech Republic

[2]Department of Physical and Macromolecular Chemistry, Charles University in Prague, Faculty of Science, Hlavova 2030, CZ-128 40, Prague 2, Czech Republic

Received 11 October 2007; accepted 21 December 2007
DOI: 10.1002/pola.22600
Published online in Wiley InterScience (www.interscience.wiley.com).

Keywords: alkyne polymerization; conjugated polymers; metathesis; Mo heterogeneous catalysts; polyacetylenes

INTRODUCTION

Conjugated polymers attract a particular attention as functional materials for electronics, photonics, and related applications as well as for gas separation and pervaporation membranes.[1–5] These polymers are usually prepared by coordination polymerization of corresponding alkynes induced with homogeneous catalysts. The increased requirements for a high purity of these polymers, especially for a low level of catalyst residues, initiated the investigation of heterogeneous catalysts, the application of which enables easy and complete separation of produced polymers from catalysts.[6] Rh complexes immobilized on polymeric supports[7,8] and/or mesoporous molecular sieves[9,10] have been successfully used for polymerization of phenylacetylene and its derivatives into polymers of high purity. These catalysts failed, however, in polymerization of aliphatic alkynes.

Aliphatic alkynes, especially linear 1-alkynes, were successfully polymerized with homogeneous systems such as Ziegler-Natta catalysts based on Ti or Fe complexes,[11] metathesis catalysts based on WCl_6, $MoCl_5$,[12,13] and various W complexes.[14–16] Organometallic compounds of Mg, Al, and Sn (mostly explosive and/or poisonous) have to be often used as cocatalysts, which makes the polymerization process less friendly and creates an additional source of possible polymer contamination besides transition metal residues. Monosubstituted alkynes can also undergo radical and ionic polymerizations, producing oligomers and/or low-molecular weight polymers only (up to $M_w = 3000$).[17]

In this article, we report the application of new heterogeneous catalysts for polymerization of aliphatic alkynes: (i) MoO_3 supported on siliceous mesoporous molecular sieves of different types (MCM-41, MCM-48, and SBA-15) and (ii) Schrock type carbene $Mo(=CHCMe_2Ph)(=N\text{-}2,6\text{-}i\text{-}Pr_2C_6H_3)[OCMe(CF_3)_2]_2$ grafted on mesoporous molecular sieves MCM-41 and SBA-15, respectively. MoO_3 supported on mesoporous molecular sieves has been recently reported as an efficient catalyst for metathesis of linear alkenes, exhibiting high activity and selectivity in 1-octene metathesis under mild reaction conditions.[18,19] Easy and low-cost catalyst preparation, no Mo leaching into the reaction system, and possibility of easy catalyst recovery after alkene metathesis were the most important advantages of this catalyst. Schrock carbene complexes grafted on MCM-41 by alkoxy ligand exchange

Correspondence to: H. Balcar (E-mail: hynek.balcar@jh-inst.cas.cz)

Journal of Polymer Science: Part A: Polymer Chemistry, Vol. 46, 2593–2599 (2008)

reaction exhibited activity and selectivity in alkene metathesis similar to those of the parent complex in homogeneous phase. The activity of these heterogenized complexes was steadily bound to the heterogeneous phase and no Mo leaching was observed.[20] When these catalysts were used in ring opening metathesis polymerization of norbornene and cyclooctene, high molecular weight polymers of high purity (about 6 ppm of Mo) were obtained.[21]

EXPERIMENTAL

Catalyst Preparation

Mesoporous molecular sieves MCM-41, MCM-48, and SBA-15 were prepared by hydrothermal synthesis using sodium silicate (MCM-41), $Na_2Si_3O_7$ and fumed silica (MCM-48) or tetraethyl orthosilicate (SBA-15) as a silicon source, and hexadecyltrimethylammonium bromide (MCM-41), hexadecyltrimethylammonium hydroxide (MCM-48), and Pluronic PE 9400 (SBA-15) as structure directing agents. Details of the synthesis and characterization are given elsewhere.[18,22] Molybdenum oxide (Lachema, Czech Republic) was supported on mesoporous silica via a thermal spreading method. Physical mixtures of calculated amounts of MoO_3 and the respective molecular sieves were calcined at 500 °C for 8 h with a temperature ramp of 1 °C/min. MoO_3 supported on conventional silica (Silica gel 40, Merck, S_{BET} = 559 m^2/g, V = 0.473 cm^3/g, broad pore size distribution centered at 4.5 nm) was prepared in the same way. Loading of all MoO_3 supported catalysts was 6 wt % of Mo. $Mo(=CHCMe_2Ph)(=N\text{-}2,6\text{-}i\text{-}Pr_2C_6H_3)[OCMe(CF_3)_2]_2$ (Strem Chemicals) was supported on MCM-41 and SBA-15, respectively, from benzene solution at room temperature. The Mo content was 1 wt % of Mo. Details are given elsewhere.[20] All catalyst samples were stored in vacuum ampoules.

Alkyne Polymerization

In polymerization experiments, toluene (Lach-Ner, Czech Republic, 99%) and benzene (p.a., Lach-Ner, Czech Republic) were used as solvents. Solvents were purified by distillation and dried over metallic sodium (toluene) or calcium hydride (benzene). As for the monomers, 1-hexyne (Fluka, 97%), 2-hexyne (Alfa Aesar, 98%), 1-decyne (Aldrich, 98%), 1-tetradecyne (Fluka, purum), *t*-butylacetylene (Aldrich, 98%), and phenylacetylene (Fluka, 97%) were passed through a column of activated alumina and then dried over calcium hydride. 1-Ethynyl-4-fluorobenzene (Aldrich, 98%) and 1-ethynyl-2,4-difluorobenzene (Aldrich, 97%) were dissolved in distilled toluene and dried over calcium hydride. 1-Octene (Aldrich, 98%) was passed through the column of activated alumina and then dried over metallic Na.

In a typical experiment, 50 mg of MoO_3-based catalyst were placed into the glass reactor and activated at 500 °C in a stream of dried air for 0.5 h and in a stream of dried argon for another 10 min. After activation, the catalyst was cooled down to the preset reaction temperature in a stream of dried argon and evacuated until the pressure of 0.1 Pa was attained. Then, 2.5 mL of toluene and 0.25 mL of monomer were injected into the temperature-controlled reactor filled with argon and equipped with a magnetic stirring bar. The reaction temperature was 40 °C. After 180 min, the reaction mixture was opened on air, diluted with tetrahydrofuran (THF) (if the reaction mixture was too viscous) and the catalyst was separated by centrifugation. Then the catalyst was washed with THF twice to separate the polymer from catalyst completely. The polymer was isolated by precipitation into methanol and dried *in vacuo* at 60 °C to a constant weight. After isolating the polymer, the volatile components were evaporated from supernatant at room temperature and the nonvolatile residue was dried *in vacuo* at 60 °C. In the case of Schrock carbene complex grafted on MCM-41 and SBA-15, in a typical experiment, weighed amount of catalyst (about 40 mg) was placed into the same reactor under argon atmosphere. Then the reactor was evacuated, calculated amount of benzene was added by distillation under vacuum, the reactor was filled with argon and calculated amount of 1-hexyne was added with syringe. Initial 1-hexyne/benzene volume ratio and the 1-hexyne/Mo mole ratio were 0.03 and 100, respectively. Reaction was performed at 25 °C under stirring for 180 min. The polymer was isolated as in the previous case.

Products Characterization

For low molecular weight products identification GC-MS was used (ThermoFinnigan, FOCUS GC + DSQ II Single Quadrupole, EI, Thermo TR-5MS column, 15 m long, phase type = 5% phenyl-polysilylphenylene-siloxane, temperature range from 50 to 250 °C, He flow 1 mL/min, inlet temperature 200 °C, split ratio 50).

SEC analyses were carried out on a Watrex Chromatograph fitted with a differential refractometer Shodex RI 101. A series of two PL-gel columns (Mixed-B and Mixed-C, Polymer Laboratories Bristol, UK) and THF (flow rate 0.7 mL/min) were used. Weight-average molecular weight, M_w, and number-average molecular weight, M_n, relative to polystyrene standards are reported.

IR spectra were recorded on a Nicolet Avatar 320 FTIR spectrometer in KBr pellets. ^{1}H-NMR spectra were recorded on a Varian Unity Inova 400 instrument, tetramethylsilane was used as an internal standard. The determination of Mo concentration in polymers was made in the Research Institute of

Table 1. Sorption Characteristics of Supports and MoO_3-Based Catalysts with 6 wt % Mo Determined from Nitrogen Adsorption Isotherms

Sample	S_{BET} (m^2/g)	d (nm)	V (cm^3/g)
MCM-41	1,071	3.1	0.841
MoO_3/MCM-41	811	2.9	0.590
MCM-48	1,334	2.8	0.927
MoO_3/MCM-48	1,172	2.7	0.780
SBA-15	784	5.4	1.054
MoO_3/SBA-15	683	5.3	0.906

Inorganic Chemistry, Czech Republic, using ETA-AAS spectrometer equipped with a graphite cuvette.

RESULTS AND DISCUSSION

Mesoporous Molecular Sieves Supported MoO_3 Catalysts

Textural properties of individual supports and catalysts prepared are summarized in Table 1. Surface area S_{BET}, void volume V, and pore diameter d were determined from nitrogen adsorption isotherms at −196 °C. From Table 1, it is seen that the catalysts maintained the mesoporous structure of their parent supports. The formation of molybdenum oxide active phase led only to some decrease in the surface area and void volume, which was observed previously[23]; the differences in the pore size between catalysts and corresponding parent supports were practically negligible.

To test the activity of the prepared catalysts, 1-hexyne was used as a model monomer. The results obtained in the polymerization of 1-hexyne with MoO_3 supported on mesoporous sieves and conventional silica (MoO_3/MCM-41, MoO_3/MCM-48, MoO_3/SBA-15, and MoO_3/SiO_2) are summarized in Table 2. Polymerization of 1-hexyne with MoO_3/MCM-41 proceeded smoothly and products were continuously released into the liquid phase (increase in viscosity and yellow color of liquid phase were observed). After 15 min of the reaction, a slightly yellow polymer of M_w = 19,000 was isolated in 7% yield (Table 2, No. 1). After 90 min, the yield of polymer increased to 34% (Table 2, No. 2). At prolonged reaction times, the viscosity of a liquid phase increased significantly and the rate of the reaction ceased. After 3 h, polymer of M_w = 23,000 was isolated in 38% yield (Table 2, No. 3). Evaporation residue of grease consistence (22% yield) consisted mainly of higher oligomers (SEC peak area = 43%, M_w = 2700) and cyclotrimers (SEC peak area = 54%). Cyclotrimers (1,3,5-tributylbenzene and 1,2,4-tributylbenzene) were found in roughly equimolar ratio by GC-MS. Formation of cyclotrimers is well known to accompany the polymerization of substituted acetylenes.[17]

The structure of the prepared polymers was evaluated using ^{1}H-NMR and FTIR. ^{1}H-NMR spectrum of poly(1-hexyne) (Fig. 1, spectrum b) confirmed a typical polyacetylene structure consisting of conjugated main chain with *n*-butyl pendant groups.[11]

Table 2. Polymerization of 1-Hexyne with MoO_3-Based Catalysts

No.	Catalyst	Polymer Yield (%)	Evaporation Residue Yield (%)	Polymer Molecular Weight	
				M_w	M_n
1	MoO_3/MCM-41[a]	7	6	19,000	7,500
2	MoO_3/MCM-41[b]	34	n.d.	n.d.	n.d.
3	MoO_3/MCM-41	38	22	23,000	10,000
4	MoO_3/MCM-48	22	n.d.	8,800	2,700
5	MoO_3/SBA-15	64	n.d.	30,000	7,500
6	MoO_3/SiO_2	4	3	6,800	2,200
7	MoO_3/MCM-41[c]	3	12[d]	13,000	7,000
8	MoO_3/MCM-41[e]	0	18[d]	n.d.	n.d.
9	MoO_3/MCM-41[f]	18	n.d.	6,100	1,600

Toluene, reaction time = 3 h; reaction temperature = 40 °C; mole ratio 1-hexyne/Mo = 70; n.d. = not determined.
[a] Reaction time 15 min.
[b] Reaction time 90 min.
[c] 1-Octene was added in equimolar amount to 1-hexyne.
[d] Yield with respect to 1-hexyne.
[e] 1-Octene was added in excess to 1-hexyne (mole ratio 1-octene/1-hexyne = 5).
[f] Reactivated catalyst, M_w and M_n = polymer weight average molecular weight and number average molecular weight, respectively.

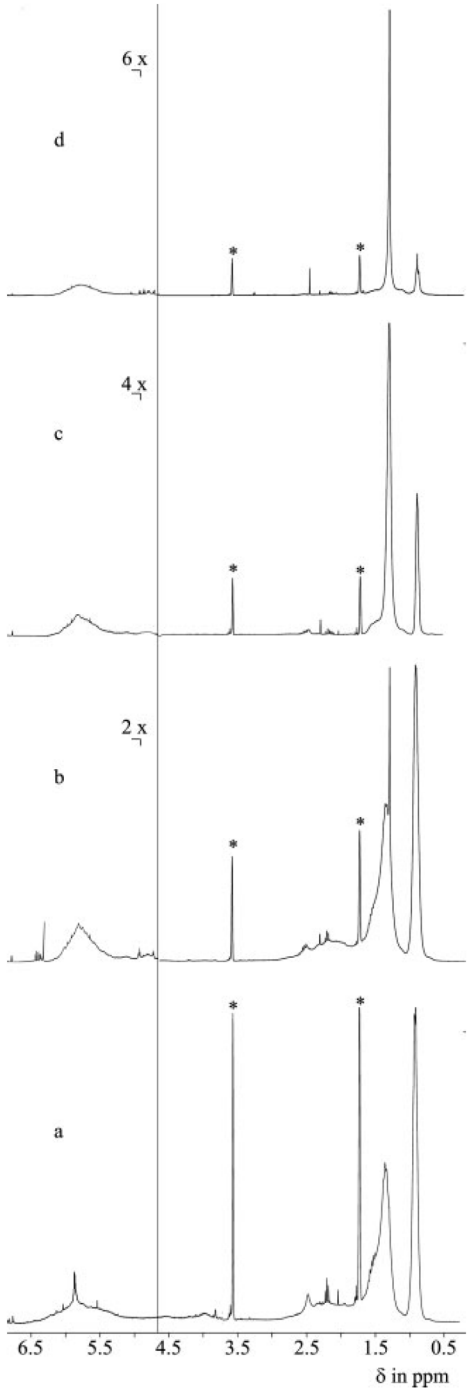

Figure 1. ^{1}H-NMR spectra of poly(1-hexyne)-(a,b), poly(1-decyne)-(c), and poly(1-tetradecyne)-(d) prepared with MoO_3/MCM-41 (b,c,d) and with Mo^{carb}/MCM-41 (a). THF-d_8, room temperature, *signal of solvents.

The broad signal of olefinic proton (δ from 5.0 to 6.5 ppm) suggests the presence of irregular polymer microstructure (*cis*- and *trans*-double bonds randomly distributed along the main chain, randomness in head-to-head and head-to-tail monomer linkage).

The content of Mo in polymer samples was 8 ppm. This result corresponds well with the high purity polyacetylenes prepared with Rh immobilized catalysts.[6]

MoO_3/MCM-48 and MoO_3/SBA-15 were tested in 1-hexyne polymerization as well and polymer yields achieved at 3 h of reaction were 22 and 64%, respectively. (Table 2, Nos. 4 and 5). Both the polymer yield and M_w increased in the order MoO_3/MCM-48 <MoO_3/MCM-41 <MoO_3/SBA-15. It suggests that the increasing pore size of the support positively affects the catalyst activity in this type of reaction. However, this finding should not be generalized as (i) the architecture of MCM-41 and MCM-48 is different (i.e., of hexagonal and cubic symmetry, respectively) and (ii) the process of catalyst operation is complex and individual factors influencing catalyst activity (i.e., Mo dispersion on the surface, type and stability of active sites, and diffusion rate of monomer and polymer in the catalyst channels) may depend on the pore size in different ways. On the other hand, MoO_3/SiO_2 exhibited very low activity, providing only 4% polymer yield in addition to 3% yield of oligomeric fraction (Table 2, No. 6). It is in agreement with a large activity difference between MoO_3 supported on mesoporous molecular sieves and on conventional silica, respectively, reported earlier for metathesis of neat linear alkenes.[18] In a blank experiment with pure MCM-41, no polymer was formed even after 20 h of the reaction (not given in Table 2).

In principle, alkyne polymerizations with transition metal catalysts proceed in either metathesis or insertion mode.[24–26] As MoO_3-based heterogeneous catalysts are well known to be active in alkene metathesis,[27] it can be anticipated that in the case of alkyne polymerization they operate in the metathesis mode as well. To support this assumption, experiments with 1-octene added to the feedstock were performed (Table 2, Nos. 7, 8). When mole ratio 1-octene to 1-hexyne was 1.0, significant reduction in polymer yield and in polymer M_w was observed. At 1-octene/1-hexyne mole ratio = 5, only oligomers were formed (higher oligomers of M_w = 2600 with 12% yield, and cyclotrimers with 6% yield with respect to 1-hexyne). Thus, 1-octene evidently acted as a chain transfer agent, which supports the assumption of metathesis mode of polymerization of pure 1-hexyne.

In experiments without chain transfer agents, we assume that the polymer is disconnected from the catalyst due to the chain transfer by polymer. We assume backbiting-like mechanism, in which the growing polymer chain reacts with catalytic species located on catalyst surface in their vicinity.[28] In addition, the rest of polymer may be liberated from the

Table 3. Polymerization of Different Alkynes with MoO_3/MCM-41 Catalyst

No	Monomer	Polymer Yield %	M_w	M_n
1	1-Hexyne	38	23,000	10,000
2	1-Decyne	38	18,000	8,400
3	1-Tetradecyne	35	20,000[a]	13,000[a]
4	*tert*-Butylacetylene	11	300,000	39,000
5	2-Hexyne	1	200,000[a]	22,000[a]
6	Phenylacetylene	1	16,000	4,700
7	4-Fluorophenylacetylene	10	5,200	2,800
8	2,4-Difluorophenylacetylene	8[b]	1,900	1,500

Toluene, reaction time = 3 h; reaction temperature = 40 °C; alkyne/Mo mole ratio = 70.
[a] THF soluble part.
[b] MeOH soluble product.

catalyst in the course of separation of liquid phase from catalyst performed on air (by reaction with oxygen).[29]

After product separation, the spent MoO_3/MCM-41 catalyst (from experiment No. 3, Table 2) was reactivated by calcination in air at 500 °C for 3 h. However, both the polymer yield and polymer M_w in the second polymerization cycle were significantly reduced (Table 2, No. 9). This is in contradiction to the 1-alkene metathesis experiments, where complete recovery of MoO_3/MCM-41 catalyst activity and selectivity was observed after the same reactivation procedure.[30]

MoO_3/MCM-41 was also used in the polymerization of a series of different alkynes (Table 3). MoO_3/MCM-41 was chosen as the application of MoO_3/SBA-15 might lead to the polymers of higher molecular weight and consequently lower solubility. Aliphatic 1-alkynes with longer chain (1-decyne and 1-tetradecyne) underwent polymerization under formation of corresponding poly(1-alkynes) with similar yields as 1-hexyne (from 35 to 38%). While poly(1-decyne) was completely soluble in THF, poly(1-tetradecyne) became only partially soluble in THF after isolation and, therefore, its molecular weight characteristics and NMR spectrum are referred to the soluble part only. Molecular weights of both poly(1-decyne) and poly(1-tetradecyne) are close to those of poly(1-hexyne). Their ^{1}H-NMR spectra (Fig. 1, spectra c and d) exhibit the same features as that of poly(1-hexyne), but with properly increased intensity of methylene proton signal at δ = 1.3 ppm. Broad signals of main chain protons also indicate irregular polymer microstructure.

The applicability of MoO_3/MCM-41 catalyst in the polymerization of other type of alkynes is significantly reduced in comparison with aliphatic linear 1-alkynes. *tert*-Butylacetylene gave polymer of M_w = 300,000, but its yield was 11% only, probably as a result of limited release of polymer from the catalyst pores. In the case of 2-hexyne, only negligible amount of partially soluble polymer was obtained. The yield of poly(phenylacetylene) was 1% only together with ca 0.2% of cyclotrimers (confirmed by SEC analysis of mixture of 1,3,5- and 1,2,4-triphenylbenzenes prepared according to Refs. 31 and 32). The introduction of electron-withdrawing fluorosubstituents on the phenyl ring (monomers: 4-fluoro-, and 2,4-difluorophenylacetylene) had only marginal effect on the monomer polymerizability, in contradiction to the positive effect of these substituents on polymerizability of fluorophenylacetylenes with Rh catalysts.[33]

Schrock-Type Mo Carbene Complex Supported on Mesoporous Molecular Sieves

Mo alkylidene complexes are known to polymerize various monosubstituted alkynes, even via living polymerization mode in some cases.[34–36] Commercially available Mo(=CHCMe$_2$Ph)(=*N*-2,6-*i*-Pr$_2$C$_6$H$_3$)[OCMe(CF$_3$)$_2$]$_2$ (Mo^{carb}) belongs to the most active alkylidene complexes of this type. (Mo^{carb}) grafted on MCM-41 and SBA-15, respectively, (Mo^{carb}/MCM-41, Mo^{carb}/SBA-15) were tested in polymerization of 1-hexyne. For a comparison, an experiment with Mo^{carb} used as homogeneous catalyst was conducted. The results are summarized in Table 4.

With Mo^{carb} applied as homogeneous catalyst, poly(1-hexyne) was formed in nearly quantitative yield. With Mo^{carb}/MCM-41 and Mo^{carb}/SBA-15 the polymer yields were lower and were comparable with those resulted over MoO_3 supported on mesoporous

Table 4. 1-Hexyne Polymerization with Schrock-Type Mo Carbene-Based Catalysts

Catalyst	Polymer Yield (%)	M_w	M_n
Mo^{carb}/MCM-41	34	7,500	2,800
Mo^{carb}/SBA-15	59	4,900	1,900
Mo^{carb} [a]	98	17,000	10,000

Benzene, reaction temperature = 25 °C; reaction time = 3 h, mole ratio 1-hexyne/Mo = 100.
[a] Mo^{carb} in benzene as homogeneous catalyst.

molecular sieves. In addition, Mo^{carb}/MCM-41 and Mo^{carb}/SBA-15 provided poly(1-hexyne)s of lower molecular weight, as compared with MoO_3 supported catalysts. High polydispersity index of polymers prepared with anchored Mo^{carb} catalysts (M_w/M_n = 2.6) indicates that the polymerization is very far from a "living" one. Different accessibility of individual propagating centers located on different places of the catalyst surface (e.g., external surface, pore mouth, pore walls of different distances from mouth) and/or chain transfer processes, responsible for polymer releasing from catalyst during polymerization, may result in the increase in polymer polydispersity index and probably also in the decrease in molecular weight averages in comparison with polymer prepared with Mo^{carb} homogeneous system.

^{1}H-NMR spectra of polymers prepared with Mo^{carb}-based catalysts differed from the spectra of polymers prepared with MoO_3-based catalysts in the region of main-chain protons. Polymers prepared with both Mo^{carb}/MCM-41 and Mo^{carb}/SBA-15 exhibited in ^{1}H-NMR spectra a narrow signal at δ = 5.9 ppm (Fig. 1, spectrum a), the sharpness of which indicates an increased polymer regularity. The similar 5.9 ppm signal was found also in poly(1-hexyne) prepared with Mo^{carb} in homogeneous system (not given in Fig. 1). It indicates that polymerization selectivity leading to the polymers of increased microstructure regularity is an inherent property of Mo^{carb} catalyst, which is preserved also after immobilization. This might be connected with a uniform type of addition of 1-hexyne molecules to the propagating carbene[34] that minimizes the interaction with bulky ligands in Mo coordination sphere and leads to the uniform head-to-tail linkage of monomeric units in the polymer chains.

Poly(1-alkyne)s with a sharp ^{1}H-NMR signal at about 5.9 ppm have already been reported in the literature. Nevertheless, the assignment of this signal to a particular main chain configuration was not unequivocal. For poly(1-alkyne)s prepared with Rh homogeneous catalysts,[25,37,38] the 5.9 ppm signal was mostly assigned to the main-chain olefinic proton on double bonds with *cis* configuration. This assignment came from the *cis*-transoidal stereoselectivity of Rh-based catalysts, which was well proved in the case of polymerization of phenylacetylene type monomers.[39] On the other hand, authors who reported poly(1-alkynes) of increased microstructure regularity prepared with W- and Fe-based catalysts ascribed the 5.9 ppm signal to the protons on the *trans* main chain double bonds.[11,40,41] In some cases, this assignment was supported by IR spectra in the fingerprint region.[11,40] The FTIR spectra of poly(1-hexyne)s prepared with MoO_3- and Mo^{carb}-based catalysts were very close to each other exhibiting in this region following bands (cm^{-1}): 728, 900, 938, 964, 1102. Moreover, these spectra were very similar to the spectrum of a reference poly(1-hexyne) sample of high microstructure uniformity (narrow ^{1}HNMR signal at δ = 5.9 ppm) and $M_w = 3 \times 10^4$ prepared with [Rh(NBD)acac] catalyst (NBD = 1,5-norbornadiene, acac = acetylacetonato).[25] The absence of the band traditionally ascribed to the vibration of =C—H in *cis* configuration (740–780 cm^{-1}), refs. 11 and 42, in spectra of all studied polymers and the known complexity of IR spectra in fingerprint region did not allow us to draw the unambiguous conclusions about the prevailing main chain configuration of poly(1-hexyne)s prepared with Mo^{carb} catalysts studied.

CONCLUSIONS

New efficient heterogeneous catalysts for 1-alkyne polymerization enabling easy separation of polymeric product from the catalysts and providing polymers free of catalyst residues were described:

i. MoO_3 supported on siliceous mesoporous molecular sieves MCM-41, MCM-48, and SBA-15 was found to be efficient catalysts for polymerization of aliphatic 1-alkynes. In polymerization of internal alkynes and phenylacetylenes, its efficiency was considerably lower. Polymerization via metathesis mechanism was proposed.
ii. $Mo(=CHCMe_2Ph)(=N\text{-}2,6\text{-}i\text{-}Pr_2C_6H_3)[OCMe(CF_3)_2]_2$ immobilized on MCM-41 and SBA-15, respectively, can be also used as catalysts for polymerization of aliphatic 1-alkynes.

The authors thank M. Horáček from J. Heyrovský Institute for GC-MS analysis of low molecular weight products. The financial support from the Grant Agency of the Czech Republic (project 203/05/2194), the Grant Agency of the Academy of Science of the Czech Republic (project A4040411), the Academy of Sciences of the Czech Republic (KAN100400701), and from long term research plan of the Ministry of Education of the Czech Republic No. MSM0021620857 is gratefully acknowledged.

REFERENCES AND NOTES

1. Handbook of Organic Conductive Molecules, Nalva, H. S.; Ed.; Wiley: New York, 1996.
2. Lam, J. W. Y.; Tang, B. Z. Acc Chem Res 2005, 38, 745–754.
3. Masuda, T. J. Polym Sci Part A: Polym Chem 2007, 45, 165–180.
4. Takada, K.; Matsuya, H.; Masuda, T.; Higashimura, T. J Appl Polym Sci 1985, 30, 1605–1616.
5. Nagase, Y.; Takamura, Y.; Matsui, K. J Appl Polym Sci 1991, 42, 185–190.
6. Svoboda, J.; Bláha, M.; Sedláček, J.; Vohlídal, J.; Balcar, H.; Mav-Golež, I.; Žigon, M. Acta Chim Slov 2006, 53, 407–416.

7. Sedláček, J.; Pacovská, M.; Rédrová, D.; Balcar, H.; Biffis, A.; Corrain, B.; Vohlídal, J. Chem Eur J 2002, 8, 366–371.
8. Mastrorilli, P.; Nobile, C. F.; Rizzuti, A.; Suranna, G. P.; Acierno, D.; Amendola, E. J Mol Catal A 2002, 178, 35–42.
9. Balcar, H.; Čejka, J.; Sedláček, J.; Svoboda, J.; Zedník, J.; Bastl, Z.; Bosáček, V.; Vohlídal, J. J Mol Catal A 2003, 203, 287–298.
10. Balcar, H.; Sedláček, J.; Svoboda, J.; Žilková, N.; Rathouský, J.; Vohlídal, J. Collect Czech Chem Commun 2003, 68, 1861–1876.
11. Petit, A.; Moulay, S.; Aouak, T. Eur Polym Mater 1999, 35, 953–963.
12. Yokota, K.; Ohtubo, M.; Hirabayashi, T.; Inai, Y. Polym J 1993, 25, 1079–1086.
13. Masuda, T.; Okano, Y.; Tamura, K.; Higashimura, T. Polymer 1985, 26, 793–797.
14. Nakayama, Y.; Mashima, K.; Nakamura, A. Macromolecules 1993, 26, 6267–6272.
15. Ymamoto, H.; Saito, Y.; Nagase, Y.; Fuchikami, T. Chem Lett 1994, 1329–1332.
16. Lucas, C.; Soum, A.; Fontanille, M. Makromol Chem Macromol Chem Phys 1989, 190, 377–387.
17. Masuda, T.; Higashimura, T. Adv Polym Sci 1987, 81, 121–165.
18. Topka, P.; Balcar, H.; Rathouský, J.; Žilková, N.; Verpoort, F.; Čejka, J. Micropor Mesopor Mater 2006, 96, 44–54.
19. Balcar, H.; Topka, P.; Žilková, N.; Pérez-Pariente, J.; Čejka, J. In Nanoporous Materials IV; Jaroniec, M.; Sayari, A., Eds.; Elsevier: Amsterdam, 2005; pp 795–802; Studies in Surface Science Catalysis 156.
20. Balcar, H.; Žilková, N.; Sedláček, J.; Zedník, J. J Mol Catal A 2005, 232, 53–58.
21. Balcar, H.; Čejka, J. In New Frontiers in Metathesis Chemistry: From Nanostructure Design to Sustainable Technologies for Synthesis of Advanced Materials, Imamoglu, Y.; Dragutan, V., Eds.; Springer: Dordrecht, 2007; pp 151–166; NATO Security through Science Series, Series C.
22. Čejka, J.; Krejčí, A.; Žilková, N.; Dědeček, J.; Hanika, J. Micropor Mesopor Mater 2001, 44, 499–507.
23. Li, Z.; Gao, L.; Zheng, S. Appl Catal A 2002, 236, 163–171.
24. Masuda, T.; Sanda, F. In Handbook of Metathesis; Grubbs, R. H., Ed.; Wiley WCH: Weinheim, 2003; Vol. 3, p 375.
25. Sedláček, J.; Vohlídal, J. Collect Czech Chem Commun 2003, 68, 1745–1790.
26. Vohlídal, J.; Sedláček, J.; Patev, N.; Pacovská M.; Lavastre, O.; Cabioch, S.; Dixneuf, P. H.; Blechta, V.; Matějka, P.; Balcar, H. Collect Czech Chem Commun 1998, 63, 1815–1838.
27. Ivin, K. J.; Mol, J. C. Olefin Metathesis and Metathesis Polymerization; Academic Press: London, 1997; Chapter 2.4.2.
28. Lee, L.-B. W.; Register, R. A. Polymer 2004, 45, 6479–6485.
29. Perrot, M. G.; Novak B. M. Macromolecules 1995, 28, 3492–3494.
30. Topka, P.; Balcar, H.; Žilková, N.; Čejka, J. In Proceedings of the 10th International Symposium on Catalyst Deactivation, Berlin, Germany, February 5–8, 2006; Book of extended abstract, p 239.
31. Niki, A.; Masuda, T.; Higashimura, T. J Polym Sci Part A: Polym Chem 1987, 25, 1553–1562.
32. Štěpnička, P.; Císařová, I.; Sedláček, J.; Vohlídal, J.; Polášek, M. Collect Czech Chem Commun 1997, 62, 1577–1584.
33. Balcar, H.; Sedláček, J.; Čejka, J.; Vohlídal, J. Macromol Rapid Commun 2002, 23, 32–37.
34. Schrock, R. R.; Luo, S.; Lee, J. C., Jr.; Zanetti, N. C.; Davis, W. M. J Am Chem Soc 1996, 118, 3883–3895.
35. Balcar, H.; Sedláček, J.; Zedník, J.; Vohlídal, J.; Blechta, V. In Ring Opening Metathesis Polymerization and Related Chemistry; Khosravi, E.; Szymanska-Buzar, T., Eds.; Kluwer Academic Publishers: Dordrecht, 2002; pp 417–424; NATO Science Series II, Vol. 56.
36. Mayershofer, M. C.; Wagner, M.; Anders, U.; Nuyken, O. J Polym Sci Part A: Polym Chem 2004, 42, 4466–4477.
37. Mitsuyama, M.; Ishii, R.; Kondo, K. J Polym Sci Part A: Polym Chem 2000, 38, 3419–3427.
38. Zhou, J. L.; Chen, X. F.; Fan, X. H.; Chai, C. P.; Lu, C. X.; Zhao, X. D.; Pan, Q. W.; Tang, H. Y.; Gao, L. C.; Zhou Q. F. J Polym Sci Part A: Polym Chem 2006, 44, 4532–4545.
39. Furlani, A.; Licoccia, S.; Russo, M. V.; Camus, A.; Marsich, N. J Polym Sci 1986, 24, 991–1005.
40. Leclerc, M.; Prud'homme, R. E.; Soum, A.; Fontanille, M. J Polym Sci Polym Phys Ed 1985, 23, 2031–2041.
41. Masuda, T.; Deng, Y. X.; Higashimura, T. Bull Chem Soc Jap 1983, 56, 2798–2801.
42. Chien, J. C. W. Polyacetylene-Chemistry, Physics and Material Science; Academic Press: Orlando, Florida, 1984; pp 206–216.

Journal of Polymer Science: Part A: Polymer Chemistry
DOI 10.1002/pola